The background of the slide is a microscopic image of *Scenedesmus obliquus* cells. These are small, green, oval-shaped organisms. Many of them contain bright, yellowish, spherical oil droplets, which are the focus of the study. The cells are distributed across the frame, with some appearing more clearly than others.

# The dynamics of oil accumulation in *Scenedesmus obliquus*

Guido Breuer



# **The dynamics of oil accumulation in *Scenedesmus obliquus***

Guido Breuer

## **Thesis committee**

### **Promotor**

Prof. Dr R.H. Wijffels  
Professor of Bioprocess Engineering  
Wageningen University

### **Co-promotors**

Dr D.E. Martens  
Assistant professor, Bioprocess Engineering  
Wageningen University

Dr P.P. Lamers  
Assistant professor, Bioprocess Engineering  
Wageningen University

### **Other members**

Prof. Dr V. Fogliano, Wageningen University  
Dr J.C. Weissman, Exxonmobil, Annandale, USA  
Prof. Dr B. Teusink, VU University Amsterdam  
Dr L.M. Trindade, Wageningen University

This research was conducted under the auspices of the Graduate School VLAG (Advanced studies in Food Technology, Agrobiotechnology, Nutrition and Health Sciences).

# **The dynamics of oil accumulation in *Scenedesmus obliquus***

**Guido Breuer**

## **Thesis**

submitted in fulfilment of the requirements for the degree of doctor

at Wageningen University

by the authority of the Rector Magnificus

Prof. Dr M.J. Kropff,

in the presence of the

Thesis Committee appointed by the Academic Board

to be defended in public

on Friday 6 March 2015

at 1:30 p.m. in the Aula.

G. Breuer

The dynamics of oil accumulation in *Scenedesmus obliquus*,  
268 pages.

PhD thesis, Wageningen University, Wageningen, NL (2015)  
With references, with summaries in Dutch and English

ISBN 978-94-6257-234-8







# Contents

<b>Chapter 1</b>	Introduction	9
<b>Chapter 2</b>	Analysis of Fatty Acid Content and Composition in Microalgae	19
<b>Chapter 3</b>	The impact of nitrogen starvation on the dynamics of triacylglycerol accumulation in nine microalgae strains	37
<b>Chapter 4</b>	Effect of light intensity, pH, and temperature on triacylglycerol (TAG) accumulation induced by nitrogen starvation in <i>Scenedesmus obliquus</i>	67
<b>Chapter 5</b>	Superior triacylglycerol (TAG) accumulation in starchless mutants of <i>Scenedesmus obliquus</i> : Evaluation of TAG yield and productivity in controlled photobioreactors	89
<b>Chapter 6</b>	Photosynthetic efficiency and carbon partitioning in nitrogen-starved <i>Scenedesmus obliquus</i>	109
<b>Chapter 7</b>	Opportunities to improve the areal oil productivity of microalgae	143
<b>Chapter 8</b>	General discussion	193
<b>References</b>		221
<b>Summary</b>		239
<b>Samenvatting</b>		247
<b>Dankwoord</b>		257
<b>About the author</b>		263
<b>List of publications</b>		265
<b>Overview of completed training activities</b>		266



# **Chapter 1** Introduction

### **1.1 Microalgae as a sustainable substitute for plant products**

Global demands for food and fuels are rapidly increasing as a result of an increasing world population and wealth of developing countries (Godfray et al., 2010).

Furthermore, renewable and sustainable alternatives for fossil-oil-derived fuels and chemicals are required because of depleting fossil resources, and concerns for climate change. Currently, these alternatives are mainly derived from agricultural crops. Their products can be used directly for food, fuel or chemical production (e.g. production of biodiesel from vegetable oil) or are converted by heterotrophic microbial fermentation to fuels and chemicals (e.g. fermentation of sugars, starch or lignocellulose to for example ethanol-fuel). The production of food and renewable-fuel commodities currently thus relies heavily on the cultivation of agricultural crops. The areal productivity of commonly used crops is reaching a ceiling and the availability of arable land, as well as of fresh water and nutrients, is limited (Godfray et al., 2010). Novel sustainable and renewable sources for both food-commodities and fuels are therefore highly desired (Draaisma et al., 2013).

Microalgae-derived products are often considered as a promising substitute for these crop-derived commodities (Draaisma et al., 2013; Wijffels & Barbosa, 2010). Microalgae are essentially unicellular plants (Fig. 1.1A) and can produce the same products as terrestrial crops. Microalgae can produce large quantities of protein, vegetable oil, and carbohydrates (Draaisma et al., 2013). Cultivation of microalgae has several advantages over the use of traditional agricultural crops. Microalgae can achieve much higher photosynthetic efficiencies. As a result, much higher areal productivities can be accomplished (Chisti, 2007; Moody et al., 2014; Wijffels & Barbosa, 2010). Furthermore, microalgae are cultivated in photobioreactors (Fig. 1.1B) and do therefore not require arable land. Potentially, microalgae can even be cultivated off-shore. Some microalgae species can grow efficiently on seawater, which can largely reduce freshwater requirements (Wijffels & Barbosa, 2010). Finally, fertilizer requirements could be reduced because no nutrients are lost to the environment in a photobioreactor (Chisti, 2013).

Despite these advantages of microalgae, the technology for production of microalgae needs to be further developed before large scale production is feasible. Today, the cost for production and the energy consumption involved in construction and operation of photobioreactors are too high (Ación et al., 2012; Brentner et al., 2011; Davis et al., 2011; Norsker et al., 2011). Current estimates claim that a several fold reduction in

cost-price needs to be realized before the production of bulk products using microalgae can become feasible (Klok et al., 2014). Such improvements could for example be made by increasing the microalgal productivity.

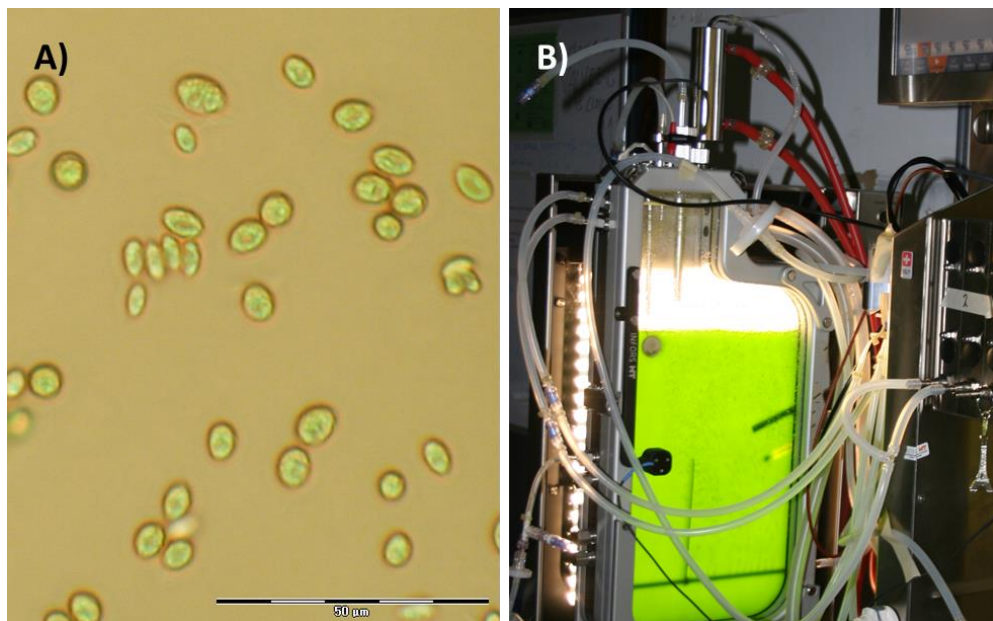


**Fig. 1.1.** Microscopic photograph of the microalga *Scenedesmus obliquus* (A). The scale bar indicates 50µm. Photograph of a lab-scale photobioreactor that was used for the work performed for this thesis (B).

## 1.2 TAG production by microalgae

Although microalgae could be a source for a large variety of commodities, the work presented in this thesis focusses on the production of triacylglycerol (TAG). TAGs are a lipid consisting of a glycerol backbone containing three fatty acid groups (Box 1). TAGs are the main component of vegetable oil and the composition of microalgal derived TAGs is similar to that of currently used vegetable oils derived from oil-crops (Draaisma et al., 2013). These TAGs are therefore suitable as a resource for both food and biofuel applications (Chisti, 2007; Draaisma et al., 2013; Wijffels & Barbosa, 2010).

In potential, TAG production using microalgae can be more sustainable and productive than TAG production using agricultural oil-crops. However, with current technology TAG production is not yet cost-effective and still requires more energy input than is produced in the form of TAG. An increase in the TAG productivity can help to decrease the cost-price and specific energy consumption of the production process. To achieve these high

TAG productivities, a quantitative understanding of the processes involved in microalgal TAG production is essential.

**Box 1. Lipids in microalgae.**

Lipid is an ambiguous term and lipids often refers to hydrophobic organic molecules or to the fraction of the biomass that is soluble in a specific organic solvent (e.g. hexane or chloroform). Because a large variety of lipid classes are produced by microalgae, and the relative abundance of these lipids can vary to a large extent, it is important to distinguish between these lipids. From a chemical point of view, these lipids could be classified as fatty-acyl lipids and non-fatty-acyl lipids.

**Table 1.1.** Lipids in microalgae. The values represent typical values found for most microalgae and can be used as a rule of thumb. For specific species, exceptions exist that exceed these values (e.g. large quantities of hydrocarbons in *Botryococcus braunii* or  $\beta$ -carotene in *Dunaliella salina*).

Component		Main function	Abundance (% DW)	Reference
fatty acyl-lipids	triacylglycerol (TAG)	storage or as energy sink	0-50	(Breuer et al., 2012; Hu et al., 2008)
	mono-, and diacylglycerols	phospholipids	5-10	(Breuer et al., 2012)
		galactolipids		
	carotenoid-fatty-acyl-esters	secondary & primary pigments (photoprotective & photosynthesis)	0-5	(Mulders et al., 2014a; Mulders et al., 2014b)
non-fatty-acyl lipids	carotenoids	primary pigments (photosynthesis)	1-3	(Mulders et al., 2014a; Mulders et al., 2014b)
	chlorophylls	various, including structural and signalling	5-20	Estimated <sup>1</sup>
	Other	e.g. waxes, sterols, hydrocarbons		

<sup>1</sup>Estimated from total lipids (15-25%)(Griffiths & Harrison, 2009; Pruvost et al., 2009; Renaud et al., 1999) minus the other lipid classes. Based on nitrogen replete conditions.

Microalgae produce many different types of lipids (Table 1.1). These lipids serve various cellular functions. Triacylglycerol (TAG) is present as droplets in the cell and serves to store carbon and energy. Cell, organelle, and thylakoid membranes mainly consist of diacylglycerols and these have a structural role. Pigments such as chlorophylls and carotenoids have a role in photosynthesis for light harvesting or photo-protection. Other lipids present in microalgae include waxes, sterols, and hydrocarbons. Among other roles, these lipids have a function in cell signalling, or contribute to the structure of, for

example, membranes (Table 1.1).

Fatty-acyl lipids are lipids that contain fatty acid groups. An important example of these fatty-acyl lipids is TAG. TAG consists of a glycerol backbone with three fatty acid groups (Fig. 1.2). Of all microalgal lipids, TAGs receive most attention because these TAGs are similar to vegetable oil and can be used as an edible oil. In addition, especially TAGs, but also other fatty-acyl lipids, are of interest because these can be trans-esterified using methanol to yield fatty acid methyl esters (FAMES). These FAMES can be used as a biodiesel.



**Fig. 1.2.** Chemical structure of a triacylglycerol containing three oleic acid (C18:1) groups (triolein).

Under balanced growth conditions, total lipid (fatty acyl and non-fatty acyl lipids) contents are typically 15-25% of the cell dry weight (Griffiths & Harrison, 2009; Pruvost et al., 2009; Renaud et al., 1999) and approximately half of these total lipids are fatty acyl-lipids (Table 1.1). Under these conditions, TAG is only produced in very low quantities (0-3% of DW). During nutrient starvation however, these TAGs can be produced in very large amounts, ranging up to 50% of the cell dry weight (Table 1.1).

Microalgae are a large and diverse group of microorganisms and large differences exist between species. Not all of these microalgae species produce large amounts of TAG. Microalgae that do accumulate large quantities of TAG are called oleaginous microalgae. The classification of oleaginous and non-oleaginous species is rather arbitrarily, but commonly, microorganisms that can accumulate more than 20% of their dry weight as TAGs are referred to as being oleaginous (Ratledge & Cohen, 2008). During conditions optimal for cell growth, even in the most-oleaginous species, only negligible amounts of TAG are produced. TAG is a secondary metabolite and is only accumulated as a response to physiological stress, such as nutrient starvation (Hu et al., 2008). The most commonly used technique to induce TAG production is the use of nitrogen starvation (Hu et al., 2008). Here, microalgae are first cultivated under nitrogen replete growth conditions to produce biomass. Subsequently, the microalgae are deprived from all nitrogen sources to induce TAG synthesis (Rodolfi et al., 2009).

Under these conditions, some species can accumulate up to 50% of their dry weight as TAGs (Chisti, 2007; Griffiths & Harrison, 2009; Hu et al., 2008).

The physiological reason for TAG accumulation during nitrogen starvation is twofold. First, the accumulated TAG can serve as a carbon and energy source upon repletion of nitrogen. Second, the production of TAG or other secondary metabolites consumes excess photosynthetic products. When these products are not consumed, over-reduction of the photosynthetic machinery will occur. This in turn results in the formation of reactive oxygen species and ultimately cell damage or death (Asada, 2006; Hu et al., 2008).

When generalized, the TAG productivity is determined by 1) the rate of light absorption, 2) the photosynthetic efficiency, and 3) the proportion of the photosynthetic rate that is used for TAG synthesis (Fig. 1.3).

- 1) The amount of TAG that can be produced is ultimately determined by the amount of light absorbed. Microalgae absorb light using light harvesting pigments. On a cellular level, the amount of light absorbed can vary greatly, but in a photobioreactor, the amount of light absorbed by a microalgal culture is determined by the amount of sunlight that falls onto the surface of the photobioreactor, and on the amount falling through the reactor. The quantification of the amount of light absorbed by the culture is important to evaluate the performance of the culture.
- 2) Absorbed photons are used to liberate electrons from  $H_2O$  to produce  $O_2$  and regenerate NADPH and ATP. This NADPH and ATP are used to fixate  $CO_2$  to  $C_3$  carbon intermediates (photosynthesis). However, not all photons that are absorbed are used for photosynthesis. Part of these photons is thermally dissipated. The ratio between the part that is used for photosynthesis and the part that is thermally dissipated determines the photosynthetic efficiency.
- 3) The photosynthetically produced  $C_3$  carbon intermediates are used as building blocks for the production of various biomass constituents. The ratio in which these biomass constituents are produced is highly variable. During balanced growth conditions, carbon is mostly partitioned towards protein and structural carbohydrates (cell wall) and structural lipids (membranes). During nitrogen starvation, the synthesis of proteins is impaired because nitrogen is required for protein synthesis. Under these conditions, the carbon intermediates are used for the synthesis of secondary metabolites, such as TAG (Fig. 1.3).



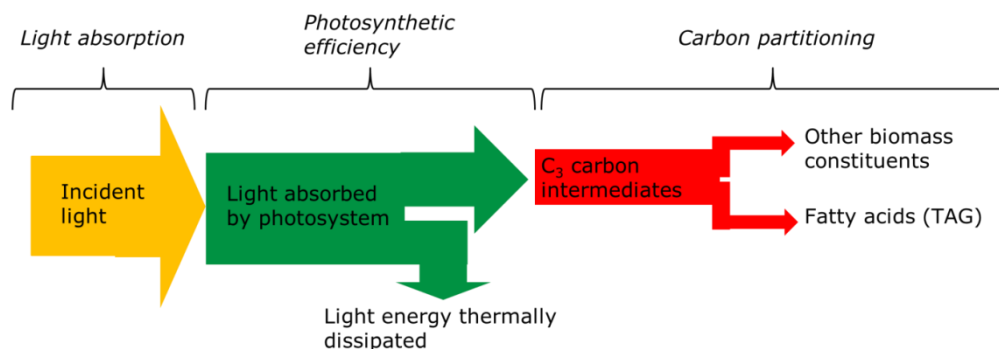


**Fig. 1.3.** Schematic representation of phototrophic TAG production during nitrogen starvation. TAG productivity is the product of the amount of light absorbed, the photosynthetic efficiency, and the fraction of photosynthetic products partitioned towards TAG synthesis. During nitrogen starvation, the synthesis of protein and other nitrogen-containing biomass constituents is impaired. This liberates photosynthetic capacity that is then used for the production of storage metabolites, such as starch and TAG.

For a high TAG productivity, a high photosynthetic efficiency is required and a large part of the photosynthetic capacity should be directed towards TAG synthesis. Unfortunately, the conditions that result in a high photosynthetic efficiency and the conditions under which large amounts of TAG are produced do not coincide (Griffiths & Harrison, 2009). Namely, the photosynthetic efficiency and carbon partitioning towards TAG are oppositely affected by nitrogen starvation. Photosynthesis and carbon partitioning can also be affected by other stress-factors or factors such as light intensity and cultivation conditions such as temperature and pH. Also, large differences exist between microalgae species. A detailed understanding of the physiology behind photosynthesis and carbon partitioning during nitrogen starvation is needed to improve the TAG productivity in microalgae cultures.

At the start of the work presented in this thesis, little was known about the quantitative aspects of photosynthesis and TAG production during nitrogen starvation. Projections of microalgal TAG production that were commonly used, were therefore poorly supported by scientific evidence and were based on erroneous estimations using both maximum photosynthetic efficiencies and maximum TAG contents. This contributed to a large uncertainty in what could be expected from microalgae. To give more accurate projections and to improve TAG production, a better understanding of the microalgal response to nitrogen starvation, that results in TAG production, is needed.

### 1.3 Aim and outline of this thesis

The aim of this thesis is therefore to obtain a quantitative understanding of the physiology of TAG production that is induced by nitrogen starvation. This understanding will be used to improve TAG productivity and to evaluate what can be expected from large-scale microalgae cultivation.

Because a variety of lipid classes are produced by microalgae, in a highly variable ratio, it is important to distinguish between these different lipids. **Chapter 2** therefore presents an analytical method to analyse the fatty acid content and composition in microalgae.

Large differences exist in the response to nitrogen starvation between microalgae species, but clear quantitative data on these differences were lacking. **Chapter 3** therefore compares the response of nine microalgae species, which were selected based on an extensive literature search, to nitrogen starvation in detail. From these microalgae, *Scenedesmus obliquus* was identified as the most promising microalga because of its ability to retain a high photosynthetic efficiency during nitrogen starvation for a long time and its ability to accumulate large quantities of TAG. *S. obliquus* was therefore used in all subsequent research performed for this thesis.

Cultivation conditions can have a large impact on both the photosynthetic efficiency and the carbon partitioning towards TAG. Therefore, **chapter 4** investigates the impact of the incident light intensity, pH, and temperature on the physiological response to nitrogen starvation in *S. obliquus*. It was found that suboptimal pH and temperature negatively affect both the photosynthetic efficiency and the maximum TAG content. The light intensity did not affect the maximum TAG content, but did have a large impact on the photosynthetic efficiency.

In chapters 3 and 4, it was found that under all conditions, and in all species, various other secondary metabolites, such as starch, are produced simultaneously with TAG. This co-product formation reduces the potential TAG productivity. To test if the TAG productivity can be improved if competing pathways are eliminated, **chapter 5** compares the carbon partitioning in the wild-type with the *slm1* starchless mutant of *S. obliquus*. It was found that wild-type *S. obliquus*, initially produces large quantities of starch simultaneously with TAG. This starch is subsequently degraded when nitrogen starvation progresses and likely used as a substrate for TAG synthesis. The starchless mutant of *S. obliquus* immediately partitions all photosynthetic capacity, that is used for starch synthesis in the wild-type, towards TAG synthesis. This improves the TAG yield on light by over 50%.

Insight in the carbon partitioning mechanism could be used to increase carbon partitioning towards TAG. Therefore, the mechanism behind carbon partitioning was investigated in more detail in **chapter 6**. It was investigated how the light intensity during nitrogen starvation and the photoacclimated state at the onset of nitrogen starvation influence the photosynthetic efficiency and carbon partitioning during nitrogen starvation. A novel experimental setup was developed to be able to independently investigate the impact of light intensity during nitrogen starvation and the photoacclimated state.

To investigate how the TAG productivity can be improved, the novel insights from the previous chapters, as well as existing knowledge from scientific literature, were condensed in a mechanistic model that describes photosynthesis and carbon partitioning during nitrogen starvation, as presented in **chapter 7**. This model was used to investigate how reactor design and strain improvement can help to improve TAG productivity. These outcomes were used to project TAG productivities of microalgae using current and future technology.

To evaluate what needs to be done to make microalgal TAG production economically and energetically feasible, **chapter 8** evaluates the outcomes of published life cycle assessment (LCA) studies and techno-economic (TE) studies. The cultivation step is the largest uncertainty in these studies and this propagates into uncertainty in the predicted cost-price and specific energy consumption. To improve the reliability of these studies, better, more realistic combinations of productivities and biochemical compositions were derived for several production scenarios, based on the previous chapters of this thesis. The implications of these new values on the outcomes of TE and LCA studies are discussed.

Altogether, this thesis provides a quantitative understanding of the factors that influence photosynthesis and carbon partitioning during nitrogen starvation. Using these insights, it is illustrated how the TAG productivity could be increased. Estimates for productivities and biochemical composition that can be achieved in a production process were presented. These insights will help to estimate and reduce the cost-price and specific energy consumption for microalgal TAG production. This can ultimately help to enable the replacement of current sources of fossil and vegetable oil.



## **Chapter 2** Analysis of fatty acid content and composition in microalgae

**This chapter has been published as:**

Guido Breuer, Wendy A.C. Evers, Jeroen H. de Vree, Dorinde M. M. Kleinegris, Dirk E. Martens, René H. Wijffels, Packo P. Lamers (2013), Analysis of fatty acid content and composition in microalgae, *Journal of Visualized experiments*, 80:e50628

### **Abstract**

A method to determine the content and composition of total fatty acids present in microalgae is described. Fatty acids are a major constituent of microalgal biomass. These fatty acids can be present in different acyl-lipid classes. Especially the fatty acids present in triacylglycerol (TAG) are of commercial interest, because they can be used for production of transportation fuels, bulk chemicals, nutraceuticals ( $\omega$ -3 fatty acids), and food commodities. To develop commercial applications, reliable analytical methods for quantification of fatty acid content and composition are needed. Microalgae are single cells surrounded by a rigid cell wall. A fatty acid analysis method should provide sufficient cell disruption to liberate all acyl lipids and the extraction procedure used should be able to extract all acyl lipid classes. With the method presented here all fatty acids present in microalgae can be accurately and reproducibly identified and quantified using small amounts of sample (5 mg) independent of their chain length, degree of unsaturation, or the lipid class they are part of. This method does not provide information about the relative abundance of different lipid classes, but can be extended to separate lipid classes from each other. The method is based on a sequence of mechanical cell disruption, solvent based lipid extraction, transesterification of fatty acids to fatty acid methyl esters (FAMES), and quantification and identification of FAMES using gas chromatography (GC-FID). A TAG internal standard (tripentadecanoin) is added prior to the analytical procedure to be able to correct for losses during extraction and incomplete transesterification.

## 2.1 Introduction

Fatty acids are one of the major constituents of microalgal biomass and typically make up between 5 and 50% of the cell dry weight (Breuer et al., 2012; Chisti, 2007; Hu et al., 2008). They are mainly present in the form of glycerolipids. These glycerolipids in turn mainly consist of phospholipids, glycolipids, and triacylglycerol (TAG). Especially the fatty acids present in TAG are of commercial interest, because they can be used as a resource for production of transportation fuels, bulk chemicals, nutraceuticals ( $\omega$ -3 fatty acids), and food commodities (Chisti, 2007; Draaisma et al., 2013; Wijffels & Barbosa, 2010; Wijffels et al., 2010). Microalgae can grow on sea water based cultivation media, can have a much higher areal productivity than terrestrial plants, and can be cultivated in photobioreactors at locations that are unsuitable for agriculture, possibly even offshore. For these reasons microalgae are often considered a promising alternative to terrestrial plants for the production of biodiesel and other bulk products (Chisti, 2007; Draaisma et al., 2013; Wijffels & Barbosa, 2010; Wijffels et al., 2010). Potentially no agricultural land or fresh water (when cultivated in closed photobioreactors or when marine microalgae are used) is needed for their production. Therefore, biofuels derived from microalgae are considered 3<sup>rd</sup> generation biofuels.

The total cellular content of fatty acids (% of dry weight), the lipid class composition, as well as the fatty acid length and degree of saturation are highly variable between microalgae species. Furthermore, these properties vary with cultivation conditions such as nutrient availability, temperature, pH, and light intensity (Breuer et al., 2012; Hu et al., 2008). For example, when exposed to nitrogen starvation, microalgae can accumulate large quantities of TAG. Under optimal growth conditions TAG typically constitutes less than 2% of dry weight, but when exposed to nitrogen starvation TAG content can increase to up to 40% of the microalgal dry weight (Breuer et al., 2012). Microalgae mainly produce fatty acids with chain lengths of 16 and 18 carbon atoms, but some species can make fatty acids of up to 24 carbon atoms in length. Both saturated as well as highly unsaturated fatty acids are produced by microalgae. The latter include fatty acids with nutritional benefits ( $\omega$ -3 fatty acids) like C20:5 (eicosapentaenoic acid; EPA) and C22:6 (docosahexaenoic acid; DHA) for which no vegetable alternatives exist (Breuer et al., 2012; Draaisma et al., 2013; Guschina & Harwood, 2006; Hu et al., 2008). The (distribution of) fatty acid chain length and degree of saturation also determines properties and quality of algae derived biofuels and edible oils (Draaisma et al., 2013; Schenk et al., 2008).

To develop commercial applications of microalgal derived fatty acids, reliable analytical methods for quantification of fatty acid content and composition are needed.

As also pointed out by Ryckebosch et al. (2011), analysis of fatty acids in microalgae distinguishes itself from other substrates (e.g. vegetable oil, food products, animal tissues etc.) because 1) microalgae are single cells surrounded by rigid cell walls, complicating lipid extraction; 2) microalgae contain a wide variety of lipid classes and the lipid class distribution is highly variable (Guschina & Harwood, 2006). These different lipid classes have a wide variety in chemical structure and properties such as polarity. Also, lipid classes other than acyl lipids are produced; 3) microalgae contain a wide variety of fatty acids, ranging from 12 to 24 carbon atoms in length and containing both saturated as well as highly unsaturated fatty acids. Therefore, methods developed to analyze fatty acids in substrates other than microalgae, might not be suitable to analyze fatty acids in microalgae.

As reviewed by Ryckebosch et al. (2011), the main difference between commonly used lipid extraction procedures is in the solvent-systems that are used. Because of the large variety of lipid classes present in microalgae, each varying in polarity, the extracted lipid quantity will vary with solvents used (Grima et al., 1994; Iverson et al., 2001; Laurens et al., 2012). This leads to inconsistencies in lipid content and composition presented in literature (Laurens et al., 2012; Ryckebosch et al., 2011). Depending on the solvent system used, methods based on solvent extraction without cell disruption through, for example, bead beating or sonication, might not extract all lipids because of the rigid structure of some microalgae species (Lee et al., 2010; Ryckebosch et al., 2011). In the case of incomplete lipid extraction, the extraction efficiency of the different lipid classes can vary (Guckert et al., 1988). This can also have an effect on the measured fatty acid composition, because the fatty acid composition is variable among lipid classes (Guschina & Harwood, 2006).

Our method is based on a sequence of mechanical cell disruption, solvent based lipid extraction, transesterification of fatty acids to fatty acid methyl esters (FAMES), and quantification and identification of FAMES using gas chromatography in combination with a flame ionization detector (GC-FID). An internal standard in the form of a triacylglycerol (tripentadecanoin) is added prior to the analytical procedure. Possible losses during extraction and incomplete transesterification can then be corrected for. The method can be used to determine the content as well as the composition of the fatty acids present in microalgal biomass. All fatty acids present in the different acyl-lipid classes, including storage (TAG) as well as membrane lipids (glycolipids, phospholipids), are detected, identified and quantified accurately and reproducibly by this method using only small amounts of sample (5 mg). This method does not provide information about the relative abundance of different lipid classes. However, the method can be extended to separate



lipid classes from each other (Breuer et al., 2012). The concentration and fatty acid composition of the different lipid classes can then be determined individually.

In literature several other methods are described to analyze lipids in microalgae. Some methods focus on total lipophilic components (Pruvost et al., 2009), where other methods focus on total fatty acids (Griffiths et al., 2010; Ryckebosch et al., 2011). These, alternatives include gravimetric determination of total extracted lipids, direct trans-esterification of fatty acids combined with quantification using chromatography, and staining cells with lipophilic fluorescent dyes.

A commonly used alternative to quantification of fatty acids using chromatography is quantification of lipids using a gravimetric determination (Bligh & Dyer, 1959; Folch et al., 1956). Advantages of a gravimetric determination are the lack of requirements for advanced and expensive equipment like a gas chromatograph; ease to set up the procedure, because of the availability of standardized analytical equipment (e.g. Soxhlet); and a gravimetric determination is less time-consuming than chromatography based methods. The major advantage of using chromatography based methods on the other hand is that in such a method only the fatty acids are measured. In a gravimetric determination the non-fatty acid containing lipids, like pigments or steroids, are also included in the determination. These non-fatty acid containing lipids can make up a large proportion (>50%) of total lipids. If one is only interested in the fatty acid content (for example for biodiesel applications), it will be overestimated when a gravimetric determination is used. In addition, in a gravimetric determination the accuracy of the analytical balance used to weigh the extracted lipids determines the sample size that needs to be used. This quantity is typically much more than the amount needed when chromatography is used. Finally, another advantage of using chromatography over gravimetric determination is that chromatography provides information about the fatty acid composition.

Another alternative to our presented method is direct transesterification (Griffiths et al., 2010; Lepage & Roy, 1984; Welch, 1977). In this method lipid extraction and transesterification of fatty acids to FAMES are combined in one step. This method is quicker than a separate extraction and transesterification step, but combining these steps limits the solvents that can be used for extraction. This might negatively influence extraction efficiency. Another advantage of a separate lipid extraction and transesterification step is that it allows for an additional lipid class separation between these steps (Breuer et al., 2012). This is not possible when direct transesterification is used.

Other commonly used methods to determine the lipid content in microalgae include staining the biomass with lipophilic fluorescent stains such as Nile red or BODIPY and measuring the fluorescence signal (Chen et al., 2009; Cooper et al., 2010). An advantage of these methods is that they are less laborious than alternative methods. A disadvantage of these methods is that the fluorescent response is, for various reasons, variable between species, cultivation conditions, lipid classes, and analytical procedures. As an example, several of these variations are caused by differences in uptake of the dye by the microalgae. Calibration using another quantitative method is therefore needed, preferably performed for all the different cultivation conditions and growth stages. Finally, this method does not provide information about the fatty acid composition and is less accurate and reproducible than chromatography based methods. The presented method is based on the method described by Lamers et al. (2010) and Santos et al. (2012) and has also been applied by various other authors (Breuer et al., 2012; Kliphuis et al., 2012; Lamers et al., 2012; Mulders et al., 2013). Also other methods are available that are based on the same principles and could provide similar results (Ryckebosch et al., 2011; Wang & Benning, 2011).

## **2.2 Protocol Text**

### **1) Sample preparation**

**There are two alternate protocols for sample preparation included as steps 1.1 and 1.2. Both methods are equally suitable and give similar results, but if a limited amount of algae culture volume is available, method 1.1 is recommended.**

NOTE: For either protocol, prepare two additional bead beater tubes according to the entire protocol but without adding algae to them to be used as a blank. In this way, peaks in the GC chromatogram resulting from extraction of components from materials used can be identified and quantified.

#### **1.1) Sample preparation protocol option 1: recommended when a limited amount of algae culture is available**

- 1.1.1) Determine the algae dry weight concentration (g/l) in the culture broth, for example as described by Breuer et al. (2012).
- 1.1.2) Transfer a volume of culture broth that contains 5-10 mg algae dry weight to a glass centrifuge tube. Calculate the exact amount of biomass transferred using the biomass concentration determined in step 1.1.1.
- 1.1.3) Centrifuge 5 minutes at 1200g.

1.1.4) Discard part of the supernatant, leave approximately 0.25 mL in the tube

1.1.5) Re-suspend the algae in the remaining supernatant by gentle pipetting the pellet up and down and transfer the complete cell pellet to a bead beater tube using a 200 µl pipet.

1.1.6) Rinse the centrifuge tube and glass pipet with  $\pm 0.15$  mL milliQ water and transfer the liquid to the same bead beater tube.

1.1.7) Centrifuge bead beater tubes for one minute at maximum rpm to make sure no air bubbles remain in the bottom of the tubes. It is possible to store closed bead beater tubes at  $-80^{\circ}\text{C}$ .

1.1.8) Lyophilize the bead beater tubes containing the sample. It is possible to store the closed bead beater tubes at  $-80^{\circ}\text{C}$ .

## **1.2) Sample preparation protocol option 2**

1.2.1) Centrifuge an undetermined volume of algae culture broth and discard supernatant. It is not necessary to determine the biomass concentration or to measure the volume used.

1.2.2) Measure or calculate the osmolarity of the culture medium using the concentration of the main salts present in the culture medium.

1.2.3) Wash the cell pellet by resuspending the cell pellet in the same volume, as used in step 1.2.1, of an ammonium formate solution, which approximates the osmolarity of the culture medium. An equiosmolar ammonium formate solution prevents cell lyses during washing of the cells.

NOTE: Washing the cells is necessary to remove salts present in the culture medium. This is especially important for fatty acid analysis in marine microalgae because of the high salt concentrations in their culture medium. If salts would still be present, this would cause overestimation of the amount of cell dry weight which will be determined later in this protocol. Ammonium formate is used to wash cells because this solution will completely evaporate during lyophilisation and not leave any residue.

1.2.4) Centrifuge algae suspension and discard supernatant.

1.2.5) Lyophilize the cell pellet.

1.2.6) Weigh 5-10 mg lyophilized microalgae powder into a bead beater tube. Record the exact weight that was used.

## **2) Cell disruption and lipid extraction**

NOTE: This section describes an extensive cell disruption procedure. Possibly, some of the cell disruption steps are redundant and less extensive cell disruption might yield the

same results for some microalgae species or for biomass derived from certain cultivation conditions. This would need validation for each specific situation however. Therefore the proposed extensive disruption protocol is recommended as a universal method suitable for all microalgal material.

2.1) Weigh an exact amount of tripentadecanoin (triacylglycerol containing three C15:0 fatty acids) and add it to an exactly known amount of 4:5 (v/v) chloroform:methanol. In this way the concentration of tripentadecanoin is exactly known. Aim for a concentration of 50 mg/l. Tripentadecanoin serves as the internal standard for fatty acid quantification.

2.2) Add 1ml chloroform:methanol 4:5(v/v) containing tripentadecanoin to each beating tube (specified in the reagents and equipment table). Check if there are no beads remaining inside the cap of the beadbeater tube, this will result in leaking of the tubes. Use a positive displacement pipet for accurate addition of solvents.

2.3) Bead beat the bead beater tubes 8 times at 2500rpm for 60 seconds, each time with a 120 second interval between each beating.

2.4) Transfer the solution from the bead beater tubes to a clean heat-resistant 15mL glass centrifuge tube with Teflon insert screw-caps. Be sure to transfer all the beads from the bead beater tube as well.

2.5) To wash the bead beater tube, add 1ml chloroform:methanol 4:5(v/v) containing tripentadecanoin into the bead beater tube, close cap and mix, and transfer this solution to the same glass tube from step 2.4. Wash the tube three times (in total 4 ml of chloroform:methanol 4:5(v/v) containing tripentadecanoin is used per sample – 1mL added in step 2.2 and 3 mL for 3 washing steps).

2.6) Vortex the glass tubes for 5 seconds and sonicate in a sonication bath for 10 minutes.

2.7) Add 2.5ml of MilliQ water, containing 50 mM 2-Amino-2-hydroxymethyl-propane-1,3-diol (Tris) and 1 M NaCl, which is set to pH 7 using a HCl solution. This will cause a phase separation between chloroform and methanol:water. 1M NaCl is used to enhance the equilibrium of lipids towards the chloroform phase.

2.8) Vortex for 5 seconds and then sonicate for 10 minutes.

2.9) Centrifuge for 5 minutes at 1200 g.

2.10) Transfer the entire chloroform phase (bottom phase) to a clean glass tube using a glass Pasteur pipette. Make sure not to transfer any interphase or top phase.

2.11) Re-extract the sample by adding 1ml chloroform to old tube (containing the methanol:water solution).

- 2.12) Vortex for 5 seconds and then sonicate for 10 minutes.
- 2.13) Centrifuge for 5 minutes at 1200 g.
- 2.14) Collect the chloroform phase (bottom phase) using a glass Pasteur pipette and pool with the first chloroform fraction from step 2.10.
- 2.15) If difficulties are experienced in collecting the entire chloroform fraction in the previous step, repeat steps 2.11-2.14. Otherwise proceed with step 2.16.
- 2.16) Evaporate the chloroform from the tube in a nitrogen gas stream. After this step samples can be stored at -20 °C under a nitrogen gas atmosphere.

### **3) Transesterification to fatty acid methyl esters**

- 3.1) Add 3ml methanol containing 5%(v/v) sulfuric acid to the tube containing the dried extracted lipids (tube originally containing the chloroform fraction) and close the tube tightly.
- 3.2) Vortex for 5 seconds.
- 3.3) Incubate samples for 3 hours at 70°C in a block heater or water bath. Periodically (every  $\pm 30$  min) ensure that the samples are not boiling (caused by an improperly closed lid) and vortex tubes. During this reaction fatty acids are methylated to their fatty acid methyl esters (FAMES).
- 3.4) Cool samples to room temperature and add 3ml MilliQ water and 3ml n-hexane.
- 3.5) Vortex for 5 seconds and mix for 15 minutes with a test tube rotator.
- 3.6) Centrifuge for 5 minutes at 1200 g.
- 3.7) Collect 2ml of the hexane (top) phase and put in fresh glass tube using a glass Pasteur pipette.
- 3.8) Add 2ml MilliQ water to the collected hexane phase to wash it.
- 3.9) Vortex for 5 seconds and centrifuge for 5 minutes at 1200 g. After this step it is possible to store the samples at -20 °C under nitrogen gas atmosphere (phase separation not necessary).

### **4) Quantification of FAMES using gas chromatography**

- 4.1) Fill GC vials with the hexane phase (upper phase) using a glass Pasteur pipette.
- 4.2) Place the caps on the GC vials. Make sure the caps are completely sealed, and cannot be turned, to prevent evaporation from the vial.
- 4.3) Refill the GC wash solvents (hexane), empty the waste vials, and put sample vials in auto-sampler. Before running the actual samples on the GC, first run 2 blanks containing only hexane on the GC.

4.4) Run the samples on a GC-FID with a Nukol column (30m x 0.53mm x 1.0 $\mu$ m). Use inlet temperature of 250°C and use helium as carrier gas, pressure of 81.7 kPa and split ratio of 0.1:1, total flow rate: 20 mL/min. FID detector temperature of 270°C with H<sub>2</sub> flow rate of 40 ml/min, air flow rate of 400 ml/min and He flow rate of 9.3 ml/min. Set injection volume to 1 $\mu$ l/sample. Pre and post wash injector with n-hexane. Initial oven temperature is set to 90°C for 0.5 min and then raised with 20°C/min until an oven temperature of 200°C is reached. Oven temperature is then maintained at 200°C for 39 minutes. Total run time is 45 minutes.

### 2.3 Representative Results

A typical chromatogram that is obtained via this process is shown in Fig. 2.1. FAMES are separated by size and degree of saturation by the GC column and protocol used. Shorter chain length fatty acids and more saturated fatty acids (less double bonds) have shorter retention times. The used GC column and protocol do not intend to separate fatty acid isomers (same chain length and degree of saturation, but different positions of double bonds), but this could be achieved by using a different GC column and protocol.

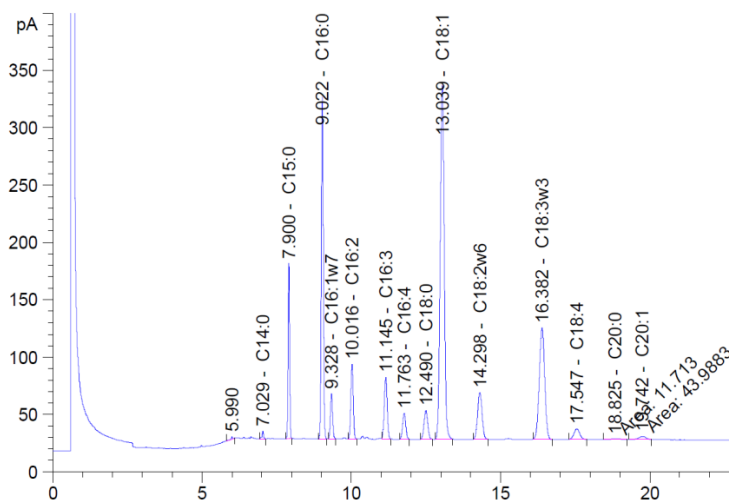


**Fig. 2.1:** Representative GC-FID chromatogram. A sample derived from *Scenedesmus obliquus* exposed to nitrogen starvation was used. Only the first 20 minutes of the chromatogram are shown. After 20 minutes no peaks were detected in this sample.

The fatty acid concentration and composition can be calculated using the area of the GC peaks, internal standard concentration (mg/l) (step 2.1), and the amount of biomass

added to the sample (mg) (step 1.1.2 or 1.2.6, depending on which sample preparation protocol was chosen).

The content of each individual fatty acid in the biomass (mg fatty acid/g dry weight) can be determined by

$$FA \text{ content } \left( \frac{mg}{g} \right) = \frac{IS \text{ added } \left( \frac{mg}{sample} \right) \cdot \frac{Area \text{ of individual FAME}}{Area \text{ of C15:0 FAME} \cdot Rel. Resp. Factor individual FAME}}{amount \text{ of biomass added in step 1.1.1 or 1.2.6 (g)}}$$

With Area of individual FAME as determined by integration of the GC chromatogram (Fig. 2.1); Area of C15:0 FAME as determined by integration of the GC chromatogram (Fig. 2.1);

$$IS \text{ added } \left( \frac{mg}{sample} \right) = 4 \text{ (ml)} \cdot [IS] \cdot \frac{3 \cdot MW_{C15:0 FA}}{MW_{C15:0 TAG}}$$

With [IS] the concentration of tripentadecanoin in the chloroform:methanol solution as determined in step 2.1;  $MW_{C15:0 FA}$  the molecular weight of the C15:0 fatty acid (242.4 g/mol);  $MW_{C15:0 TAG}$  the molecular weight of tripentadecanoin (765.24 g/mol);

*Rel. Resp. Factor individual FAME*

$$= \frac{[C15:0 FAME \text{ in calibration solution}]}{[individual FAME \text{ in calibration solution}]} \cdot \frac{Area \text{ of individual FAME in calibration curve}}{Area \text{ of C15:0 FAME in calibration curve}}$$

As determined by running calibration solutions on the GC, constituting out of mixtures of C15:0 FAME and FAMES of all individual fatty acids expected in the sample, with [C15:0 FAME in calibration solution] the concentration of C15:0 FAME in the calibration solution (mg/l); [individual FAME in calibration solution] the concentration of the individual FAME in the calibration solution (mg/l); and the areas as determined by integration of the GC chromatogram of the calibration solution.

The total fatty acid content can be calculated as the sum of all individual fatty acids. The relative abundance of each fatty acid can be calculated by dividing the concentration of each individual fatty acid by the total fatty acid content.

The fatty acid composition and content of *Scenedesmus obliquus* UTEX393

(Chlorophyceae) under both nitrogen replete and deplete conditions is shown in Fig. 2.2.

Fatty acid composition and content are highly affected by nitrogen starvation. In *S.*

*obliquus*, C16:0 (palmitic acid) and C18:1 (oleic acid) are the two most abundant fatty acids.

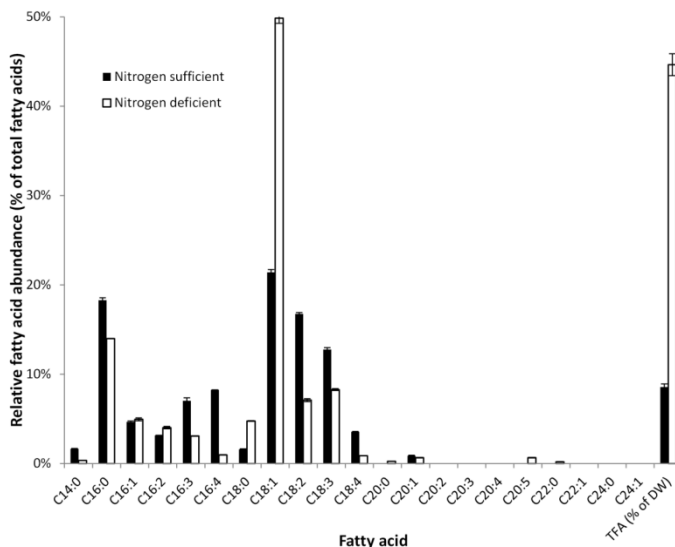


**Fig. 2.2:** Fatty acid composition (relative abundance of fatty acids) of *Scenedesmus obliquus* (Chlorophyceae) under both nitrogen sufficient (black bars) and nitrogen deprived cultivation conditions (white bars). The total fatty acid contents were  $8.6 \pm 0.5\%$  and  $44.7 \pm 1.7\%$  (% of dry weight) under nitrogen sufficient and nitrogen deprived cultivation conditions, respectively. Error bars indicate the highest and lowest value of two analytical replicates.

The fatty acid composition and content of *Phaeodactylum tricornutum* UTEX640 (diatom) under both nitrogen replete and deplete conditions are shown in Fig. 2.3. Similar to *S. obliquus*, the fatty acid content and composition are highly affected by nitrogen starvation. *P. tricornutum* also produces substantial amounts of highly unsaturated fatty acids such as C20:5 (eicosapentaenoic acid, EPA) as well as very long chain fatty acids (lignoceric acid, C24:0) that can be detected by this method.



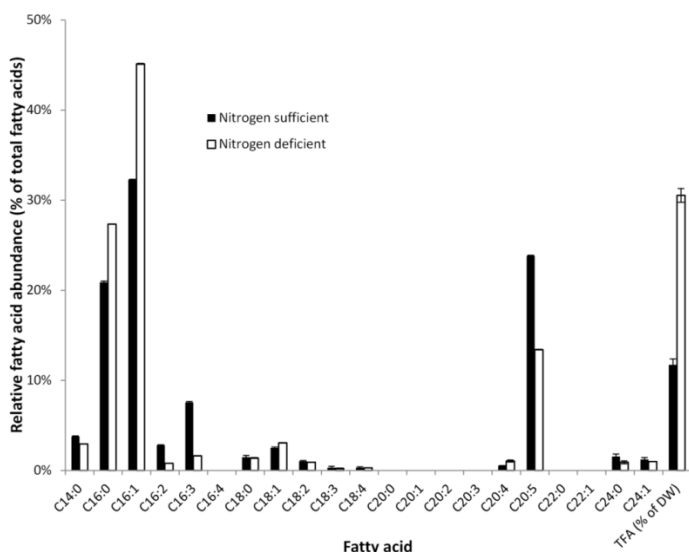


**Fig. 2.3:** Fatty acid composition (relative abundance of fatty acids) of *Phaeodactylum tricornutum* (diatom) under both nitrogen sufficient (black bars) and nitrogen deprived cultivation conditions (white bars). The total fatty acid contents were  $11.7 \pm 0.9\%$  and  $30.5 \pm 1.1\%$  (% of dry weight) under nitrogen sufficient and nitrogen deprived cultivation conditions, respectively. Error bars indicate the highest and lowest value of two analytical replicates.

## 2.4 Discussion

The described method can be used to determine the content as well as the composition of total fatty acids present in microalgal biomass. Fatty acids derived from all lipid classes, including storage (TAG) as well as membrane lipids (phospholipids and glycolipids), are detected. All fatty acid chain lengths and degrees of saturation that are present in the microalgae can be detected and distinguished. The method is based on mechanical cell disruption, solvent based lipid extraction, transesterification of fatty acids to FAMES, and quantification of FAMES using gas chromatography in combination with a flame ionization detector (GC-FID). This method requires small amounts of sample (5 mg), is accurate and reproducible and can be used among a wide variety of microalgae species. This method is intended to be used for analytical purposes and is specifically tailored for using small sample sizes. The method is not intended to be scaled-up and used for extracting large quantities of microalgal fatty acids. A limitation of this method is that it is laborious and it can take a few days from starting the procedure to obtaining results. Especially in the case of process monitoring for industrial microalgal fatty acid production this might be considered a limitation. If faster results are required, other options such as staining with lipophilic fluorescent dyes might be

more suitable. The following recommendations are made with regard to performing the analytical procedure:

1. Extraction and transesterification procedure are standardized by using a triacylglycerol (tripentadecanoin) as an internal standard. The use of an internal standard is commonly used for quantification of FAMES in samples using gas-chromatography, but most often a FAME internal standard is used. It is recommended to use a TAG internal standard rather than a FAME internal standard and to add it before cell disruption and solvent extraction. Possible losses during lipid extraction or incomplete transesterification can then be corrected for, since it is expected that similar losses would occur to the internal standard. An internal standard should be used that does not co-elute with fatty acids produced by microalgae. Because microalgae only produce fatty acids with even carbon numbers, a TAG containing a fatty acid with an odd number of carbon atoms is a good candidate. Because the GC column and protocol not only separate on chain length but also on degree of unsaturation, a saturated odd numbered fatty acid could hypothetically co-elute with an unsaturated even numbered fatty acid. It should be validated that the used internal standard does not co-elute with fatty acids naturally present in the sample. In our experience with various microalgae, tripentadecanoin (TAG containing three C15:0 fatty acids) does not co-elute with fatty acids naturally present in microalgae.
2. Saturated and highly unsaturated fatty acids give different GC-FID responses (peak areas) at identical concentrations. Therefore standards of FAMES should be used for calibration and determination of relative response factors of individual fatty acids as described in the representative results section. Standards of FAMES can also be used to determine retention times of individual fatty acids. Alternatively, GC-MS can be used for fatty acid identification.
3. Both the retention time and relative response factor of individual fatty acids will change with GC equipment age. Frequent calibration of retention time and relative response factor is therefore recommended.
4. Mechanical cell disruption is an important step in this method. It is realized by a combination of lyophilisation, bead beating and sonication. Without cell disruption it is possible that not all lipids are extracted (Lee et al., 2010; Ryckebosch et al., 2011). Possibly, some of the cell disruption steps are redundant and less extensive cell disruption (for example shorter bead beating

times) might yield the same results for some microalgae species or for biomass derived from certain cultivation conditions. This would need validation for each specific situation however, therefore the proposed extensive disruption protocol is recommended.

5. During the analytical procedure, the solvents used might extract components from the plastic tubes and pipette tips used. These extracted components might interfere with detection of the FAMES using GC-FID. Especially, long bead-beat times and high temperature during bead-beating will result in contaminating components. Our experience is that components extracted from the bead-beat tubes will result in a few additional peaks in the GC-FID chromatogram, some of which overlay with algae derived FAMES (mainly the saturated fatty acids). When the method is executed as proposed, this is never more than 1-2% of the total peak area. Cooling of the bead-beater tubes during bead-beating and using larger amounts of biomass per sample will reduce the relative peak area of these plastic derived peaks. It is recommended to use glass pipettes and glass tubes as much as possible throughout the protocol. Furthermore, the use of blanks to check and correct for the components extracted from plastics, but also to check and correct for contaminations in for example the used solvents, is recommended.
6. During the bead-beating process, both the bead-beater and the bead-beater tubes will heat up. When bead-beating for a much longer time or much higher rpm than proposed in this method, and when no cooling is applied in between, this can result in boiling of the solvents and eventually rupture of the tubes. This will result in a loss of sample. In our experience, this situation occurs when bead-beating for more than 6 minutes at 6000 rpm.
7. Microalgae can produce highly unsaturated fatty acids, which can be prone to oxidation. Ryckebosch et al. (Ryckebosch et al., 2011) observed no change in fatty acid composition caused by oxidation of unsaturated fatty acids during various extraction procedures. It was proposed that antioxidants naturally occurring in microalgae protect these unsaturated fatty acids from oxidation. If it is suspected that oxidation might occur, a possibility would be to add a synthetic antioxidant such as butylhydroxytoluene (BHT) as long as the antioxidant does not co-elute with FAMES, and as long as the amount of antioxidant used does not interfere with the chromatography (Ryckebosch et al.,

2011). To prevent oxidation during long term storage, it is recommended to store samples at -80°C under a nitrogen gas atmosphere.

8. Lipases present in microalgae can potentially hydrolyze lipids during the analytical procedure and therefore affect the results. Ryckebosch et al. (2011) found that lyophilisation inactivates lipases. Moreover, lipases do not degrade fatty acids, but just detach them from the glycerol group of glycerolipids. Hence, lipase activity should not interfere with the presented fatty acid protocol. Enzymes involved in fatty acid degradation act on Coenzyme A activated fatty acids and the occurrence of such degradation during the extraction thus does not seem likely. Nevertheless, in case it is suspected that enzymatic breakdown of fatty acids from glycerolipids might affect results, a possibility would be to add a lipase inhibitor, such as isopropanol, as long as the inhibitor does not interfere with the analytical procedure itself (Ryckebosch et al., 2011).

This method could be extended to quantify and determine the fatty acid composition of neutral lipids (TAG) and polar lipids (phospholipids, glycolipids) by using a solid phase extraction (SPE) separation step between step 2 (lipid extraction) and step 3 (transesterification) as described by for example Breuer et al. (2012). Alternatively, a Thin Layer Chromatography (TLC) step can be used to separate various polar lipid classes, for example as described by Wang and Benning (2011).

This method could be extended to be used in, for example, plants, animal tissues and other micro-organisms. Because of the emphasis on cell disruption, this method is mainly suitable for analysis of fatty acids in materials that are very difficult to extract. The extraction part of the method (steps 1 and 2) could be used for extraction of pigments and other lipophilic components (Lamers et al., 2010; Mulders et al., 2013). The cell disruption procedure could be used for extraction of other components such as starch or carbohydrates by using other solvent systems (including water).

### **Acknowledgments**

A part of this work was financially supported by the Institute for the Promotion of Innovation by Science and Technology—Strategic Basic Research (IWT-SBO) project Sunlight and Biosolar cells. Erik Bolder and BackKim Nguyen are acknowledged for their contribution to the optimization of the bead beating procedure.





## **Chapter 3**    The impact of nitrogen starvation on the dynamics of triacylglycerol accumulation in nine microalgae strains

**This chapter has been published as:**

Guido Breuer, Packo P. Lamers, Dirk E. Martens, René B. Draaisma, René H. Wijffels (2012), The impact of nitrogen starvation on the dynamics of triacylglycerol accumulation in nine microalgae strains, *Bioresource Technology* 124, 217-226

### **Abstract**

Microalgae-derived lipids are an alternative to vegetable and fossil oils, but lipid content and quality vary among microalgae strains. Selection of a suitable strain for lipid production is therefore of paramount importance. Based on published results for 96 species, nine strains were selected to study their biomass, total fatty acid, and triacylglycerol (TAG) production under nitrogen-sufficient and deficient cultivation conditions. Under nitrogen-deficient conditions, *Chlorella vulgaris*, *Chlorella zofingiensis*, *Neochloris oleoabundans*, and *Scenedesmus obliquus*, accumulated more than 35% of their dry weight as TAGs. Palmitic and oleic acid were the major fatty acids produced. The main difference between these strains was the amount of biomass that was produced (3.0 to 7.8-fold increase in dry weight) and the duration that the biomass productivity was retained (2 to 7 days) after nitrogen depletion. *Scenedesmus obliquus* (UTEX 393) and *Chlorella zofingiensis* (UTEX B32) showed the highest average TAG productivity (322 and 243 mg l<sup>-1</sup> day<sup>-1</sup>).



### 3.1 Introduction

Microalgae-derived lipids are considered as an alternative to lipids derived from terrestrial plants because of their much higher areal productivity (Chisti, 2007). Microalgae can be cultivated on non-arable land and, when cultivated in closed photobioreactors, require less fresh water than terrestrial plants. Furthermore, production is not seasonally limited and microalgae can be harvested daily (Gouveia & Oliveira, 2008). In addition to their use in biofuels, microalgal lipids could also be used as feedstock for food (bulk edible oils and/or nutraceuticals), fish feed, and chemicals (Wijffels & Barbosa, 2010).

Many lipid classes are produced by microalgae, but triacylglycerols (TAGs) are considered the preferred lipid class for most applications. Bulk edible oils are composed of TAGs and TAGs are also preferred for biodiesel production, because of their high content (%w/w) of fatty acids (glycerol backbone with three fatty acids) and the absence of other chemical constituents besides glycerol, in contrast to, for example, phospholipids or glycolipids. Many microalgal strains have the ability to accumulate large quantities of lipids in the form of TAGs under environmental stress conditions such as nitrogen starvation (Hu et al., 2008). TAGs serve as energy and carbon storage compounds and as an electron sink in situations where the electron supply provided by photosynthesis exceeds the requirements for growth (Hu et al., 2008).

Large scale production of microalgae-derived lipids is currently uneconomical as costs exceed those for the production of vegetable oils (Ratledge & Cohen, 2008). However, the costs could be reduced several fold by improving process design and operation, for example by improving irradiation conditions, photosynthetic efficiency, and reducing the costs for nutrient usage (Norsker et al., 2011; Wijffels & Barbosa, 2010). Other important factors are lipid content, productivity, and lipid composition of the microalgal strains (Griffiths & Harrison, 2009). To develop a competitive production process, selection of a suitable microalgal strain is therefore of paramount importance.

Studies to identify promising oleaginous microalgal strains have already been done (Gouveia & Oliveira, 2008; Griffiths & Harrison, 2009; Huerlimann et al., 2010; Rodolfi et al., 2009; Sheehan et al., 1998) but different experimental conditions were applied resulting in large variations in performance and observed optima, making it difficult to compare the studies with each other. Furthermore, it was not always confirmed that optimal accumulation had been achieved and valuable information on TAG content and

composition as well as the dynamics of TAG or lipid accumulation were not always provided.

The aim of the present study was to compare the impact of nitrogen starvation on the dynamics of TAG accumulation in different promising oleaginous microalgal strains. Knowledge about the dynamics of TAG accumulation during nitrogen starvation and the differences that exist between strains could direct the selection of suitable strains for large scale TAG production. The ideal microalgal strain should be able to simultaneously accumulate large amounts of TAG and maintain substantial biomass productivity. Nine promising microalgal strains were selected on the basis of a literature survey among 96 microalgal species for TAG and fatty acid production. Selection criteria included lipid and TAG content under both nutrient-sufficient and deficient conditions, volumetric lipid and biomass productivity, and growth characteristics. In these nine strains, TAG accumulation was investigated in batch cultures under both nitrogen-sufficient (control) and deficient conditions as a function of time for up to two weeks after nitrogen depletion. It was confirmed that this was sufficiently long to study the dynamics of TAG accumulation. Nitrogen starvation was accomplished by centrifugation of the biomass and re-suspension in medium lacking a nitrogen source. In this way, it was possible to identify four promising strains that were able to accumulate more than 35% TAG (% of dry weight).

### 3.2 Material and Methods

#### 3.2.1 Strains, growth medium and pre-cultivation conditions

Freshwater microalgal strains *Chlorella vulgaris* UTEX 259, *Chlorella zofingiensis* UTEX B32, *Nannochloris* sp. UTEX 1999, *Neochloris oleoabundans* UTEX 1185 and *Scenedesmus obliquus* UTEX 393 as well as marine strains *Dunaliella tertiolecta* UTEX LB 999, *Isochrysis aff. galbana* UTEX LB 2307, *Phaeodactylum tricornutum* UTEX 640 and *Porphyridium cruentum* UTEX 161 were obtained from the University of Texas Culture Collection of Algae (UTEX). Prior to the experiments, cultures were maintained in shake flasks at 25°C, 40  $\mu\text{mol m}^{-2} \text{s}^{-1}$  incident light intensity in a 16:8 hour light/dark cycle. For culture maintenance, atmospheric air not enriched in CO<sub>2</sub> was used. Flasks were placed in incubators and orbitally shaken at 120 rpm.

Culture media for the freshwater and marine strains consisted out of (in mM, unless stated otherwise): NaCl 0 (freshwater), 450 (marine); KNO<sub>3</sub> 16.8 (pre-cultivation medium), 33.6 (N+ medium), 0 (N- medium); KCl 0 (pre-cultivation medium and N+

medium), 33.6 (N- medium); Na<sub>2</sub>SO<sub>4</sub> 0.7 (freshwater), 3.5 (marine); 2-[4-(2-hydroxyethyl)piperazin-1-yl]ethanesulfonic acid (HEPES) 100; MgSO<sub>4</sub>·7H<sub>2</sub>O 1 (freshwater), 5 (marine); CaCl<sub>2</sub>·2H<sub>2</sub>O 0.5 (freshwater), 2.5 (marine); K<sub>2</sub>HPO<sub>4</sub> 2.5; NaHCO<sub>3</sub> 10; NaFeEDTA 28 µM; Na<sub>2</sub>EDTA·2H<sub>2</sub>O 80 µM, MnCl<sub>2</sub>·4H<sub>2</sub>O 19 µM, ZnSO<sub>4</sub>·7H<sub>2</sub>O 4 µM, CoCl<sub>2</sub>·6H<sub>2</sub>O 1.2 µM, CuSO<sub>4</sub>·5H<sub>2</sub>O 1.3 µM, Na<sub>2</sub>MoO<sub>4</sub>·2H<sub>2</sub>O 0.1 µM; Biotin 0.1 µM, vitamin B1 3.7 µM, vitamin B12 0.1 µM. The pH was adjusted with NaOH to pH 7.0 for the freshwater and pH 7.5 for the marine media. The high buffer capacity of the medium ensured that the change in pH value was never more than 0.6 pH units in nitrogen-sufficient cultures, and that the pH did not change in nitrogen-deficient cultures.

### 3.2.2 Batch TAG accumulation

Algae were inoculated in 250-ml glass Erlenmeyer flasks (100 ml liquid volume) at an OD<sub>750nm</sub> of 0.2. An average incident light intensity of 150 µmol m<sup>-2</sup> s<sup>-1</sup> was provided by GroLux fluorescent tubes (Sylvania F36W/GRO) and cultures were continuously illuminated. Air enriched with 5% CO<sub>2</sub> was provided to the incubator head space to ensure CO<sub>2</sub> sufficiency. Flasks were placed in an orbitally shaking incubator (120 rpm) at 25°C. Cultures were first grown under nitrogen-sufficient conditions until the biomass concentration reached 1 to 1.5 g/l. Subsequently, duplicate flasks were pooled to ensure an equal initial biomass composition between duplicate experiments and culture broth was divided in an N-sufficient (N+) control pool and an N-deficient (N-) pool. Both pools were centrifuged for 5 minutes at 400-600 x g after which the pellet was washed once with the same volume of medium containing 33.6 mM KNO<sub>3</sub> (N+) or equimolar KCl (N-). Subsequently, the pellet was re-suspended in the same volume of either N+ or N-medium. Due to their high viscosity, the cell suspensions of *P. cruentum* were diluted twice with the corresponding medium before centrifugation and then centrifuged at 2400 x g to ensure pellet formation. The moment of re-suspension was considered the start of cultivation and is referred to as t=0. Subsequently, cultures were cultivated for 13 to 14 days under the abovementioned conditions. Samples were always taken around the same time (morning). Both N+ and N- experiments were performed in duplicate.

### 3.2.3 Determination of dry weight concentration

Dry weight concentration was determined as described by Lamers et al. (2010). For the freshwater algae, 0.2 µm filtered demineralised water and for marine algae 35 g/l 0.2 µm filtered ammonium formate solution were used as washing buffers.

### 3.2.4 Fatty acid analysis

Fatty acid extraction and quantification were performed as described by Lamers et al. (2010) and Santos et al. (2012), with the exception that the cell pellets were immediately transferred to bead-beating tubes after centrifugation and freeze dried before analysis. A 30-min bead-beating time was used. The method is based on extraction of lipids in chloroform:methanol, followed by methylation of fatty acids to their methyl esters (FAMES) and quantification of FAMES using gas chromatography, as described in detail by Lamers et al. (2010) and Santos et al. (2012). Tripentadecanoin was used as an internal standard for fatty acid quantification. Total fatty acid concentration was calculated as the sum of all individual fatty acids.

### 3.2.5 Triacylglycerol analysis

Total lipids were extracted as described in section 3.2.4 and dissolved in 0.5 ml hexane. TAGs were purified from this mixture using an SPE silica gel cartridge (Waters; product number 186004617). The cartridge was pre-washed with 6 ml hexane and subsequently the sample was loaded onto the cartridge. TAGs were eluted using 10 ml 87:13 (%v/v) hexane:diethylether. TAG content in the undiluted eluent was quantified using gas chromatography (Fisons instruments GC-8610 with FID detector; column: Varian CP-Sil-5 low bleed (CB-MS) (CP7858), 10 m \* 0.32 mm ID, DF=0.12µm (COL-GC-265); carrier gas: H<sub>2</sub>; column pressure: 30 kPa ~3.7 ml/min (constant flow); FID pressures H<sub>2</sub>: 50 kPa, air: 100 kPa, make-up N<sub>2</sub>: 80-100 ml/min; temperature profile: 80°C (2 min), 10°C /min, 360°C (5 min); detector temp: FID 370°C; injector volume: 1.0 µl). Tripentadecanoin was used as an internal standard and TAG concentration was calculated using the area of the internal standard.

TAG fatty acid composition was determined by evaporation of all solvents in the eluent followed by methylation of the residue and quantification of FAMES using gas chromatography, as described in section 3.2.4.

### 3.2.6 Calculations

The average volumetric productivity (mg l<sup>-1</sup> day<sup>-1</sup>) was calculated by dividing the amount of product per culture volume formed during cultivation (i.e. biomass, total fatty acids, or TAG), by the cultivation time.

$$\text{Average productivity}_i = \frac{c_i(t_{end}) - c_i(t_0)}{t_{end} - t_0} \quad \text{Eq. 1}$$

The maximum volumetric productivity ( $\text{mg l}^{-1} \text{ day}^{-1}$ ) during the cultivation was calculated as the highest productivity observed between two consecutive sample points.

$$\text{Max. prod} = \max_j \left[ \frac{c_i(t_{j+1}) - c_i(t_j)}{t_{j+1} - t_j} \right] \quad \text{Eq. 2}$$

With  $c_i$  the concentration of component  $i$  ( $\text{mg/l}$ ), in which  $i$  represents either the dry weight, fatty acid or TAG concentration, and  $t$  the time (days).

To determine whether the increase in biomass can completely be explained by accumulation of fatty acids, the content of other major constituents was estimated. In terms of significant contribution to the cell mass, the biomass dry weight was assumed to be the sum of protein, lipids, and carbohydrates. The lipid fraction was measured analytically as described in section 3.2.4, the protein fraction was calculated using a mass balance over nitrogen, and the carbohydrate fraction was assumed to be the remaining biomass. Other nitrogen containing constituents, for example chlorophyll and nucleic acids, were lumped into the protein fraction.

Although protein turnover might occur, it was assumed that the net volumetric protein content remained constant during N-deficient cultivation at the value present at the start of nitrogen depletion ( $\text{g/l}$ ) and that there is no net release of nitrogen to the culture medium (Eq. 3). The protein content per gram dry weight during N-deficient cultivation was calculated by dividing the volumetric protein content by the dry weight concentration ( $\text{g/l}$ ). In the situation where release of nitrogen would occur, the assumptions would lead to an overestimation of the protein fraction and an underestimation of the remaining carbohydrate fraction. The initial volumetric protein content was estimated by multiplying the initial biomass concentration by the average protein content of functional biomass (i.e. biomass with a composition of non-stressed cells). The average protein content of functional biomass was estimated by dividing the average nitrogen content of functional biomass ( $0.09 \text{ g/g}$ ) by an assumed average nitrogen content in protein ( $0.16 \text{ g/g}$ ), resulting in an initial protein content of  $0.5625 \text{ g/g}$  (Eq. 3).

$$\text{Protein content}_t = \frac{X_{t=0} \frac{0.09}{0.16}}{X_t} \quad \text{Eq. 3}$$

Where  $X_{t=0}$  and  $X_t$  represent the biomass concentrations (g dry weight  $l^{-1}$ ) at the start of nitrogen depletion and at time  $t$ , respectively.

The total fatty acid (lipid) fraction was measured analytically as described in section 3.2.4, and is therefore not affected by our assumptions. Carbohydrate content is calculated by subtracting protein and lipid content from the total biomass fraction (Eq. 4).

$$\text{CHO content}_t = 1 - \text{Protein content}_t - \text{Lipid content}_t \quad \text{Eq. 4}$$

### 3.3 Results and discussion

#### 3.3.1 Literature survey

Ninety-six microalgal species belonging to seven different taxa, and including fresh water and marine strains were included in a literature survey to identify promising photoautotrophic TAG producing microalgae. The outcomes of this literature survey can be found in Supplementary data 2 of the online published version of this chapter (Breuer et al., 2012). Selection criteria for promising strains included lipid and TAG content under both nutrient-sufficient and deficient conditions, growth characteristics, and volumetric lipid and biomass productivity. Out of these 96 species, 21 species were considered promising for TAG production because they showed (i) a high lipid content, (ii) a considerable increase in lipid content upon nutrient starvation, (iii) a high lipid productivity, and/or (iv) a large TAG fraction of total lipids.

As pointed out by (Griffiths & Harrison, 2009), it is difficult to select a promising strain for TAG production solely based on a literature review due to differences in methods and information provided; therefore nine strains were selected for further studies.

#### 3.3.2 Dry weight concentration, total fatty acid and TAG content

Biomass concentration and total fatty acid content under both N-sufficient and deficient cultivation of the chlorophyte *S. obliquus* UTEX 393 and the diatom *P. tricornutum* UTEX 640 as a function of time are shown as an example (Fig. 3.1). These examples were chosen because these strains are widely studied for lipid accumulation. In addition, *S.*

*obliquus* was chosen because it showed the highest volumetric fatty acid and TAG productivity. The time courses for the other seven strains are provided in Appendix A.

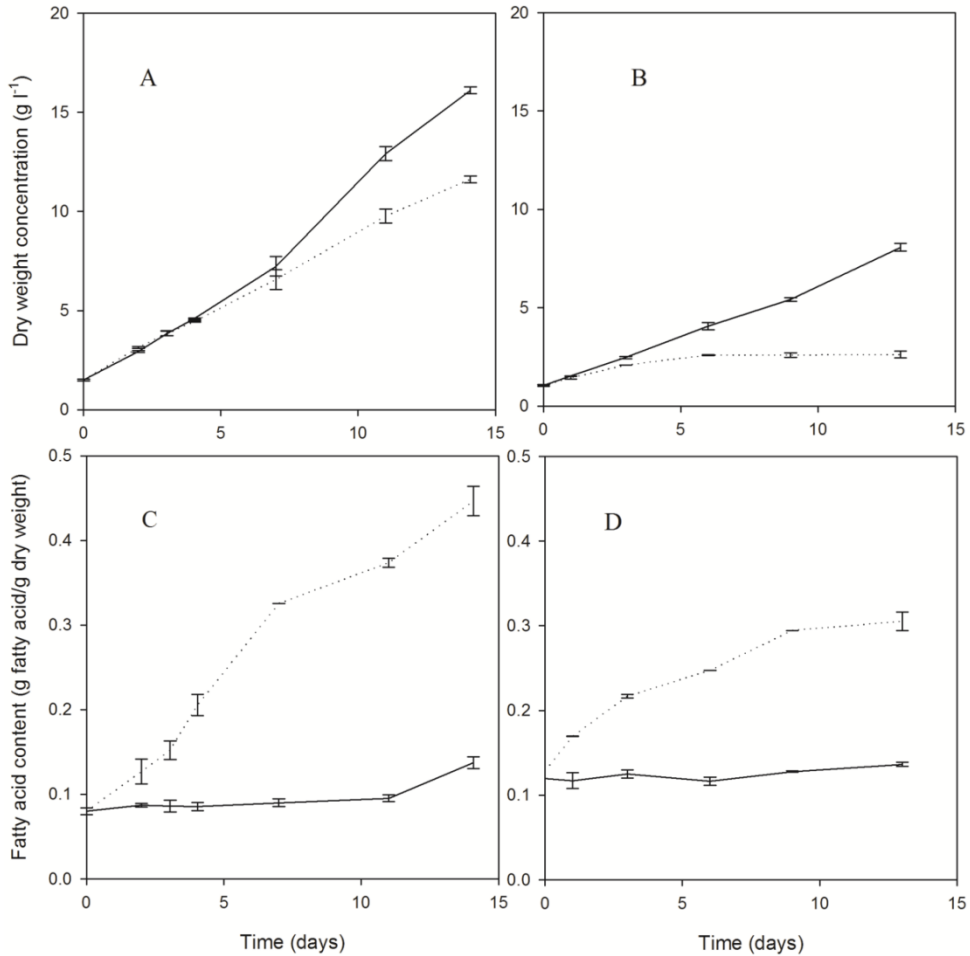


**Fig. 3.1.** Biomass concentration (a,b) and total fatty acid content (c,d) in *S. obliquus* (a,c) and *P. tricornutum* (b,d) under nitrogen-sufficient (solid lines) and deficient conditions (dotted lines). Average values of duplicate culture replicates are shown. Error bars indicate the deviation of both cultures from the average.

N-sufficient experiments were started with a  $\text{KNO}_3$  concentration of 33.6 mM. This was sufficient for the formation of an additional 5.3 g/l biomass with a nitrogen content of 9% (w/w). Most N-sufficient cultures eventually achieved biomass concentrations exceeding this concentration and thus experienced nitrogen limitation at the end of the

experiments. Although these data-points are shown in Fig. 3.1 and Appendix A, they were not used for calculations.

In all cultures, dry weight concentrations increased under both N-sufficient and deficient conditions (Fig. 3.1 and Appendix A). The fold increase in dry weight concentrations in N-starved cultures varied greatly among strains (Fig. 3.2a), but it was always smaller than the fold increase in N-sufficient cultures (Fig. 3.1 and Appendix A). The smallest increase in biomass concentration was observed for *I. galbana* and *Nannochloris* sp., which increased  $1.4 \pm 0.1$  and  $2.2 \pm 0.1$  fold in biomass concentration upon nitrogen starvation, respectively. The largest increase was observed for *S. obliquus* and *C. zofingiensis*. The biomass concentration of these strains increased  $7.8 \pm 0.3$  and  $6.8 \pm 0.2$  fold, respectively, upon nitrogen starvation. The ability to increase in biomass concentration during initial nitrogen starvation is commonly observed for many microalgal strains (da Silva et al., 2009; Guarnieri et al., 2011; Li et al., 2008; Lv et al., 2010; Msanne et al., 2012; Packer et al., 2011; Pal et al., 2011; Pruvost et al., 2009; Pruvost et al., 2011). Such an increase in biomass concentration could be explained by accumulation of storage compounds such as TAG (da Silva et al., 2009; Msanne et al., 2012; Pal et al., 2011).

For all strains except *I. galbana*, the volumetric biomass productivities ( $\text{mg l}^{-1} \text{ day}^{-1}$ ) for the N-deficient cultivations were similar to those of the N-sufficient cultivations for a certain period of time. Thereafter, the productivities of N-deficient cultures became smaller than those of N-sufficient cultures. The duration of this period was highly strain-specific and varied between one day to a maximum of seven days (Fig. 3.1 and Appendix A). The similar biomass productivities indicate that photosynthetic or carbon fixation rates ( $\text{mg C mg}^{-1} \text{ biomass day}^{-1}$ ) were maintained during early nitrogen starvation. Some strains can maintain these rates longer than others. During this initial period, biomass dry weight concentration could increase up to 4.5-fold (*S. obliquus*). Similar biomass productivities during initial N-deficient and sufficient growth were also observed by Guarnieri et al. (2011) for *C. vulgaris*. After the initial period of similar productivities, biomass productivities decreased in N-deficient cultures compared to N-sufficient cultures and were eventually completely halted, except for *S. obliquus* and *C. zofingiensis*. These two strains still showed an increasing dry weight concentration at the end of the experiment, suggesting that an even larger increase in dry weight concentration could be achieved under nitrogen starvation. *I. galbana*, *Nannochloris* sp.



and *N. oleoabundans* decreased in dry weight concentration after a maximum was reached.

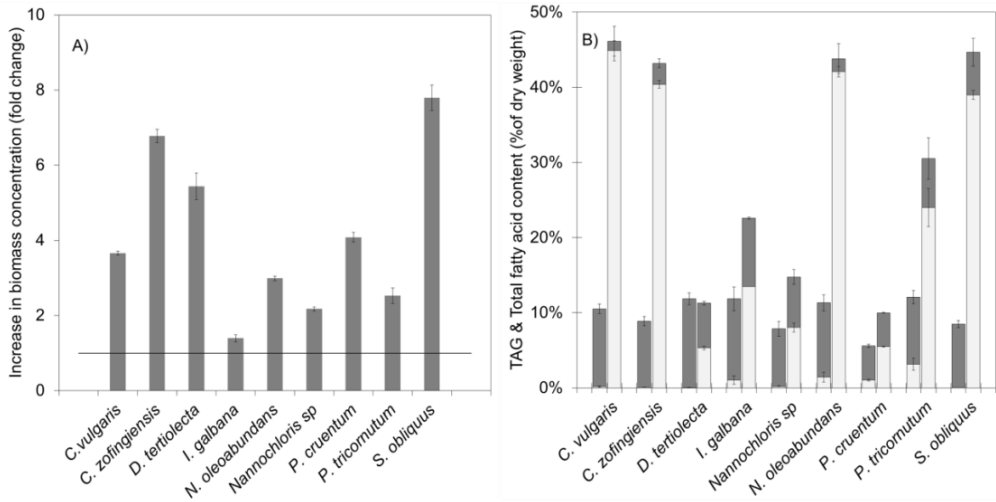


**Fig. 3.2.** a) Fold increase in biomass dry weight concentration when exposed to nitrogen starvation. The highest observed dry weight concentration was used to calculate the fold increase. This was at the end of the experiment for all strains, except for *Nannochloris* sp., *I. galbana*, and *N. oleoabundans*, for which the biomass concentration 3 days, 3 days, and 6 days after re-suspension in nitrogen free medium were used, respectively. Black horizontal line represents initial biomass concentration (1 fold change). Average values of duplicate culture replicates are shown. Error bars indicate the deviation of both cultures from the average. b) Cellular total fatty acid (dark grey bars) and TAG (light grey bars) content under nitrogen-sufficient (bars on left hand side) and deficient (bars on right hand side) conditions. Bars under nitrogen-sufficient conditions represent average values during nitrogen-sufficient cultivation. Bars under nitrogen-deficient conditions represent the highest achieved fatty acid and TAG content. This was at the end of the experiment for all strains except for *Nannochloris* sp. and *I. galbana*, for which the fatty acid and TAG contents 6 days after re-suspension in nitrogen free medium were used. Average values of duplicate culture replicates are shown. Error bars indicate the deviation of both cultures from the average.

The total fatty acid content (% of dry weight) did not significantly change during N-sufficient cultivation but upon nitrogen starvation all strains showed an increase in total fatty acid content, except *D. tertiolecta*, which showed a minor decrease (Fig. 3.2b). *Nannochloris* sp. and *P. cruentum* only increased slightly in total fatty acid content upon nitrogen starvation (Fig. 3.2b). This result is, for unknown reasons, in contrast to that observed by Takagi et al. (2006) for *D. tertiolecta* and by Takagi et al. (2000) and Yamaberi et al. (1998) for *Nannochloris* sp. Large differences were observed in maximal total fatty acid contents between strains, but in the four strains that accumulated the

most fatty acids, these differences were minor (Fig. 3.2b). Highest fatty acid contents were observed in *S. obliquus*, *N. oleoabundans*, *C. vulgaris*, and *C. zofingiensis*, reaching total fatty acid contents of  $44.7\% \pm 1.7$ ,  $43.8\% \pm 1.9$ ,  $46.1\% \pm 1.5$ , and  $43.2\% \pm 0.2$  (% of dry weight), respectively. *I. galbana* and *Nannochloris* decreased in total fatty acid content after a maximum was reached (Appendix A3.1).

Fatty acid content was affected within one day after re-suspension in nitrogen-free medium (Fig. 3.1b,d). This observation confirms that, as expected, cultures became nitrogen limited within one day. Fatty acid accumulation continued for 2 to 14 days, depending on the strain (Fig. 3.1 and Appendix A3.1). The rate at which the total fatty acid content increased varied among strains, also between the strains that achieved similar final total fatty acids contents (Fig. 3.3b).

TAG content was determined at the start of the experiment and once in the N-sufficient culture and once in the N-deficient culture for the time-point in which the total fatty acid content was highest (total fatty acid content was determined analytically for each sample; for most strains the highest values were found at the end of the experiment). For the six strains that showed a substantial increase in total fatty acid content upon nitrogen starvation, the increase could completely be accounted for by the accumulation of TAGs. TAGs constituted up to 90% of total fatty acids and over 40% of dry weight in some strains (Fig. 3.2b). The content of other lipids, estimated as the difference between total fatty acid and TAG content, decreased upon nitrogen starvation, possibly caused by a reduction in the thylakoid membrane or cellular membrane content (Bar et al., 1995; Guckert & Cooksey, 1990).

### **3.3.3 Biomass composition**

In the absence of a nitrogen source, protein and chlorophyll synthesis is reduced and their content (% of dry weight) can decrease almost an order of magnitude (da Silva et al., 2009; Lv et al., 2010; Pruvost et al., 2011). Protein content in N-deficient cultures was estimated using a mass balance over nitrogen. The volumetric protein content (g/l) was assumed to remain constant after nitrogen depletion and the nitrogen content in exponentially growing biomass and in proteins was assumed as 9% and 16% (w/w), respectively. The protein content per dry weight (g/g) was subsequently calculated using Eq. 3. Due to the increase in dry weight concentration after nitrogen depletion, the protein content (% w/w) decreased. This decrease in protein content was highest in *S. obliquus* with an estimated decrease of 56% at the start of the experiment to less than

8% (w/w) after 14 days (Fig. 3.3a). This observation can be explained by the accumulation of storage compounds, such as TAGs.

The increase in biomass concentration during nitrogen starvation can at least partly be explained by *de novo* fatty acid synthesis. However, depending on the strain, the increase in volumetric fatty acid content can account for only 42% to 69% of the increase in biomass dry weight concentration in the oleaginous strains. This difference indicates simultaneous *de novo* production of other components, most likely carbohydrates. Several oleaginous microalgal strains are known to simultaneously increase in carbohydrate content upon nitrogen starvation to over 60% of dry weight (Jakob et al., 2007; Lv et al., 2010; Pruvost et al., 2011). The putative carbohydrate fraction of biomass, estimated using Eq. 4, increased from 30% to 50-60% in the first 2-4 days of N-deficient cultivation. Hereafter, it slightly decreased again and then remained constant during the rest of the cultivation (Fig. 3.3c). Initially, the rate at which the fraction of fatty acids increased was lower than the rate at which the putative carbohydrate fraction increased (Fig. 3.3b,c). Carbohydrate accumulation prior to, and simultaneous with, TAG accumulation was observed by Msanne et al. (2012) for *Chlamydomonas reinhardtii* and *Coccomyxa* sp. and by Li et al. (2011) for *Pseudochlorococcum* sp. Therefore, Li et al. (2011) suggested that carbohydrates are used as a primary and TAG is used as a secondary storage product. Possibly, carbohydrates are even converted into TAGs when nitrogen starvation progresses.

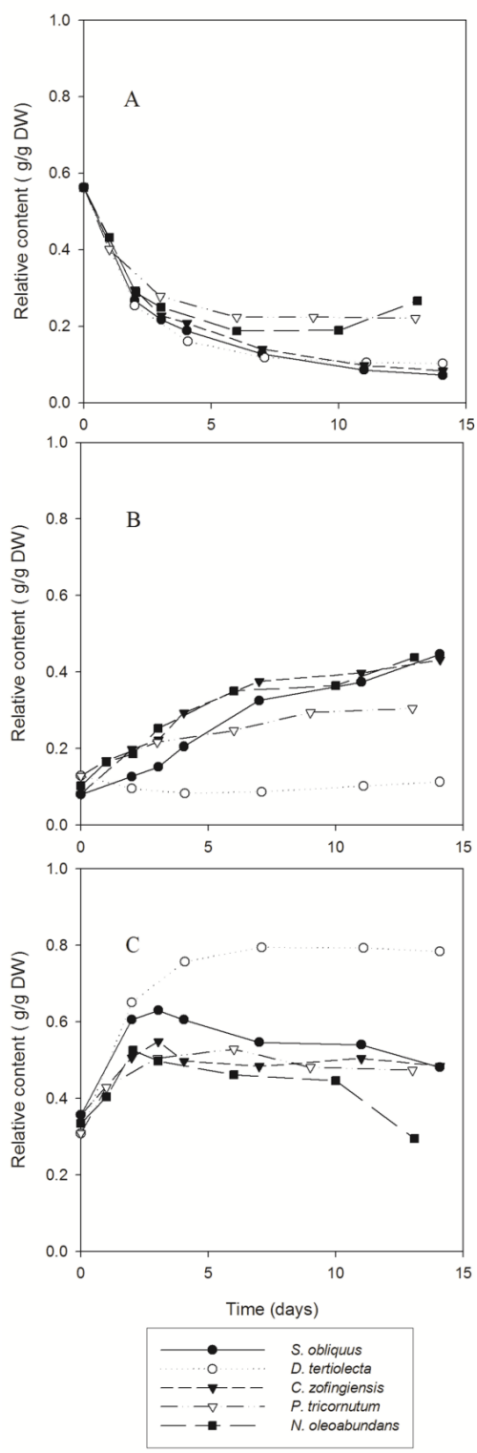


**Fig. 3.3.** Dynamics of protein (a), lipid (b) and putative carbohydrate (c) content during nitrogen-deficient cultivation. *S. obliquus*, *D. tertiolecta*, *C. zoefingiensis*, *P. tricornutum*, and *N. oleoabundans* are shown as an example. Protein and carbohydrate content were estimated using Eq. 3 and Eq. 4. Total fatty acid (lipid) content was measured analytically.

### 3.3.4 Fatty acid composition

The fatty acid composition of total fatty acids was determined as a function of time in both N-sufficient and deficient cultures. Examples for *S. obliquus* and *P. tricornutum* are shown in Fig. 3.4 and data for all other strains are provided in Appendix A.

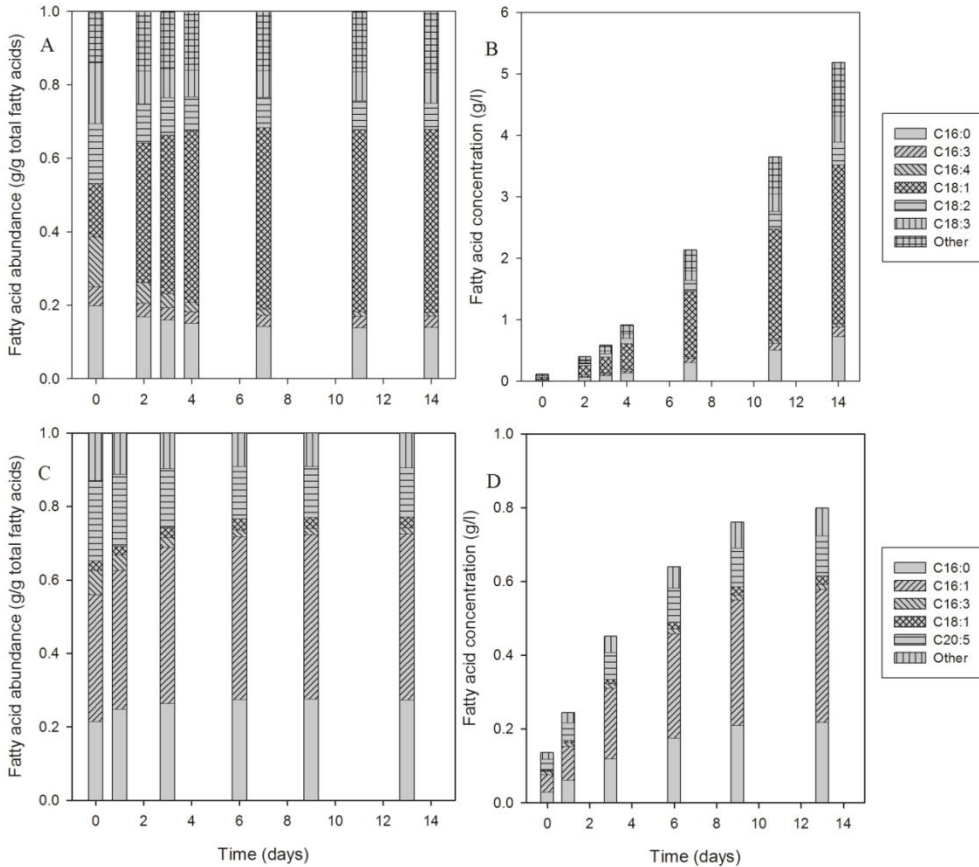


**Fig. 3.4.** Change in fatty acid composition during nitrogen-deficient growth. Change in abundance of fatty acids as percentage of total fatty acids (a,c) and increase in concentration in the culture medium of individual fatty acids (b,d). *S. obliquus* (a,b) and *P. tricornutum* (c,d) are shown as examples. Average values of duplicate culture replicates are shown.

Fatty acid composition during N-sufficient growth did not change significantly (Table 3.1a) but upon nitrogen starvation, a major shift in the fatty acid profile was observed (Table 3.1b). The largest change in composition was observed in the first 1 or 2 days. The composition continued to change until fatty acid content remained constant (Fig. 3.4a,c and Appendix A). All strains, including the ones that did not accumulate substantial amounts of fatty acids, showed a major change in fatty acid composition

upon nitrogen starvation. In the oleaginous strains, this can be explained by the accumulation of TAG, with a different fatty acid composition than that of functional and structural lipids. In the non-oleaginous strains this could indicate a shift in lipid class composition, for example a reduction in thylakoid membrane content. Strains that accumulated the largest amounts of fatty acids also showed the largest change in fatty acid composition.

In the strains that accumulated more than 40% fatty acids (all belonging to the chlorophyceae), fatty acid compositions after nitrogen starvation were very similar. In these strains oleic acid was the dominant fatty acid, constituting up to 50% of total fatty acids. This is a commonly observed phenomenon for green algae (Ben-Amotz et al., 1985; Griffiths et al., 2011; Guckert & Cooksey, 1990).

The average degree of unsaturation of total fatty acids (expressed as the average number of double bonds per fatty acid) decreased upon nitrogen starvation. Depending on the strains, the degree of unsaturation decreased by 10 to 38% in nitrogen starved cultures (average reduction of 27%). This reduction was mainly caused by an increase in oleic acid abundance and a decrease in more unsaturated fatty acid abundance (Table 3.1).

Although the relative abundance of some fatty acid types decreased, the absolute abundance ( $\text{mg l}^{-1}$ ) of all fatty acid types in the oleaginous strains increased due to the large increase in volumetric fatty acid content in nitrogen-starved cultures (Fig. 3.4b,d). This finding suggests that the change in fatty acid profile is a result of a change in the relative *de novo* fatty acid production rates.

To meet the EN 14214 biodiesel standard, the contents of linolenic acid (C18:3) and fatty acids of more than four double bonds should be less than 12% and 1% (w/w), respectively. These requirements were met by all green algae, except *C. vulgaris* when exposed to nitrogen starvation (Table 3.1b). Furthermore, the ideal composition of biodiesel is a ratio of 5:4:1 of C16:1, C18:1 and C14:0 (Schenk et al., 2008). This ratio was not present in any of the strains but C16:1, C18:1 and C14:0 were produced in large quantities by *P. tricornutum*, all oleaginous chlorophyceae, and *I. galbana* (Table 3.1). As proposed by Huerlimann et al. (2010), mixing of fatty acids derived from different strains might be a feasible option for the production of biodiesel with a desirable composition.

**Table 3.1.** Fatty acid composition during nitrogen-sufficient and deficient cultivation (continues next page).

A)	<i>C. vulgaris</i>	<i>C. zofigiensis</i>	<i>D. tertiolecta</i>	<i>I. galbana</i>	<i>Nannochloris</i> sp.	<i>N. oleoabundans</i>	<i>P. cruentum</i>	<i>P. tricornutum</i>	<i>S. obliquus</i>
<b>Saturated</b>									
C14:0	2	2	2	17	2 †	2	1	4	2
C16:0	20	18	18	9	26	22	32	20	18
C18:0	1	2	1	1	1	1	3	2	1
<b>Total</b>	<b>22</b>	<b>21</b>	<b>21</b>	<b>28</b>	<b>29</b>	<b>24</b>	<b>37</b>	<b>26</b>	<b>21</b>
<b>Mono-unsaturated</b>									
C16:1	1	1	1	4 †	3	3 †		31	5
C18:1	4 †	18	5 †	14	9 †	8 †	5 †	3 ‡	22
<b>Total</b>	<b>5</b>	<b>19</b>	<b>6</b>	<b>18</b>	<b>12</b>	<b>11</b>	<b>5</b>	<b>34</b>	<b>27</b>
<b>Poly-unsaturated</b>									
C16:2	11	7	2		8	6	1	3 †	3
C16:3	14	9	4 †	2	8	12		8	6 †
C16:4		2 ‡	20						9
C18:2	19	20	11	13 †	31	27	14	1	15
C18:3	28	18	35	9	11	20			13
C18:4		2	1	10					3
C20:4				1			31		
C20:5				1			7 ‡	24	
C22:6				15					
<b>Total</b>	<b>72</b>	<b>58</b>	<b>73</b>	<b>51</b>	<b>58</b>	<b>65</b>	<b>54</b>	<b>36</b>	<b>49</b>
Other		1		3	1		5	4	2
<b>B)</b>									
<b>Saturated</b>									
C14:0			1	22	1	1	1	3	
C16:0	17	15	25	14	37	23	28	27	14
C18:0	2	3	2	1	2	3	4	1	5
<b>Total</b>	<b>19</b>	<b>18</b>	<b>28</b>	<b>37</b>	<b>41</b>	<b>26</b>	<b>33</b>	<b>32</b>	<b>19</b>
<b>Mono-unsaturated</b>									
C16:1	1	1	1	2	2	3		45	5
C18:1	47	47	14	27	27	41	5	3	50
<b>Total</b>	<b>48</b>	<b>48</b>	<b>15</b>	<b>29</b>	<b>29</b>	<b>44</b>	<b>6</b>	<b>48</b>	<b>55</b>
<b>Poly-unsaturated</b>									
C16:2	3	4	1		2	3		1	4
C16:3	6	2	2		3	2		2	3
C16:4			12						1
C18:2	10	17	9	3	18	21	30	1	7
C18:3	14	8	31	4	6	3			8
C18:4			1	10					1
C20:4							23	1	
C20:5				2			3	13	1
C22:6				12					
<b>Total</b>	<b>33</b>	<b>32</b>	<b>56</b>	<b>32</b>	<b>30</b>	<b>29</b>	<b>56</b>	<b>18</b>	<b>25</b>
Other		1		3	1		5	2	1

†Relative standard deviation between 10% and 25%.

‡Relative standard deviation between 25% and 60%.

**Table 3.1 (continued).** a) Average fatty acid composition of total fatty acids during nitrogen-sufficient cultivation. Relative deviation of duplicate culture replicates (*i.e.* measured value minus average value divided by average value) during nitrogen-sufficient growth was less than 10% or as indicated otherwise. The reproducibility for fatty acids with a relative abundance of less than 2% was not considered. b) Fatty acid composition of total fatty acids under nitrogen-deficient conditions. Data shown are from the time point at which cellular fatty acid content was maximal and corresponds to the time points shown in Fig. 3.2b. This is at the end of the experiment for all strains except for *Nannochloris* sp. and *I. galbana*, for which the fatty acid compositions 6 days after re-suspension in nitrogen free medium are shown. The average values of duplicate culture replicates are shown. Relative deviation of duplicate culture replicates was less than 5%. The reproducibility for fatty acids with a relative abundance of less than 2% was not considered.

The marine strains included well known producers of (long chain) poly-unsaturated fatty acids that can be used as a nutraceuticals or in fish feed (Apt & Behrens, 1999; Wijffels & Barbosa, 2010). Eicosapentaenoic acid (EPA) was produced by *P. tricornutum* (22%) and *P. cruentum* (10%), arachidonic acid (ARA) was produced by *P. cruentum* (26%) and docosahexaenoic acid (DHA) was produced by *I. galbana* (16%) during cultivation under N-sufficient conditions. When exposed to nitrogen starvation, the relative abundance of these fatty acids decreased (% of total fatty acids) but absolute concentrations of these fatty acids ( $\text{mg l}^{-1}$ ) increased during N-deficient cultivation due to increased volumetric fatty acid contents. The decrease in relative abundance of these fatty acids in the marine strains was counterbalanced by an increase in saturated and mono-unsaturated fatty acids, except for *P. cruentum*, which showed an increase in linoleic acid (C18:2) abundance (30%).

### 3.3.5 Productivity

Volumetric and areal fatty acid productivity are considered key parameters to predict performance of fatty acid production by microalgal strains (Griffiths & Harrison, 2009; Griffiths et al., 2011; Rodolfi et al., 2009). It is generally accepted that the total fatty content is enhanced under nitrogen-deficient conditions, but biomass productivity is decreased (Griffiths et al., 2011; Pruvost et al., 2011; Rodolfi et al., 2009). Both fatty acid content and biomass productivity contribute to fatty acid productivity, illustrating the importance of both parameters. Therefore, it is often debated whether highest fatty acid productivities are achieved under N-sufficient or deficient cultivation conditions. In the present study, all oleaginous strains showed the highest fatty acid productivity under nitrogen-deficient conditions (Table 3.2).



**Table 3.2.** Average productivities (calculated using Eq. 1) and the highest observed productivity between two consecutive time points (Eq. 2) of biomass, total fatty acids, as well as the average TAG productivity (Eq. 1) for nitrogen-sufficient (N+) and deficient (N-) cultures. Nitrogen-sufficient productivities were calculated using the data until nitrogen became limiting. Nitrogen-deficient average productivities were calculated over the entire cultivation or as indicated otherwise. Underlined values represent the highest observed productivity among all strains in nitrogen-deficient cultures and bold values represent the highest observed productivity between all strains in nitrogen-sufficient cultures. Average values of duplicate culture replicates are shown. Relative deviation of duplicate culture replicates was less than 5% or as indicated otherwise.

Species	Volumetric biomass productivity ( $\text{mg l}^{-1} \text{ day}^{-1}$ )		Volumetric fatty acid productivity ( $\text{mg l}^{-1} \text{ day}^{-1}$ )		Average volumetric TAG productivity ( $\text{mg l}^{-1} \text{ day}^{-1}$ )
	Average	Max	Average	Max	
<i>C. vulgaris</i> N-	217	489	130	173 <sup>c</sup>	134
<i>C. vulgaris</i> N+	668 <sup>b</sup>	771 <sup>b</sup>	77 <sup>b</sup>	91 <sup>c</sup>	1 <sup>b</sup>
<i>C. zofingiensis</i> N-	508	674	251	301	242
<i>C. zofingiensis</i> N+	<b>792</b>	<b>973</b>	<b>80</b>	97	3 <sup>a</sup>
<i>D. tertiolecta</i> N-	341	680	38	46	22 <sup>a</sup>
<i>D. tertiolecta</i> N+	487	503 <sup>b</sup>	56	61 <sup>a</sup>	0 <sup>b</sup>
<i>I. galbana</i> N-	149 <sup>†, b</sup>	276	65 <sup>†</sup>	76	26 <sup>†</sup>
<i>I. galbana</i> N+	401 <sup>b</sup>	620 <sup>b</sup>	56 <sup>b</sup>	67	1 <sup>b</sup>
<i>N. oleoabundans</i> N-	426 <sup>†</sup>	799 <sup>b</sup>	202 <sup>†</sup>	265 <sup>a</sup>	216 <sup>†</sup>
<i>N. oleoabundans</i> N+	451 <sup>a</sup>	776 <sup>b</sup>	62	122 <sup>b</sup>	15 <sup>c</sup>
<i>Nannochloris</i> sp. N-	264 <sup>†</sup>	340 <sup>a</sup>	36 <sup>†, a</sup>	40	15 <sup>a</sup>
<i>Nannochloris</i> sp. N+	524	776	46	56 <sup>a</sup>	2
<i>P. cruentum</i> N-	308	679 <sup>b</sup>	38 <sup>a</sup>	58 <sup>c</sup>	8 <sup>b</sup>
<i>P. cruentum</i> N+	679 <sup>a</sup>	710 <sup>b</sup>	35	37 <sup>b</sup>	<b>21</b>
<i>P. tricornutum</i> N-	122 <sup>a</sup>	413 <sup>a</sup>	51	109 <sup>b</sup>	45
<i>P. tricornutum</i> N+	486	530 <sup>a</sup>	64	73 <sup>b</sup>	11 <sup>c</sup>
<i>S. obliquus</i> N-	<u>719</u>	<u>822<sup>b</sup></u>	<u>360</u>	<u>498<sup>a</sup></u>	<u>323</u>
<i>S. obliquus</i> N+	767	883 <sup>a</sup>	68 <sup>a</sup>	73 <sup>c</sup>	6 <sup>b</sup>

<sup>†</sup> In cultivations where biomass concentration or total fatty acid content started to decrease after a maximum was reached, the average productivity until the start of this decrease was used.

<sup>a</sup> Relative standard deviation between 5 and 10%.

<sup>b</sup> Relative standard deviation between 10 and 25%.

<sup>c</sup> Relative standard deviation between 25 and 75%.

The highest average volumetric fatty acid and TAG productivity were achieved by *S. obliquus* (360  $\text{mg fatty acid l}^{-1} \text{ day}^{-1}$  and 322  $\text{mg TAG l}^{-1} \text{ day}^{-1}$ ) and *C. zofingiensis* (250  $\text{mg fatty acid l}^{-1} \text{ day}^{-1}$  and 243  $\text{mg TAG l}^{-1} \text{ day}^{-1}$ ). These values are high compared to previously reported values (Griffiths & Harrison, 2009; Mata et al., 2010), but productivity parameters are highly dependent on cultivation conditions, making it difficult to compare results obtained in the present study to those obtained under different cultivation conditions. Productivities in lab-scale experiments cannot directly be extended to productivities that can be achieved in outdoor photo-bioreactors, but can serve as a tool for strain selection.

Simultaneous fatty acid accumulation and continuation of biomass productivity was observed. For example, in *S. obliquus*, fatty acid content reached over 30% of dry weight in N-deficient cultures before biomass productivity started to decrease compared to N-sufficient cultivation (Fig. 3.1a,c). During this period, a 4.5-fold increase in dry weight concentration was achieved. Large differences were observed between the lengths of the periods during which biomass productivity could be maintained by the different strains (Fig. 3.1 and Appendix A).

Fatty acid productivity is a combination of the increase in biomass concentration and fatty acid content. The difference in fatty acid productivities between the four most productive strains is mainly caused by the difference in achieved biomass concentration rather than by differences in achieved fatty acid content. This finding could mean that fatty acid productivities of strains with a relatively low fold increase in biomass concentration could be enhanced by optimizing the biomass concentration at which nitrogen depletion starts or by optimizing the initial nitrogen concentration. However, this approach would increase the usage of the nitrogen source (fertilizer), which in turn would increase the environmental impact of the overall production process. These phenomena make the extent to which the biomass concentration, and especially TAG concentration, can increase under nitrogen-starved conditions an important microalgal characteristic and should be considered when selecting an appropriate strain and production strategy.

### **3.4 Conclusions**

*S. obliquus* (UTEX 393) and *C. zofingiensis* (UTEX B32) are most promising for TAG production. These strains accumulated over 35% of their dry weight as TAGs and achieved the highest average TAG productivity (322 and 243 mg l<sup>-1</sup> day<sup>-1</sup>, respectively). The duration that biomass productivity was retained after nitrogen depletion was the biggest contributor to the differences observed in these TAG productivities, and is therefore an important microalgal characteristic. Further research on what determines the length of this period, the distribution of carbon over TAGs and carbohydrates during nitrogen starvation, and the yield of TAGs on light is recommended.

### **Acknowledgements**

This research project is financially supported by the Food and Nutrition Delta program of Agentschap NL (FND10007) and Unilever. We thank Marcia de Rooy and Hans-Gerd Janssen from Unilever Research and Development, Vlaardingen, The Netherlands for the development of the TAG analysis method and analysis of the TAG samples.

## Appendix A. Biomass concentration, lipid content and fatty acid composition of all algae species.

### *Chlorella vulgaris*

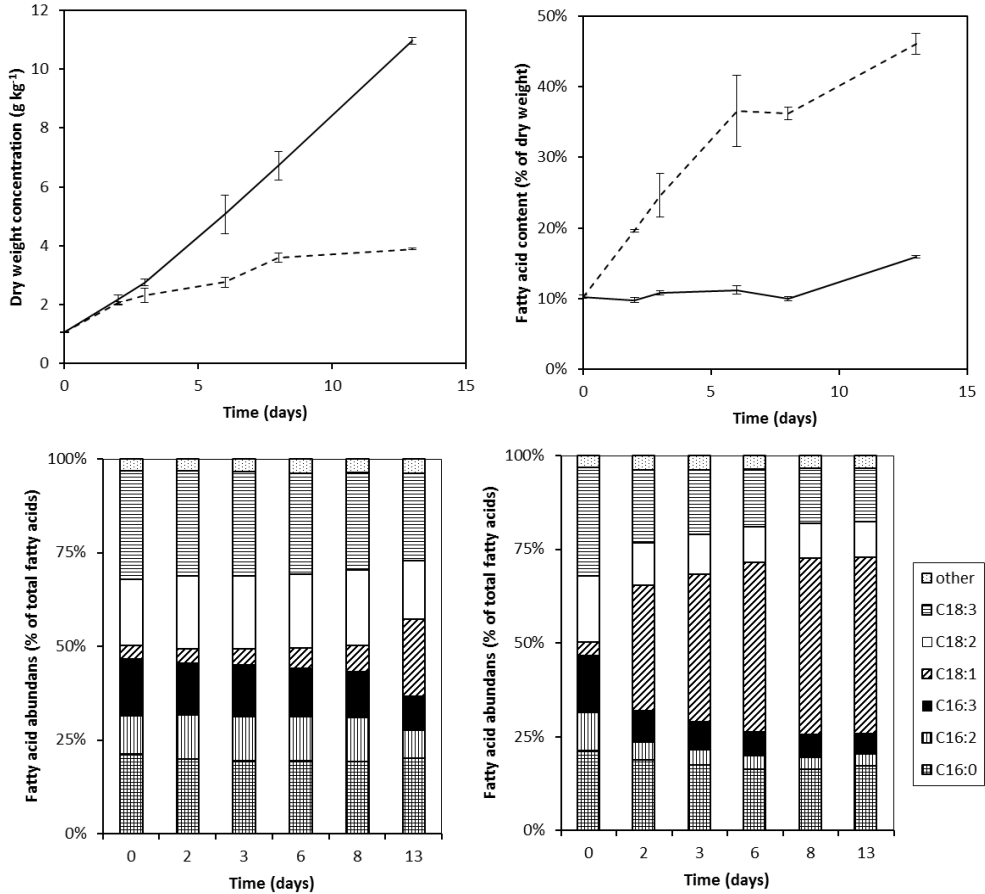


**Fig. A.1** Biomass concentration (top-left), lipid content (top-right), fatty acid composition during nitrogen replete cultivation (bottom-left), and fatty acid composition during nitrogen deplete cultivation (bottom-right) of *C. vulgaris*. In the top figures, solid lines indicate nitrogen replete conditions and dotted lines indicate nitrogen-depleted conditions.

*Chlorella zofingiensis*

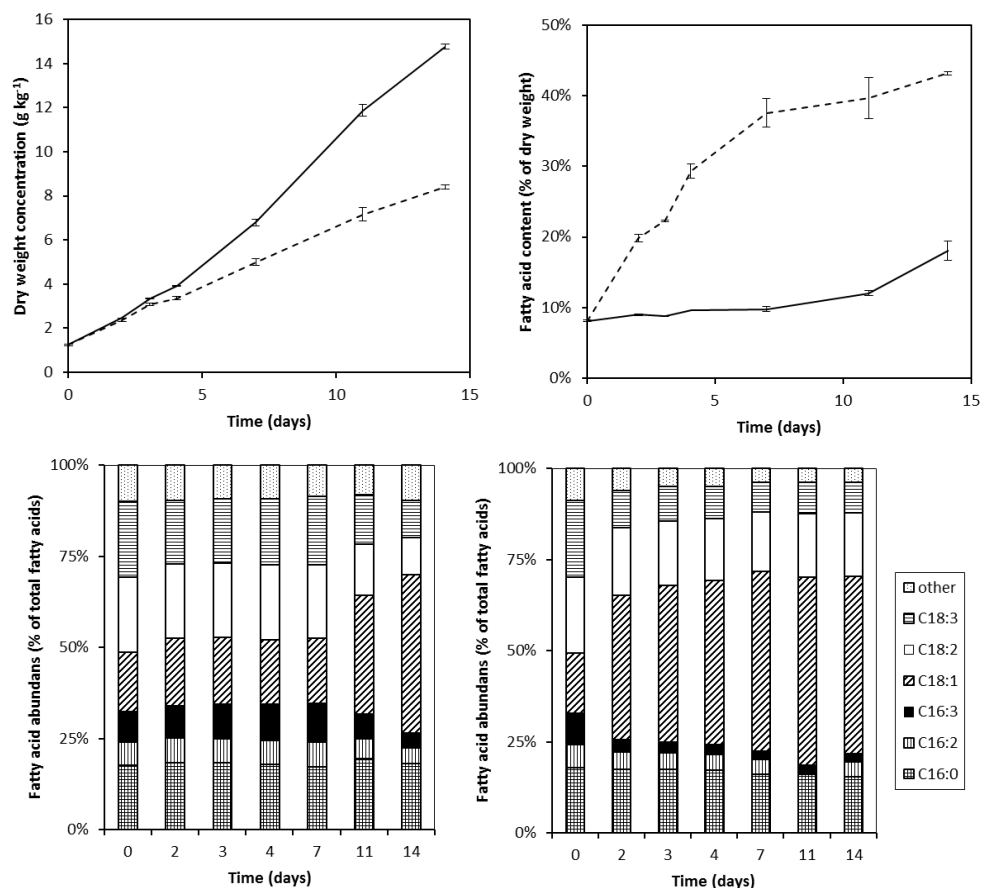


**Fig. A.2** Biomass concentration (top-left), lipid content (top-right), fatty acid composition during nitrogen replete cultivation (bottom-left), and fatty acid composition during nitrogen deplete cultivation (bottom-right) as a function of time in *C. zofingiensis*. In the top figures, solid lines indicate nitrogen replete conditions and dotted lines indicate nitrogen-depleted conditions.

### *Dunaliella tertiolecta*

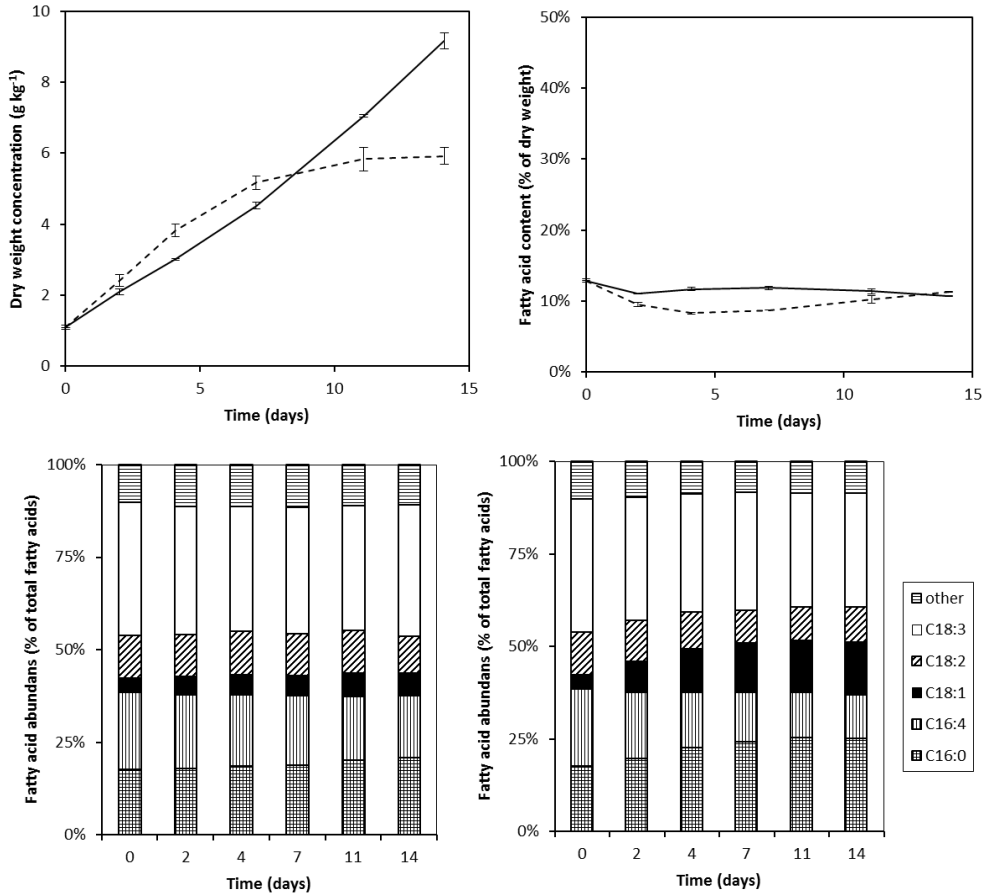


**Fig A.3** Biomass concentration (top-left), lipid content (top-right), fatty acid composition during nitrogen replete cultivation (bottom-left), and fatty acid composition during nitrogen deplete cultivation (bottom-right) as a function of time in *D. tertiolecta*. In the top figures, solid lines indicate nitrogen replete conditions and dotted lines indicate nitrogen-depleted conditions.

*Isochrysis galbana*

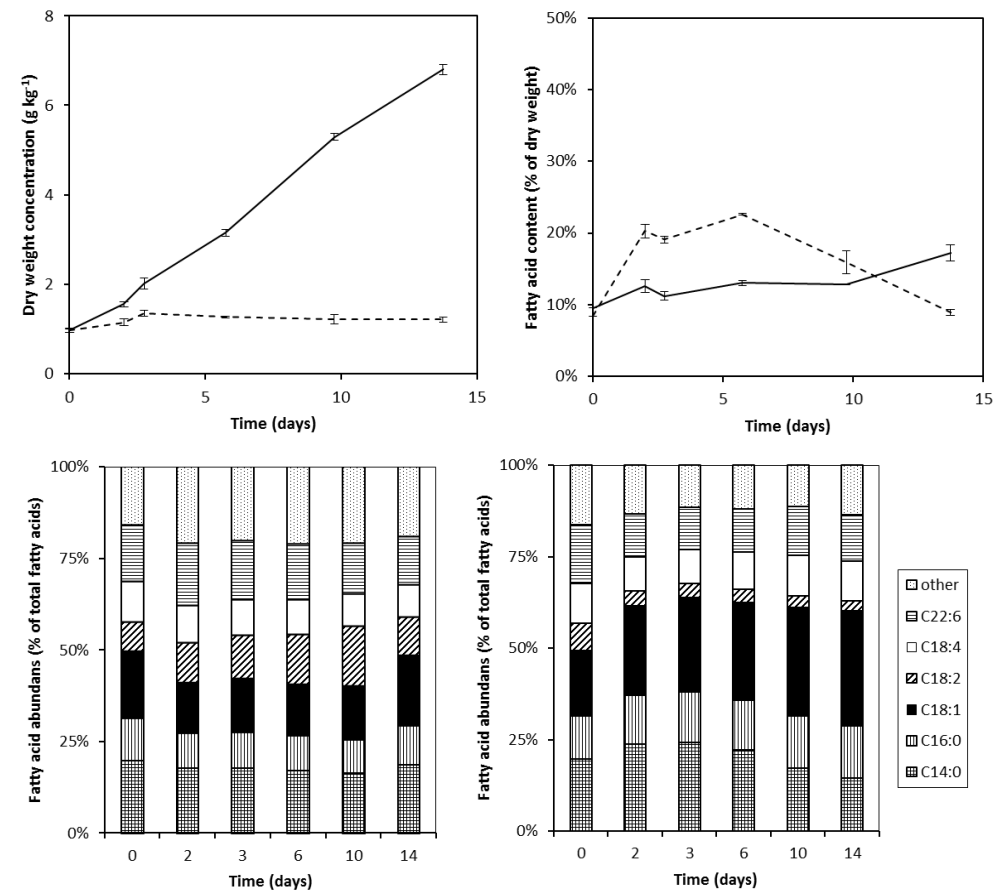


**Fig. A.4** Biomass concentration (top-left), lipid content (top-right), fatty acid composition during nitrogen replete cultivation (bottom-left), and fatty acid composition during nitrogen deplete cultivation (bottom-right) as a function of time in *I. galbana*. In the top figures, solid lines indicate nitrogen replete conditions and dotted lines indicate nitrogen-depleted conditions.

*Nannochloris* sp.

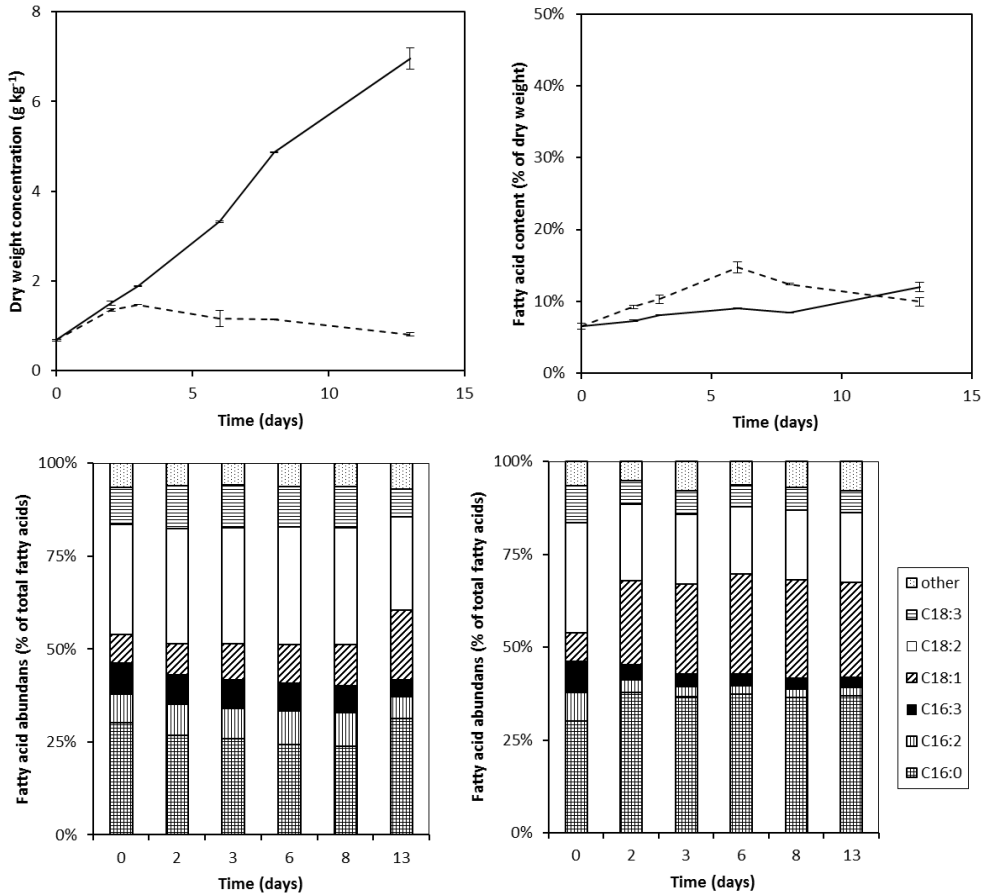


**Fig. A.5** Biomass concentration (top-left), lipid content (top-right), fatty acid composition during nitrogen replete cultivation (bottom-left), and fatty acid composition during nitrogen deplete cultivation (bottom-right) as a function of time in *Nannochloris* sp.. In the top figures, solid lines indicate nitrogen replete conditions and dotted lines indicate nitrogen-depleted conditions.

*Neochloris oleoabundans*

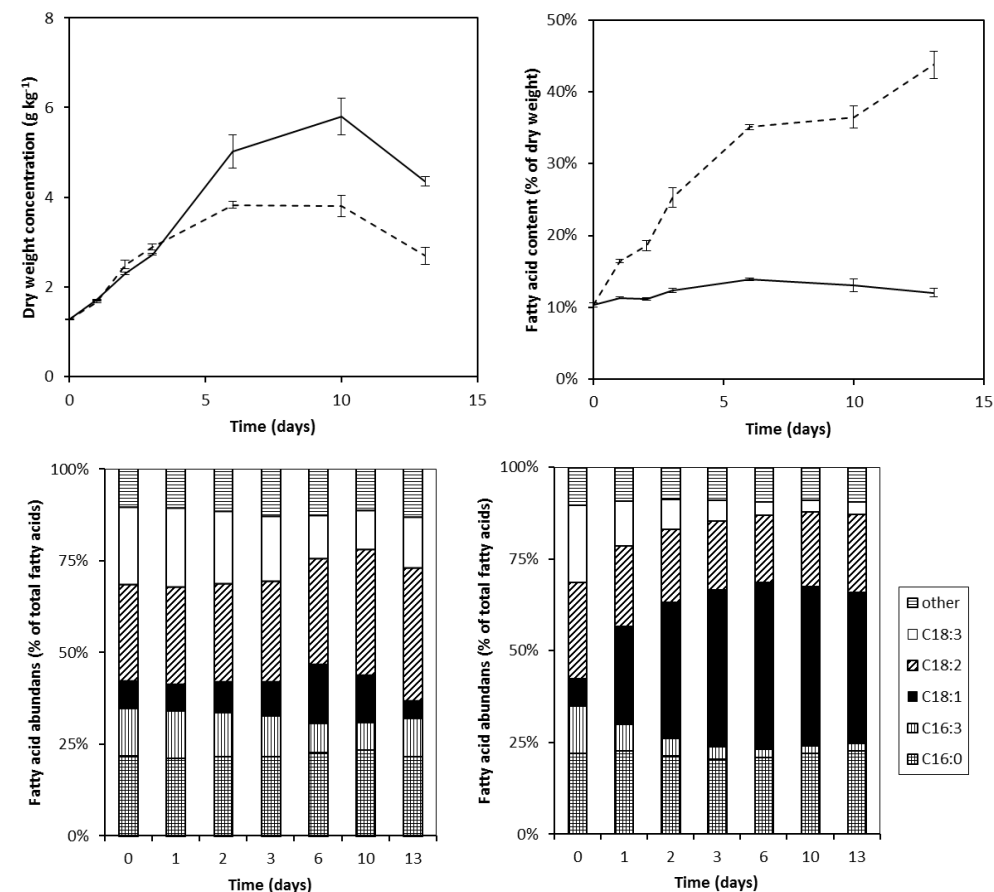


**Fig. A.6** Biomass concentration (top-left), lipid content (top-right), fatty acid composition during nitrogen replete cultivation (bottom-left), and fatty acid composition during nitrogen deplete cultivation (bottom-right) as a function of time in *N. oleoabundans*. In the top figures, solid lines indicate nitrogen replete conditions and dotted lines indicate nitrogen-depleted conditions.



### *Phaeodactylum tricornutum*

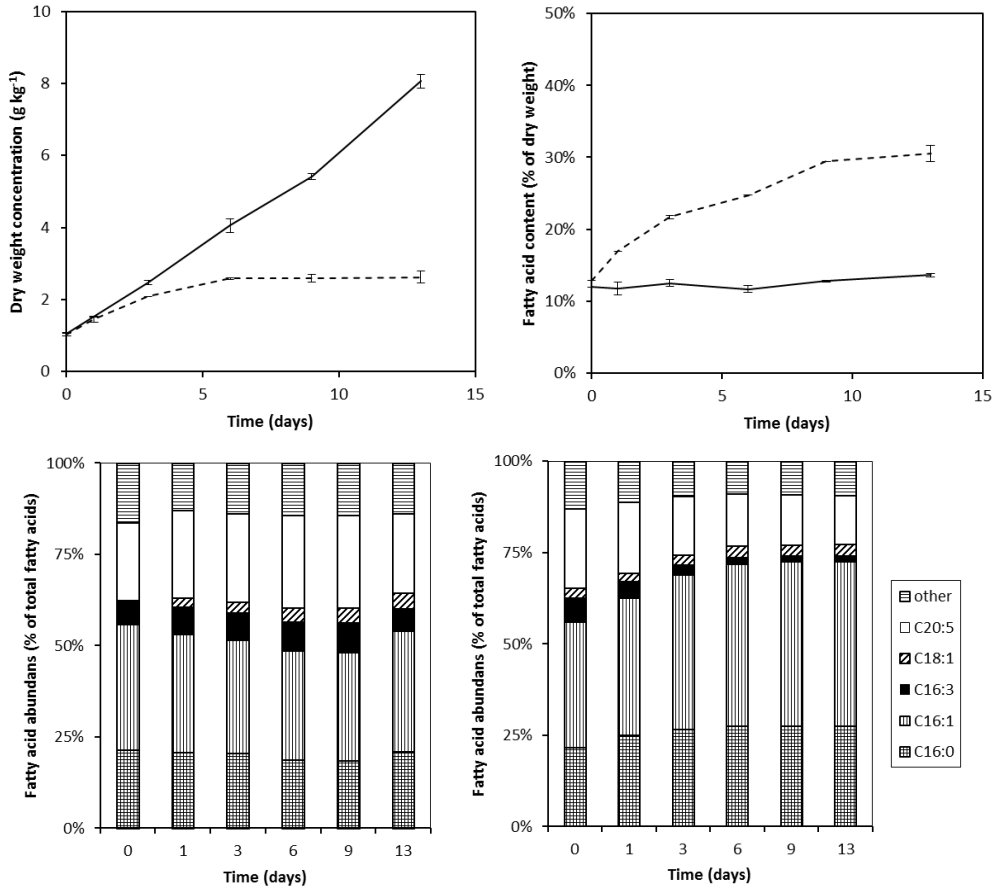


**Fig. A.7** Biomass concentration (top-left), lipid content (top-right), fatty acid composition during nitrogen replete cultivation (bottom-left), and fatty acid composition during nitrogen deplete cultivation (bottom-right) as a function of time in *P. tricornutum*. In the top figures, solid lines indicate nitrogen replete conditions and dotted lines indicate nitrogen-depleted conditions.

*Porphyridium cruentum*

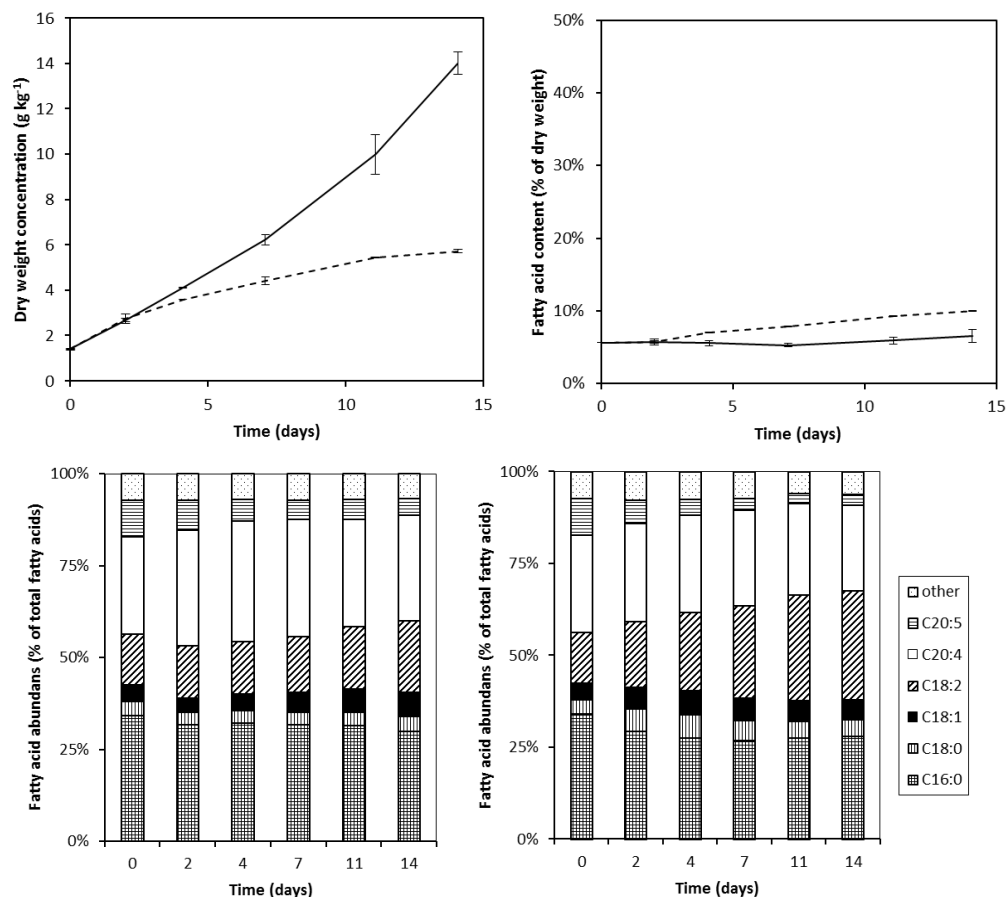


**Fig. A.8** Biomass concentration (top-left), lipid content (top-right), fatty acid composition during nitrogen replete cultivation (bottom-left), and fatty acid composition during nitrogen deplete cultivation (bottom-right) as a function of time in *P. cruentum*. In the top figures, solid lines indicate nitrogen replete conditions and dotted lines indicate nitrogen-depleted conditions.

### *Scenedesmus obliquus*

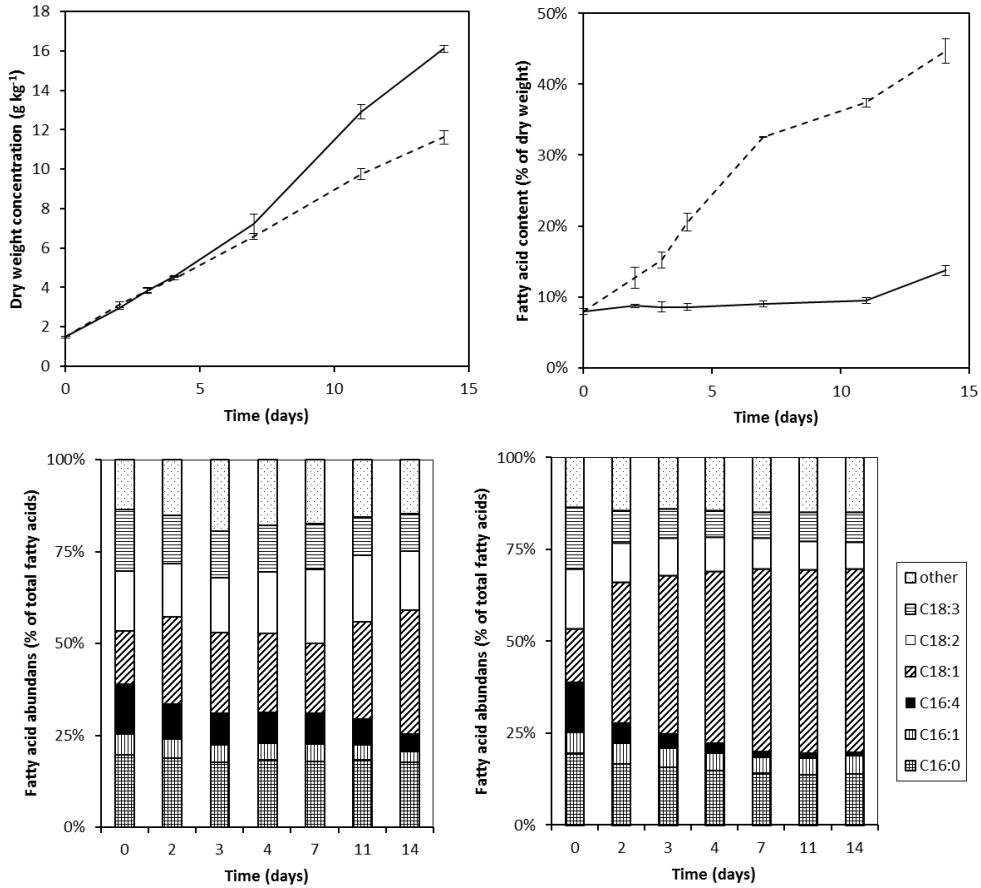


**Fig. A.9** Biomass concentration (top-left), lipid content (top-right), fatty acid composition during nitrogen replete cultivation (bottom-left), and fatty acid composition during nitrogen deplete cultivation (bottom-right) as a function of time in *S. obliquus*. In the top figures, solid lines indicate nitrogen replete conditions and dotted lines indicate nitrogen-depleted conditions.



## **Chapter 4**    Effect of light intensity, pH, and temperature on triacylglycerol (TAG) accumulation induced by nitrogen starvation in *Scenedesmus obliquus*

**This chapter has been published as:**

Guido Breuer, Packo P. Lamers, Dirk E. Martens, René B. Draaisma, René H. Wijffels (2013), Effect of light intensity, pH, and temperature on triacylglycerol (TAG) accumulation induced by nitrogen starvation in *Scenedesmus obliquus*, *Bioresource Technology* 143, 1-9

### **Abstract**

Microalgae-derived lipids in the form of triacylglycerols (TAGs) are considered an alternative resource for the production of biofuels and food commodities. Large scale production of microalgal TAGs is currently uneconomical. The cost price could be reduced by improving the areal and volumetric TAG productivity. The economic value could be increased by enhancing the TAG quality. To improve these characteristics, the impact of light intensity, and the combined impact of pH and temperature on TAG accumulation were studied for *Scenedesmus obliquus* UTEX 393 under nitrogen starved conditions. The maximum TAG content was independent of light intensity, but varied between 18% and 40% of dry weight for different combinations of pH and temperature. The highest yield of fatty acids on light (0.263 g/mol photon) was achieved at the lowest light intensity, pH 7 and 27.5°C.

#### 4.1 Introduction

Microalgae are considered one of the most promising future feedstocks for sustainable supply of commodities for both food and non-food products (Draaisma et al., 2013; Wijffels & Barbosa, 2010). Lipids derived from microalgae in the form of triacylglycerol (TAG) can for example be used for biodiesel production (Chisti, 2007) and certain microalgal oils might in part substitute functionalities of major vegetable oils in food applications (Draaisma et al., 2013).

Many microalgae species have the ability to produce TAG. Under optimal growth conditions they produce very low quantities of TAG, but when exposed to nitrogen starvation TAG accumulation is induced and contents as high as 40% of dry weight can be reached (Breuer et al., 2012). When exposed to nitrogen limitation, the production rate of functional biomass (i.e. protein, DNA, RNA, chlorophyll) is impaired. The difference between the rate at which electrons are generated by photosynthesis and the lower rate at which these electrons can be used to produce functional biomass can at least partially be used to produce TAG. TAG functions as a storage component for energy and carbon, but in addition its formation also prevents photo-oxidative damage to the cell by incorporating excess photosynthetically derived electrons (Hu et al., 2008). Costs of large scale production of microalgae-derived TAGs currently exceed those for the production of vegetable oils (Norsker et al., 2011; Ratledge & Cohen, 2008). The cost price could be reduced by improving the areal and volumetric productivity of TAG. Furthermore, the economic value could be enhanced by improving the TAG quality, which is determined by its fatty acid composition. TAG content and quality vary between microalgae species and depend on cultivation conditions (Breuer et al., 2012; Griffiths et al., 2011). Selection of a suitable species and optimization of cultivation conditions is therefore of paramount importance.

In previous research, nine microalgae species were selected as most promising for TAG production from a literature survey among 96 microalgae strains. These nine strains were experimentally evaluated and *Scenedesmus obliquus* UTEX 393 was identified as the most promising strain for TAG production (Breuer et al., 2012).

Light intensity, pH, and temperature are important cultivation parameters for microalgal growth and could therefore affect TAG productivity, yield and quality (Hu et al., 2008). Many investigations focussed on the impact of these process conditions on nitrogen replete growth whereas only little information is available about the impact of these process conditions on TAG accumulation induced by nitrogen starvation. For example, the impact of light intensity on the photosynthetic rate and photosynthetic efficiency under light limited growth is investigated extensively for many different microalgal

species (Janssen et al., 2000; Jassby & Platt, 1976; MacIntyre et al., 2002). Also, the impact of cultivation conditions on the nutritional value of marine microalgae for aquaculture applications, such as temperature (Renaud et al., 2002; Renaud et al., 1995) or light intensity (Guedes et al., 2010), has been the topic of many publications. Finally, many investigations focussed on determining cultivation conditions that result in maximum growth rates. For example, optimal conditions for nitrogen replete growth of *S. obliquus* are pH 7 (Hodaifa et al., 2010a) and a temperature of 25-30°C (Hodaifa et al., 2010b; Xin et al., 2011).

These investigations did not aim at maximizing TAG content or TAG productivity and neither did these cultivation conditions contribute to high TAG contents or productivities. TAG accumulation is most commonly achieved by applying nitrogen starvation. Optimal cultivation conditions for TAG accumulation under these nitrogen deplete conditions may be very different from those for growth under nitrogen replete conditions.

Knowledge about this topic is limited. Most knowledge is available about the impact of light intensity on TAG accumulation under nitrogen starved conditions, but a clear consensus is lacking. For example, both observations that lipid content is affected only to a minor extent by light intensity (Pal et al., 2011; Simionato et al., 2011) as well as observations that lipid content increases with light intensity have been made (Liu et al., 2012). Too few results are available to draw conclusions about the exact impact of pH and temperature on TAG accumulation under nitrogen starved conditions. However, it has been reported that high pH values can contribute to TAG accumulation (Gardner et al., 2010; Guckert & Cooksey, 1990; Santos et al., 2012).

In addition to the limited availability of knowledge on this topic, reported results are sometimes difficult to interpret because the impact of nitrogen starvation on TAG accumulation is not always completely isolated from the impact of the other investigated cultivation conditions. For example, in some investigations lipid accumulation was only evaluated at one arbitrarily chosen time point, while the investigated cultivation condition affected the moment at which the culture became nitrogen starved, and thus varying the duration of nitrogen starvation. This may lead to erroneous interpretation of the results and the outcomes might have been different when a different time point would have been chosen. It is therefore important to determine the point at which nitrogen is depleted and to monitor the entire accumulation process rather than looking at one arbitrarily chosen time point.

In this paper, the quantitative impact of light intensity, pH, and temperature on TAG accumulation induced by nitrogen starvation in *S. obliquus* is determined under well-defined and controlled conditions.



## 4.2 Materials and Methods

### 4.2.1 Culture, medium, and pre-cultivation

*Scenedesmus obliquus* UTEX 393 was used in all experiments and obtained from the University of Texas culture collection of algae (UTEX). Prior to the TAG accumulation experiments, cultures were maintained as described by Breuer et al. (2012). Cultivation medium used in the TAG accumulation experiment consisted of KNO<sub>3</sub> 10 mM; Na<sub>2</sub>SO<sub>4</sub> 0.7 mM; MgSO<sub>4</sub>•7H<sub>2</sub>O 1 mM; CaCl<sub>2</sub>•2H<sub>2</sub>O 0.5 mM; K<sub>2</sub>HPO<sub>4</sub> 2.5 mM; NaHCO<sub>3</sub> 10 mM; NaFeEDTA 28 µM; Na<sub>2</sub>EDTA•2H<sub>2</sub>O 80 µM; MnCl<sub>2</sub>•4H<sub>2</sub>O 19 µM; ZnSO<sub>4</sub>•7H<sub>2</sub>O 4 µM; CoCl<sub>2</sub>•6H<sub>2</sub>O 1.2 µM; CuSO<sub>4</sub>•5H<sub>2</sub>O 1.3 µM; Na<sub>2</sub>MoO<sub>4</sub>•2H<sub>2</sub>O 0.1 µM; Biotin 0.1 µM; vitamin B1 3.7 µM; vitamin B12 0.1 µM. Medium pH was adjusted to pH 7.0 with NaOH and the medium was filter sterilized prior to use.

### 4.2.2 Batch TAG accumulation experiments

TAG accumulation experiments were performed in batch-wise operated, aseptic, heat-sterilized, flat-panel, airlift-loop photobioreactors (Fig. 4.1). The liquid volume in the reactors was 380 ml with a light path (reactor depth) of 14 mm.

All cultures were continuously illuminated (24h per day) and illumination was provided on the culture side of the reactor (left side in Fig. 4.1B) using LED lamps with a warm white light spectrum (Bridgelux, BXRA W1200). The incident light intensity was determined as the average of measurements over the entire surface of the inside of the front glass panel of the reactor. Aeration and mixing was provided by sparging filtered air at 1.5 vvm. pH was controlled by adding on-demand CO<sub>2</sub> to the airflow. It was assured that the percentage of CO<sub>2</sub> in the airflow, in combination with the total gas flow rate, was sufficient to meet the CO<sub>2</sub> demand of the microalgae. In addition, cultures at pH 5 were supplied with a dilute HCl solution (0.5 M), because CO<sub>2</sub> sparging alone could not maintain the desired pH value. The temperature was controlled using a water jacket on the backside (other side than illuminated surface) of the reactor.

The reactor was inoculated at a biomass dry weight concentration between 0.02 and 0.05 g/l. The cultivation conditions directly after inoculation were: an incident light intensity of 100 µmol m<sup>-2</sup> s<sup>-1</sup>, pH 7, and temperature of 27.5°C. Once the biomass concentration reached 0.25-0.5 g/l dry weight, which was typically after 2-3 days, the set-points for incident light intensity, temperature, and pH were changed to the values to be investigated (200, 500, 800, and 1500 µmol m<sup>-2</sup> s<sup>-1</sup> incident light intensity; pH 5, 7, and 9; temperature of 20, 27.5, and 35°C). The moment at which these set-points were changed was considered the start of the experiment and is referred to as t=0. Typically one to two days after the start of the experiment, nitrogen was depleted from

the culture medium (at a biomass dry weight concentration of approximately 1.5-2 g/l) and TAG accumulation commenced. Cultivation was continued until the biomass concentration remained constant or decreased for several consecutive days, which was typically about two weeks after nitrogen depletion.

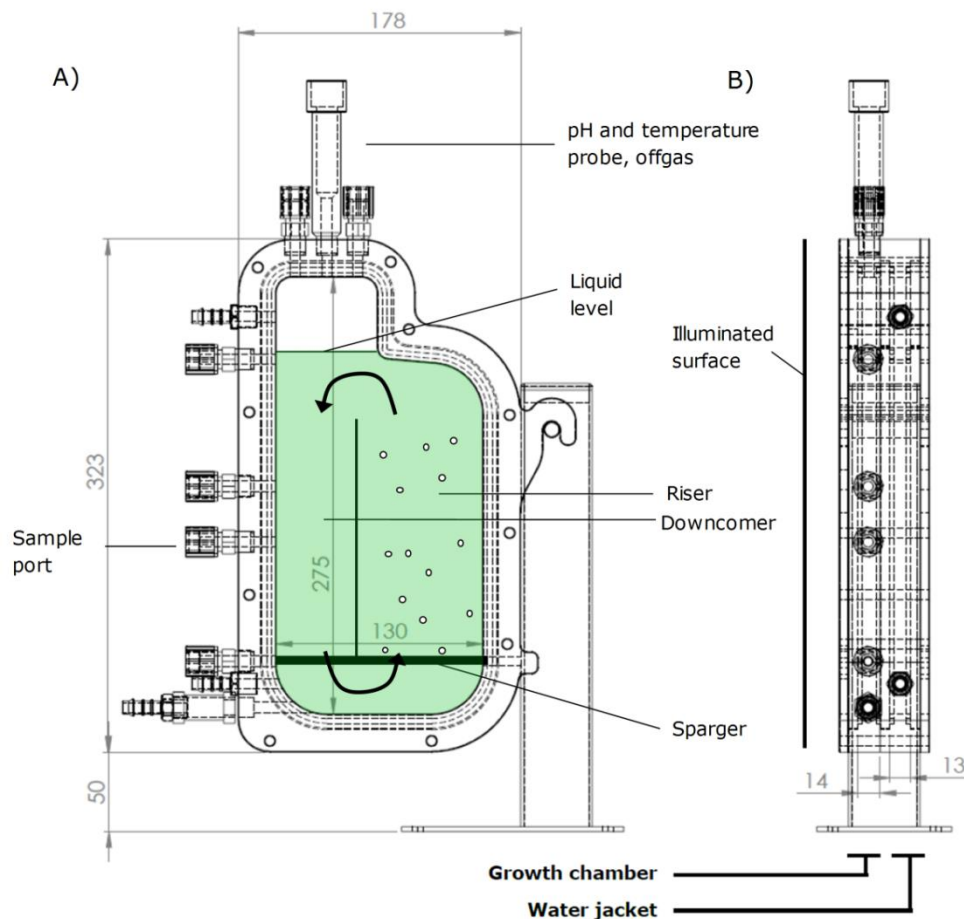


**Fig. 4.1.** Design of the bioreactor used. The water jacket was connected to an external temperature-controlled water bath. Illumination was provided from the side of the growth chamber (left side of Fig. B). The depth of the growth chamber was 14mm and the working volume in the growth chamber was 380 ml.

Periodically, a sample was taken directly from the reactor (10-20 ml sample volume) and analysed for dry weight concentration, dissolved (residual) nitrate, total fatty acid concentration and composition, TAG concentration and TAG fatty acid composition. After taking a sample, the reactor volume was restored by adding 0.2 $\mu$ m-filtered

demineralized water, to ensure that the pH and temperature probe remained submerged. It is acknowledged that this resulted in a dilution of the culture, but this dilution was similar for the different experiments. Heat sterilized 1% (v/v) antifoam (Antifoam B, J.T. Baker) was added to the reactor manually when foaming was visible.

### **4.2.3 Cultivation parameters and data analysis**

To study the combined impact of pH and temperature, experiments were performed at all combinations of pH 5, 7, and 9, with temperatures of 20, 27.5, and 35°C (9 combinations). In these experiments, an incident light intensity of  $500 \mu\text{mol m}^{-2} \text{s}^{-1}$  was used. To study the impact of light intensity, experiments were performed with an incident light intensity of 200, 500, 800, and  $1500 \mu\text{mol m}^{-2} \text{s}^{-1}$ . In these experiments, the pH and temperature were maintained at pH 7 and 27.5°C.

The reproducibility was investigated by performing replicate experiments for the experiments at pH 7, 27.5°C (duplicate), pH 5, 20°C (triplicate), and pH 9, 35°C (duplicate). Interpolation was used for data interpretation. Interpolation was performed using the Matlab (MathWorks inc., USA) function 'interp2' using the 'spline' algorithm.

### **4.2.4 Analyses**

#### **4.2.4.1 Dry weight concentration.**

The dry weight concentration was determined by filtrating culture broth over glass fibre filters and measuring the mass increase of the dried filters as described by Kliphuis et al. (2012).

#### **4.2.4.2 Total fatty acid concentration and composition.**

The total fatty acid concentration and composition were determined by a sequence of mechanical cell disruption, solvent based lipid extraction, transesterification of fatty acids to fatty acid methyl esters (FAMES), and quantification of FAMES using gas chromatography (GC-FID) as described by Lamers et al. (2010) and Santos et al. (2012) with modifications as described by Breuer et al. (2012).

#### **4.2.4.3 TAG and polar acyl lipid concentration and composition**

All lipophilic components were extracted as described by Breuer et al. (2012). This lipid fraction was fractionated into a TAG pool and polar acyl lipid pool using a solid phase extraction (SPE) column as described by Breuer et al. (2012). First, TAG was eluted from the column using 10ml 7:1 (v/v) hexane:diethylether. Thereafter, polar acyl lipids were eluted using 10ml 2:2:1 (v/v/v) methanol:acetone:hexane. Subsequently all solvents

were evaporated and the fatty acid concentration and composition in the two pools were determined by transesterification of fatty acids to FAMES. FAMES were subsequently quantified using GC-FID as described by Breuer et al. (2012).

#### **4.2.4.4 Dissolved nitrate and nitrite concentration.**

The dissolved  $\text{NO}_3^-$  and  $\text{NO}_2^-$  (potentially formed by reduction of nitrate) concentrations in 0.2 $\mu\text{m}$ -filtrated culture broth were estimated using colorimetric strips (Merck; product number 1100200001) according to manufacturer's instructions. Nitrite ( $\text{NO}_2^-$ ) concentrations were always below the detection limit.

#### **4.2.5 Calculation of time-specific, time-averaged yield, and maximum time-averaged yield**

Yields of biomass, total fatty acids, and TAG on light (g/mol photon) were calculated by dividing the amount produced in a certain period by the amount of light supplied in that period. The amount of light supplied was calculated by multiplying the incident light intensity (photon flux density), illuminated reactor surface area (0.0271  $\text{m}^2$ ), and duration of illumination.

All yields presented in this paper were calculated based on the incident light intensity. Calculated yields based on absorbed light would be only slightly higher, since the high biomass concentrations in the bioreactor ensured that only a small fraction of the incident light was not absorbed.

A distinction is made between the time-specific yield and the time-averaged yield. The time-specific yield is calculated between two consecutive time points. The time-averaged yield is calculated for each time point over the period between that time point and the start of the experiment ( $t=0$ ). The maximum time-averaged yield is then defined as the maximum value of all time-averaged yields observed during one experiment.

### **4.3 Results and discussion**

#### **4.3.1 Batch TAG accumulation experiments**

Among all investigated cultivation conditions, similar growth and TAG accumulation patterns, but different final concentrations and yields were observed. This paragraph discusses the general patterns observed using the cultivation at pH 7, temperature of 27.5°C, and an incident light intensity of 500  $\mu\text{mol m}^{-2} \text{s}^{-1}$  as an example (Fig. 4.2). The other paragraphs discuss the main differences observed between the different cultivation conditions. The dynamics of all cultivation conditions are shown in supplementary data 1 of the online published version of this chapter (Breuer et al., 2013b).

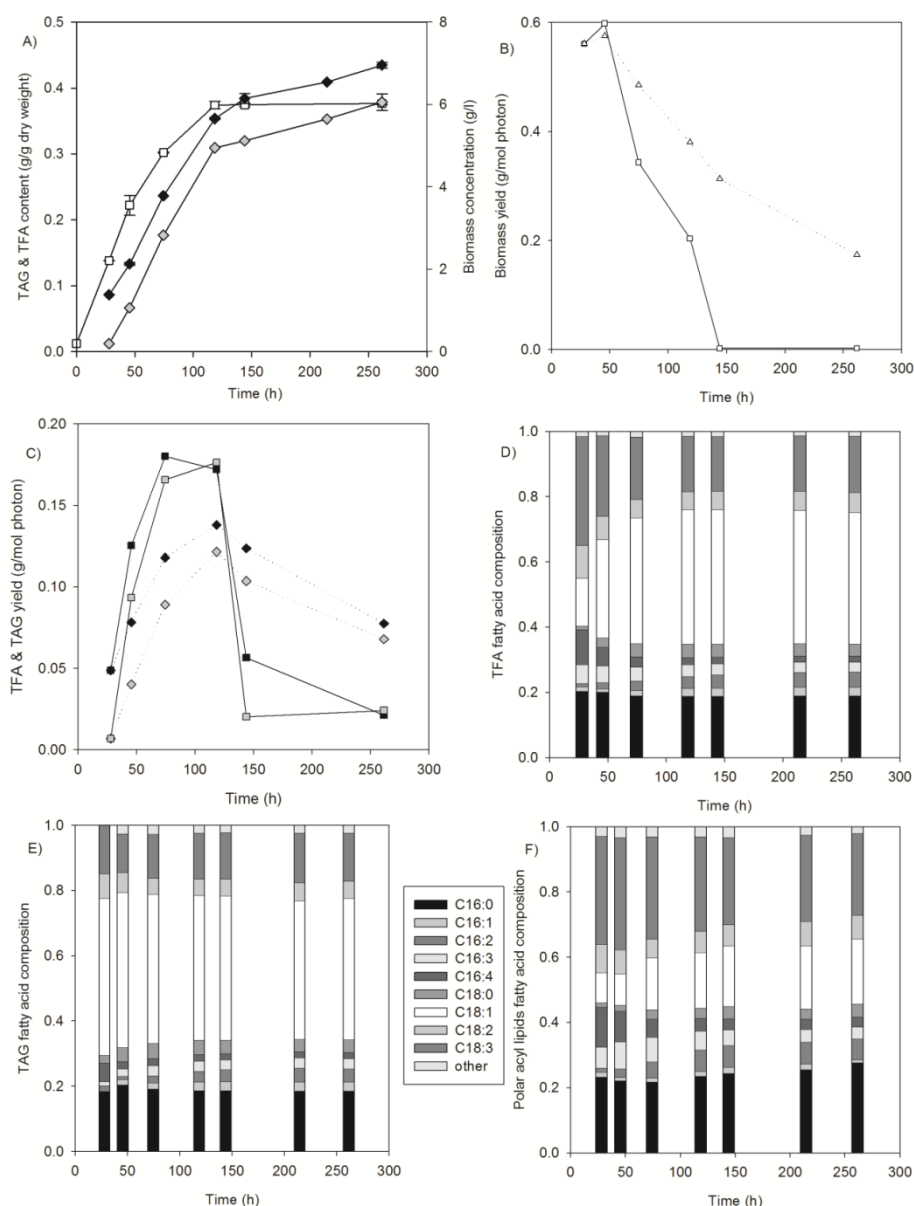


**Fig. 4.2.** Dynamics of TAG accumulation induced by nitrogen starvation. A: biomass concentration (white rectangles), total fatty acid content (black diamonds), and TAG content (grey diamonds); B: biomass yield between two consecutive time points (rectangles) and yield averaged over the period between  $t=0$  and each time point (triangles); C: TFA (black) and TAG (grey) yield between two consecutive time points (rectangles) and the yield averaged over the period between  $t=0$  and each time point (diamonds); D: fatty acid composition of total fatty acids; E: fatty acid composition of fatty acids in TAG pool; F: fatty acid composition of fatty acids in polar acyl lipids pool.

Sufficient nitrate was added to the culture medium (10 mM) to achieve a biomass concentration of 1.5-2 g/l without nitrogen limitation. After this concentration was reached and nitrate was depleted (confirmed as described in paragraph 2.4.4), the biomass concentration continued to increase at a constant rate ( $\text{g l}^{-1} \text{ day}^{-1}$ ) for typically 50 to 100 hours. Hereafter, the biomass productivity was significantly reduced, halted, or even a decrease in biomass concentration was observed. Maximum biomass concentrations reached were between 2 and 8 g/l, depending on cultivation conditions (Fig. 4.2A).

The total fatty acid (TFA) content increased from 7-9% (% of dry weight) under nitrogen replete conditions to a maximum of 30-45% during nitrogen starvation. The TAG content increased from approximately 2% to typically 30-40% (% of dry weight). The TFA and TAG content typically increased during a period of 150 to 250 hours (Fig. 4.2A).

From the results, the time-specific and the time-averaged yields of TFA, TAG, and biomass were calculated. The time-specific yield provides information about the actual efficiency at which photons are used and gives insight into the actual production rates of individual components at every moment during the experiment. The time-averaged yield can be used to determine the optimal time of harvest and it is also an important parameter for the comparison of different process designs. Furthermore, because the amount of light supplied to a certain area is fixed, the time-averaged yield on light is directly proportional to the areal productivity and can therefore be used to extrapolate lab-scale data to areal productivities of large scale outdoor photobioreactors.

For example, extrapolation of the yields obtained in this study, using basic assumptions and solar irradiance data, results in areal productivities ranging from 2.5 to 34.6 metric tonne fatty acids  $\text{ha}^{-1} \text{ year}^{-1}$ , depending on geographic location and photobioreactor design (Appendix A).

The time-specific yield of biomass on light was highest during the initial part of the cultivation during which nitrogen was not yet depleted. Once nitrogen was depleted, the time-specific yield of biomass on light decreased rapidly (Fig. 4.2B).

Both the time-specific and time-averaged yields of TFA and TAG on light, on the other hand, were initially low because absorbed photons were mainly used for the production of biomass other than TFA and TAG (e.g. proteins). After nitrogen was depleted, both the time-specific and time-averaged yield of TFA and TAG on light increased rapidly, after which the time-specific yield remained constant for a short period. During this period, TFA and TAG were produced with the maximum efficiency that was attainable under the cultivation conditions of the respective experiment. After this period, both the time-specific and time-averaged yield decreased again (Fig. 4.2C) but TFA and TAG

accumulation continued. The maximum time-averaged yield of TFA and TAG on light was therefore achieved before fatty acid accumulation was complete. In some cases, degradation of biomass, TFA, or TAG was observed at the end of the experiment, characterized by a negative yield on light.

In the presented example, the maximum time-averaged yield of TFA and TAG was achieved after 119h of cultivation (138 and 122 mg/mol photon for TFA and TAG, respectively). At this point the TFA and TAG contents were 35% and 31% of dry weight, respectively, while at the end of the cultivation final contents of 44% and 38% (% of dry weight) were achieved, respectively.

As commonly observed, a large change in the fatty acid composition of TFA was observed once nitrogen was depleted (Breuer et al., 2012; Griffiths et al., 2011). The relative abundance of C18:1 increased, counterbalanced by a decrease in C18:3 and C16:4. The C16:0 abundance remained more or less constant. The largest shift in the composition of TFA was observed in the first two days of nitrogen starvation (Fig. 4.2D). As also shown by Popovich et al. (2012) for *Neochloris oleoabundans*, this change in fatty acid composition is a result of a change in lipid class composition, since the fatty acid composition of both the TAG and the polar acyl lipid pool remained more or less constant during the experiment (Fig. 4.2E,F).

As explained in paragraph 2.2, after sampling, the culture volume was restored by adding 0.2 $\mu$ m-filtered demineralized water. This resulted in a dilution of the culture, which could result in an underestimation of the achievable concentrations and yields. This dilution was similar between different experiments and the impact of the dilution on the results was much smaller than the differences observed between the different experiments.

#### **4.3.2 Effect of pH and Temperature on TAG accumulation**

To study the impact of pH and temperature on TAG accumulation, experiments were performed at all combinations of pH 5, 7, and 9, and 20, 27.5, and 35°C. All experiments were performed at the same incident light intensity of 500  $\mu$ mol m<sup>-2</sup> s<sup>-1</sup>. TAG accumulated under all conditions. The highest final biomass concentration (Fig. 4.3A) and the highest initial biomass productivity (Fig. 4.3B) were observed at pH 7, 27.5°C. In general, conditions that favoured biomass formation also resulted in higher TAG and TFA contents. Final TFA content varied between 28% and 43% of dry weight (Fig. 4.3C) and TAG accounted for 69% to 93% of TFA (Fig. 4.3D) resulting in final TAG contents between 18% and 40% of dry weight (Fig. 4.3E). At 20 and 35°C, the TFA and TAG content increased with increasing pH. This is in accordance with the observation

that a high pH, especially in combination with nitrogen starvation, can enhance TAG accumulation (Gardner et al., 2010; Guckert & Cooksey, 1990; Santos et al., 2012). The highest maximum time-averaged yield of TFA on light was observed at pH 7, 27.5°C (0.138 g/mol) and decreased as much as 5 fold at sub optimal pH and temperature (Fig. 4.3F). This TFA yield corresponded with a yield of TAG on light of 0.122 g/mol. Despite the fact that at a temperature of 27.5°C and pH 7 the highest time-averaged yields and productivities were observed, the economic and energetic optimum for TAG production might differ. Cultivation at suboptimal temperature or pH can save energy and investments in equipment for cooling, heating, or CO<sub>2</sub> transfer. The presented results can be used as a tool to calculate the reduction in productivity and yield when cultivated at suboptimal biological conditions. This can in turn be used to calculate the energetic and economic optimum when information is available about the relation between the cultivation conditions and the energy and costs involved in heating, cooling, and aeration of the photobioreactor.

#### **4.3.3 Effect of light intensity on TAG accumulation**

To study the impact of light intensity on TAG accumulation, experiments were performed at incident light intensities of 200, 500, 800, and 1500  $\mu\text{mol m}^{-2} \text{s}^{-1}$ . These experiments were performed at pH 7 and a temperature of 27.5 °C, the optimum for TAG production as determined in paragraph 3.2.

Similar maximum biomass concentrations were observed between all incident light intensities investigated (Fig. 4.4A). This suggests that the biomass concentrations that were achieved in the experiments were not limited by the light intensity, but were limited by the amount of nitrogen provided. Maximum achievable TAG and TFA content were also found to be independent of the incident light intensity (Fig. 4.4B). In existing literature, both observations that lipid content and lipid accumulation are only affected to a minor extend by light intensity (Pal et al., 2011; Simionato et al., 2011) as well as observations that lipid content increases with light intensity have been made (Liu et al., 2012). These differences can partly be explained by the fact that the impact of light intensity was not always isolated from the impact of nutrient starvation.



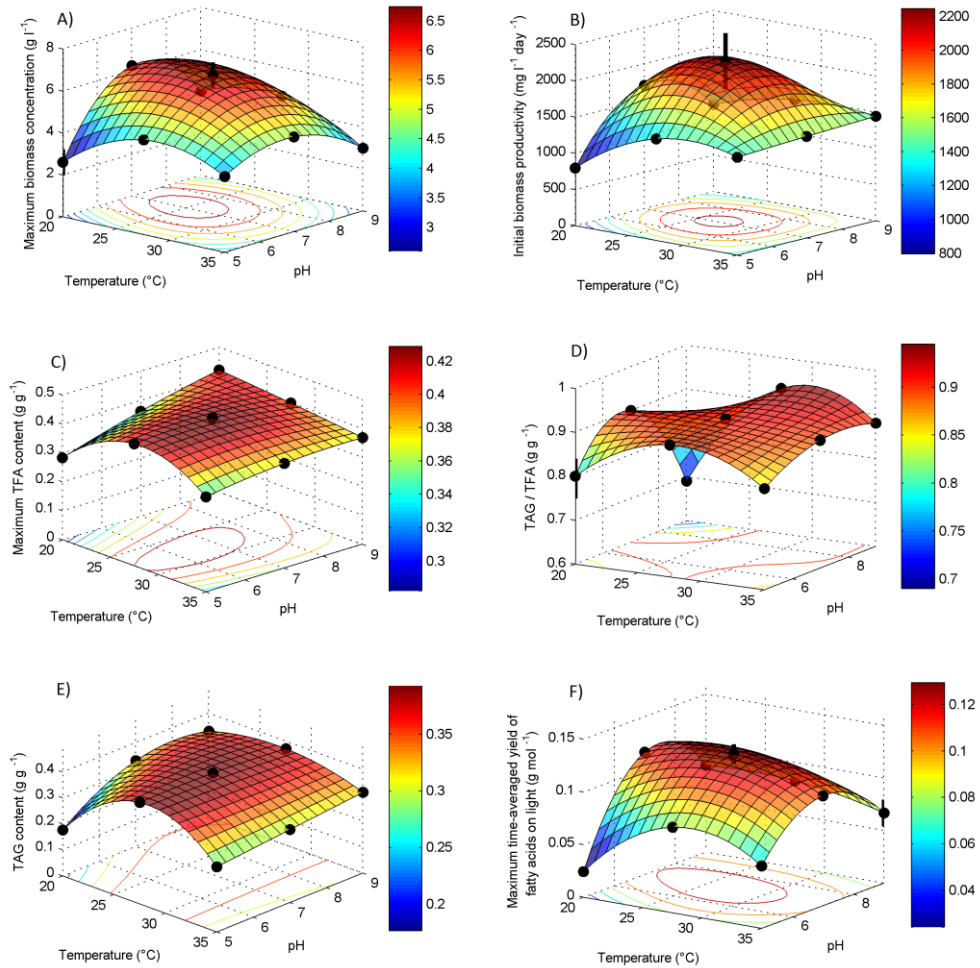


**Fig. 4.3.** The impact of pH and temperature on the maximum biomass concentration, initial biomass productivity, maximum TFA content, TAG fraction of TFA (determined when TFA content was maximum), TAG content (determined when TFA content was maximum), and maximum time-averaged yield of TFA on light. Interpolation between data-points was done using the Matlab function `interp2` using the 'spline' algorithm. Average values between replicates are shown (black dots) and the black vertical bars represent minimum and maximum values observed in replicate experiments ( $n=2$  for pH 7, 27.5°C and pH 9, 35°C;  $n=3$  for pH 5, 20°C;  $n=1$  for all other experiments).

In contrast to the impact on the biomass concentration and the maximum achievable TAG and TFA content, large differences were observed in the maximum time-averaged yield of TFA and biomass on light at the different light intensities. For example, between incident light intensities of 200 to 1500  $\mu\text{mol m}^{-2} \text{s}^{-1}$ , the maximum time-averaged yield

of TFA on light decreased from 0.263 to 0.048 g TFA per mol photons provided (Fig. 4.4C).

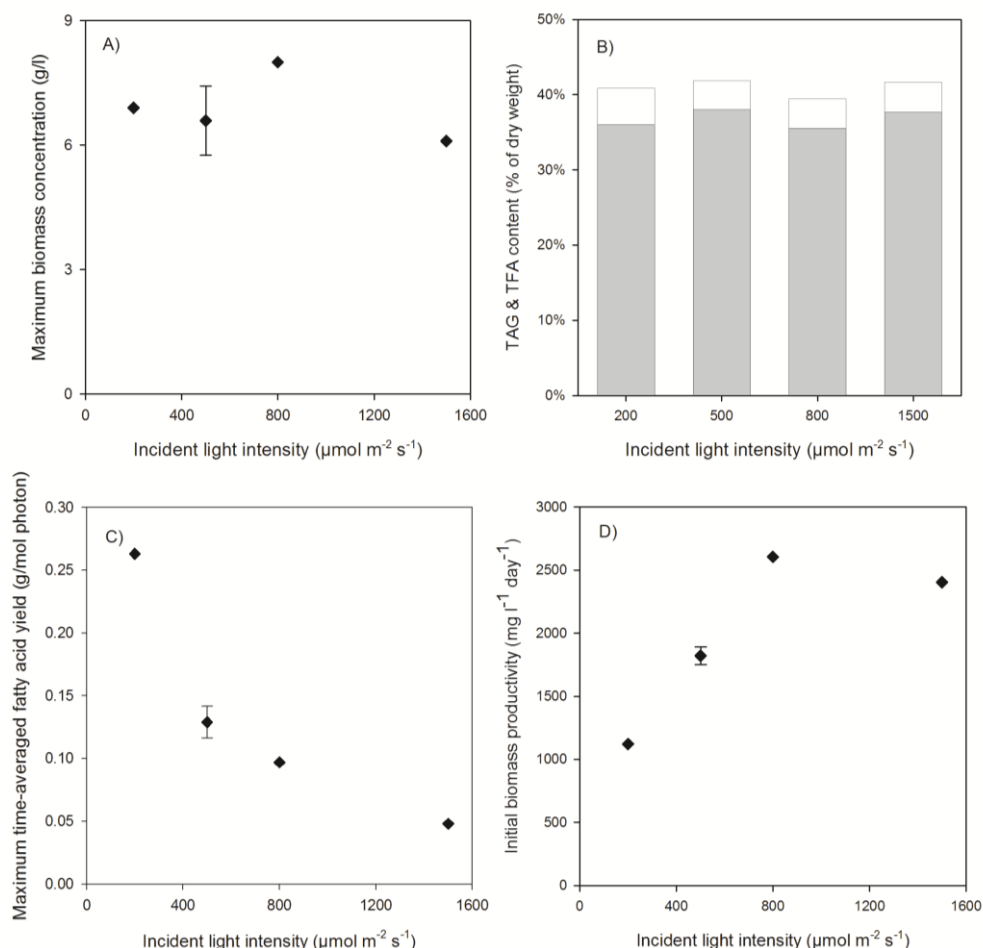


**Fig. 4.4.** The impact of light intensity on biomass formation and TAG accumulation. A: Maximum biomass concentration achieved during cultivation; B: TAG (grey bars) and polar acyl lipids (white bars) content when TFA content was maximal. The sum of the two bars represents the total fatty acid content; C: Maximum time-averaged yield of fatty acids on light; D: Initial biomass productivity. For all experiments  $n=1$  except for an incident light intensity of 500  $\mu\text{mol m}^{-2} \text{s}^{-1}$ , where  $n=2$ .

From these results it can be concluded that a low incident light intensity is most beneficial for TAG production, since similar biomass concentrations and maximum achievable TAG contents are achieved compared to high light intensities, but at a higher time-averaged yield.

In the case of outdoor production, a very high incident light intensity is provided by direct sunlight, but to utilize the full potential of the microalgae, a low light intensity is required. As suggested by Cuaresma et al. (2011) and Wijffels & Barbosa (2010), this could for a part be achieved by using vertically oriented reactors, under the condition that they are constructed from light diffusing/reflective material. This distributes the light over a larger reactor area and lowers the incident light intensity on the reactor surface.

To the best of our knowledge, this is the first report of yields of TFA and TAG on photons under nitrogen starved conditions. Although, some areal lipid productivities have previously been reported in combination with solar radiation data, from which yields can be deduced. For example, from the results of Bondioli et al. (2012) an average yield of 0.21 g total lipids/mol PAR photons can be deduced (average irradiance of  $26 \text{ MJ m}^{-2} \text{ day}^{-1}$  in combination with an average lipid productivity of  $6.5 \text{ g m}^{-2} \text{ day}^{-1}$ ) or from the results of Rodolfi et al. (2009) an average yield 0.30 g total lipids/mol PAR photons can be deduced (average irradiance of  $15.4 \text{ MJ m}^{-2} \text{ day}^{-1}$  in combination with an average lipid productivity of  $9 \text{ g m}^{-2} \text{ day}^{-1}$ ), both for *Nannochloropsis* sp. In these calculations, it is assumed that photons in the photosynthetic active radiation (PAR) spectrum have an energy content of 0.217 MJ/mol and it is assumed that 42% (J/J) of the irradiance has a wavelength within the PAR spectrum. It should be noted, however, that the areal lipid productivities reported by Rodolfi et al. (2009) and Bondioli et al. (2012) were determined using total lipid measurements, rather than total fatty acid measurements. Total lipid contents (and thus productivities and yields) will always be higher than total fatty acid contents since not all lipophilic components contain fatty acids.

#### **4.3.4 Effect of light intensity, pH, and temperature on fatty acid composition**

The fatty acid composition was found to be dependent on pH and temperature. TAG consisted mainly of C16:0, C18:1, and C18:3 fatty acids under all investigated cultivation conditions. Among all investigated cultivation conditions, the relative abundance of these fatty acids in the TAG pool varied between 14-27%, 32-53%, and 12-21% respectively.

The degree of unsaturation (average number of double bonds per fatty acid) decreased with both increasing temperature and pH (Fig. 4.5A). In many microalgae species a general trend towards a higher degree of fatty acid unsaturation at lower temperatures is observed (Hu et al., 2008). At the individual fatty acid level, large variations were observed in the relative abundance of the three most abundant fatty acids between the different cultivation conditions (Fig. 4.5B-D).

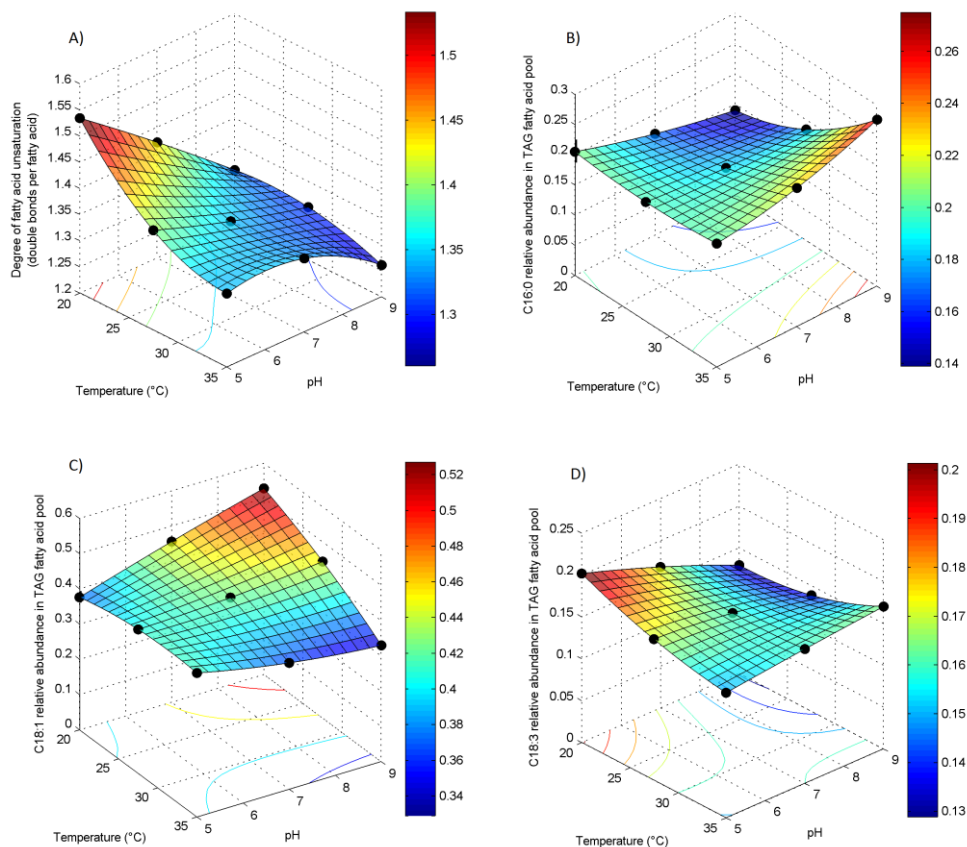


**Fig. 4.5.** The impact of pH and temperature on the fatty acid composition of the TAG fatty acid pool. A: Degree of unsaturation (average number of double bonds per fatty acid); B: Relative abundance of C16:0; C: Relative abundance of C18:1; D: Relative abundance of C18:3. Interpolation between data-points was done using the Matlab function `interp2` using the 'spline' algorithm. Average values between replicates are shown (black dots) and the black vertical bars represent minimum and maximum values observed in replicate experiments ( $n=2$  for pH 7, 27.5°C and pH 9, 35°C;  $n=3$  for pH 5, 20°C;  $n=1$  for all other experiments).

In accordance with other reports (Liu et al., 2012; Pal et al., 2011), light intensity had only a minor impact on the fatty acid composition. The relative abundance of C18:3 in the TAG pool increased with increasing light intensity under nitrogen starved conditions (Fig. 4.6A). This resulted in an increase of the degree of unsaturation with light intensity from a value of 1.26 at  $200 \mu\text{mol m}^{-2} \text{s}^{-1}$  to a value of 1.43 at  $1500 \mu\text{mol m}^{-2} \text{s}^{-1}$ . Variations were observed in the fatty acid composition of the polar acyl lipids but no clear trends were observed (Fig. 4.6B).

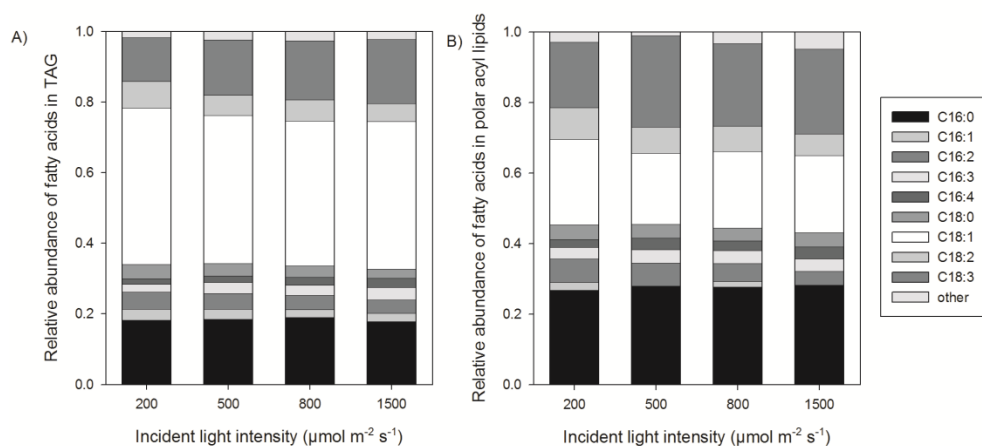


**Fig. 4.6.** Effect of the incident light intensity on the fatty acid composition under nitrogen starved conditions. A: fatty acid composition of TAG; B: Fatty acid composition of polar acyl lipids. The fatty acid compositions correspond to the TAG and polar acyl lipids contents in Fig. 4.4.

#### 4.4 Conclusions

The highest time-averaged yield of fatty acids on light (0.263 g fatty acids/mol photons) was observed at pH 7, 27.5°C, and an incident light intensity of 200  $\mu\text{mol m}^{-2} \text{s}^{-1}$ .

Suboptimal pH and temperatures reduced both TAG content and yield. Higher light intensities resulted in the same TAG content, but resulted in lower yields. The maximum time-averaged yields were observed before TAG accumulation was complete.

#### Acknowledgements

This research project is financially supported by the Food and Nutrition Delta program of Agentschap NL (FND10007) and Unilever.

**Appendix A: Extrapolation of photosynthetic TAG yields to areal productivities.**

Most extrapolations of lab-scale data to areal lipid productivities are based on multiplication of the maximum achievable lipid content under nitrogen deplete conditions with biomass productivities or photosynthetic efficiencies under nitrogen replete conditions (Quinn et al., 2011b). This will lead to erroneous results because nitrogen starvation reduces the photosynthetic efficiency. This reduction needs to be taken into account.

Since the amount of light supplied to a certain area is fixed, the areal productivity is directly proportional to the time-averaged yield on light. This makes the time-averaged yield on light a very important characteristic. The yields of TAG on light that are found in this work include the impact of nitrogen starvation.

The highest time-averaged yield of TFA on light in *S. obliquus* was obtained at pH 7, 27.5°C and was strongly dependent on the incident light intensity. Between incident light intensities of 200 to 1500  $\mu\text{mol m}^{-2} \text{s}^{-1}$ , the maximum time-averaged yield of TFA decreased from 0.263 to 0.048 g TFA per mol photons provided.

When it is assumed that, under outdoor production conditions, yields can be achieved that are similar to our lab-scale experiments, these yields can be used to extrapolate lab-scale data to estimations of areal lipid productivities using basic assumptions and solar irradiance data.

**A.1 Calculation and assumptions**

The areal productivity can be calculated by multiplying the annual areal supply of photons in the photosynthetic active radiation (PAR) spectrum with the time-averaged yield of total fatty acids on photons as determined experimentally. This value is corrected for losses during nocturnal respiration and downtime of the photobioreactor (Eq 1).

$$\text{Areal productivity (g TFA m}^{-2} \text{ year}^{-1}) = Y_{\text{TFA,I}} \cdot \frac{I \cdot \text{PAR}}{E} \cdot (1 - r) \cdot \text{Operation} \quad (\text{Eq 1}).$$

All values used are listed in Table A1.

**Table A1.** Assumptions and constants used in the extrapolation of measured yields of total fatty acids on light to areal productivities.

Constant	Description	Value	Unit
h	Planck's constant	$6.626 \cdot 10^{-34}$	J s
c	Speed of light	$2.998 \cdot 10^8$	m s <sup>-1</sup>
N <sub>A</sub>	Number of Avogadro	$6.022 \cdot 10^{23}$	mol <sup>-1</sup>
λ	Wavelength		nm
I <sub>ph</sub> (λ)	Photon flux density of wavelength λ in reference solar spectrum <sup>1</sup>		μmol m <sup>-2</sup> s <sup>-1</sup> nm <sup>-1</sup>
I <sub>PAR</sub>	Cumulative photon flux density of all wavelengths in PAR spectrum in reference solar spectrum <sup>1</sup>	$\int_{400}^{700} I_{ph}(\lambda) d\lambda$	μmol m <sup>-2</sup> s <sup>-1</sup>
E	Average energy of photons in PAR range of reference solar spectrum	$N_A \int_{400}^{700} \frac{I_{ph}(\lambda)}{I_{PAR}} \frac{h \cdot c}{\lambda} d\lambda$ =0.217233	MJ mol <sup>-1</sup>
I	Annual insolation <sup>2</sup>	NE <sup>3</sup> = 3600 SE <sup>4</sup> = 6480 SH <sup>5</sup> = 9000	MJ m <sup>-2</sup> year <sup>-1</sup>
PAR	Fraction of photosynthetic active radiation (PAR) in solar spectrum <sup>1</sup>	0.4234	J J <sup>-1</sup>
Y <sub>TFA,I</sub>	Maximum time-averaged yield of total fatty acids on light as determined experimentally	low: 0.048 high: 0.263	g mol <sup>-1</sup>
r	Fraction of absorbed energy lost to nocturnal respiration	0.1	J J <sup>-1</sup>
Operation	Annual duration that photobioreactor is in use	10/12	month month <sup>-1</sup>

<sup>1</sup>Solar spectrum obtained from ASTM International (<http://rredc.nrel.gov/solar/spectra/am1.5/ASTMG173/ASTMG173.html>)

<sup>2</sup>Irradiance data from SolarGis (<http://solargis.info/>)

<sup>3</sup>NE = Northern Europe

<sup>4</sup>SE = Southern Europe.

<sup>5</sup>SH = Sahara

## A.2 Results and Discussion

The areal productivity was calculated for both a high yield scenario in which it is assumed that illumination in the photobioreactor is always optimal. The (higher) maximum time-averaged yield obtained in experiments at low incident light intensity

( $200 \mu\text{mol m}^{-2} \text{s}^{-1}$ ) was used to calculate this scenario. Also a low yield scenario was considered, in which it was assumed that illumination is not optimized in the photobioreactor. In this scenario, the maximum time-averaged yield at a high incident light intensity ( $1500 \mu\text{mol m}^{-2} \text{s}^{-1}$ ) was used. Three geographic locations were considered: Northern Europe, Southern Europe, and the Sahara. These locations respectively have a low, medium, and high irradiance. These extrapolations result in estimated areal productivities ranging from 2.5 to 34.6 metric tonne TFA  $\text{ha}^{-1} \text{year}^{-1}$  (Table A2).

The areal fatty acid productivity of *S. obliquus* could thus be up to 6 times higher than is currently achieved with the most productive terrestrial plant (Chisti, 2007). Our estimations are low, when compared to extrapolations based on multiplication of biomass productivity or photosynthetic efficiency under nitrogen replete conditions with maximum achievable lipid contents under nitrogen deplete conditions (Quinn et al., 2011b). However, our estimations, despite being based on yields obtained under continuous light, are consistent with reported areal lipid productivities obtained under outdoor cultivation conditions (Bondioli et al., 2012; Quinn et al., 2012; Rodolfi et al., 2009).

**Table A2.** Extrapolated areal total fatty acid productivity of *S. obliquus* cultivated in photobioreactors designed with both non-optimized and optimized illumination, in three different geographic locations (low, medium, and high irradiance).

	<b>Areal productivity (metric tonne of fatty acids <math>\text{ha}^{-1} \text{year}^{-1}</math>)</b>		
	<b>Northern Europe<sup>1</sup> I=3600 MJ <math>\text{m}^{-2}</math> year<sup>-1</sup></b>	<b>Southern Europe<sup>1</sup> I=6480 MJ <math>\text{m}^{-2}</math> year<sup>-1</sup></b>	<b>Sahara<sup>1</sup> I=9000 MJ <math>\text{m}^{-2}</math> year<sup>-1</sup></b>
Non-optimized illumination photobioreactor ( $Y_{\text{TFA,I}} = 0.048 \text{ g mol}^{-1}$ )	2.5	4.5	6.3
Optimized illumination in photobioreactor ( $Y_{\text{TFA,I}} = 0.263 \text{ g mol}^{-1}$ )	13.8	24.9	34.6

<sup>1</sup> Irradiance data from SolarGis (<http://solargis.info/>)







## **Chapter 5** Superior triacylglycerol (TAG) accumulation in starchless mutants of *Scenedesmus obliquus*: Evaluation of TAG yield and productivity in controlled photobioreactors

**This chapter has been published as:**

Guido Breuer<sup>†</sup>, Lenny de Jaeger<sup>†</sup>, Valentin P. G. Artus, Dirk E. Martens, Jan Springer, René B. Draaisma, Gerrit Eggink, René H. Wijffels, Packo P. Lamers (2014), Superior triacylglycerol (TAG) accumulation in starchless mutants of *Scenedesmus obliquus*: (II) evaluation of TAG yield and productivity in controlled photobioreactors, *Biotechnology for Biofuels* 7:70

<sup>†</sup>Both authors contributed equally to this work.

**Abstract**

Many microalgae accumulate carbohydrates simultaneously with triacylglycerol (TAG) upon nitrogen starvation, and these products compete for photosynthetic products and metabolites from the central carbon metabolism. As shown for starchless mutants of the non-oleaginous model alga *Chlamydomonas reinhardtii*, reduced carbohydrate synthesis can enhance TAG production. However, these mutants still have a lower TAG productivity than wild-type oleaginous microalgae. Recently, several starchless mutants of the oleaginous microalga *Scenedesmus obliquus* were obtained which showed improved TAG content and productivity.

The most promising mutant, *slm1*, is compared in detail to wild-type *S. obliquus* in controlled photobioreactors. In the *slm1* mutant, the maximum TAG content increased to  $57 \pm 0.2\%$  of dry weight versus  $45 \pm 1\%$  in the wild-type. In the wild-type, TAG and starch were accumulated simultaneously during initial nitrogen starvation, and starch was subsequently degraded and likely converted into TAG. The starchless mutant did not produce starch and the liberated photosynthetic capacity was directed towards TAG synthesis. This increased the maximum yield of TAG on light by 51%, from  $0.144 \pm 0.004$  in the wild-type to  $0.217 \pm 0.011$  g TAG/mol photon in the *slm1* mutant. No differences in photosynthetic efficiency between the *slm1* mutant and the wild-type were observed, indicating that the mutation specifically altered carbon partitioning while leaving the photosynthetic capacity unaffected.

The yield of TAG on light can be improved by 51% by using the *slm1* starchless mutant of *S. obliquus*, and a similar improvement seems realistic for the areal productivity in outdoor cultivation. The photosynthetic performance is not negatively affected in the *slm1* and the main difference with the wild-type is an improved carbon partitioning towards TAG.

## 5.1 Introduction

Microalgae are well known for their ability to produce large quantities of triacylglycerol (TAG), which can be used as a resource for food, feed, and fuel production (Draaisma et al., 2013; Wijffels & Barbosa, 2010). Microalgae-derived TAGs can be competitive to oils derived from terrestrial plants due to the higher areal productivities of microalgae and because no arable land is required for their cultivation (Wijffels & Barbosa, 2010). However, the economic costs and carbon footprint of photobioreactors make it necessary to improve the areal TAG productivity even further (Brentner et al., 2011; Norsker et al., 2011).

The dogma on the physiological role of TAG synthesis is that TAG serves as a compact energy and carbon storage pool when formation of functional biomass is impaired. Furthermore, TAG can serve as an electron sink under unfavourable conditions for growth. An electron sink under these conditions prevents the build-up of photosynthetic products which would otherwise have resulted in over-reduction of the electron transport chains. Such over-reduction can result in the transfer of electrons to O<sub>2</sub>, which results in the formation of reactive oxygen species (ROSs), such as H<sub>2</sub>O<sub>2</sub>, or superoxide (Asada, 2006). These ROS can cause damage to the cell. Production of TAG can thus protect the cell against the damage induced by adverse growth conditions (Hu et al., 2008). This is reflected by the fact that under nutrient replete conditions only trace amounts of TAG are produced. However, as a response to nitrogen starvation, TAG can be accumulated to over 40% of dry weight by many oleaginous microalgae species (Breuer et al., 2012; Griffiths et al., 2011; Hu et al., 2008).

Although nitrogen starvation reduces photosynthetic efficiency (Klok et al., 2013a), photosynthesis and carbon assimilation continue for a certain period when the microalgae are exposed to nitrogen depleted conditions (Simionato et al., 2013). This is supported by the observation of an up to eight-fold increase in biomass dry weight concentration after nitrogen depletion in some species (Breuer et al., 2012). This increase in biomass can be explained by de novo production of nitrogen-free storage molecules such as TAG and carbohydrates. Even in the most oleaginous species, the increase in dry weight cannot solely be explained by the observed TAG production (Breuer et al., 2012). Other storage components such as starch are simultaneously accumulated and can easily account for over 40% of the newly produced biomass (Breuer et al., 2012; Klok et al., 2013b; Li et al., 2011; Zhu et al., 2013). Diverting this

large carbon flow away from carbohydrates towards TAG could substantially enhance TAG productivity (Li et al., 2010a).

The partitioning of assimilated carbon between TAG and carbohydrates during nitrogen starvation is a complex and highly regulated process as indicated by the activity of transcription factors and the observed changes in transcriptome and proteome during nutrient starvation (Blaby et al., 2013; Boyle et al., 2012; Dong et al., 2013; Valenzuela et al., 2012). In addition, it is often proposed that the production rates of TAG and storage carbohydrates are influenced by competition for common pre-cursors, that is, intermediates of the central carbon metabolism such as glyceraldehyde-3-phosphate (GAP) or acetyl coenzyme A (acetyl-CoA) (Fan et al., 2012; Msanne et al., 2012). Modifying the activity of either pathway using strain improvement techniques could therefore potentially affect the carbon partitioning between TAG and storage carbohydrates (Li et al., 2010a). One commonly attempted strategy to accomplish this is to over-express reactions in the TAG synthesis pathway, such as the initial step in fatty acid synthesis catalysed by acetyl-CoA carboxylase (Dunahay et al., 1996) or the acyl-transfer step catalysed by diacylglycerol acyltransferase (DGAT) (La Russa et al., 2012). However, attempts to improve TAG production by increasing the expression of genes involved in the TAG biosynthesis pathway have been mostly unsuccessful as reviewed by Li et al. (2010b).

Another commonly employed strategy is to down-regulate or inhibit the competing carbohydrate (for example, starch) synthesis. Several successful attempts have been made to enhance TAG production by reducing or eliminating starch synthesis (Li et al., 2010a; Li et al., 2010b; Ramazanov & Ramazanov, 2006; Siaux et al., 2011; Wang et al., 2009). For example, Li et al. (2010b) observed an eight-fold increase in TAG content (reaching a TAG content of 32.6% of dry weight) under mixotrophic conditions and Li et al. (2010a) observed a four-fold increase in volumetric TAG productivity under photoautotrophic conditions, both using the starchless BAFJ5 mutant of *Chlamydomonas reinhardtii*.

Although cellular TAG contents are generally enhanced in starchless or impaired mutants, the overall TAG productivity of such mutant cultures is not always improved. This is because their biomass productivity under nitrogen starvation conditions is often largely reduced or even completely impaired compared to their wild-type strains (Li et al., 2010b). This reduction in biomass productivity is often poorly characterized with the focus only directed at the TAG content, making conclusive evaluations of the mutant

performance difficult. The decrease in biomass productivity could, among other possible explanations, be a result of additional mutations in, for example, the photosynthetic machinery (Siaut et al., 2011) or of insufficient capacity to channel all excess photosynthate towards TAG. Especially in the latter case, the impact of starch deficiency on oleaginous microalgae might be fundamentally different from that on non-oleaginous microalgae. Namely, a starchless oleaginous microalga might be able to redirect most of the light energy that would otherwise have been used for starch synthesis towards TAG, whereas a non-oleaginous microalga might be unable to utilize this light energy. For a non-oleaginous microalga, this could thus lead to a quick build-up of photosynthetic products, which in turn could result in over-reduction of the photosynthetic machinery and the formation of harmful ROSs (Asada, 2006). This might occur at a lower rate in starchless oleaginous microalgae that are able to channel most excess photosynthate towards TAG synthesis.

Most previous work on starchless mutants is performed in the non-oleaginous model alga *C. reinhardtii* and shows that the use of starchless mutants can be a feasible strategy to enhance TAG production. However, even these starchless mutants under-achieve in TAG production compared to good-performing wild-type oleaginous microalgae. The TAG contents of these *C. reinhardtii* mutants are at best comparable to those of oleaginous microalgae (Breuer et al., 2012; Li et al., 2010a; Li et al., 2010b). In addition, upon nitrogen starvation their biomass productivity decreases to a much bigger extent than that of wild-type oleaginous microalgae (Breuer et al., 2012; Li et al., 2010b). Therefore, it is important to study the effect of disabling starch formation on TAG production in good-performing oleaginous microalgae.

In previous research, *Scenedesmus obliquus* (recently suggested to be reclassified to *Acutodesmus obliquus* (Krienitz & Bock, 2012)) was identified as a very promising microalga to produce TAG (Breuer et al., 2012; Griffiths et al., 2011) and recently several starchless mutants of *S. obliquus* were obtained (de Jaeger et al., 2014). In shake-flask studies, the *slm1* mutant showed both an enhanced TAG content during initial nitrogen starvation and a biomass productivity comparable to that of the wild-type, resulting in a net increase in volumetric TAG productivity (de Jaeger et al., 2014). In this work, a more detailed and quantitative comparison, performed in controlled photobioreactors, of the *S. obliquus* wild-type and this starchless mutant is presented.

## 5.2 Results and discussion

### 5.2.1 TAG and starch accumulation

For both the wild-type (wt) *S. obliquus* (UTEX 393) and a starchless mutant (slm1) of *S. obliquus* (de Jaeger et al., 2014), duplicate nitrogen run-out experiments were performed to investigate the difference in carbon partitioning between the wt and the slm1 under nitrogen depleted conditions (Fig. 5.1). Reactors were inoculated at 50 mg DW/l and cultivated at an incident light intensity of  $100 \mu\text{mol m}^{-2} \text{s}^{-1}$  until the biomass concentration was 0.3-1 g DW/l, after which the incident light intensity was increased to  $500 \mu\text{mol m}^{-2} \text{s}^{-1}$ . The moment of inoculation is considered as  $t=0$ .

Nitrogen was depleted from the culture medium at a biomass concentration of approximately 1.5-2 g/l and occurred 70 to 100h after inoculation (Fig. 5.1). After nitrogen was depleted, carbon assimilation and biomass formation continued, mainly as a result of accumulation of TAG (both the wt and the slm1) and starch (the wt only), which is consistent with previous observations (Breuer et al., 2013b; Breuer et al., 2012; de Jaeger et al., 2014). The wt increased more rapidly in biomass concentration than the slm1 during initial nitrogen starvation and also achieved a higher maximum biomass concentration (Fig 5.1A,B).

In the wt cultivation, starch and TAG were accumulated simultaneously after nitrogen was depleted. Initially starch was produced at a much higher rate than TAG (Fig. 5.1C) but when nitrogen starvation progressed starch synthesis stopped. Starch reached a maximum content of  $38 \pm 2\%$  (average of duplicate cultivations  $\pm$  deviation of duplicates from average) of dry weight after  $168 \pm 2$  h and a maximum concentration of  $3.6 \pm 0.2$  g/l after  $223 \pm 10$  h. Subsequently starch was degraded. The starch concentration at the end of the cultivation decreased to 0.5 g/l (6% of dry weight). During this period TAG synthesis continued and the TAG content reached a maximum of  $45 \pm 1\%$  of dry weight ( $4.5 \pm 0.1$  g/l) (Fig. 5.1C; Fig. 5.2A). The simultaneous degradation of starch and production of TAG in the wt could indicate that degradation products of starch are used for the synthesis of TAG. This inter-conversion has also been suggested previously for *Pseudochlorococcum* sp. (Li et al., 2011), *C. reinhardtii* (Msanne et al., 2012), *Coccomyxa* sp. (Msanne et al., 2012), and *Chlorella zofingiensis* (also known as *Chromochloris zofingiensis*) (Zhu et al., 2013), as well as for conversion of chrysolaminarin into TAG in the diatom *Cyclotella cryptica* (Roessler, 1988).



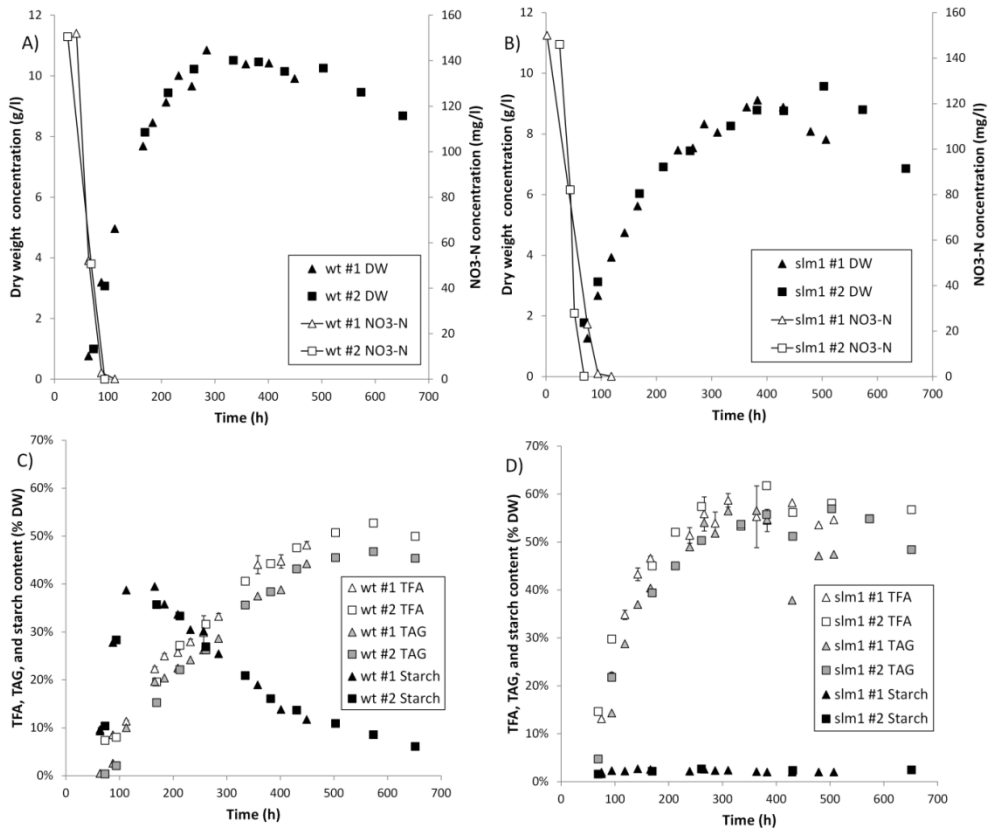


**Fig. 5.1** Duplicate batch nitrogen run-out cultivations of the wt and the slm1 *S. obliquus*. Left: wild-type. Right: slm1. Top: biomass concentration (g DW/l) and dissolved NO<sub>3</sub>-N concentration. Bottom: total fatty acid (TFA), TAG, and starch content. As indicated in the legend boxes in the figure, in the top figure, the black symbols represent the dry weight concentration and the open symbols represent the NO<sub>3</sub>-N concentration. In the bottom figures, the open symbols represent the total fatty acid content (TFA), the grey symbols represent the TAG content, and the black symbols represent the starch content. The results indicated with #1 and #2 in the figure legend represent the replicate cultivations.

In the slm1, the production of starch is negligible. As a result, the TAG content increases more rapidly in the slm1 than in the wt during initial nitrogen starvation; the TAG content in the slm1 reached a maximum of  $57 \pm 0.2\%$  of dry weight ( $5.2 \pm 0.2$  g/l) after  $433 \pm 70$  h (Fig. 5.1C,D; Fig. 5.2A).

In neither the wt nor the slm1 can the combined accumulation of starch and TAG completely account for the increase in dry weight after nitrogen depletion. This difference between the measured biomass constituents and dry weight concentration is

relatively constant and accounts for approximately 20 to 30% of dry weight during the entire cultivation for both the wt and the slm1. Proteins are most likely not part of this residual biomass as no nitrogen source is available for protein synthesis; also protein synthesis out of non-protein nitrogen present in the biomass can only contribute very little, because this fraction of non-protein nitrogen in the biomass is very small (Becker, 2007). It is likely that the cell wall will account for a substantial part of this residual biomass. Although little is known about the cell wall composition of *S. obliquus* and other microalgae, it is hypothesized that this residual biomass consists largely of carbohydrates (other than starch) such as cellulose, which is known to be a major constituent of the cell wall of *S. obliquus* and other microalgae (Aguirre & Bassi, 2013; Burczyk et al., 1970).

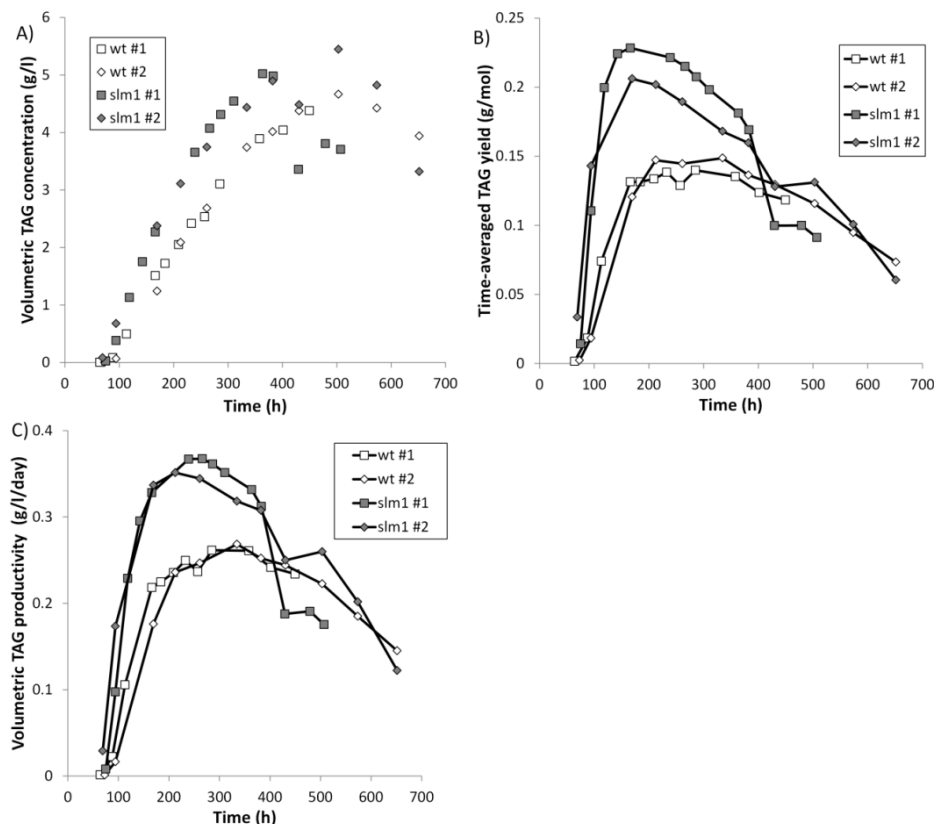


**Fig 5.2.** TAG concentration (A), time-averaged yield of TAG on photons (B), and time-averaged volumetric TAG productivity (C). Open symbols: wt. Grey symbols: slm1. The time-averaged yield and volumetric productivity are calculated over the period between inoculation and each time-point. The Results indicated with #1 and #2 in the figure legend represent the replicate cultivations.

### 5.2.2 Yields, productivity and implications for large-scale production

Using the measured TAG concentration at each time point (Fig. 5.2A) and the amount of light supplied specific to the reactor volume (calculated as the incident light intensity multiplied by the area-to-volume ratio of the reactor), the time-averaged yield of TAG on photons was calculated for each time-point (the yield of TAG on light achieved over the period between inoculation and each time point) (Fig. 5.2B). Because almost no TAG is produced during nitrogen replete conditions, this yield of TAG on light is very low during the initial part of the cultivation. After nitrogen depletion, the time-averaged yield increases to a maximum of  $0.217 \pm 0.011$  and  $0.144 \pm 0.004$  g TAG/mol photon for the *slm1* and wt, respectively (Fig. 5.2B). This illustrates that the *slm1* can achieve a 51% higher time-averaged yield of TAG on light than the wt. Similarly, the maximum volumetric productivity, calculated between inoculation and each time-point, was enhanced in the *slm1* by 35% compared to the wt and increased from a maximum of  $0.265 \pm 0.004$  in the wt to a maximum of  $0.359 \pm 0.008$  g TAG l<sup>-1</sup> day<sup>-1</sup> in the *slm1* (Fig. 5.2C). During the period that these maxima in yield and volumetric productivity were maintained, the TAG content increased to over 40% of dry weight for both the wt and the *slm1* (Fig. 5.1C,D; Fig. 5.2B,C).

After these maxima in yield and volumetric productivity were achieved, the difference in performance of the wt and the *slm1* became smaller when the cultivation progressed. This can be explained by the degradation of starch in the wt and possible inter-conversion into TAG. This could enhance the TAG contents in the wt at the end of the cultivation, resulting in a smaller difference between the *slm1* and wt at the end of the cultivation.

Due to the different behaviour of the wt and *slm1*, there is a difference in the biomass concentration in the wt and *slm1* cultivation (Fig. 5.1). This did not result in a difference in light absorption rates between the wt and *slm1* because nearly all light was absorbed in all cultures; therefore, a difference in the biomass concentration or pigmentation will only result in a difference in the light gradient in the photobioreactor. Furthermore, because all cultures were provided with the same amount of NO<sub>3</sub>, the amount of light absorbed per N-mol and per amount of catalytic biomass (assuming that the amount of catalytic biomass is proportional to the amount of nitrogen) is exactly the same.

When algae are cultivated using sunlight, the amount of light that can be provided to the photobioreactor is limited to the insolation to that area. The maximum areal productivity

is therefore directly proportional to the yield on light that can be achieved. Maximizing this yield of TAG on light can therefore contribute to improving the areal productivity of microalgal TAG production. The time-point where the highest time-averaged yield of TAG on light is achieved is therefore proposed as the optimum time-point to harvest the culture. Previously it has been shown that this yield can be enhanced by improving the photobioreactor design (Cuaresma et al., 2011; Wijffels & Barbosa, 2010) as well as optimizing cultivation conditions (Breuer et al., 2013b). In this work it is shown that this yield on light can be improved by 51% by using a starchless mutant, and a similar improvement seems realistic for the areal productivity in outdoor cultivation. It should be noted that at the moment this maximum was reached, the TAG content was over 40% of the dry weight.

In this work, all cultivations were performed using continuous illumination. However, during day-night cycles starch contents in microalgae oscillate, and starch can likely provide energy for nocturnal respiration (de Winter et al., 2013; Ral et al., 2006). This might complicate cultivation of starchless mutants in day-night cycles. In higher plants such as *Arabidopsis thaliana* it is indeed reported that starchless mutants show decreased growth rates and decreased net photosynthesis rates when grown under day-night cycles, whereas these are indistinguishable from their wild-types during continuous illumination (Caspar et al., 1985; Radakovits et al., 2010). The *slm1* mutant, however, does not show decreased growth under day-night cycles under nitrogen replete conditions and possibly the role of starch can be taken over by other storage metabolites (de Jaeger et al., 2014). Further investigation of the behaviour of *slm1* under day-night cycles and nitrogen depleted conditions would be of future interest.

### **5.2.3 Photosynthetic energy distribution in the wt compared to the *slm1***

The biomass productivity was lower in the *slm1* than in the wt during the initial period of nitrogen starvation. Because exactly the same amount of light was supplied, this might at first suggest a reduced photosynthetic efficiency in the *slm1*. However, lipids (for example TAG) are much more energy dense than carbohydrates, (37.6 kJ/g for lipids compared to 15.7 kJ/g for carbohydrates (Jakob et al., 2007)). The difference in metabolic costs required to produce TAG and starch can completely explain the observed difference in biomass productivity. To illustrate this, we compare the photosynthetic requirement for the observed biomass production after nitrogen depletion in the wt and the *slm1*. To calculate this photosynthetic requirement, it is assumed that after nitrogen depletion only TAG, starch, and other carbohydrates (such as cell wall cellulose) are

produced. The TAG and starch concentration are measured at each time-point (Fig. 5.1) and it is assumed that the remaining newly produced biomass consists of other carbohydrates (calculated as the amount of dry weight produced minus the amounts of TAG and starch produced). The photosynthetic requirement to produce the biomass that is made between nitrogen depletion and time-point  $t$  can then be calculated by summing the quotients of the measured concentration of each biomass constituent at time-point  $t$  and the photosynthetic yield of that biomass constituent (Eq. 1):

$$\text{Photosynthetic requirement}(t) = C_{\text{TAG}}(t)/Y_{\text{TAG,light}} + C_{\text{starch}}(t)/Y_{\text{starch,light}} + C_{\text{carbohydrate}}(t)/Y_{\text{carbohydrate,light}} \quad \text{Eq. 1}$$

In Eq. 1,  $C_i(t)$  represents the concentration of component  $i$  (g/l) at time-point  $t$  and  $Y_{i,\text{light}}$  represents the photosynthetic yield of component  $i$  (g product/mol photon). These photosynthetic yields are estimated to be 1.02 g TAG/mol photon, 3.24 g starch/mol photon, and 3.24 g carbohydrate/mol photon (see Appendix A).

Using this calculation, it appears that although the *slm1* has a lower biomass productivity, the minimum photosynthetic requirement to produce that biomass is similar (Fig. 5.3). This indicates that the *slm1* does not have a reduced photosynthetic efficiency, but only seems to differ from the wt in terms of carbon partitioning.

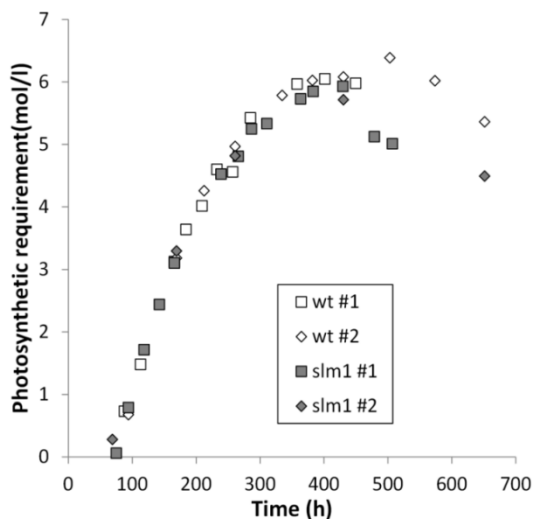


**Fig. 5.3.** Theoretical minimum amount of photons required to produce the observed biomass after nitrogen is depleted. Open symbols: wt. Grey symbols: *slm1*. The Results indicated with #1 and #2 in the figure legend represent the replicate cultivations.

In the wt, the calculated photosynthetic requirement also increases at the end of the cultivation, where no substantial increase in dry weight concentration is observed. This can be explained by an increase in energy density of the biomass due to a change in biomass composition (increase in TAG and decrease in starch content). This requires additional energy, which is provided by photosynthesis.

In these calculations it was assumed that the residual biomass (difference between the produced dry weight and the measured amounts of TAG and starch) consists for a large part of cell wall material that is made of carbohydrates such as cellulose (Burczyk et al., 1970). If this were a different biomass constituent with a different photosynthetic yield than carbohydrates, it would affect the calculated photosynthetic requirement. However, the estimated amount of this remaining fraction is similar in the wt and the slm1.

Therefore, this will not result in a biased comparison.

It is observed in the wt that starch is first produced and subsequently degraded (Fig. 5.1). This turnover is not taken into account in these calculations. However, the turnover of starch (synthesis of starch out of GAP and subsequent degradation of starch into GAP) only costs 1 ATP per glucose monomer and would only result in a minor change in the calculated photosynthetic requirement.

#### **5.2.4 Photosynthesis**

The pigmentation of the cell determines the amount of light that can be absorbed and ultimately be used for photosynthesis. The absorbance cross section of the biomass was measured and used as a proxy for the pigmentation. An up to eight-fold decrease in the biomass specific absorbance cross section ( $\text{m}^2/\text{g DW}$ ) was observed at the end of the cultivation compared to the point before nitrogen depletion in both the wt and the slm1 (Fig. 5.4B). A decrease in pigmentation during nitrogen starvation is commonly observed in microalgae (Geider et al., 1998a). The volumetric absorbance cross section ( $\text{m}^2/\text{l}$ ), however, remained more or less constant throughout the entire experiment. This suggests that the decrease in biomass specific absorbance cross section is mainly a result of dilution of pigments over newly formed biomass and is likely caused to a lesser extent by net degradation of pigments.

In addition to a change in absorbance cross section, the absorbance spectrum, and thus the pigment class composition, changed drastically (Fig. 5.4C). Photo-protective pigments (carotenoids) can be produced in response to physiological stress to prevent photo-oxidative damage (Geider et al., 1998a; Lamers et al., 2008). The ratio of chlorophyll over carotenoids decreased during nitrogen starvation as is apparent from

the increase in absorbance at 483nm (the observed absorbance maximum of carotenoids) relative to the absorbance at 680nm (the observed absorbance maximum of chlorophyll) (Fig. 5.4D). The decrease in absorbance cross section between the *slm1* and wt was similar but the *slm1* showed a higher ratio of absorbance at 483nm/680nm as the nitrogen starvation progressed. This suggests that the *slm1* has relatively more carotenoids than the wt. This difference between the *slm1* and wt became more apparent when nitrogen starvation progressed (Fig. 5.4D). These observations suggest that a progressively smaller fraction of the absorbed light is available for photosynthesis when nitrogen starvation progresses due to an increased carotenoid/chlorophyll ratio.

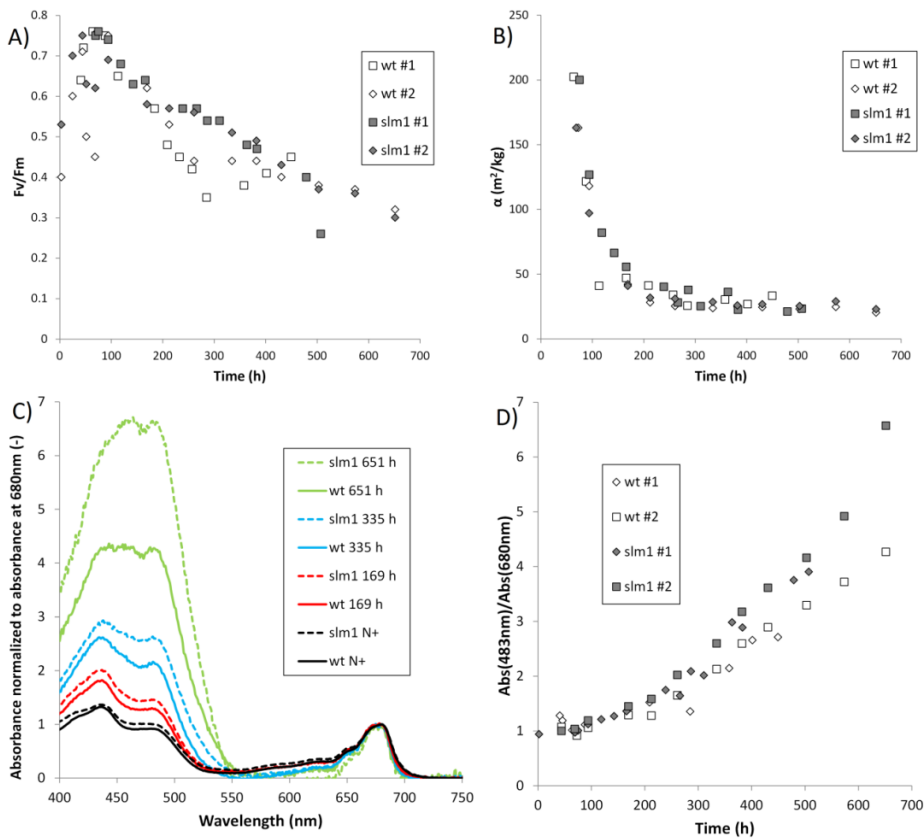


**Fig. 5.4.** Impact of nitrogen starvation on photosynthesis. A: Fv/Fm ratio. B: Absorbance cross section. C: Absorbance spectrum of the *slm1* and wt under nitrogen replete and nitrogen depleted conditions, normalized to the absorbance at 680nm. D: Ratio of absorbance at 483nm and 680nm. In figure C, the time indicated in the figure legend represents the time after inoculation. Nitrogen starvation commenced 70 to 100 h after inoculation. The spectrum that is indicated with N+ in the figure legend represents the spectrum before nitrogen was depleted. Open symbols indicate the wt and grey symbols indicate the *slm1*. The results indicated with #1 and #2 in the figure legend represent the replicate cultivations.

The variable fluorescence/maximum fluorescence ratio (Fv/Fm) was measured and can be used as a proxy for the intrinsic (or maximum) PSII quantum yield (Li et al., 2010b; Simionato et al., 2013). Although it does not directly reflect the photosynthetic efficiency achieved in the photobioreactor, it is often used as a diagnostic value for the photosynthetic performance (Maxwell & Johnson, 2000). Immediately after inoculation, the Fv/Fm ratio started substantially below the maximum value that was observed (Fig. 5.4A). This could possibly be due to a shock in biomass concentration and light intensity as a result of inoculation. During the nitrogen replete growth phase, the Fv/Fm ratio increased gradually to a maximum of 0.78, which is consistent with maximum values observed in other studies (Li et al., 2010b). Once nitrogen was depleted, the Fv/Fm ratio gradually decreased, as is commonly observed (Li et al., 2010b; Simionato et al., 2013). This could be an indication of increased damage to the photosystems. Fv/Fm ratios in the *slm1* are comparable to, or even slightly higher than the Fv/Fm ratios in the wt. This is consistent with the observation presented in Fig. 5.3, that the photosynthetic performance is not negatively affected in the *slm1* and that the main difference with the wt is an improved carbon partitioning towards TAG in the *slm1*.

### 5.3 Conclusions

The maximum TAG content increased from  $45\pm 1\%$  in wild-type to  $57\pm 0.2\%$  of dry weight in starchless *S. obliquus* (*slm1*). The *slm1* had a lower biomass productivity, which can completely be explained by the higher energy requirement to produce TAG compared to starch. The maximum yield of TAG on light in the mutant increased from  $0.144\pm 0.004$  to  $0.217\pm 0.011$  g TAG/mol photon, and a 51% improvement in areal TAG productivity therefore seems realistic for outdoor cultivation. This work highlights the potential of improved carbon partitioning using a starchless mutant to increase TAG productivity in oleaginous microalgae.

### 5.4 Methods

#### 5.4.1 Strains, pre-culture conditions, and cultivation medium

Wild-type (wt) *S. obliquus* UTEX 393 (recently suggested to be reclassified to *Acutodesmus obliquus* (Krienitz & Bock, 2012)) was obtained from the University of Texas Culture collection of algae (UTEX). The starchless mutant (*slm1*) was obtained using UV radiation-induced random mutagenesis on the wild-type strain of *S. obliquus* (de Jaeger et al., 2014). The culture medium was similar to that described by Breuer et al. (2013b) with the exception that all vitamins were omitted from the culture medium. The culture medium was autotrophic and contained 10 mM KNO<sub>3</sub> as the limiting nutrient.



All other required nutrients were present in excess. Pre-cultures were maintained in 16:8h light:dark cycles as described by Breuer et al. (2012). Both the wt and the *slm1* were able to continue growing after multiple serial dilutions while being cultivated autotrophically under these day-night cycles (16:8 light:dark).

#### 5.4.2 Experimental conditions

Batch cultivations were performed in flat-panel airlift-loop photobioreactors with a working volume of 1.7 l (Labfors 5 Lux, Infors HT, Switzerland). The reactor design is similar to that described by Klok et al. (2013a). The reactors were sparged with air containing 2% CO<sub>2</sub> at 1 l/min. The reactors were continuously illuminated (24h/day) using LED lamps with a warm white spectrum located on the culture side of the reactor. The incident light intensity was calibrated by measuring the average light intensity on the culture side of the front glass plate. The light path (reactor depth) was 2 cm. The temperature was controlled at 27.5°C and the pH was controlled at pH 7 using automatic addition of 1M HCl. These values for pH and temperature were found to be optimal for both growth and TAG accumulation in *S. obliquus* in previous research (Breuer et al., 2013b). A few millilitres of a 1% Antifoam B solution (J. T. Baker) were added manually when excessive foaming was visible. Prior to inoculation, reactors were heat-sterilized and subsequently filled with 0.2 µm filter-sterilized medium. Reactors were inoculated at 50 mg algae dry matter/l and grown at an incident light intensity of 100 µmol m<sup>-2</sup> s<sup>-1</sup> until the biomass density reached 0.3 to 1 g dry weight (DW)/l (typically after 48 h). At this point the incident light intensity was increased to 500 µmol m<sup>-2</sup> s<sup>-1</sup>. Periodically, samples were taken aseptically and analysed for dry weight concentration, biomass composition, residual dissolved NO<sub>3</sub><sup>-</sup>, Fv/Fm ratio, absorbance spectrum, and absorbance cross section. After nitrogen was depleted, more than 95% of the incident light was absorbed. Therefore, for simplicity, in the calculations it is assumed that the absorbed light is identical to the incident light intensity.

Although a condenser was installed at the gas exhaust of the reactor, water losses were present due to evaporation. Evaporation was quantified in a separate reactor that was filled with water and operated under the same conditions as during cultivation. The evaporation rate was 0.9 ml/h. Evaporation results in concentration of the biomass, which thus has an effect on the measured dry weight concentration. The measured biomass composition is unaffected. The biomass concentration was corrected for evaporation using  $C_{x,corrected} = \frac{V_{observed}}{V_{without\ evaporation}} C_{x,observed}$ . The correction factor decreased from 1 at the start of the cultivation to a minimum between 0.60 and 0.71 (depending

on the duration of the cultivation) at the end of the cultivation. All presented results and calculations throughout this work are based on the concentrations corrected for evaporation. Evaporation rates were similar in all experiments and therefore did not result in a biased comparison between the *slm1* and *wt* in any way. However, evaporation and the accompanying concentration effect did increase the steepness of the light gradient in the reactor and reduced light penetration and biomass specific light absorption rates.

### **5.4.3 Analyses**

#### **5.4.3.1 Dry weight**

The dry weight concentration was determined by filtrating culture broth over pre-weighted glass fibre filters and measuring the weight increase of the filters after drying at 95°C as described by Kliphuis et al. (2012).

#### **5.4.3.2 Total fatty acid**

The total fatty acid (TFA) concentration was determined by a sequence of cell disruption, total lipid extraction in chloroform:methanol, trans-esterification of acyl lipids to fatty acid methyl esters (FAMES) and quantification of FAMES using gas chromatography as described by Breuer et al. (2013a). Tripentadecanoin was used as an internal standard.

#### **5.4.3.3 TAG**

The TAG concentration was determined by separating the total lipid extract, obtained using the aforementioned method, into a TAG and polar lipid pool using a solid phase extraction column (SPE) as described by Breuer et al. (2013b), followed by transesterification and quantification of the fatty acids in the TAG pool as described by Breuer et al. (2013a).

#### **5.4.3.4 Starch**

The starch concentration was determined using an AA/AMG Total Starch Kit (Megazyme, Ireland) with modifications as described by de Jaeger et al. (2014). The procedure consisted of a sequence of cell disruption, starch precipitation using an aqueous solution of 80% ethanol, enzymatic hydrolysis of starch to glucose monomers using  $\alpha$ -amylase and amyloglucosidase, and a spectrophotometric based assay for quantification of glucose monomers.

#### 5.4.3.5 Dissolved nitrate

Dissolved nitrate was analysed in supernatant using a Seal analytical AQ2 nutrient analyser (SEAL Analytical Inc., USA) according to the manufacturer's instructions.

#### 5.4.3.6 Fv/Fm

Pulse amplitude modulation (PAM) fluorometry was used to determine the Fv/Fm ratio using an AquaPen AP-100 fluorescence spectrophotometer (PSI, Czech Republic) according to the manufacturer's instructions. Cultures were diluted in demineralized water to an optical density of 0.4 at 750nm in a cuvette with a light path of 10mm (equivalent to a concentration of 0.2 g DW/l) and adapted to dark conditions for 15 minutes prior to the measurement. It was confirmed that longer dark-adaptation times did not affect the results.

#### 5.4.3.7 Absorption spectrum and absorption cross section

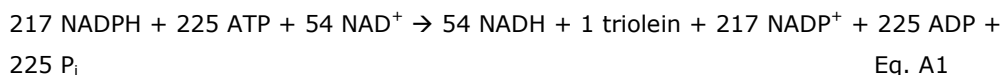
Cell suspensions were diluted to an optical density at 750nm of 1.4 to 1.6 as measured in a cuvette with a 1 cm light path. Subsequently, the absorption spectrum was measured in these diluted cell suspensions with a Shimadzu UV-2600 integrating sphere spectrophotometer in the spectrum 300 to 750nm, which results in the absorption spectrum corrected for scattering. Residual scattering was calculated as the average absorption between 740 and 750nm and subtracted from the absorption spectrum. From this absorption spectrum, the average biomass dry weight specific absorption cross section between 400 and 700nm ( $\alpha$ , unit: m<sup>2</sup>/g) was calculated as  $\alpha = \frac{\sum_{400}^{700} abs_{\lambda} \frac{\ln(10)}{z}}{300 DW}$ . Where  $abs_{\lambda}$  is the absorbance at wavelength  $\lambda$ ,  $z$  the light path of the cuvette (0.002 m), and DW the dry weight concentration (g/m<sup>3</sup>).

#### Acknowledgements

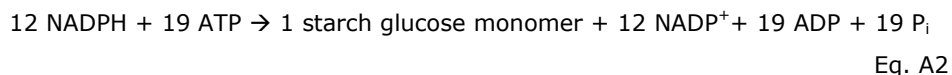
This research project is financially supported by the Food and Nutrition Delta program of Agentschap NL (FND10007) and Unilever.

**Appendix A: Calculation of the photosynthetic yield of biomass constituents**

TAG consists of a glycerol backbone with three fatty acids. Because approximately 50% of the fatty acids in TAG are oleic acid molecules in *S. obliquus* (Breuer et al., 2013b), triolein is used as the reference TAG molecule to calculate the photosynthetic yield of TAG. In the production of one molecule of oleic acid from CO<sub>2</sub>, 70 molecules of NADPH and 71 molecules of ATP are required and 18 molecules of NADH are produced. In the production of the glycerol backbone 7 NADPH and 9 ATP are consumed (Johnson & Alric, 2013). Finally, in the condensation of the fatty acids to the glycerol backbone, it is assumed that 1 ATP is consumed for each fatty acid. This results in the net utilization of cofactors as presented in Eq. A1.



Similarly, one glucose monomer of starch can be produced out of 19 ATP and 12 NADPH (Eq. A2). It is assumed that production of other carbohydrates (such as cell wall cellulose) is similar to production of starch in terms of metabolic requirements.



The required cofactors can be provided using photosynthesis through either linear electron transport (theoretical maximum: 8 photons → 3 ATP + 2 NADPH) or cyclic electron transport (theoretical maximum: 2 photons → 1 ATP). Furthermore, it is assumed that oxidative phosphorylation can be used to provide 2.5 ATP using 1 NADH. Using these stoichiometric relationships, it can be calculated that a minimum of 868 photons are required to produce 1 mol of triolein and a minimum of 50 photons are required to produce 1 mol of starch glucose monomers. Using the molecular weights of triolein (885 g/mol) and starch glucose monomers (162 g/mol), theoretical maximum yields of 1.02 g TAG/mol photon and 3.24 g starch/mol photon can be found. Note that according to the stoichiometric relationship of triolein production, additional NADH is produced (Eq. A1). If this NADH can be used to reduce NADP<sup>+</sup> to NADPH, the yield of TAG on photons could increase to 1.36 g TAG/mol photon.





## **Chapter 6**    Photosynthetic efficiency and carbon partitioning in nitrogen-starved *Scenedesmus obliquus*

**This chapter has been submitted for publication as:**

Guido Breuer, Dirk E. Martens, René B. Draaisma, René H. Wijffels, Packo P. Lamers,  
Photosynthetic efficiency and carbon partitioning in nitrogen-starved *Scenedesmus  
obliquus*

**Abstract**

This work investigates how the photoacclimated state at the onset of nitrogen starvation and the light intensity during nitrogen starvation influence carbon partitioning and photosynthetic efficiency in nitrogen-starved *Scenedesmus obliquus*. Nitrogen-depleted batch cultivations were performed at an incident light intensity of 200 and 1000  $\mu\text{mol m}^{-2} \text{s}^{-1}$ . These nitrogen-depleted batch cultivations were started with biomass that was photoacclimated to an incident light intensity of either 200 or 1000  $\mu\text{mol m}^{-2} \text{s}^{-1}$  under nitrogen replete conditions. During initial nitrogen starvation, fatty acids and starch are produced in a 1:4 ratio. This ratio progressively increased towards only fatty acid synthesis. Hereafter, the initially accumulated starch was degraded and likely used as a substrate for fatty acid synthesis. The ratio between starch and fatty acid synthesis correlated strongly to the biomass nitrogen content. Slightly more carbon was partitioned to starch synthesis at high light intensities, and carbon partitioning was not affected by the photoacclimated state at the onset of nitrogen starvation. Likely, this observed carbon partitioning is caused by competition between fatty acid and starch synthesis for a common carbon pre-cursor. The photosynthetic efficiency decreased 2-fold at high versus low light intensities but was not affected by photoacclimation.



## 6.1 Introduction

Oleaginous microalgae can produce large amounts of fatty acids in the form triacylglycerol (TAG). These TAGs are of commercial interest as a resource for food, feed, and biofuels (Draaisma et al., 2013; Wijffels & Barbosa, 2010). Microalgae can be seen as 'microplants' and have several advantages over agricultural crops that are currently used to produce these commodities. Microalgae have the potential to reach much higher productivities than terrestrial plants, can be cultivated on non-arable land, and have lower freshwater and fertilizer requirements than agricultural crops (Draaisma et al., 2013; Hu et al., 2008; Wijffels & Barbosa, 2010).

Microalgal TAGs are only produced under conditions of physiological stress (Hu et al., 2008). The most common approach to induce TAG production in microalgae is using nitrogen starvation (Hu et al., 2008). During nitrogen starvation, not only TAG accumulation is induced, but also the photosynthetic efficiency and carbon assimilation rate decrease progressively in time, leading to progressively decreasing TAG accumulation rates (Breuer et al., 2012; Klok et al., 2013a). Furthermore, even in the best TAG producing microalgae species, TAG only accounts for approximately half of the biomass produced after the depletion of nitrogen (Breuer et al., 2012). Other biomass constituents, such as starch, are produced simultaneously (Breuer et al., 2014). The overall TAG productivity during nitrogen starvation is thus determined by the product of the photosynthetic rate during nitrogen starvation and the fraction thereof that is partitioned towards TAG synthesis.

Both the light intensity during the nitrogen replete growth phase and the light intensity during the nitrogen starvation phase can affect the photosynthetic efficiency and carbon partitioning during nitrogen starvation, as discussed below.

### *Light intensity during nitrogen starvation*

It is generally accepted that the photosynthetic efficiency is strongly dependent on the light intensity (Jassby & Platt, 1976; MacIntyre et al., 2002). At low light intensities, photosynthesis is limited by light absorption but at high light intensities photosynthesis is limited by the capacity of the photosynthetic machinery. The excess absorbed light is then thermally dissipated, resulting in a decreased photosynthetic efficiency at high light intensities (Jassby & Platt, 1976; MacIntyre et al., 2002). A high light intensity during nitrogen starvation will thus also reduce the photosynthetic efficiency during nitrogen starvation (Breuer et al., 2013b; Klok et al., 2013a).

Also carbon partitioning may be affected by the light intensity during nitrogen starvation. Many studies report the impact of the light intensity on carbon partitioning towards TAG. The conclusions of these studies are contradicting however. Some studies hypothesize that TAG production is the result of an overflow metabolism where excess photosynthetic products are used for TAG synthesis. These studies report that partitioning towards TAG increases with light intensity and suggest that optimal TAG production will be achieved at high light intensities (Kandilian et al., 2014; Liu et al., 2012; Van Vooren et al., 2012). Other studies report that the light intensity does not affect carbon partitioning and maximum TAG content, but does influence TAG productivities and yields, because the light intensity affects the photosynthetic rate and photosynthetic efficiency (Breuer et al., 2013b; Pal et al., 2011; Simionato et al., 2011). Yet different studies claim that starch is the primary accumulation product, and that low light intensities result in increased partitioning towards TAG (Klok et al., 2013b; Solovchenko et al., 2007). Note that the carbon partitioning response to light intensity might very well be species specific, making comparison of aforementioned studies difficult. In conclusion, it is clear that no consensus exists on how the light intensity during nitrogen starvation influences carbon partitioning.

#### *Light intensity during the nitrogen replete growth phase*

Microalgae acclimate to the light intensity (MacIntyre et al., 2002). The light intensity prior to the onset of nitrogen starvation thus determines the photoacclimated state at the onset of nitrogen starvation. The effects induced by this photoacclimated state are likely to persist during nitrogen starvation because acclimation to a change in light intensity typically occurs with half-times in the order of 10h, during nitrogen replete conditions (Neidhardt et al., 1998; Sukenik et al., 1990). This means that the effects of the photoacclimated state will at least persist during initial nitrogen starvation. But because protein synthesis is impaired during nitrogen starvation, re-acclimation likely occurs at a much slower rate (Neidhardt et al., 1998; Prézelin & Matlick, 1983). The effects of the photoacclimated state might therefore also persist during prolonged nitrogen starvation.

The photoacclimation state is reflected in the pigmentation and composition of the photosystem. A change in photoacclimation state can thus have a large impact on the photosynthetic efficiency (MacIntyre et al., 2002; Melis, 2009; Melis et al., 1999). This can also affect carbon partitioning in the case that energetic imbalances are the driving force behind carbon partitioning, as is often proposed (Kandilian et al., 2014; Van Vooren et al., 2012). It has for example been proposed that microalgae, that are first

acclimated to a low light intensity and are subsequently exposed to a high light intensity during nitrogen starvation, can have an enhanced TAG accumulation because of the increased energetic shock (Simionato et al., 2011). Photoacclimation can also affect the biochemical composition of the biomass, and potentially also the composition of the enzymatic machinery for fatty acid and starch synthesis. When the composition of the enzymatic machinery persists during nitrogen starvation, this can also affect carbon partitioning during nitrogen starvation.

In summary, little is known about the effects of the photoacclimated state at the onset of nitrogen starvation on the photosynthetic efficiency and carbon partitioning during nitrogen starvation, because typically the same light intensity is used during the nitrogen replete phase and nitrogen-depleted phase of a batch cultivation. This makes it impossible to distinguish between the effects of the light intensity during nitrogen starvation and the photoacclimated state. Also no consensus exists on the impact of the light intensity during nitrogen starvation on carbon partitioning. Therefore, in this work, we investigate how the light intensity during nitrogen starvation and the photoacclimated state at the onset of nitrogen starvation influence carbon partitioning and the photosynthetic efficiency during nitrogen starvation in the oleaginous microalga *Scenedesmus obliquus*.

To do so, light-limited, nitrogen replete, chemostat cultivations were performed at a low and a high light intensity to obtain two differently photoacclimated cultures. Subsequently, these differently photoacclimated cultures were used to perform nitrogen-depleted batch cultivations at either a low or a high light intensity (4 experimental conditions in total). The chemostat operation allowed for a high degree of control over the photoacclimated state of the biomass. Furthermore, this setup ensured that the transition from a low to a high, and from a high to a low light intensity was simultaneous with the onset of nitrogen starvation.

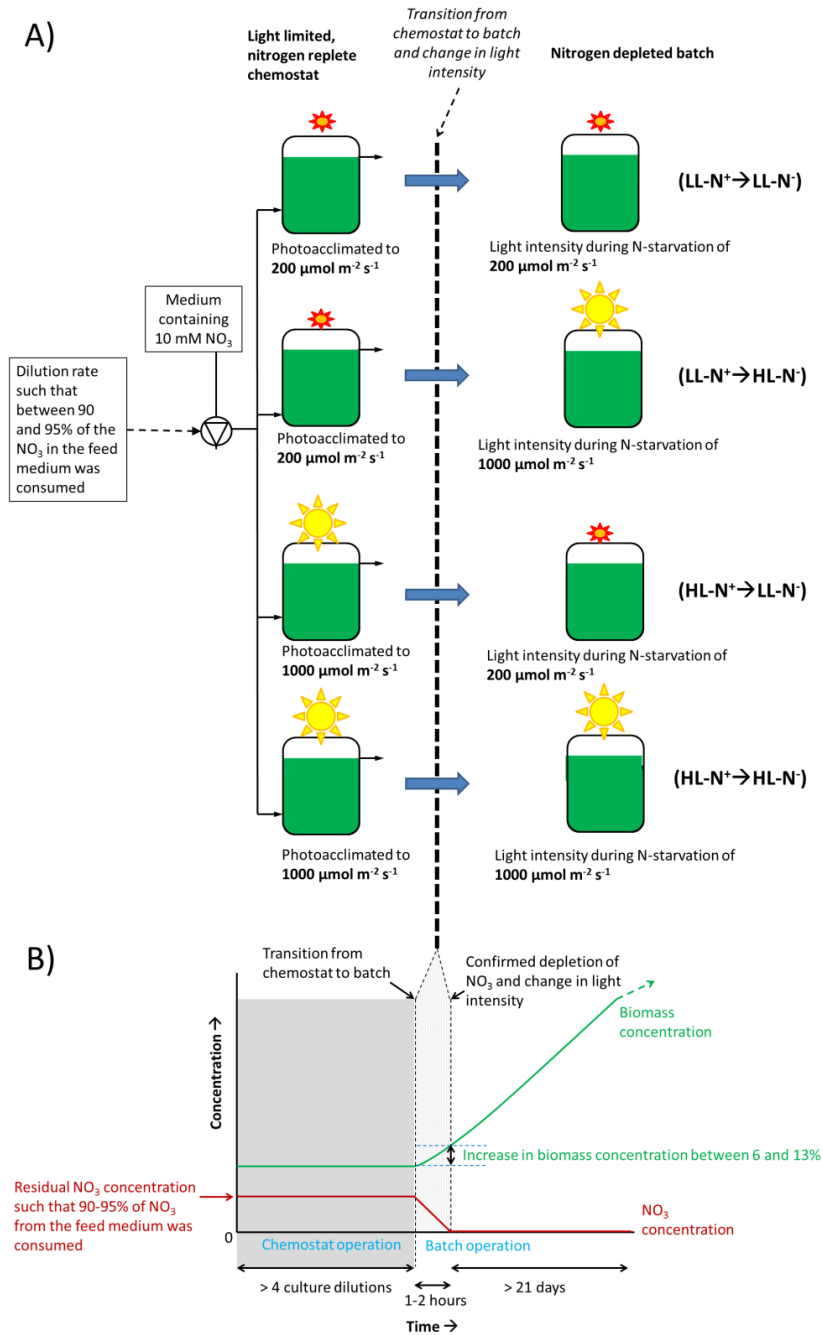


**Fig. 6.1.** (A) schematic overview of the experimental design. Cultures were photoacclimated to either 200 or 1000  $\mu\text{mol m}^{-2} \text{s}^{-1}$  in light-limited, nitrogen replete, chemostat cultivations (LL-N<sup>+</sup> and HL-N<sup>+</sup>, respectively). **Continues next page.**

**Fig. 6.1 (continued).** In these cultivations, the dilution rate was adjusted such that  $\text{NO}_3^-$  was almost completely consumed (90-95%). This resulted in similar biomass concentrations for all chemostat cultivations. Subsequently, both these differently photoacclimated cultures were continued as a nitrogen-depleted batch, at an incident light intensity of either 200 or 1000  $\mu\text{mol m}^{-2} \text{s}^{-1}$  (LL- $\text{N}^-$  and HL- $\text{N}^-$ , respectively). (B) transition from light-limited chemostat operation to nitrogen-starved batch operation. After the chemostat operation was terminated, the residual  $\text{NO}_3^-$  was consumed within 2 hours. After confirmation that all residual  $\text{NO}_3^-$  was completely consumed, the light intensity was set according to the scheme shown in figure A. In the period between transition of chemostat to batch operation and change in light intensity/depletion of  $\text{NO}_3^-$ , the biomass concentration increased between 6 and 13% compared to the steady-state biomass concentration during the chemostat operation (Table 6.1).

## 6.2 Material and Methods

### 6.2.1 Experimental design

All experiments were started as light-limited, nitrogen replete, chemostat cultivations. These chemostat cultivations were operated at an incident light intensity of 200 or 1000  $\mu\text{mol m}^{-2} \text{s}^{-1}$  to obtain two differently photoacclimated cultures. In these chemostat cultivations, the dilution rate was chosen such that between 90 and 95% of the  $\text{NO}_3^-$  present in the feed-medium (10 mM) was consumed (Appendix A). Once steady state conditions were achieved (evaluated based on a constant biomass concentration and absorption cross section), chemostat cultivation was continued for more than 4 culture dilutions. During this period,  $\text{NO}_3^-$  was at no point depleted. Hereafter, chemostat operation was terminated, and batch operation was initiated (Fig. 6.1B). This was accomplished by stopping the medium-inflow and overflow pumps. Because of the near complete  $\text{NO}_3^-$  consumption during the chemostat operation, all residual  $\text{NO}_3^-$  was consumed within two hours (Fig. 6.1B). During this period the consumption of residual  $\text{NO}_3^-$  was measured every 30 minutes until all  $\text{NO}_3^-$  was consumed. Once depletion of  $\text{NO}_3^-$  was confirmed, the light intensity was set to 200 or 1000  $\mu\text{mol m}^{-2} \text{s}^{-1}$  (depending on the experimental condition) and batch operation was followed for at least 21 days (Fig 6.1B).

There was a short period between the transition from chemostat to batch-operation and the moment of nitrogen starvation/change in light intensity during which nitrogen was not yet depleted. As a consequence, there was a small increase in biomass concentration in this period (Fig. 6.1B). To quantify this difference, a sample was taken when nitrogen was depleted to measure the change in biomass concentration in the period between termination of chemostat operation and complete consumption of  $\text{NO}_3^-$ . This increase in dry weight (DW) concentration was in all cases less than 13% (Table 6.1). All experiments were performed in duplicate.

### 6.2.2 Reactor design and operation

Cultivations were performed in flat-panel airlift-loop photobioreactors with a working volume of 1.7 l and a light path of 2 cm (Labfors 5 Lux, Infors HT, Switzerland), as described by (Breuer et al., 2014). The reactors were aerated with air enriched with 2% (v/v) CO<sub>2</sub> at 1 l/min. The condenser was operated at 2°C to prevent water losses due to evaporation. The reactors were continuously illuminated (24h/day) using a panel containing 260 LED lamps, with a warm-white spectrum (as specified in the user manual of the Labfors 5 Lux; colour temperature of 4000 K), located on the culture side of the reactor. The temperature was controlled at 27.5°C and the pH was controlled at pH 7 using automatic addition of a 5% (v/v) H<sub>2</sub>SO<sub>4</sub> solution. The O<sub>2</sub> and CO<sub>2</sub> concentration in the off-gas were measured online using a mass spectrometer (Prima dB, Thermo Scientific). Prior to inoculation, the composition of the ingoing gas was measured. This was subtracted from the measured concentrations in the cultivation off-gas to determine the  $\Delta\text{O}_2$  and  $\Delta\text{CO}_2$ . For chemostat operation, filter-sterilized medium was pumped into the reactor at a constant flow rate. A pump with a higher capacity pumped liquid, from the top, out of the reactor to maintain a constant liquid level. This harvested liquid was collected in an overflow bottle that was weighted daily. The sum of this harvested liquid and sample size (10-30 ml/day) was used to calculate the actual dilution rate. During both nitrogen replete chemostat operation and nitrogen-depleted batch cultivation, between 95 and 100% of the incident light was absorbed. Calculations for yield on light are based on the absorbed light.

### 6.2.3 Species, medium, and pre-culture conditions

Wild-type *S. obliquus* UTEX 393 was used in all experiments and obtained from the University of Texas culture collection of algae (UTEX). The culture medium and pre-culture conditions were similar to those described by Breuer et al. (2014). The culture medium did not contain any added carbon source and contained 10 mM KNO<sub>3</sub> (for the nitrogen replete chemostat cultivations that were used in combination with the nitrogen-depleted batch cultivations; from which the results are shown in the main text) or 34 mM KNO<sub>3</sub> (for the nitrogen replete chemostat cultivations used to determine the photoacclimation behaviour; from which the results are shown in Appendix A and 2). All other required nutrients were present in excess.

### 6.2.4 Analyses

Biomass DW, dissolved nitrate, total fatty acid (TFA), and starch concentration were measured as described previously (Breuer et al., 2014; Breuer et al., 2013a). The

absorption cross section was measured and calculated as described by Vejrazka et al. (2011) between 400 and 700nm using a Shimadzu UV-2600 integrating sphere spectrophotometer. In addition, the ratio of the absorption cross sections between 550-700nm and 400-700nm was used as a proxy for the pigment class composition. Chlorophylls have an absorption maximum at both 400-500nm and 600-700nm, where carotenoids only have an absorption maximum between 400-500nm. The ratio between the absorption cross section between 550-700 and 400-700 can thus be used as a proxy for the relative chlorophyll abundance in total pigments or the chlorophyll/carotenoid ratio. This ratio does not quantitatively represent a ratio in concentrations and can only be used qualitatively. A higher value for this ratio indicates a higher chlorophyll abundance in total pigments and higher chlorophyll/carotenoid ratio.

### 6.2.5 Statistical analysis

Statistical significance was determined using paired samples student t-tests using SPSS 19. Differences were considered significant when  $p < 0.05$ .

## 6.3 Results

To investigate how the light intensity during nitrogen starvation and the photoacclimated state at the onset of nitrogen starvation affect carbon partitioning and the photosynthetic efficiency in nitrogen-starved *S. obliquus*, the experimental setup as presented in Fig. 6.1 was used. Nitrogen-depleted batch cultivations were performed at incident light intensities of 200 and 1000  $\mu\text{mol m}^{-2} \text{s}^{-1}$ . These are from now on referred to as LL-N<sup>-</sup> and HL-N<sup>-</sup>, respectively (in which LL stands for low light and HL stands for high light). These nitrogen-depleted batch cultivations were started using *S. obliquus* cultures that were photoacclimated to an incident light intensity of either 200 or 1000  $\mu\text{mol m}^{-2} \text{s}^{-1}$  in light-limited, nitrogen replete, chemostat cultivations (Fig. 6.1A). This photoacclimated state is from now on referred to as LL-N<sup>+</sup> and HL-N<sup>+</sup>, respectively. *S. obliquus* that was acclimated to a light intensity of 200  $\mu\text{mol m}^{-2} \text{s}^{-1}$  (LL-N<sup>+</sup>) had a 1.7-fold higher absorption cross section, a higher chlorophyll/carotenoid ratio, a slightly higher TFA content ( $9.2 \pm 0.5$  compared to  $6.9 \pm 0.1\%$  of DW) and lower starch content ( $7.1 \pm 0.5$  compared to  $13.9 \pm 0.4\%$  of DW) than cultures that were photoacclimated to 1000  $\mu\text{mol m}^{-2} \text{s}^{-1}$  (HL-N<sup>+</sup>) (Table 6.1; Appendix A). Photoacclimation also had an impact on the fatty acid composition. In the LL-N<sup>+</sup> acclimated *S. obliquus*, the relative abundance of C18:3 was lower and that of C18:2 was higher than in HL-N<sup>+</sup> acclimated *S. obliquus* (Supplementary Fig. S1). The photosynthetic biomass yield was 1.8-fold

lower during the HL-N<sup>+</sup> cultivation than during the LL-N<sup>+</sup> cultivation ( $0.65 \pm 0.03$  compared to  $1.19 \pm 0.03$  g/mol)(Table 6.1; Appendix A).

The dilution rate in the nitrogen replete chemostat cultivations was chosen such that between 90-95% of the NO<sub>3</sub><sup>-</sup> present in the feed medium was consumed (Table 6.1). It was confirmed that this low residual NO<sub>3</sub><sup>-</sup> concentration was not limiting for growth and did not affect photoacclimation (Appendix A). Because the same NO<sub>3</sub><sup>-</sup> concentration (10 mM) was used in all cultivations, the steady-state biomass concentration was approximately 1.5 g/l in all chemostat cultivations (Table 6.1). After the transition from nitrogen replete chemostat operation to nitrogen-depleted batch operation, all residual NO<sub>3</sub><sup>-</sup> was consumed within 2 hours. The biomass concentration increased less than 13% during this period in all cases (Table 6.1). Because the light intensity was not changed during this period, this only resulted in a minor change in light gradient and a minor adjustment of the photoacclimated state during this 2-hour period. For example, the change in absorption cross section in this period was in all cases less than 4%. When depletion of NO<sub>3</sub><sup>-</sup> was confirmed, the light intensity was set to either 200 or 1000  $\mu\text{mol m}^{-2} \text{s}^{-1}$  (Fig. 6.1). This transition from chemostat to batch operation of one of the experiments is shown as an example in Supplementary Fig. S2.

In total, four combinations of photoacclimated state and light intensity were investigated (Fig. 6.1A), in duplicate. In this paper, these combinations are from now on referred to as "photoacclimated state at onset of nitrogen starvation" → "light intensity during nitrogen starvation", e.g. LL-N<sup>+</sup> → HL-N<sup>-</sup> (Fig. 6.1).



	LL-N <sup>+</sup>				HL-N <sup>+</sup>			
	LL-N <sup>+</sup> replicate #1 n = 4	LL-N <sup>+</sup> replicate #2 n = 4	HL-N <sup>+</sup> replicate #1 n = 3	HL-N <sup>+</sup> replicate #2 n = 5	LL-N <sup>+</sup> replicate #1 n = 4	LL-N <sup>+</sup> replicate #2 n = 4	HL-N <sup>+</sup> replicate #1 n = 4	HL-N <sup>+</sup> replicate #2 n = 3
Biomass concentration (g/l)	1.42 ± 0.04	1.50 ± 0.04	1.43 ± 0.02	1.46 ± 0.05	1.48 ± 0.01	1.48 ± 0.07	1.47 ± 0.03	1.53 ± 0.03
Photosynthetic biomass yield (g/mol)	1.19 ± 0.08	1.19 ± 0.01	1.16 ± 0.03	1.23 ± 0.04	0.66 ± 0.02	0.62 ± 0.03	0.64 ± 0.04	0.68 ± 0.01
Specific growth rate (day <sup>-1</sup> )	0.71 ± 0.02	0.67 ± 0.01	0.68 ± 0.01	0.71 ± 0.02	1.87 ± 0.04	1.76 ± 0.02	1.86 ± 0.03	1.89 ± 0.04
TFA content (% DW)	8.8 ± 0.2	9.1 ± 0.0	9.9 ± 0.1	8.9 ± 0.2	6.9 ± 0.2	6.4 ± 0.0	6.9 ± 0.2	6.8 ± 0.0
Starch content (% DW)	7.5 ± 0.3	6.8 ± 0.0	7.2 ± 0.2	6.6 ± 0.8	13.9 ± 0.5	15.0 ± 0.0	14.2 ± 0.9	13.5 ± 1.0
Absorption cross section between 400-700nm (m <sup>2</sup> /kg)	213 ± 5	246 ± 6	238 ± 1	227 ± 5	138 ± 3	131 ± 4	136 ± 3	131 ± 4
Ratio of absorption cross section between 550-700nm and 400-700nm (-)	0.70 ± 0.01	0.72 ± 0.00	0.73 ± 0.00	0.72 ± 0.01	0.62 ± 0.00	0.62 ± 0.00	0.62 ± 0.00	0.64 ± 0.00
Residual NO <sub>3</sub> <sup>-</sup> (%)	8 ± 2	7 ± 1	8 ± 3	5 ± 0	9 ± 3	5 ± 1	7 ± 0	8 ± 3
Increase in biomass concentration in the period between transition of chemostat to batch operation and depletion of nitrogen/change in light intensity (%)	8	6	7	7	13	9	10	9

**Table 6.1.** Steady state values obtained in the eight different nitrogen replete chemostat cultivations for the biomass concentration, photosynthetic biomass yield, biomass composition, absorption cross section, and residual NO<sub>3</sub><sup>-</sup> concentration. The N<sup>+</sup> conditions (LL-N<sup>+</sup> and HL-N<sup>+</sup>) in the table refer to the light intensity that was used during the chemostat operation. The N<sup>-</sup> conditions listed in the table refer to the nitrogen-depleted experiments (see Fig. 6.1A). These values represent the average±standard deviation of samples taken over several culture dilutions during the steady state operation of the nitrogen replete chemostat cultivation (the number of samples taken on consecutive days that were used to calculate the average and standard deviation are indicated with n). In addition, the increase in biomass concentration between the transition of chemostat operation to batch operation and the depletion of NO<sub>3</sub><sup>-</sup> from the culture medium is shown.

### 6.3.1 Biomass productivity and biomass composition during nitrogen starvation

The light intensity during nitrogen starvation had a large impact on the biomass productivity and photosynthetic efficiency during nitrogen starvation. For the HL-N<sup>-</sup> conditions, the biomass productivity during the first two days of nitrogen starvation was approximately 2.2-fold higher than for the LL-N<sup>-</sup> conditions ( $2.6 \pm 0.1$  compared to  $1.2 \pm 0.1$  g l<sup>-1</sup> day<sup>-1</sup>). When it is considered that the light intensity was 5-fold higher in the HL conditions, the photosynthetic biomass yield (g biomass/mol photon) was 2.3-fold lower in the HL-N<sup>-</sup> condition than in the LL-N<sup>-</sup> conditions (0.6 vs 1.4 g/mol). The differently photoacclimated cultures that were cultivated at the same nitrogen-depleted light intensity had similar biomass productivities, as can be seen from their increase in DW as a function of time (Fig. 6.2A). For all conditions, the dry weight (DW) concentration increased 7 to 8-fold during nitrogen starvation (Fig. 6.2A).

The increase in biomass was mainly a result of the production of starch and fatty acids. Together, the accumulated starch and fatty acids accounted for approximately 70% of the biomass produced during nitrogen starvation (Supplementary Fig. S3). For all conditions, starch accumulation commenced immediately upon nitrogen depletion (Fig. 6.2C). Starch accumulation continued for several days and then stopped. Hereafter, degradation of starch was initiated (Supplementary Fig. S4). Total fatty acids (TFA) accumulation commenced approximately 1 day after the depletion of NO<sub>3</sub><sup>-</sup> and continued until the end of the cultivation (Fig. 6.2B). As a response to nitrogen starvation, also a major shift in TFA composition was observed. During nitrogen starvation, the relative abundance of C16:4, C18:2, and C18:3 decreased and the relative abundance of C18:0 and C18:1 increased (Supplementary Fig. S1). In this work, we only measured TFA, because in previous work it has been shown that in *S. obliquus*, cultivated under similar conditions, the complete increase in TFA after the depletion of nitrogen is caused by the production of TAG (Breuer et al., 2014; Breuer et al., 2013b; Breuer et al., 2012).

Although the same general trends were observed for all treatments, the light intensity during nitrogen starvation did have an effect on the biomass composition during nitrogen starvation. In the HL-N<sup>-</sup> experiments, higher maximum starch contents were reached and these maxima were achieved earlier than in the LL-N<sup>-</sup> experiments (Fig. 6.2C). Maxima in starch content were 32-35% of DW after 4-6 days for the LL-N<sup>-</sup> cultivations, and 37-42% of DW after approximately 2 days for the HL-N<sup>-</sup> cultivations. In the HL-N<sup>-</sup> experiments, the TFA content increased slightly faster than in the LL-N<sup>-</sup> experiments, but only minor differences in maximum TFA content were observed

between the different conditions (Fig. 6.2B). No differences in starch and TFA content were observed between the differently photoacclimated cultures (LL-N<sup>+</sup> and HL-N<sup>+</sup>) when these were cultivated at the same nitrogen-depleted light intensity (LL-N<sup>-</sup> or HL-N<sup>-</sup>).

The reduction in the photosynthetic biomass yield at high light intensities resulted in a threefold reduction in the maximum time-averaged TFA yield on light in the HL-N<sup>-</sup> compared to the LL-N<sup>-</sup> experiments (Table 6.2). No difference in the maximum time-averaged TFA yield on light was observed between the differently photoacclimated cultures, when these were cultivated at the same nitrogen-depleted light intensity (Table 6.2). This time-averaged TFA yield on light was calculated for each time-point as the yield of TFA on light (g TFA/mol photon) between that time-point and the onset of nitrogen starvation (t=0)(Supplementary Fig. S5). The maximum time-averaged yield was then obtained by taking the maximum among these yields. This correlation between the TFA yield on light and the incident light intensity is consistent with previous observations for *S. obliquus* (Breuer et al., 2013b).

**Table 6.2.** Maximum time-averaged TFA yields on light. The time-averaged TFA yield on light was calculated for each time-point as the yield of TFA on light (g TFA/mol photon) between that time-point and the onset of nitrogen starvation (t=0)(Supplementary Fig. S5). The maximum time-averaged yield was then obtained by taking the maximum among these yields. The values indicate the average±deviation from the average of the duplicate cultivations.

Experimental condition	Maximum time-averaged TFA yield on light (g/mol)
LL-N <sup>+</sup> → LL-N <sup>-</sup>	0.295±0.033
LL-N <sup>+</sup> → HL-N <sup>-</sup>	0.103±0.004
HL-N <sup>+</sup> → LL-N <sup>-</sup>	0.291±0.000
HL-N <sup>+</sup> → HL-N <sup>-</sup>	0.095±0.000

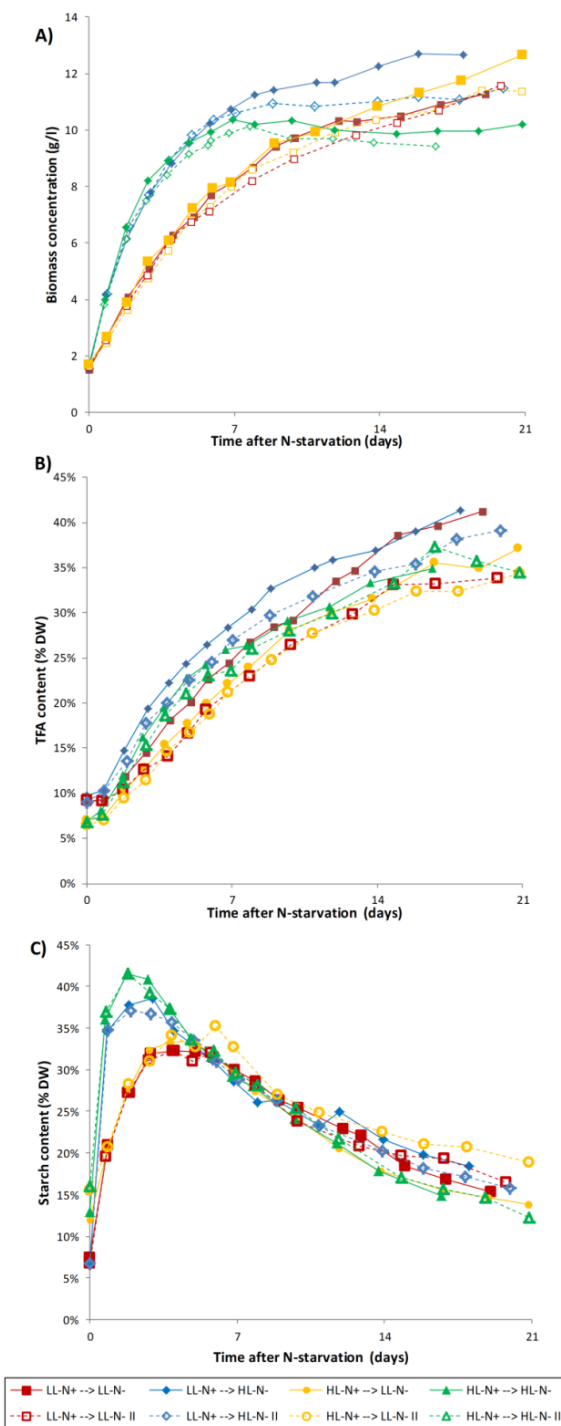


**Fig. 6.2.** Biomass concentration (A), TFA content as percentage of DW (B), and starch content as percentage of DW (C) during the nitrogen-depleted batch cultivation. Red: LL-N<sup>+</sup>→LL-N<sup>-</sup>; blue: LL-N<sup>+</sup>→HL-N<sup>-</sup>; yellow: HL-N<sup>+</sup>→LL-N<sup>-</sup>; green: HL-N<sup>+</sup>→HL-N<sup>-</sup>. The closed symbols/solid lines and open symbols/dashed lines represent replicate cultivations. Time = 0 represents the onset of nitrogen starvation.

### 6.3.2 The ratio between fatty acid and starch synthesis changes during nitrogen starvation

Starch and fatty acids are produced simultaneously during nitrogen starvation, but in a continuously changing ratio. To investigate how the ratio between starch and fatty acids synthesis progresses during nitrogen starvation, we calculated the carbon partitioning ratio as a function of the extent of nitrogen starvation (Fig. 6.3). This carbon partitioning is defined as the amount of fatty acids produced (g/l) between two consecutive time-points ( $\Delta\text{TFA}$ ) divided by the combined fatty acid and starch production (g/l) in that same period ( $\Delta\text{TFA} + \Delta\text{Starch}$ ). The nitrogen content of the biomass, expressed here as the dry weight/N ratio (DW/N ratio), was used as a proxy for the extent of nitrogen starvation. This biomass-nitrogen content is commonly used as a state-variable to describe nitrogen-starvation-related processes (Bernard, 2011; Packer et al., 2011). Given the fact that all  $\text{NO}_3^-$  was consumed from the cultivation medium, this DW/N ratio was calculated from the measured dry weight concentration and from the nitrogen concentration originally present in the cultivation medium (10 mM).

For all conditions, fatty acids and starch were produced in a 1:4 ratio immediately after the depletion of nitrogen, as can be seen from a  $\Delta\text{TFA} / (\Delta\text{TFA} + \Delta\text{Starch})$  ratio of 20% at the lowest DW/N ratios (Fig. 6.3). When nitrogen starvation progressed (DW/N ratio increased), this ratio shifted more towards fatty acid synthesis, ultimately reaching the point where only fatty acids were being produced (the  $\Delta\text{TFA} / [\Delta\text{TFA} + \Delta\text{Starch}]$  ratio reached 100%)(Fig. 6.3). Hereafter, starch was degraded (at a DW/N ratio of  $63 \pm 5$  and  $69 \pm 6$  for the LL- $\text{N}^-$  and HL- $\text{N}^-$  conditions, respectively)(Supplementary Fig. S4). In the partitioning ratio of Fig. 6.3, only net production is considered.  $\Delta\text{Starch}$  was therefore set to 0 when net degradation of starch was observed. This resulted in a partitioning of 100% towards fatty acids, also after starch degradation was initiated (*i.e.* at very high DW/N ratios).

The general trend in how the fatty acid:starch synthesis ratio increased as a function of the DW/N ratio was similar for all combinations of photoacclimated states (LL- $\text{N}^+$  and HL- $\text{N}^+$ ) and light intensities during nitrogen starvation (LL- $\text{N}^-$  and HL- $\text{N}^-$ ). Nevertheless, the light intensity during nitrogen starvation did have a minor impact on how the fatty acid:starch synthesis ratio progressed. At the same extent of nitrogen starvation (same DW/N ratio), more carbon was partitioned to fatty acid synthesis in the LL- $\text{N}^-$  experiments than in the HL- $\text{N}^-$  experiments. This can be seen from the slightly higher

$\Delta\text{TFA} / (\Delta\text{TFA} + \Delta\text{Starch})$  ratios in the LL-N<sup>-</sup> experiments than in the HL-N<sup>-</sup> experiments, at the same DW/N ratio (Fig. 6.3). Differences were minor however.

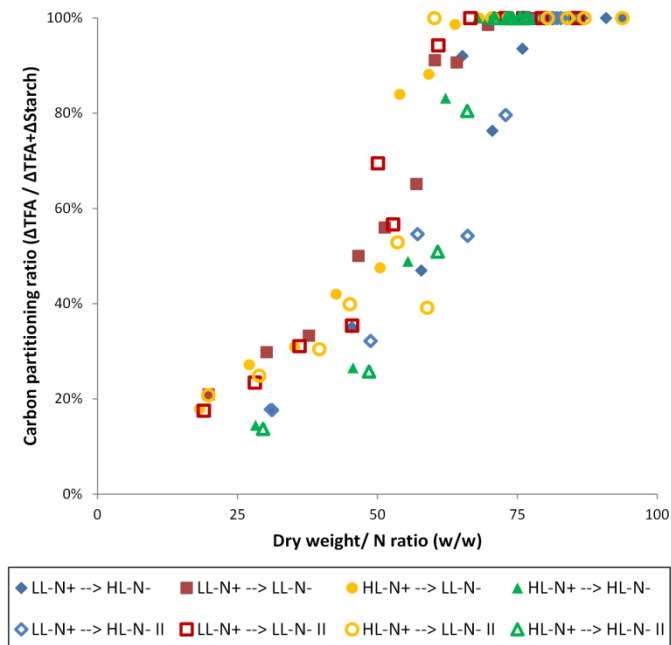


**Fig. 6.3.** Carbon partitioning between starch and fatty acids during nitrogen starvation. The carbon partitioning ratio is plotted versus the extent of nitrogen starvation, which is represented here by the dry weight/N ratio (DW/N ratio). Nitrogen replete *S. obliquus* contains approximately 9% (% of DW) nitrogen and thus has a DW/N ratio of 11. When nitrogen starvation progresses, the DW/N ratio increases. The carbon partitioning ratio was quantified as the amount of fatty acids produced between two consecutive time-points ( $\Delta\text{TFA}$ ) divided by the combined fatty acid and starch production in that same period ( $\Delta\text{TFA} + \Delta\text{Starch}$ ). Fatty acid and starch production together contributed 70% to the increase in DW during nitrogen starvation (Supplementary Fig. S3). At a low light intensity (LL-N<sup>-</sup>), carbon partitioning was favoured slightly more towards fatty acid synthesis at the same extent of nitrogen starvation (DW/N ratio), compared to a high light intensity. The photoacclimated state at the onset of nitrogen starvation (LL-N<sup>+</sup> compared to HL-N<sup>+</sup>) did not have an effect on how the carbon partitioning ratio progressed during nitrogen starvation. Red: LL-N<sup>+</sup>→LL-N<sup>-</sup>; blue: LL-N<sup>+</sup>→HL-N<sup>-</sup>; yellow: HL-N<sup>+</sup>→LL-N<sup>-</sup>; green: HL-N<sup>+</sup>→HL-N<sup>-</sup>. The closed and open symbols represent replicate cultivations.

The photoacclimated state at the onset of nitrogen starvation did not have an effect on how the fatty acid:starch synthesis ratio progressed during nitrogen starvation, as no differences were observed between the  $\Delta\text{TFA} / (\Delta\text{TFA} + \Delta\text{Starch})$  ratios of the differently photoacclimated cultures (LL-N<sup>+</sup> and HL-N<sup>+</sup>)(Fig. 6.3).

### 6.3.3 The effects of photoacclimation persist during nitrogen starvation

The light intensity towards which *S. obliquus* was acclimated, had a large impact on the absorption cross section and chlorophyll/carotenoid ratio at the onset of nitrogen starvation (the ratio of the absorption cross section between 550-700nm and 400-700nm is used as a qualitative proxy for the chlorophyll/carotenoid ratio as explained in the material and methods section; Table 6.1). These differences induced by photoacclimation persisted during nitrogen starvation (Fig. 6.4). In the LL-N<sup>-</sup> experiments, the difference in absorption cross sections and chlorophyll/carotenoid ratio, introduced by the photoacclimated state at the onset of nitrogen starvation, persisted for at least 2-3 days (Fig. 6.4A,B). During this period, the absorption cross section and chlorophyll/carotenoid ratio of the HL-N<sup>+</sup> acclimated culture converged to that of the LL-N<sup>+</sup> acclimated culture. This can be seen in the temporary increase in absorption cross section and chlorophyll/carotenoid ratio in the HL-N<sup>+</sup>→LL-N<sup>-</sup> experiments (Fig. 6.4A,B). The absorption cross section and chlorophyll/carotenoid ratio decreased immediately in the LL-N<sup>+</sup>→LL-N<sup>-</sup> experiment (Fig. 6.4A,B). In the HL-N<sup>-</sup> experiments, the difference in absorption cross section and chlorophyll/carotenoid ratio, introduced by the photoacclimated state at the onset of nitrogen starvation, persisted during almost the entire nitrogen starvation period (Fig. 6.4A,B).

During nitrogen starvation, a general trend towards a decreased absorption cross section and decreased chlorophyll/carotenoid ratio was observed (Fig. 6.4A,B). The absorption cross section (m<sup>2</sup>/kg) decreased more in the HL-N<sup>-</sup> experiments than in the LL-N<sup>-</sup> experiments. Also the chlorophyll/carotenoid ratio decreased more in the HL-N<sup>-</sup> experiments than in the LL-N<sup>-</sup> experiments (Fig. 6.4). The decrease in absorption cross section was mainly a result of dilution of existing pigments over newly formed biomass, as becomes apparent from the volumetric absorption cross section (m<sup>2</sup>/m<sup>3</sup>). This volumetric absorption cross section, which is a measure for the total pigment concentration in the reactor, increased during initial nitrogen starvation (Fig. 6.4C). This increase in volumetric pigment concentration is most apparent in the HL-N<sup>+</sup>→LL-N<sup>-</sup> experiments, where also the biomass-specific absorption cross section temporarily increased (Fig. 6.4A). In this specific experiment, the increase in pigmentation during initial nitrogen starvation also included *de novo* synthesis of chlorophyll as both the volumetric absorption cross section and the chlorophyll/carotenoid ratio increased (Fig. 6.4B,C). For the other treatments it is not possible to conclude whether *de novo* synthesis of chlorophyll occurred, due to the semi-quantitative nature of the measurements, but it nevertheless seems plausible.

## **6.4 Discussion**

### **6.4.1 Photosynthetic efficiency during nitrogen starvation**

The photosynthetic efficiency was strongly reduced in the HL-N<sup>-</sup> experiments compared to the LL-N<sup>-</sup> experiments. This is consistent with earlier findings (Breuer et al., 2013b) and it is commonly accepted that the photosynthetic efficiency decreases with increasing light intensities. This is because at low light intensities, photosynthesis is limited by light absorption, but at high light intensities, light absorption exceeds the capacity of the downstream photosynthetic machinery. This excess absorbed light is thermally dissipated, resulting in a decreased photosynthetic efficiency (Jassby & Platt, 1976). This is commonly called photosaturation.

Although the photoacclimated state at the onset of nitrogen starvation had a large impact on the composition of the photosystems during nitrogen starvation (e.g. pigmentation), the photoacclimated state at the onset of nitrogen starvation did not have an effect on the photosynthetic efficiency during nitrogen starvation. It is, however, often hypothesized that microalgae with a lower pigmentation can have a higher photosynthetic efficiency at high light intensities (de Mooij et al., 2014; Melis, 2009; Melis et al., 1999). It is then reasoned that the photosystem of microalgae with a lower pigmentation becomes saturated at a higher light intensity, because microalgae with a lower pigmentation have a lower light absorption rate at any given light intensity. This can increase the photosynthetic efficiency at high light intensities because less light is then thermally dissipated (de Mooij et al., 2014; Melis, 2009; Melis et al., 1999).



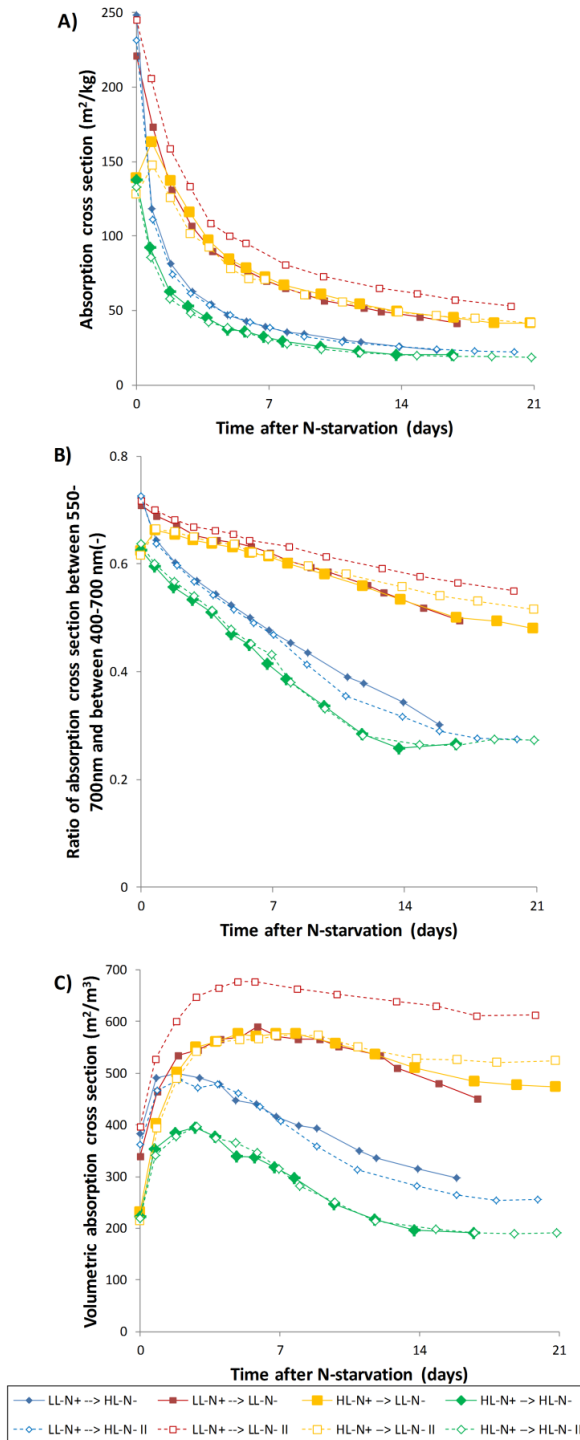


**Fig. 6.4.** Biomass-specific absorption cross section (pigmentation) **(A)**, ratio of the absorption cross section between 550-700nm and 400-700nm, used as a qualitative proxy for the chlorophyll/carotenoid ratio **(B)**, and volumetric absorption cross section ( $\text{m}^2/\text{m}^3$ ) during nitrogen starvation **(C)**. For all conditions, initially the volumetric absorption cross section increased. This illustrates *de novo* synthesis of pigments during initial nitrogen starvation. The differences in initial pigmentation and chlorophyll/carotenoid ratio, caused by the photoacclimated state (LL-N<sup>+</sup> and HL-N<sup>+</sup>), persisted during the entire nitrogen starvation period in the HL-N<sup>-</sup> experiments and persisted for at least 2-3 days in the LL-N<sup>-</sup> experiments. Time = 0 refers to the onset of nitrogen starvation. Red: LL-N<sup>+</sup> → LL-N<sup>-</sup>; blue: LL-N<sup>+</sup> → HL-N<sup>-</sup>; yellow: HL-N<sup>+</sup> → LL-N<sup>-</sup>; green: HL-N<sup>+</sup> → HL-N<sup>-</sup>. The closed symbols/solid lines and open symbols/dashed lines represent replicate cultivations.

The differently photoacclimated cultures (LL-N<sup>+</sup> and HL-N<sup>+</sup>) had an almost twofold difference in their pigmentation ( $231 \pm 14$  vs  $134 \pm 3$  m<sup>2</sup>/kg; Table 6.1). The difference in pigmentation between these differently photoacclimated cultures persisted throughout almost the entire nitrogen starvation period in the HL-N<sup>-</sup> experiments (Fig. 6.4). In theory, a twofold difference in pigmentation can result in a twofold difference in the photosaturated light intensity. This in turn can result in a twofold difference in the photosynthetic efficiency under saturating light conditions (de Mooij et al., 2014). No differences in the photosynthetic efficiency between the LL-N<sup>+</sup> and HL-N<sup>+</sup> acclimated cultures were however seen in the HL-N<sup>-</sup> experiments, as these cultures had a similar biomass productivity and biomass composition throughout the cultivation (Fig. 6.2). These results could either mean that the pigmentation did not have an effect on the photosynthetic efficiency, or it could mean that other physiological characteristics change simultaneously with the pigmentation and have an opposite effect on the photosynthetic efficiency. For example, the extent of photoinhibition also increases with light intensity. Photoinhibition is caused by light-induced damage to the photosystem reaction centres. This damage is reversible thanks to cellular repair mechanisms, but at high light intensities a larger proportion of the reaction centres is damaged. This results in a decreased photosynthetic efficiency (Rubio et al., 2003). The LL-N<sup>+</sup> acclimated cultures are thus expected to have a lower extent of photoinhibition than the HL-N<sup>+</sup> acclimated cultures. The extent of photoinhibition does not change instantaneously when the light intensity is changed and is thus likely to persist during (at least initial) nitrogen starvation (Appendix B)(Neidhardt et al., 1998; Sukenik et al., 1990). This means that the potential negative effects of a high pigmentation can possibly be counteracted by a lower extent of photoinhibition in the LL-N<sup>+</sup> acclimated cultures, resulting in a similar net photosynthetic efficiency as in the HL-N<sup>+</sup> acclimated cultures that have a low pigmentation but possibly also a higher extent of photoinhibition.

Similar observations were made for a change in light intensity under nitrogen replete conditions. After a transition from a high to a low light intensity, the photosynthetic rate (quantified using the  $\Delta O_2$  and the  $\Delta CO_2$  concentration in the reactor off-gas) was temporarily lower than the steady state photosynthetic rate that was ultimately reached. This is an indication that the photosynthetic efficiency was temporarily lower and that the detrimental effects of photoinhibition possibly persisted after a transition from a high to a low light intensity (Appendix B). After a transition from a low to a high light intensity, the photosynthetic rate was temporarily higher than the steady state photosynthetic rate that was ultimately reached. Exactly the opposite would have been expected based on the higher pigmentation caused by acclimation to the low light

intensity (Table 6.1). It could however be explained if the microalgae that were acclimated to a low light intensity had a lower extent of photoinhibition which improved their photosynthetic efficiency during these high light intensity conditions (Appendix B).

#### **6.4.2 Carbon partitioning during nitrogen starvation**

It was found that 70% of the biomass produced during nitrogen starvation consisted of starch and fatty acids (Supplementary Fig. S3). The ratio in which fatty acids and starch were produced was highly variable and dependent on the extent of nitrogen starvation, which was quantified as the DW/N ratio (Fig. 6.3). At the lowest DW/N ratios (immediately after the onset of nitrogen starvation), fatty acids and starch were produced in a 1:4 ratio. At the highest DW/N ratios (end of nitrogen starvation), only fatty acids were produced and the initially accumulated starch was degraded (Fig. 6.3; Supplementary Fig. S4). Likely, the degradation products of starch are used as a substrate for fatty acid synthesis (Breuer et al., 2014). The synthesis of starch, or other carbohydrates, simultaneous with fatty acid synthesis has also been observed for various other microalgae species (Breuer et al., 2012; Dillschneider & Posten, 2013; Fernandes et al., 2013; Klok et al., 2013b; Siaut et al., 2011). And in *Neochloris oleoabundans*, it was also found that relatively more TAG is produced at lower biomass nitrogen content (more severe nitrogen limitation)(Klok et al., 2013a; Klok et al., 2013b). The inter-conversion of carbohydrates to fatty acids has also been described for various other microalgae species (Li et al., 2011; Msanne et al., 2012; Roessler, 1988; Zhu et al., 2013). It has up to now, however, never been quantified how these processes progress during nitrogen starvation and how these are influenced by the light intensity or photoacclimated state.

The same general trend in carbon partitioning was observed for all combinations of the light intensity during nitrogen starvation and the photoacclimated state at the onset of nitrogen starvation (Fig. 6.2; Fig. 6.3). However, at high light intensities, slightly more carbon was partitioned towards starch at similar DW/N ratios (Fig. 6.3). This difference is reflected by the slightly higher maximum starch content that was achieved in the HL-N<sup>-</sup> experiments (Fig. 6.2C). Similar observations were made for *N. oleoabundans*, where it was also found that at higher light intensities, and at a given DW/N ratio, more light energy is partitioned towards starch (Klok et al., 2013a; Klok et al., 2013b). The photoacclimated state at the onset of nitrogen starvation did not have any effect on how the fatty acid:starch partitioning ratio progressed during nitrogen starvation (Fig. 6.2; Fig. 6.3).

It is often proposed that fatty acid accumulation during nitrogen starvation is caused by an “overflow-metabolism”-like response, in which excess light energy is used for fatty acid synthesis (Kandilian et al., 2014; Packer et al., 2011). It is however unlikely that such a mechanism controls fatty acid accumulation in *S. obliquus*. In that case, a very large increase in carbon partitioning towards fatty acid synthesis would be expected with increasing light intensities. This is not observed. In fact, slightly more light energy is partitioned towards starch at high light intensities. This means that if any overflow metabolism would be active during nitrogen starvation, starch is the most likely overflow metabolite. Such a hypothesis is seemingly supported by the observation that during initial nitrogen starvation mainly starch is accumulated. Starchless mutants of *S. obliquus*, however, do not show a decreased photosynthetic efficiency during nitrogen starvation and can efficiently redirect the liberated photosynthetic capacity towards fatty acid synthesis (Breuer et al., 2014). This makes it unlikely that starch functions as an overflow metabolite.

A more likely explanation for the observed partitioning between fatty acids and starch is that it is caused by competition for a common carbon pre-cursor between the fatty acid and starch synthesis pathways (Fan et al., 2012; Li et al., 2010a; Msanne et al., 2012). This is supported by the fact that fatty acid synthesis and starch synthesis are simultaneously active, and share the products of the Calvin cycle as a common carbon pre-cursor. Furthermore, fatty acid synthesis can readily take over the carbon flux through the starch synthesis pathway when this pathway is eliminated in starchless mutants of *S. obliquus* (Breuer et al., 2014; de Jaeger et al., 2014). Finally, it is unlikely that starch or fatty acid synthesis are limited by the capacity of their synthesis machinery during nitrogen starvation. This becomes apparent from the observation that, at the same extent of nitrogen starvation (DW/N ratio), the ratio between starch and fatty acid synthesis is mostly independent of the light intensity and corresponding biomass productivity (Fig. 6.3). This means that both the fatty acid and starch synthesis rate increase roughly proportionally to the biomass productivity. More evidence that the fatty acid synthesis capacity is not limiting is provided by the observation that starchless mutants can achieve much higher fatty acid synthesis rates than their wild-types (Breuer et al., 2014; de Jaeger et al., 2014; Li et al., 2010a).

The ratio between fatty acid and starch synthesis does however change when nitrogen starvation progresses. This changing ratio could be explained by a changing activity of their pathways over time. The observation that this ratio changes independently of the

photoacclimated state and almost independently of the light intensity, suggests that the activity of both pathways is tightly regulated during nitrogen starvation. This is consistent with observations in the transcriptome of other microalgae species during nitrogen starvation, where it is found that transcript-level regulation occurs for the glycolysis, TCA cycle, and fatty acid synthesis pathways (Li et al., 2014). In addition, the activity of these pathways could be redox or allosterically regulated, as is known to occur in higher plants (Hunter & Ohlrogge, 1998).

## 6.5 Conclusion

The photoacclimated state at the onset of nitrogen starvation does not affect the photosynthetic efficiency or carbon partitioning during nitrogen starvation. High light intensities during nitrogen starvation result in lower photosynthetic efficiencies and favours carbon partitioning slightly more towards starch synthesis. Carbon partitioning between starch and fatty acids strongly correlates to the DW/N ratio. At the lowest DW/N ratios, fatty acids and starch are produced in a 1:4 ratio. At increasing DW/N ratios, this ratio progressively shifts towards only fatty acid synthesis. At these DW/N ratios, starch is degraded and likely used as a substrate for fatty acid synthesis. Likely, this observed carbon partitioning is caused by competition between fatty acid and starch synthesis for a common carbon pre-cursor.

## Abbreviations

DW: Dry weight; TAG: triacylglycerol; TFA: total fatty acids; LL-N<sup>+</sup>: photoacclimated during nitrogen replete chemostat operation to a light intensity of 200  $\mu\text{mol m}^{-2} \text{s}^{-1}$ ; HL-N<sup>+</sup>: photoacclimated during nitrogen replete chemostat operation to a light intensity of 1000  $\mu\text{mol m}^{-2} \text{s}^{-1}$ ; LL-N<sup>-</sup>: nitrogen-depleted culture at a light intensity of 200  $\mu\text{mol m}^{-2} \text{s}^{-1}$ ; HL-N<sup>-</sup>: nitrogen-depleted depleted culture at a light intensity of 1000  $\mu\text{mol m}^{-2} \text{s}^{-1}$ .

## Acknowledgements

This research project is financially supported by the Food and Nutrition Delta program of Agentschap NL (FND10007) and Unilever.

## Appendix A: Determination of required dilution rate and effects of photoacclimation

### A1.1 Methods

A 90-95% consumption of the 10 mM  $\text{NO}_3^-$  in the feed medium was desired for the chemostat cultivations presented in the main text. Because the biomass nitrogen content of nitrogen-replete-grown *S. obliquus* is approximately 9% (w/w) of DW (measured using the DUMAS method; results not shown). The corresponding biomass concentration to this 90-95% consumption is thus approximately 1.5 g/l. To find the dilution rate that results in this biomass concentration, first chemostat cultivations were performed with a  $\text{NO}_3^-$  concentration of 34 mM in which the biomass yield on light (Eq. A1) and biomass composition were determined as a function of the incident light intensity. The dilution rates of these chemostats were iteratively adapted until the steady-state biomass concentration was between 1.3 and 1.8 g/l.

To better understand the effects of photoacclimation, this was done for incident light intensities between 100 and 1400  $\mu\text{mol m}^{-2} \text{s}^{-1}$  (thus not only at incident light intensities of 200 and 1000  $\mu\text{mol m}^{-2} \text{s}^{-1}$  that were used for the experiments in the main text). This resulted in dilution rates between approximately 0.4  $\text{day}^{-1}$  at 100  $\mu\text{mol m}^{-2} \text{s}^{-1}$  and approximately 2.0  $\text{day}^{-1}$  at 1400  $\mu\text{mol m}^{-2} \text{s}^{-1}$ . These dilution rates were subsequently used as initial estimates for the required dilution rate for the 10 mM  $\text{NO}_3^-$  chemostats. Subsequently, these dilution rates in the 10 mM  $\text{NO}_3^-$  chemostats were iteratively adapted until the 90-95% consumption of  $\text{NO}_3^-$  criterion was satisfied. These dilution rates are shown in Table 6.1.

$$\text{Yield} \left[ \frac{\text{g}}{\text{mol}} \right] = \frac{\text{dilution rate} [\text{day}^{-1}] \cdot \text{biomass concentration} \left[ \frac{\text{g}}{\text{l}} \right] \cdot 10^3 \left[ \frac{\text{l}}{\text{m}^3} \right]}{\text{light intensity} [\mu\text{mol m}^{-2} \text{s}^{-1}] \cdot \frac{1}{\text{reactor thickness} [\text{m}]} \cdot 10^{-6} \left[ \frac{\text{mol}}{\mu\text{mol}} \right] \cdot 60 \cdot 60 \cdot 24 \left[ \frac{\text{s}}{\text{day}} \right]}$$

Eq.  
A1

### A1.2 Results

The results of these chemostat cultivations, that were operated with a residual  $\text{NO}_3^-$  concentration of 0.5-1 mM (90-95% consumption of the initial 10mM  $\text{NO}_3^-$  in the culture medium), are shown in the main text and were compared to the chemostat cultivations that were operated at the same dilution rate, but with a  $\text{NO}_3^-$  concentration in the feed-medium of 34mM (residual  $\text{NO}_3^-$  concentration of approximately 24 mM). In these experiments similar biomass concentrations, yields, and absorption cross sections were

achieved (Fig. A1). This confirmed that this 0.5-1 mM residual  $\text{NO}_3^-$  was not limiting for growth during the chemostat cultivation nor affected photoacclimation (Fig. A1). Both the photosynthetic biomass yield and absorption cross section were approximately twofold lower at high light intensities than at low light intensities (Fig. A1). The biomass yield on light decreased from approximately 1.25 to 0.6 g/mol and the absorption cross section decreased from 200-250 to 120  $\text{m}^2/\text{kg}$  between incident light intensities ranging from 100 to 1400  $\mu\text{mol m}^{-2} \text{s}^{-1}$  (Fig. A1; Table 6.1). Also the pigment class composition changed towards a reduced chlorophyll/carotenoid ratio with increasing light intensities, as is apparent in the ratio of the absorption cross section between 550-700nm and between 400-700nm (Fig. A1; Table 6.1).

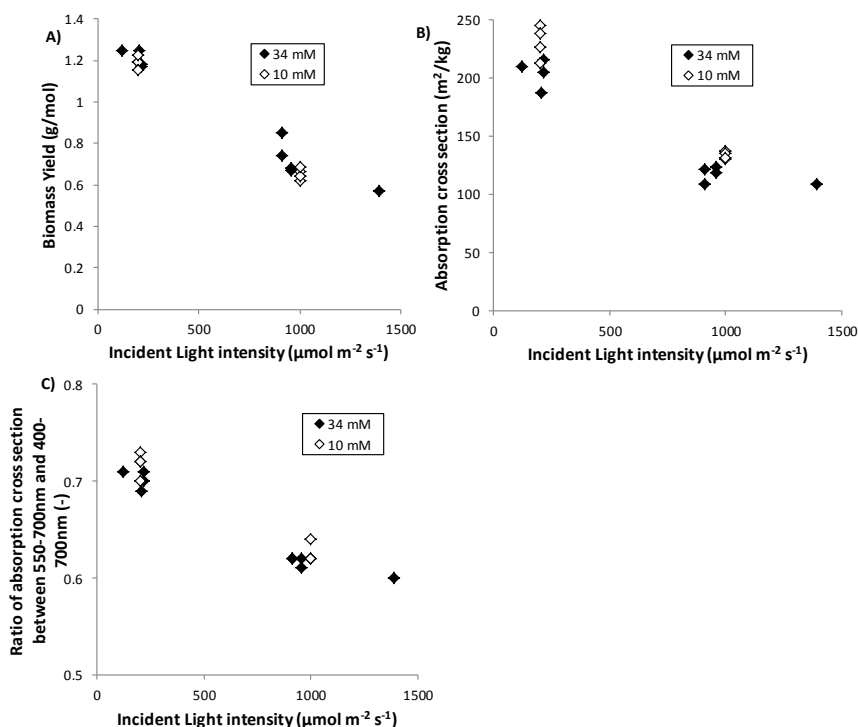


**Fig. A1.** The photosynthetic biomass yield (A), absorption cross section (B), and ratio of absorption cross section between 550-700nm and 400-700nm (C) during nitrogen replete chemostat cultivation are dependent on the incident light intensity. Values shown are steady-state values obtained from light-limited, nitrogen replete, chemostat cultivations. The results of the chemostat cultivations that were operated with a 5-10% residual  $\text{NO}_3^-$  concentration of the initial 10mM in the culture medium (open symbols) and of the chemostat cultivations operated at the same dilution rate, but with a  $\text{NO}_3^-$  concentration in the culture medium of 34mM (closed symbols) are both shown. The biomass concentration was in all cases between 1.3 and 1.8 g/l.

## **Appendix B: Dynamics of photoacclimation in response to a change in light intensity**

### **B2.1 Methods**

To investigate how *S. obliquus* acclimates to a change in light intensity during nitrogen replete conditions, chemostat cultivations similar as described in Appendix A (using a  $\text{NO}_3^-$  concentration of 34 mM) were performed, at an incident light intensity of 200 and 1000  $\mu\text{mol m}^{-2} \text{s}^{-1}$ . Subsequently, the steady-state operation of these chemostat cultivations was perturbed by changing the incident light intensity and measuring the subsequent photoacclimation. To maintain a constant biomass concentration, the dilution rate was changed accordingly, simultaneously with the change in light intensity. The required dilution rate was determined as described in Appendix A and the biomass concentration was between 1.4 and 1.9 g/l at all times.

Experiments were performed in which the incident light intensity was increased from 200 to 1000  $\mu\text{mol m}^{-2} \text{s}^{-1}$  (LL→HL), and experiments were performed in which the incident light intensity was decreased from 1000 to 200  $\mu\text{mol m}^{-2} \text{s}^{-1}$  (HL→LL). The biomass concentration, absorption cross section and the  $\Delta\text{O}_2$  and  $\Delta\text{CO}_2$  concentration (absolute difference between the concentration in the ingoing gas and off-gas of the reactor) were measured during this transition. The  $\Delta\text{O}_2$  and  $\Delta\text{CO}_2$  concentration were used as a proxy for the photosynthetic rate.

### **B2.2 Results**

The acclimation of the pigmentation (as quantified using the absorption cross section) and pigment class composition (as quantified using the ratio of absorption between 550-700 and between 400-700nm) to a change in light intensity took more than two days, equivalent to at least one culture dilution (i.e. at least one biomass replication), before new steady-state values were achieved (Fig. A2A,C). This is consistent with the observations by for example (Sukenik et al., 1990), who found that half-times of changes to the photosynthetic machinery, upon a change in light intensity, are in the order of 10h.

As measured by the  $\Delta\text{O}_2$  and  $\Delta\text{CO}_2$  concentration (absolute difference between the concentration in the ingoing gas and off-gas of the reactor), the photosynthetic rate responded immediately to a change in light intensity. Nevertheless, it took several days (and thus also biomass replications) before new steady-state values for the photosynthetic rate were reached (Fig. A2B,D). In the LL→HL transition experiment, the photosynthetic rate was initially well above the steady-state value before it decreased



towards the steady-state value. The opposite was observed in the HL→LL transition experiment, although to a lesser extent. In this case, a temporarily decreased photosynthetic rate was observed (Fig. A2D).

A temporary difference in biomass composition might explain such a temporary difference in the photosynthetic rate because different biomass constituents have a different specific photosynthetic requirement (Breuer et al., 2014). The differences in biomass composition between *S. obliquus* that was acclimated to a low and a high light were however minor (Table 6.1). Nevertheless it remains possible that the biomass composition changes temporarily upon a change in light intensity, contributing to this difference in photosynthetic rate. When disregarding any influences of this slightly different biomass composition, the photosynthetic efficiency would be directly proportional to the photosynthetic rate because nearly all incident light was absorbed (material and methods section). In that case, the results would suggest a temporarily higher photosynthetic efficiency in the LL→HL transition experiment and a temporarily lower photosynthetic efficiency in the HL→LL transition experiment (Fig. A2B,D).

It has often been proposed that microalgae with a lower pigmentation have a higher light saturated light intensity and as a consequence can have a higher photosynthetic efficiency at high light intensities (Melis, 2009; Melis et al., 1999). Similar, microalgae with a high pigmentation are expected to have a lower photosynthetic efficiency at high light intensities than microalgae with a low pigmentation. In the LL→HL transition experiment, the pigmentation was initially approximately twofold higher than the steady state pigmentation at this high light intensity (Fig. A2A). If the pigmentation would be the only difference between low and high light acclimated cells, this would decrease the photosaturating light intensity twofold and thus result in a twofold reduction in the photosynthetic efficiency under saturating light conditions. However, the observed higher pigmentation did not result in a decreased photosynthetic efficiency during this transition period (Fig. A2B). In fact, the photosynthetic efficiency was higher during this transition from a low to high light intensity.

Among possible other explanations, this temporary increase in photosynthetic efficiency could be explained by a lower extent of photoinhibition in low light acclimated microalgae. Photoinhibition is caused by light-induced damage to the photosystem. This damage is reversible, and the extent of photoinhibition is therefore a result of an equilibrium between damage and repair rates (Rubio et al., 2003). At high light intensities, this damage rate increases, resulting in a larger extent of photoinhibition

(Baroli & Melis, 1996; Rubio et al., 2003). These damaged photosystems thermally dissipate all absorbed light, resulting in a decreased photosynthetic efficiency (Baroli & Melis, 1996; Rubio et al., 2003). The extent of photoinhibition does not change instantaneously when the light intensity is changed and takes time to build up (in the case of a shift from low to high light) or to repair (in the case of a shift from high light to low light) (Baroli & Melis, 1996; Neidhardt et al., 1998). In the LL→HL transition experiment, the lower extent of photoinhibition during this transition could explain the temporarily higher photosynthetic efficiency (Fig. A2B). Similarly, in the HL→LL transition experiments, the higher extent of photoinhibition could explain the temporarily lower photosynthetic efficiency (Fig. A2D).

In summary, these results are an indication that the detrimental effects of photoinhibition can be larger than the beneficial effects of a lower pigmentation in the initial phase after a change in light intensity. In microalgae acclimated to a high light intensity, the built-up photoinhibition can thus counteract the effects of the reduced pigmentation. This also means that the behaviour of short-antennae mutants, mutants that have a natural lower pigmentation, is fundamentally different from microalgae that have a lower pigmentation as a result of photoacclimation. This is because in these antennae mutants, the lower pigmentation does not (necessarily) coincide with an increased photoinhibition, where-as in microalgae that have a low pigmentation as a result of photoacclimation, photoinhibition and a low pigmentation do coincide. These insights in photoacclimation and photoinhibition, and their timescales, can be valuable to understand the biomass production in highly variable light intensity conditions, as will be encountered in outdoor cultivation.

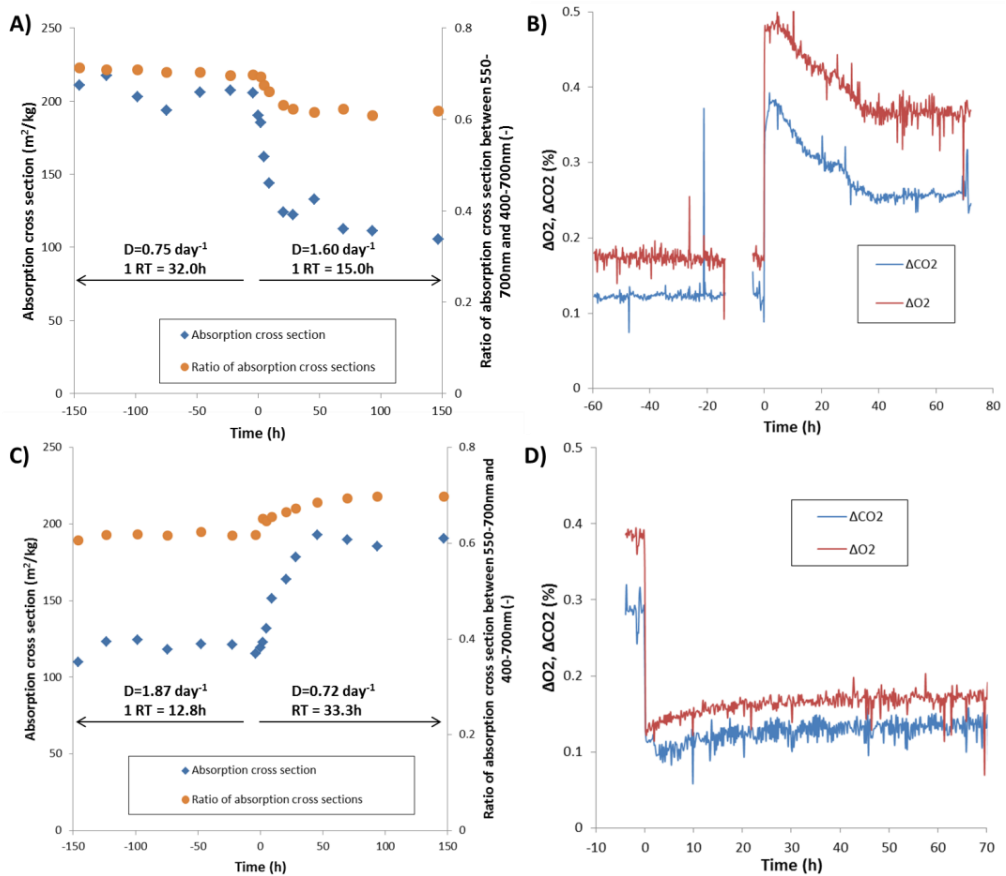
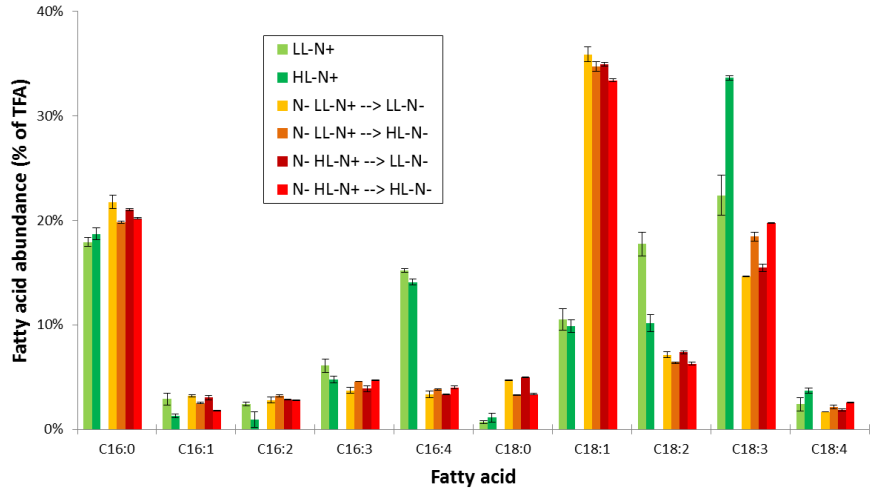
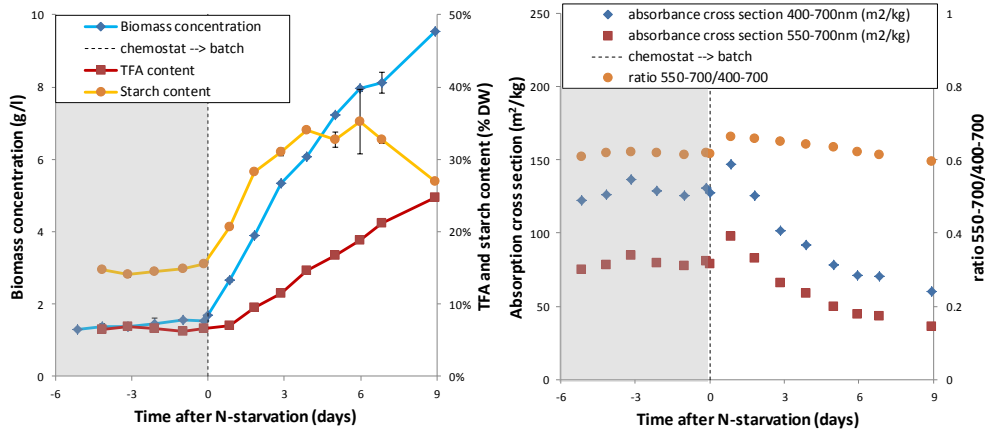


**Fig. A2.** Acclimation to a change in incident light intensity in light-limited, nitrogen replete, chemostat cultivations. A,B: Acclimation from 200 to 1000  $\mu\text{mol m}^{-2} \text{s}^{-1}$ . C,D: Acclimation from 1000 to 200  $\mu\text{mol m}^{-2} \text{s}^{-1}$ . Time = 0 refers to the moment of the change in incident light intensity. The dilution rate was adjusted simultaneously with the change in incident light intensity, such that the biomass concentration remained between 1.3 and 1.8 g/l in all cases. These dilution rates (symbol D) are indicated in figure A and C, together with the duration of one retention-time (RT; equal to  $1/D$ ). A,C: Absorption cross section and pigment composition (expressed as ratio between absorption cross section between 550-700 and 400-700nm). B,D:  $\Delta\text{O}_2$  and  $\Delta\text{CO}_2$  concentration in the reactor off-gas, used as a proxy for the photosynthetic rate. To allow for representation on the same scale, the absolute values of  $\Delta\text{O}_2$  and  $\Delta\text{CO}_2$  are shown. Nearly all incident light was absorbed, and differences in photosynthetic rate are thus a result of differences in photosynthetic efficiency and not a result of differences in the amount of light absorbed. Due to technical problems with the mass spectrometer, off-gas data between -14h and -4h (figure B) and before -4h (figure D) is not available.

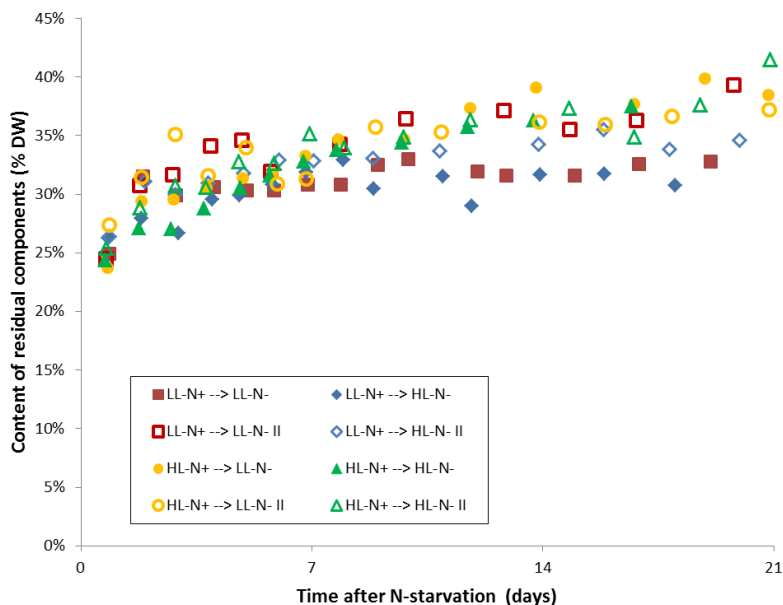
Appendix C: Supplementary figures



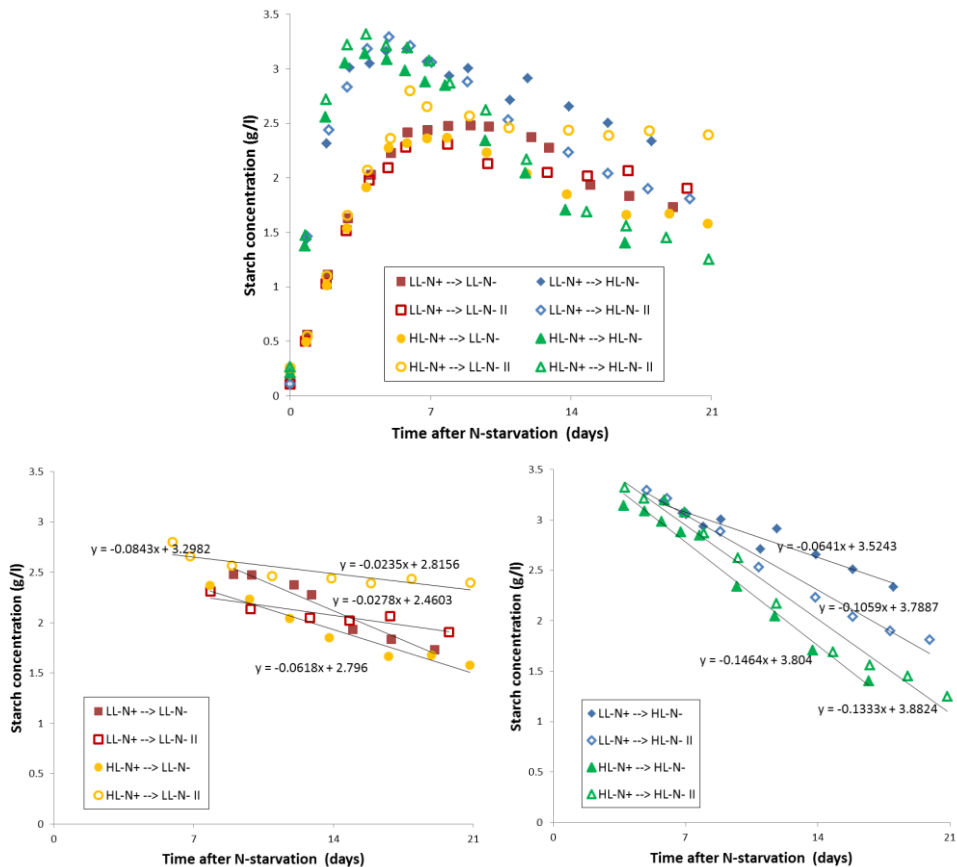
**Supplementary Fig. S1.** Fatty acid composition during nitrogen replete cultivation (green bars) and the fatty acid composition at the end of nitrogen starvation (orange to red bars). The relative fatty acid abundance of all C16 and C18 fatty acid species are shown (expressed as percentage of total fatty acids). Fatty acids with other chain lengths were detected, but only in minor amounts (<2%) and are therefore not shown. Error bars indicate the standard deviation (n=4, nitrogen replete) or deviation from average between replicate cultivations (n=2, nitrogen-depleted).



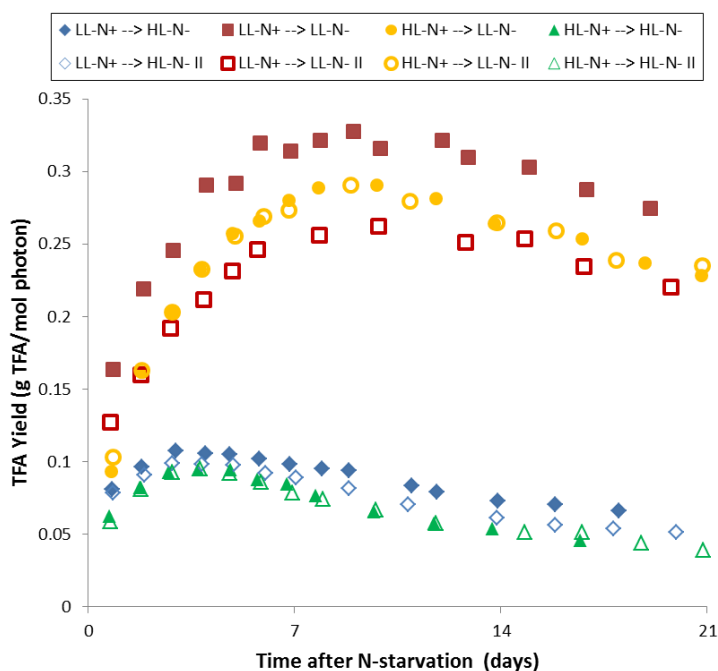
**Supplementary Fig. S2.** Example of the transition from light limited, nitrogen replete, chemostat operation to nitrogen-depleted batch operation. The grey area left of the dotted line represents the nitrogen replete chemostat part of the cultivation. The vertically dotted line represents the transition from the chemostat operation to the batch operation (at time =0). The white area right of the dotted line represents the nitrogen-depleted batch part of the cultivation (only the first 9 days are shown). The data shown correspond to the HL-N<sup>+</sup>→LL-N<sup>-</sup> II experiment. Left: biomass concentration (blue), total fatty acid (TFA) content (red), and starch content (yellow). Right: biomass-specific absorption cross section between 400-700nm (blue) and 550-700nm (red) and the ratio between both (orange). DW = dry weight.



**Supplementary Fig. S3.** Residual biomass (biomass that is produced during nitrogen starvation and is not starch or fatty acids) during nitrogen starvation. This fraction is calculated as  $residual\ biomass(t) = dry\ weight(t) - dry\ weight(t = 0) - TFA(t) - starch(t)$ , in which each term represents the corresponding concentration in g/l at timepoint  $t$ , and  $t=0$  refers to the onset of nitrogen starvation. In all experiments, this residual biomass contributed approximately 30-35% to the dry weight (DW) concentration throughout the entire nitrogen starvation period. It is hypothesized that this residual biomass constitutes of carbohydrates other than starch, for example cellulose present in the cell wall (Breuer et al., 2014). Red:  $LL-N^+ \rightarrow LL-N^-$ ; blue:  $LL-N^+ \rightarrow HL-N^-$ ; yellow:  $HL-N^+ \rightarrow LL-N^-$ ; green:  $HL-N^+ \rightarrow HL-N^-$ . The closed and open symbols represent replicate cultivations.



**Supplementary Fig. S4.** Starch concentration (g/l) throughout the nitrogen-depleted batch part of all cultivations (top). The maximum starch concentration was higher in the HL-N<sup>-</sup> experiments ( $3.24 \pm 0.09$ ) than in the LL-N<sup>-</sup> experiments ( $2.49 \pm 0.22$ ). After a maximum concentration is reached, starch is degraded. When 0<sup>th</sup>-order-degradation kinetics are assumed, these degradation rates were  $56 \pm 28$  mg l<sup>-1</sup> day<sup>-1</sup> for the LL-N<sup>+</sup>→LL-N<sup>-</sup> cultivation,  $43 \pm 19$  mg l<sup>-1</sup> day<sup>-1</sup> for the HL-N<sup>+</sup>→LL-N<sup>-</sup> cultivation,  $85 \pm 21$  mg l<sup>-1</sup> day<sup>-1</sup> for the LL-N<sup>+</sup>→HL-N<sup>-</sup> cultivation, and  $140 \pm 7$  mg l<sup>-1</sup> day<sup>-1</sup> for the HL-N<sup>+</sup>→HL-N<sup>-</sup> cultivation (bottom left and bottom right). Although, the degradation rate of starch was on average higher in the HL-N<sup>-</sup> experiments, this difference was not statistically significant (paired samples student t-test; n=4; p=0.126). Red: LL-N<sup>+</sup>→LL-N<sup>-</sup>; blue: LL-N<sup>+</sup>→HL-N<sup>-</sup>; yellow: HL-N<sup>+</sup>→LL-N<sup>-</sup>; green: HL-N<sup>+</sup>→HL-N<sup>-</sup>. The closed and open symbols represent replicate cultivations.



**Supplementary Fig. S5.** Time-averaged yield of total fatty acids on light throughout the nitrogen-starved batch cultivation. This time-averaged yield is calculated for each time-point as the yield over the period between that time-point and  $t=0$  (the onset of nitrogen starvation). The maximum observed value among these time-averaged yields for each cultivation is used as the maximum time-averaged yield in the main text (Table 6.2). These maximum time-averaged yields were  $0.294 \pm 0.034$ ,  $0.291 \pm 0.000$ ,  $0.103 \pm 0.004$ , and  $0.095 \pm 0.000$  g/mol for the cultivations of  $\text{LL-N}^+ \rightarrow \text{LL-N}^-$ ,  $\text{HL-N}^+ \rightarrow \text{LL-N}^-$ ,  $\text{LL-N}^+ \rightarrow \text{HL-N}^-$ , and  $\text{HL-N}^+ \rightarrow \text{HL-N}^-$   $\mu\text{mol m}^{-2} \text{s}^{-1}$ , respectively. Red:  $\text{LL-N}^+ \rightarrow \text{LL-N}^-$ ; blue:  $\text{LL-N}^+ \rightarrow \text{HL-N}^-$ ; yellow:  $\text{HL-N}^+ \rightarrow \text{LL-N}^-$ ; green:  $\text{HL-N}^+ \rightarrow \text{HL-N}^-$ . The closed and open symbols represent replicate cultivations.





## **Chapter 7** Opportunities to improve the areal oil productivity of microalgae

**This chapter has been submitted for publication as:**

Guido Breuer, Packo P. Lamers, Marcel Janssen, René H. Wijffels, Dirk E. Martens,  
Opportunities to improve the areal oil productivity of microalgae

### **Abstract**

New sustainable sources of vegetable oil are highly desired as global demands for food and biofuels increase rapidly. Arable land to produce these vegetable oils is however limited. Microalgae have the potential to achieve much higher oil productivities than common terrestrial plants and can be cultivated on non-arable land. Microalgae are therefore often considered as a promising alternative natural-source of vegetable oils. Projected microalgal productivities are, however, often poorly supported by scientific evidence and based on too optimistic assumptions. To provide a better insight in what can be expected from microalgae, we condensed existing knowledge and novel scientific insights into a mechanistic model that describes photosynthesis and carbon partitioning. Subsequently, we quantified the potential for improvement in oil productivity for various technologies and projected that improvements in the carbon-partitioning mechanism, photosynthesis, and reactor design can improve the oil productivity from 2.1 to up to 10.9 g m<sup>-2</sup> day<sup>-1</sup>.

## **7.1 Introduction**

New sustainable sources of vegetable oil are highly desired as global demands for food and biofuels increase rapidly. Arable land to produce these vegetable oils is however limited. Microalgae have the potential to achieve much higher oil productivities than common terrestrial plants and can be cultivated on non-arable land (Wijffels & Barbosa, 2010). Microalgae are therefore often considered as a promising alternative natural-source of vegetable oils (this oil is from here on referred to as triacylglycerol; TAG)(Draaisma et al., 2013). Although high productivities are often projected for microalgae, these projected productivities are often poorly supported by scientific evidence and based on too optimistic assumptions (Waltz, 2009). Projections that are supported by a detailed understanding of the microalgal physiology are therefore highly desired.

Oleaginous microalgae only produce TAG in response to nitrogen starvation (Breuer et al., 2012). This microalgal response to nitrogen starvation is complex, and affects both the photosynthetic efficiency and carbon partitioning. A model can help to quantify how biological traits, process conditions, and process design influence, and can be exploited to enhance, TAG production. Because existing models either focus on photosynthesis (Geider et al., 1998b; Packer et al., 2011; Quinn et al., 2011a) or carbon partitioning (Dillschneider & Posten, 2013; Klok et al., 2013b; Mairet et al., 2011) during nitrogen starvation, they only partly describe the actual response to nitrogen starvation. To provide a better insight in what can be expected from microalgae, we therefore condensed existing knowledge and novel scientific insights into a novel mechanistic model that independently describes the effects of nitrogen starvation on photosynthesis and carbon partitioning. Subsequently, we used the model to quantify how improvements in the carbon-partitioning mechanism, photosynthesis, and reactor design can improve the TAG productivity. These findings are finally used to provide projections of microalgal areal TAG productivities.

## **7.2 Results and Discussion**

### **7.2.1 Model development**

The developed model consists of a photosynthesis module and a carbon partitioning module (Appendix A.1-5). The photosynthesis module uses a photosynthesis-irradiance response curve (PI-curve) to describe the part of the absorbed photons that is used for photosynthesis and the part that is thermally dissipated, as a function of light intensity and extent of nitrogen starvation (Appendix A.2). At low light intensities, the photosynthetic rate is limited by absorption of photons and increases linearly with

increasing light intensity (Fig. 7.1a). This increase is proportional to the absorption cross section ( $\alpha$ ) and the photosynthetic quantum yield ( $\psi_N$ ). At higher light intensities, the photosynthetic machinery becomes saturated and the photosynthetic rate approaches a maximum photosynthetic rate ( $q_{hv}^{max}$ ). The values of these parameters decrease during nitrogen starvation as a result of a reduction in pigmentation (Breuer et al., 2014; da Silva et al., 2009; Kandilian et al., 2014), a reduction in the photosynthetic capacity (da Silva et al., 2009; Geider et al., 1998b), increased photoinhibition, and changes in pigment (Breuer et al., 2014; Kandilian et al., 2014) and photosystem composition (Simionato et al., 2013) (Appendix A.2). These changes affect the shape of the PI-curve (Fig. 7.1a), the photo-saturated light intensity (Fig. 7.1a), light attenuation (Fig. 7.1b), and as a consequence of these, the local photosynthetic rates in the photobioreactor (Fig. 7.1c). When assumed that characteristic times of photosynthesis are much smaller than mixing times, the average photosynthetic rate in the photobioreactor can be found as the average of these local photosynthetic rates (Vejrazka et al., 2013) (Appendix A.2).

This photosynthetic response to nitrogen starvation results in a decreased photosynthetic efficiency, but photosynthesis and carbon assimilation continue (Breuer et al., 2012). Many models that focus on the above mentioned photosynthetic response, often assume that all excess photosynthetic capacity during nitrogen starvation is used for TAG synthesis (Packer et al., 2011; Quinn et al., 2011a). This is however not the case. Various biomass constituents are made during nitrogen starvation, in a continuously changing ratio. These can account for more than half of the increase in dry weight (Breuer et al., 2012).

Therefore, we propose a novel carbon-partitioning mechanism, based on the results from chapter 5 and 6 (Fig. 7.1d). Here, the photosynthetic capacity is first used to fulfil maintenance requirements. Next, in the presence of a nitrogen source, only reproducing biomass is made. This reproducing biomass constitutes of a constant ratio of proteins, lipids, and carbohydrates (Appendix A.3). In the absence of a nitrogen source, first a fraction of the photosynthetic capacity is used for the synthesis of residual biomass other than starch and TAG (CHO), such that this fraction in the total biomass remains constant (Supplementary Fig. A.3). It is assumed that CHO constitutes of structural carbohydrates other than starch (*e.g.* cellulosic cell wall material)(Breuer et al., 2014). The remaining capacity is partitioned towards synthesis of starch and TAG. During initial nitrogen starvation, most of this capacity is used for the synthesis of starch and when nitrogen starvation progresses, more and eventually all of this capacity is used for TAG

synthesis (Supplementary Fig. A.4; chapter 6). When nitrogen starvation progresses further, starch is inter-converted into TAG (Breuer et al., 2014; Roessler, 1988).

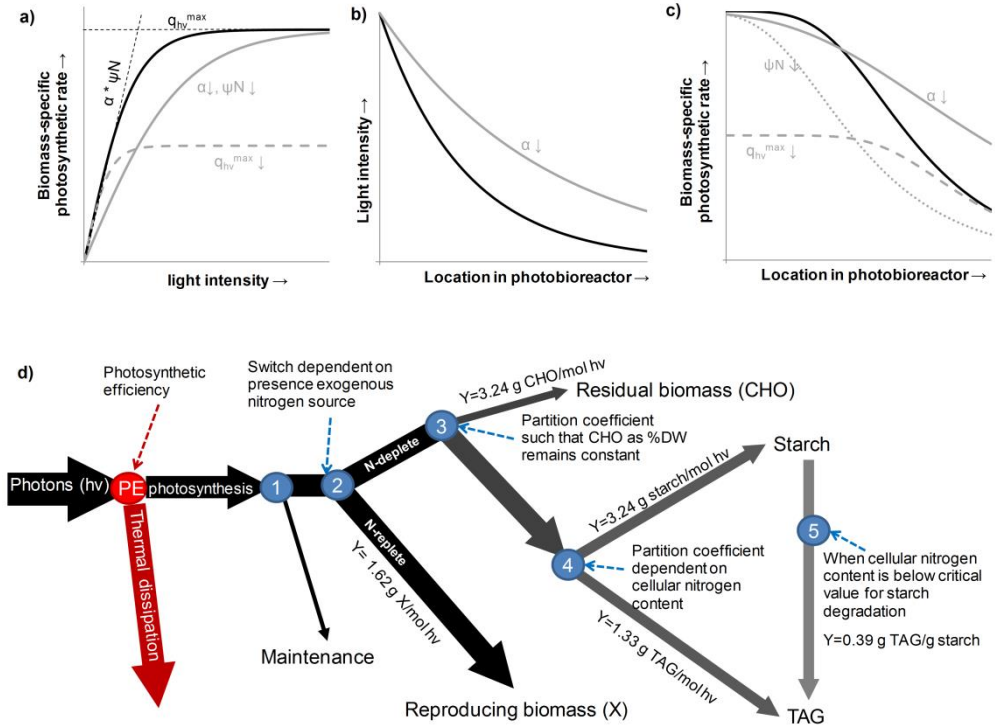


**Fig. 7.1** Nitrogen starvation affects photosynthesis and carbon partitioning. Schematic representation of the impact of a decrease in the absorption cross section ( $\alpha$ ), photosynthetic quantum yield ( $\psi_N$ ), or maximum photosynthetic rate ( $q_{hv}^{max}$ ) on the photosynthesis-irradiance response curve (**a**), and on light attenuation in a photobioreactor (**b**). Combining the photosynthesis-irradiance response curve and light attenuation gives the local biomass specific photosynthetic rate as a function of the location parallel to the incident light (**c**). The black lines represent the reference case and the grey lines represent the change caused by a reduction in  $\alpha$ ,  $\psi_N$ , or  $q_{hv}^{max}$ . Carbon partitioning in *S. obliquus* (**d**). The photosynthesis module provides the photosynthetic rate, expressed as the amount of photons (hv) that become available for metabolism (node PE). Then, the photosynthetic-rate is used to fulfil the maintenance requirements (node 1). Under nitrogen-replete conditions all remaining photosynthetic capacity is used to produce reproducing biomass (node 2). Under nitrogen deplete conditions, a fraction of the available photons is used for the synthesis of residual biomass (CHO) such that the CHO content remains constant (node 3). The remainder is partitioned between TAG and starch (node 4). This partitioning ratio is dependent on the cellular nitrogen content (% N in DW). Finally, starch is inter-converted into TAG when the cellular nitrogen content decreases below a critical value (node 5). The depicted photosynthetic and inter-conversion yields of the different biomass constituents were calculated using flux balance analysis.

To include the behaviour of starchless mutants in this model, this carbon-partitioning mechanism is adapted using the assumption that all remaining photosynthetic capacity after CHO synthesis (node 4 in Fig. 7.1d) is used for TAG synthesis in starchless mutants (Breuer et al., 2014) (Appendix A.4).

The energetic requirements to produce these various biomass constituents vary up to threefold (Breuer et al., 2014). This is commonly overlooked in existing models (Mairet et al., 2011; Packer et al., 2011; Quinn et al., 2011a) and can result in a large misunderstanding of production rates. Therefore, the photosynthetic and inter-conversion yields associated with production of these biomass-constituents were estimated, using a metabolic network and flux balance analysis (FBA), to be 1.62 g reproducing biomass/mol photon, 3.24 g starch/mol photon, 3.24 g CHO/mol photon, 1.33 g TAG/mol photon, and 0.39 g TAG/g starch (Appendix A.3).

This model is developed to describe the behaviour of both wild-type (wt) and the *slm1* starchless mutant of *Scenedesmus obliquus* (Breuer et al., 2014) (Appendix A.6), but could easily be adapted to describe the behaviour of other microalgae species. The model accurately describes experimental data from nitrogen-starved batch cultivations of both wt and *slm1* starchless mutant *S. obliquus* (Supplementary Fig. A.5).

### 7.2.2 Optimizing the photosynthetic TAG yield

*S. obliquus* is recognized as a very promising microalga to produce TAG (Breuer et al., 2012; Griffiths et al., 2011) and the recently generated starchless mutant (de Jaeger et al., 2014) showed an up to 50% improvement in TAG production (Breuer et al., 2014). Therefore, we used *S. obliquus* as a case study to discuss optimization of TAG production. The TAG yield on light (g TAG/mol photon) was used as the target optimization parameter because this yield ultimately determines the areal productivity and allows for comparison between light intensities (Breuer et al., 2013b). This TAG yield refers to the yield at the time-point where harvesting would have resulted in the highest yield. Process duration is thus optimized (Appendix A.7). First, this TAG yield was calculated as a function of the incident light intensity using the model parameter values estimated from the validation experiments (red symbols in Fig. 7.2a-d). Subsequently, we quantified how this TAG yield is impacted by the biomass concentration at the onset of nitrogen starvation ( $c_{x,n=0}$ ), reactor thickness ( $z$ ), pigmentation and maximum photosynthetic rate at the onset of nitrogen starvation ( $a_{\text{replete}}$  and  $q_{\text{hv}}^{\text{max}}$ ). These parameters were varied in the range as presented in Appendix

A.7 (blue symbols in Fig. 7.2a-d). This was done for both the wt and starchless mutant. The outcomes are briefly discussed below, and more comprehensively in Appendix A.8.

Among the parameters investigated, the incident light intensity has the most prominent impact on the TAG yield on light. The variation in the TAG yield was therefore expressed as a function of the incident light intensity in Fig. 7.2. The TAG yield increased up to threefold when the incident light intensity was reduced from 1500 to 200  $\mu\text{mol m}^{-2} \text{s}^{-1}$  (Fig. 7.2a,b). This is consistent with experimental data (Breuer et al., 2013b), and is a result of increased photosaturation at high light intensities (Fig. 7.1a). Although solar irradiation provides a given incident light intensity to a certain ground area, smart use of refraction and reflections at the reactor surface can distribute this incident light over a larger reactor area without reducing the total amount of light provided to the culture; a principle called light dilution (Slegers et al., 2011; Wijffels & Barbosa, 2010; Zemke et al., 2013) (Supplementary fig. A.7). In Supplementary fig. A.7, it is calculated that an angle between the solar irradiation and reactor surface of 83° can result in a 10-fold reduction of the incident light intensity. Furthermore, high mixing rates can be used to provide very short light/dark cycles to which the microalgae are exposed. When these cycles are short enough, the photosynthetic efficiency no longer responds to the high local light intensity, but to the lower average light intensity (Vejrazka et al., 2013) (Appendix A.8). By lowering the light intensity perceived by the microalgae, photobioreactor design can thus improve the TAG yield up to threefold.

At low  $z$  and  $c_{x,n=0}$ , only part of the incident light is absorbed. This results in a substantial loss in TAG yield (Fig. 7.2a,b). Also at high  $z$  and  $c_{x,n=0}$ , this yield can decrease because of increased cell maintenance requirements. An optimum for these values is therefore often observed (Zemke et al., 2013). In our case, this optimum is very wide due to the low maintenance coefficient (Appendix A.8). When all incident light is absorbed, variation in  $z$  and  $c_{x,n=0}$  still cause a 14% variation in the TAG yield for the wt but no variation for the starchless mutant (Fig. 7.2a,b). This difference is a consequence of the applied carbon-partitioning mechanism (Appendix A.8).

Strain improvement can be employed to improve carbon partitioning towards TAG. For the starchless mutant, a 40-48% higher TAG yield is projected than for the wt when the reference conditions are compared, consistent with experimental observations (Breuer et al., 2014). A 22-29% higher yield is projected when the best-cases are compared (Fig. 7.2a,b). In these starchless mutants, still not all photosynthetic capacity is directed towards TAG synthesis. Further improvements seem possible if the activity of other competing pathways is reduced (Appendix A.8).

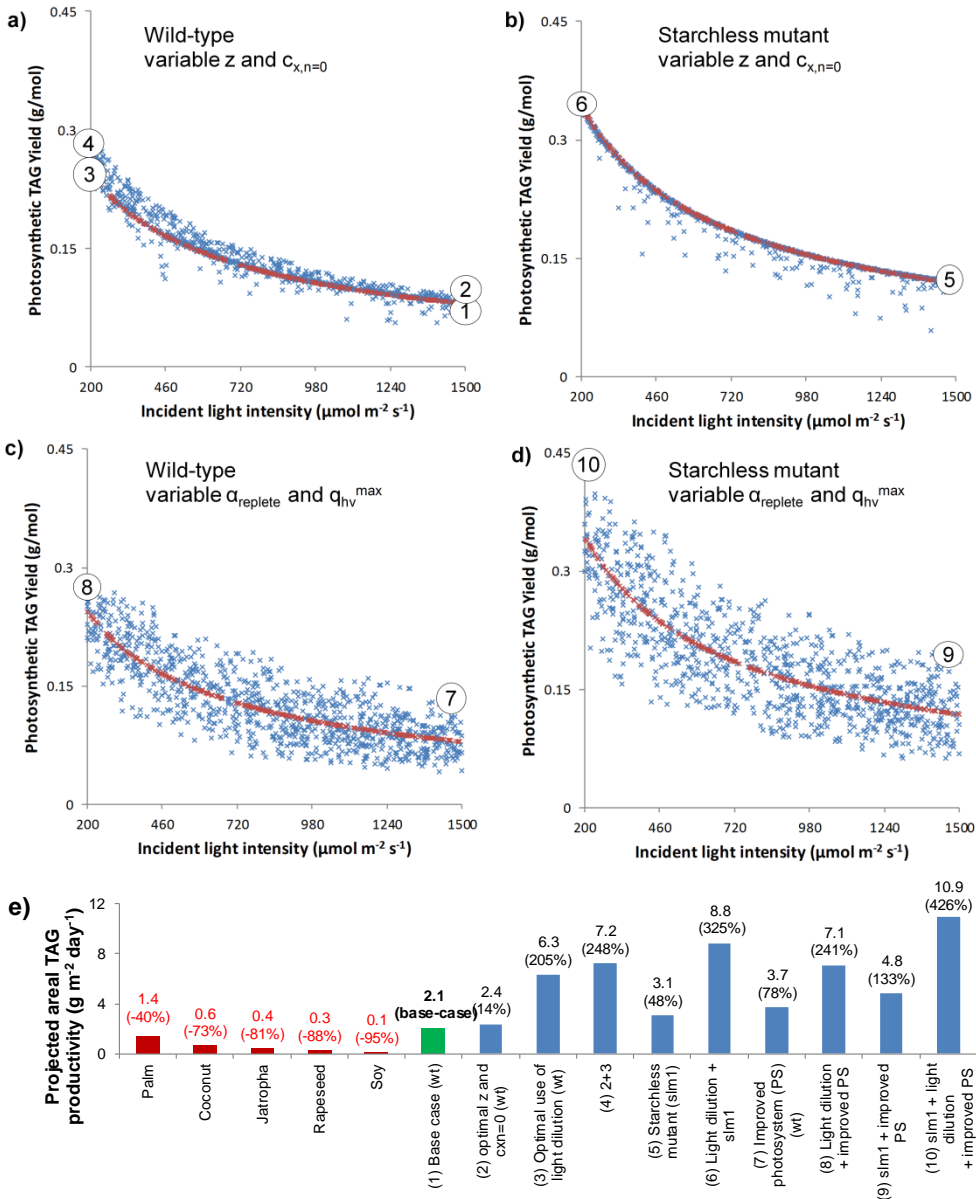


**Fig. 7.2** TAG yield on light as a function of the incident light intensity and variable reactor thickness ( $z$ ), and biomass concentration at the onset of nitrogen starvation ( $c_{X,n=0}$ ) (**a,b**) and variable  $q_{hv}^{max}$ , and  $\alpha_{replete}$  (**c,d**). Each blue point represents the outcome of one simulation, using a Monte-Carlo-sampled combination of the parameters under investigation (ranges in which these values were sampled are presented in Appendix A.7). This is done for the wt (**a,c**) and starchless mutant (**b,d**). Each red symbol represents the outcome of a simulation using the model parameter values estimated from the validation experiments. **Continues next page.**



**Fig. 7.2 (continued).** The yields indicated with the numbered white circles in figure a-d correspond to various optimization scenarios and are extrapolated to areal productivities for comparison with productivities of vegetable oils in terrestrial crops **(e)**. The values between brackets represent the improvement relative to the base-case. Productivities of terrestrial oil-crops were derived from <https://attra.ncat.org/attra-pub/summaries/summary.php?pub=312> and (Chisti, 2007).

Strain improvement can also be employed to improve the photosynthetic efficiency. A general trend towards higher TAG yields at lower pigmentations ( $\alpha_{\text{replete}}$ ) and higher maximum photosynthetic rates ( $q_{\text{hv}}^{\text{max}}$ ) is observed (Appendix A.8). The potential for improvement was 76 and 55% at  $1500 \mu\text{mol m}^{-2} \text{s}^{-1}$  and 13 and 24% at  $200 \mu\text{mol m}^{-2} \text{s}^{-1}$  (wt and starchless mutant, respectively)(Fig. 7.2c,d). This illustrates that although the potential improvement is higher at high light intensities, the photosynthetic efficiency can also be enhanced substantially at low light intensities. The range in which  $q_{\text{hv}}^{\text{max}}$  and  $\alpha_{\text{replete}}$  were varied in our simulations was chosen arbitrarily ( $\pm 50\%$  of the reference value) and it remains to be tested whether these biological parameters can be altered without negatively affecting other physiological traits. The absolute improvement in TAG yield should thus be interpreted with caution. Nevertheless, the ranges in which these parameters were varied seem realistic based on natural variation in these parameters (Appendix A.8). A reduction in pigmentation can be achieved in so-called short-antennae mutants (Melis, 2009) and the maximum photosynthetic rate could be improved by de-bottlenecking the photosynthetic chain (Peterhansel et al., 2008) by increasing the number of electron carriers in the photosystem (Chida et al., 2007) or the activity of rate-limiting enzymes for  $\text{CO}_2$  fixation (e.g. rubisco) (Suknik et al., 1987).

### 7.2.3 Areal TAG productivities

To compare our findings to other work, these yields were extrapolated to areal productivities for an insolation corresponding to southern Europe, using some basic assumptions (Appendix A.9). From the simulated yields, 10 scenarios were derived (numbered circles in Fig. 7.2a-d; Appendix A.9). The base-case is defined as the wt, no light dilution (incident light intensity of  $1500 \mu\text{mol m}^{-2} \text{s}^{-1}$ ), and reference values for  $z$ ,  $C_{x,n=0}$ ,  $\alpha_{\text{replete}}$ , and  $q_{\text{hv}}^{\text{max}}$  (scenario 1). The optimization scenarios include optimization of  $C_{x,n=0}$  and  $z$  (scenarios 2 and 4) the use of a starchless mutant (scenarios 5, 6, 9, and 10), maximal use of light dilution (scenarios 3, 4, 6, 8, and 10), and an improved photosystem (scenarios 7-10). This results in a projected areal TAG productivity of  $2.1 \text{ g m}^{-2} \text{day}^{-1}$  for the base-case. Starchless mutants, an improved photosynthetic machinery, and optimal use of light dilution can improve this productivity to 3.1, 3.7, and  $6.3 \text{ g m}^{-2}$

day<sup>-1</sup>, respectively. Productivities of up to 10.9 g m<sup>-2</sup> day<sup>-1</sup> are projected for combinations of these technologies (Fig. 7.2e).

These projected productivities are still far from the theoretical maximum productivity of 34.5 g m<sup>-2</sup> day<sup>-1</sup> (extrapolated using the theoretical maximum TAG yield of 1.33 g/mol, estimated through FBA). This maximum is not reached because of side-product formation, photosaturation, and a major reduction in the photosynthetic efficiency during nitrogen starvation. As a consequence, the base-case achieves only 6% and the most optimistic scenario 32% of this theoretical maximum TAG productivity. This emphasizes that prospects near theoretical maxima are far from realistic, even when highly optimized photobioreactor designs or well-engineered strains are used.

Peer-reviewed data of microalgal TAG or acyl-lipid productivities under representative outdoor conditions are very scarce, but published productivities for acyl-lipids (1.7-3.2 g m<sup>-2</sup> day<sup>-1</sup>) (Quinn et al., 2012), and total lipophilic-components (1.7-6.5 g m<sup>-2</sup> day<sup>-1</sup>) (Bondioli et al., 2012) are consistent with our base-case projection of 2.1 g TAG m<sup>-2</sup> day<sup>-1</sup>, when it is taken into account that these published lipid fractions only partly consist of TAG. Our projected, and these published, productivities are a substantial improvement compared to terrestrial plants (Fig. 7.2e), but much lower than what is often assumed in life-cycle (LCA) and techno-economic studies (Moody et al., 2014). These studies typically assume productivities that range from twice our base-case to more than our best case. Often, these studies combine optimistic biomass productivities under nitrogen replete conditions (20-30 g m<sup>-2</sup> day<sup>-1</sup>) with TAG contents that are only achieved during prolonged nitrogen starvation (25-50% of dry weight) to yield unrealistically high productivities. We believe that, with available technology, areal productivities for an optimized process between 2.1 (base-case) and 8.8 g TAG m<sup>-2</sup> day<sup>-1</sup> (starchless mutant and maximal use of light dilution) are more realistic.

### **Acknowledgements**

We thank René B. Draaisma for critically reviewing the manuscript. This research project is financially supported by the Food and Nutrition Delta program of Agentschap NL (FND10007) and Unilever.

## Appendix A: Model development.

### A.1 General model structure

A modular design is used to independently describe the effects of nitrogen starvation on photosynthesis and partitioning of photons towards the different biomass constituents (Fig. A.1).

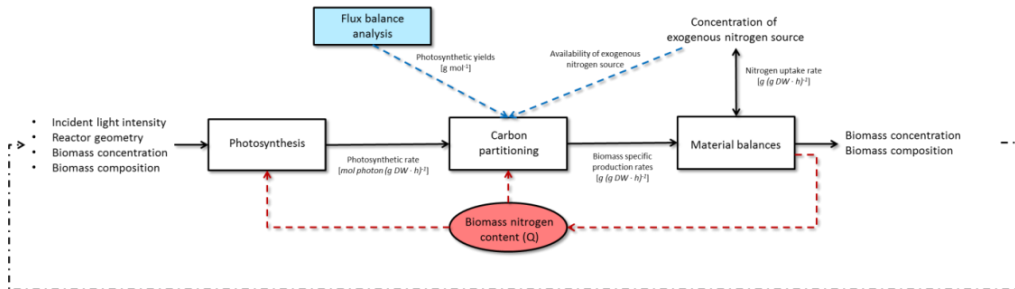


**Fig. A.1** Schematic representation of model structure. The model uses the light intensity, reactor geometry and biomass concentration and composition to calculate the biomass specific photosynthetic rate. A carbon partitioning module is used to calculate biomass specific production rates of the different macromolecules as a function of the cellular nitrogen content, using the photosynthetic rate and photosynthetic yields that are calculated using flux balance analysis. These biomass specific production rates are used to calculate the biomass concentration and composition throughout the cultivation using material balances. The cellular nitrogen content is used as the state variable that controls the regulation involved in photosynthesis and carbon partitioning. The availability of an extracellular nitrogen concentration is used as a switch between nitrogen replete and nitrogen deplete conditions.

A photosynthesis module describes absorption of photons, the part of these photons that is used for photosynthesis and the part of these photons that is dissipated (section A.2). A carbon partitioning module (section A.4) describes the partitioning of the available photons, as calculated in the photosynthesis module, towards *de novo* synthesis of four different biomass constituents: reproducing biomass (the biomass that is produced during nitrogen replete cultivation), TAG, starch, and residual biomass (CHO). In addition, this module describes conversion of starch into TAG. Flux balance analysis is used to calculate the photosynthetic yield for each biomass constituent and the inter-conversion yield of starch to TAG (section A.3). Finally, material balances are used to provide the biomass concentration and composition throughout the cultivation using the rates derived in the carbon partitioning module (Section A.5).

Both the photosynthetic module and the carbon partitioning module use the cellular nitrogen content (Q) as proxy for the extent of nitrogen starvation and as a state

variable to model metabolic regulation and the physiological changes influenced by nitrogen starvation. The approach to use the cellular nitrogen content as a control mechanism to model nitrogen starvation originates from the Droop equation (Droop, 1968) and has been implemented in most models describing nitrogen starvation in microalgae (Bernard, 2011; Geider et al., 1998b; Mairet et al., 2011; Packer et al., 2011; Quinn et al., 2011a). The extracellular nitrogen concentration is used as a switch between nitrogen replete and nitrogen starvation conditions.

In all cases, photons refer to photons in the photosynthetically active radiation (PAR) spectrum. This model assumes that the pH and temperature are kept at their optimal values and that all nutrients other than  $\text{NO}_3$  are present in excess.

The model is developed to describe the behaviour of both wild-type (wt) and the *slm1* starchless mutant (de Jaeger et al., 2014) of *Scenedesmus obliquus*, but could easily be adapted to describe the behaviour of other microalgae species. The experimental data from (Breuer et al., 2014) is used for model validation.

## **A.2 Photosynthesis**

### **A.2.1 Photosynthesis-irradiance response curve**

The photosynthetic rate and photosynthetic efficiency are dependent on the light intensity. It is generally accepted that at low light intensities, the photosynthetic rate is limited by absorption of photons and increases linearly with increasing light intensity. The slope of this increase is proportional to the photosynthetic absorption cross section ( $\alpha$ ) and the photosynthetic quantum yield ( $\psi$ ). When the light intensity increases further, the photosystem becomes saturated and the photosynthetic rate approaches a maximum photosynthetic rate ( $q_{\text{hv}}^{\text{max}}$ ). The light intensity at which this maximum photosynthetic rate is achieved is referred to as the photosaturating light intensity.

Many empirical equations are used to describe this photosynthesis-irradiance response (Jassby & Platt, 1976). These equations share the same parameters and often yield very similar results. Most photosynthetic models use the  $\text{O}_2$  production rate or the biomass specific growth rate as a proxy for the photosynthetic rate, but that makes it impossible to distinguish between the process of photosynthesis and the utilization of co-factors such as NADPH and ATP. Because different biomass constituents have different cofactor requirements, this work expresses the photosynthetic rate as the rate at which photons are channelled into the electron transport chains (thus representing the absorbed

photons minus the dissipated photons), while the use of photosynthetic products is considered separately in the carbon partitioning module.

In this model, the photosynthesis-irradiance response curve is described using the hyperbolic tangent equation (Jassby & Platt, 1976). A variable factor between 0 and 1 is introduced to describe the reduction in the quantum yield as a result of nitrogen starvation ( $\psi_N$ ). The biomass specific photosynthetic rate ( $q_{hv}$ ) at a given light intensity,  $I$ , can then be described by Eq. 1.

$$q_{hv} = q_{hv}^{max} \tanh\left(\frac{\alpha \psi_N I}{q_{hv}^{max}}\right) \quad \text{Eq. 1}$$

The values for the photosynthetic quantum yield ( $\psi_N$ ), absorption cross section ( $\alpha$ ), and maximum photosynthetic rate ( $q_{hv}^{max}$ ) are affected by nitrogen starvation and as a result are variable throughout a nitrogen depleted batch cultivation.

### **A.2.2 The absorption cross section decreases during nitrogen starvation**

During nitrogen starvation, the biomass specific absorption cross section decreases as a result of a decrease in pigmentation (da Silva et al., 2009; Geider et al., 1998a; Kolber et al., 1988). This can have various causes. Firstly, the production of storage metabolites, such as TAG and starch, causes dilution of pigments over total biomass dry weight. Secondly, the most abundant pigment, chlorophyll *a*, contains nitrogen. Nitrogen starvation can thus result in competition for nitrogen between proteins and chlorophyll *a*. This could result in degradation of chlorophyll *a* to liberate nitrogen for protein synthesis or at least inhibit the *de novo* synthesis of chlorophyll *a* when no exogenous nitrogen source is available. Finally, the reduction of pigmentation could be a result of a protective mechanism to protect the cell against photo-oxidative damage during nitrogen starvation, by actively reducing the amount pigments and thus the amount of light that is absorbed (Hu et al., 2008).

A reduction of the biomass specific absorption cross section can have an effect on light harvesting in different ways. First of all, the amount of light that can be absorbed per unit of biomass will decrease and this decreases the slope of the photosynthesis-irradiance response curve resulting in a lower photosynthetic rate at low light intensities while retaining the high photosynthetic rate at high light intensities (Fig. 7.1A). This

results in an increase in the photosaturating light intensity. Second, the biomass specific absorption cross section together with the biomass concentration determines light attenuation in the reactor. A change in the biomass specific absorption cross section can therefore also result in a different light gradient in the photobioreactor (Fig. 7.1B), and will thus affect local photosynthetic rates (Fig. 7.1C).

For *S. obliquus*, it is observed that the absorption cross section is linearly correlated to the cellular nitrogen content,  $Q$  (Fig. A.2)(Eq. 2). Similar observations were made for several other microalgae species (Bernard, 2011; Geider et al., 1998b; Griffiths et al., 2014). Nevertheless, it is possible that different correlations between the absorption cross section and cellular nitrogen content exist for other microalgae species.

$$a = a_{\text{replete}} \frac{Q}{Q_{\text{max}}} \quad \text{Eq. 2}$$

In Eq. 2,  $a_{\text{replete}}$  represents the biomass specific absorption cross section of nitrogen replete biomass and  $Q_{\text{max}}$  represents the cellular nitrogen content under nitrogen replete conditions.

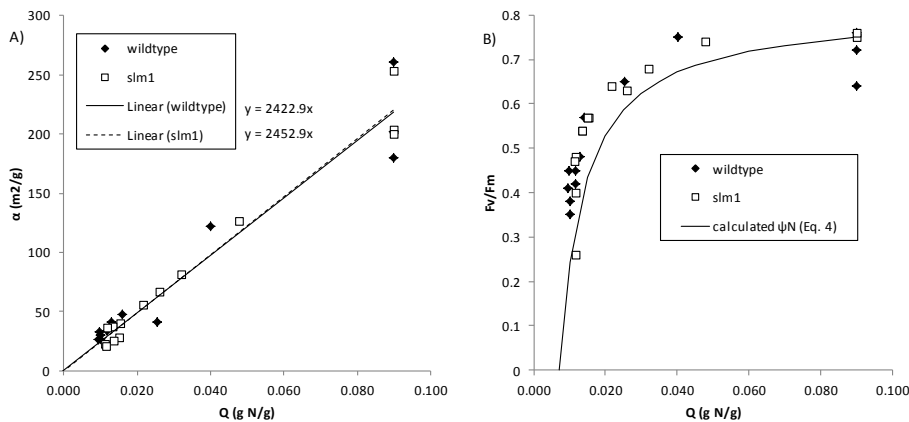


**Fig. A.2** Impact of nitrogen starvation on photosynthesis. **(A):** The absorption cross section ( $a$ ) decreases proportionally with decreasing biomass nitrogen content ( $Q$ ). **(B):** The dark adapted maximum quantum yield ( $F_v/F_m$ ) decreases with decreasing biomass nitrogen content. This decrease in  $F_v/F_m$  mimics the Droop equation that is used to describe the reduction in the photosynthetic quantum yield during nitrogen starvation ( $\psi_N$ ; Eq. 4). Experimental data derived from (Breuer et al., 2014). Black symbols: wt. Open symbols: slm1 starchless mutant of *S. obliquus*.

Because the absorption cross section correlates linearly to the biomass nitrogen content and because the amount of total biomass nitrogen remains constant after the depletion of nitrogen, the volumetric absorption cross section remains constant after the depletion of nitrogen. This also means that, according to the model, light attenuation (*i.e.* light gradients in the photobioreactor) does no longer change after nitrogen is depleted.

### A.2.3 The maximum photosynthetic rate decreases during nitrogen starvation

At light intensities above the photosaturating light intensity, the photosynthetic rate is no longer limited by the absorption capacity of the biomass but is limited by the maximum photosynthetic rate (Fig. 7.1A). This maximum photosynthetic rate is a result of the capacity of the photosystem reaction centres and downstream machinery (of for example the photosystem reaction centres, rubisco, or anabolism). Because this downstream machinery consists for a large part out of proteins, its content in the biomass decreases with decreasing nitrogen content (da Silva et al., 2009; Geider et al., 1998b). At a high (local) light intensity, this will result in a lower biomass specific photosynthetic rate. At a low (local) light intensity, however, this will not affect the biomass specific photosynthetic rate because at low light intensities only light absorption is limiting (Fig. 7.1A,C). Furthermore, a lower maximum photosynthetic rate will also result in a lower photosaturating light intensity (Fig. 7.1A).

In this work, the correlation found by (Geider et al., 1998b) is used to describe the reduction of the maximum photosynthetic rate during nitrogen starvation (Eq. 3). It describes that the maximum photosynthetic rate decreases linearly with decreasing nitrogen content reaching zero at the minimum cellular nitrogen content ( $Q_{min}$ ).

$$q_{hv}^{max} = q_{hv}^{max, replete} \left( \frac{Q - Q_{min}}{Q_{max} - Q_{min}} \right) \quad \text{Eq. 3}$$

In Eq. 3,  $q_{hv}^{max, replete}$  represents the biomass specific maximum photosynthetic rate under nitrogen replete conditions.

### A.2.4 Nitrogen starvation results in a reduction of the photosynthetic quantum yield

Changes in the absorption cross section and maximum photosynthetic rate can affect the photosynthetic efficiency, with their contribution to the photosynthetic efficiency being dependent on the (local) light intensity. In addition to these changes, various physiological changes occur that affect the photosynthetic efficiency in a way that is

independent of the (local) light intensity because they decrease the probability that an absorbed photon becomes available for photosynthesis. This results in a decrease of the photosynthetic quantum yield. Examples include photoinhibition, changes in pigment composition or ratio between the amount of PSII/PSI photosystems, as explained below.

Photoinhibition is the result of light-induced damage to the PSII D1 protein resulting in an inactivated PSII complex. Because the amount of intact D1 is a result of an equilibrium between damage and repair rates of D1, the net result of photoinhibition is a lower ratio of active/inactive PSII (Rubio et al., 2003). The inactivated PSII still contains light harvesting complexes, but absorbed photons will not be used for electron transport and will be dissipated as heat instead. This results in a reduced quantum yield at increasing photoinhibition. In the absence of an exogenous nitrogen source, protein synthesis (and repair) is entirely dependent on protein turnover. This will most likely result in slower regeneration rates of the D1 protein during nitrogen starvation and therefore reduces the relative amount of active PSII reaction centres, and thereby the photosynthetic efficiency (Kolber et al., 1988). In addition, increased photoinhibition can also reduce the maximum photosynthetic rate because the amount of active photosystem is reduced. This phenomenon is implicitly included in  $q_{hv}^{max}$  (section A.2.3).

A decrease in the ratio of light-harvesting pigments (chlorophylls) to photoprotective pigments (carotenoids) is commonly observed during nitrogen starvation (Berges et al., 1996; Breuer et al., 2014; Geider et al., 1993; Kandilian et al., 2014). These photoprotective pigments dissipate their absorbed photons, independent of the light intensity (Mulders et al., 2014b). An increased ratio of such photoprotective pigments over light harvesting pigments therefore results in a reduced photosynthetic efficiency.

The ratio in number of PSII/PSI photosystems is decreased during nitrogen starvation (Berges et al., 1996; Simionato et al., 2013). This will likely result in more photons absorbed by PSI than that it receives electrons from PSII. This imbalance will decrease the rate of linear electron transport and thereby the photosynthetic efficiency. Possibly, the excess photons absorbed by PSI can contribute to cyclic electron transport to generate ATP, but this will inevitably result in increased thermal dissipation of photons (Ort, 2001).



These physiological changes that result in a decrease in the photosynthetic quantum yield are lumped together in  $\psi_N$ . It is assumed that  $\psi_N$  decreases with decreasing cellular nitrogen content following a modified Droop equation (Droop, 1968) (Eq. 4).

$$\psi_N = \left(1 - \frac{Q_{min}}{Q}\right) \left(1 - \frac{Q_{min}}{Q_{max}}\right)^{-1} \quad \text{Eq. 4}$$

The constant  $\left(1 - \frac{Q_{min}}{Q_{max}}\right)^{-1}$  is introduced to ensure that  $\psi_N$  has a value between 0 and 1. It is often proposed to use the PSII variable fluorescence/maximum fluorescence ratio of dark adapted biomass (Fv/Fm) as a proxy for the photosynthetic quantum yield (Simionato et al., 2013). Although, the Fv/Fm measurement excludes some of the above mentioned phenomena, the decrease in  $\psi_N$  as a result of nitrogen starvation indeed mimics the observed decrease in Fv/Fm during nitrogen starvation (Fig. A.2).

#### A.2.5 Average photosynthetic rate in light gradients

A light gradient is present inside photobioreactors. Due to mixing in the reactors, cells are intermittently exposed to high light intensities and low light intensities, sometimes referred to as light-dark cycles (not to be confused with day-night cycles). Reported turnover times of the photosynthetic apparatus are in the order of 1-10 ms (Sukenik et al., 1987; Sukenik et al., 1990), whereas typical mixing times in photobioreactors (*e.g.* bubble columns) have seconds as their order of magnitude (Camacho Rubio et al., 2004). It is therefore assumed in this model that the characteristic time of photosynthesis is much smaller than the characteristic time of mixing and it is therefore assumed that the photosynthetic rate is dependent on the local light intensity in the photobioreactor and therefore varies throughout the reactor. In that case, the average photosynthetic rate of the entire photobioreactor can be found by integrating the photosynthetic rate throughout the reactor using the light gradient present in the reactor. This is often referred to as growth integration (Bernard, 2011; Vejrazka et al., 2013).

Very high mixing rates (order of ms) or very steep light gradients (as a result of high biomass densities) can result in very short light/dark cycles. When flashes of a high light intensity are compared to a continuous illumination with the lower average light intensity, it can be seen that the photosynthetic efficiency during these high light intensity flashes approaches that of the photosynthetic efficiency during the continuous lower light intensity when these cycles are short enough (Posten, 2009; Vejrazka et al., 2013). In this situation the photosynthetic efficiency can approach that of what would be

achieved in the much lower average light intensity. This can substantially reduce photoinhibition (Posten, 2009), but at the cost of large energy inputs for mixing.

In this model, the effects of scattering are neglected and the local light intensity is described using the light attenuation model of Lambert-Beer. It is assumed that all light is parallel (no diffuse light) and enters the photobioreactor perpendicular to the reactor surface. All combined, the average biomass specific photosynthetic rate for a flat panel photobioreactor ( $\overline{q_{hv}}$ ) can then be described by Eq. 5.

$$\overline{q_{hv}} = \frac{1}{z} \int_0^z q_{hv}^{max} \tanh\left(\frac{a\psi_N I_0 e^{(-a c_x z)}}{q_{hv}^{max}}\right) dz \quad \text{Eq. 5}$$

In Eq. 5,  $z$  represents the light path of the reactor,  $I_0$  the incident light intensity, and  $c_x$  the biomass concentration.

The effects of scattering, different reactor geometries, or different (variable) solar inclinations could be included as described by for example (Lee et al., 2014; Slegers et al., 2011).

### **A.3 Photosynthetic and inter-conversion yields of metabolites calculated using flux balance analysis**

#### **A.3.1 Metabolic network**

During photosynthesis, the absorbed photons that are channelled towards the electron transport chains are used to regenerate NADPH and ATP. These can subsequently be used to fixate  $\text{CO}_2$  in  $\text{C}_3$  molecules using the Calvin cycle. These  $\text{C}_3$  molecules can be converted into a wide variety of end products, which are grouped into either of the four major biomass constituents considered in this model: reproducing biomass (the biomass that is made during nitrogen replete cultivation, including a fixed amount of starch and carbohydrates), TAG, starch, and carbohydrates other than starch (CHO). It is assumed that these biomass constituents have a constant composition. These biomass constituents can be synthesized *de novo* through photosynthesis, but in addition it is assumed that starch can be converted to TAG. Conversion of polar acyl-lipids to TAG is not considered, because no net degradation of polar acyl-lipids was observed during nitrogen starvation in the validation experiments (Breuer et al., 2014).

The metabolic requirements to produce these different biomass constituents are very different due to differences in energy density and degree of reduction (Breuer et al., 2014; Klok et al., 2013b). As a result, very different photosynthetic yields are observed for these biomass constituents (g biomass constituent/mol photon). The amount of biomass that can be made at a certain photosynthetic rate is therefore dependent on the biomass composition.

The theoretical maximum photosynthetic yields of these biomass constituents can be calculated using the stoichiometry of the metabolic network. In this work, the metabolic network for *Chlamydomonas reinhardtii* as described by (Kliphuis et al., 2012) is used with some modifications that are based on (Boyle & Morgan, 2009; Falkowski & Raven, 2007; Johnson & Alric, 2013; Yang et al., 2000), as summarized below. Both *C. reinhardtii* and *S. obliquus* belong to the Chlorophyceae (green algae). It is assumed that they share a similar central carbon metabolism and compartmentalization. The number of reactions in the network is largely reduced by lumping sequential non-branched reactions into single reactions. In summary, this simplified metabolic network is split into two compartments, the chloroplast and a combined cytosol/mitochondria. In the chloroplast, cyclic (2 photon  $\rightarrow$  1 ATP) and linear electron transport (8 photon  $\rightarrow$  3 ATP + 2 NADPH) can be active, in a variable ratio. The Calvin cycle is used for CO<sub>2</sub> fixation. The Calvin cycle, the upper part of the glycolysis (between G6P and 3PG), fatty acid synthesis (from acetyl-CoA to fatty acids), reduction of NO<sub>2</sub><sup>-</sup> to NH<sub>4</sub><sup>+</sup>, glutamine, and glutamate synthesis are located in the chloroplast. The lower glycolysis (between GAP and acetyl-CoA), the oxidative pentose phosphate pathway (oxidative PPP), citric acid cycle (TCA cycle), reduction of NO<sub>3</sub><sup>-</sup> to NO<sub>2</sub><sup>-</sup>, synthesis of amino acids other than glutamine and glutamate, nucleic acid synthesis, and protein assembly are located in the cytosol/mitochondria. Starch and other carbohydrates are produced from G6P in the chloroplast. TAG is assembled from fatty acids and glycerol-3-phosphate in the cytosol. Glucose-6-phosphate (G6P), glyceraldehyde-3-phosphate (GAP), 3-phospho-glycerate (3PG),  $\alpha$ -ketoglutarate (aKG), glutamine, glutamate, acetyl-CoA, fatty acids, and NO<sub>2</sub> can be transported over the chloroplast membrane. Co-factors cannot be transported over the chloroplast membrane. Oxidative phosphorylation is assumed to produce 2.5 ATP out of 1 NADH in the cytosol/mitochondria. It is assumed that excess ATP is dissipated to heat using an ATP hydrolase. Appendix B provides a complete overview of all (lumped) reactions in the metabolic network.

It is assumed that starch and CHO consist of poly-glucose, and that all fatty acids in TAG are oleic acid (*i.e.* are triolein). The amino acid composition of protein, the nucleic acid composition, and the co-factor requirements to produce biomass constituents out of their monomers and biomass assembly are assumed to be similar as described by (Kliphuis et al., 2012). Finally, it is assumed that the reproducing biomass of the wildtype consists of 45% protein, 0.2% DNA, 6% RNA, 10% fatty acid (oleic acid), 10% starch, and 28.8% other carbohydrates. For uniformity, it is assumed that all starch in the reproducing biomass is replaced with other carbohydrates in the *slm1* starchless mutant. The ash content is neglected and assumed to be 0%. This results in an elemental nitrogen content of 9% of dry weight (DW). This is consistent with experimentally observed biomass and elemental compositions of *S. obliquus* (Breuer et al., 2014) (Fig. A.3) and other microalgae (Kliphuis et al., 2012).

### A.3.2 Calculation of yields

Using flux balance analysis, flux distributions are found that result in the highest possible yield of each of these biomass constituents on photons. In this procedure, the photon supply rate is fixed to 1 and through linear programming (MATLAB: *linprog*) a flux distribution is found that results in the highest possible production rate of a specific biomass constituent (Eq. 6).

Objective: Maximize  $v_M$  (biomass constituent production rate)

*Constrained with*

Eq. 6

$$\begin{array}{ll}
 S \cdot v = 0 & \text{(stoichiometric constraints)} \\
 v_{\text{photon}} = 1 & \text{(all rates are normalized to photosynthetic rate)} \\
 v_{\min} \leq v \leq v_{\max} & \text{(flux constraints used to describe reversibility of reactions)}
 \end{array}$$

With,  $S$ , the stoichiometry matrix and  $v$ , the vector containing the flux rates. The boundaries of the flux rates are set according to the reversibility of reactions, consistent with (Kliphuis et al., 2012).  $v_{\min}$  is set to 0 for irreversible reactions and set to -infinite for reversible reactions.  $v_{\max}$  is set to infinite (see Appendix B for an overview of all reactions and their reversibility). The photosynthetic yield of product  $M$  can then be calculated as  $v_M/v_{\text{photon}}$ . To calculate the conversion yield of TAG on starch,  $v_{\text{starch}}$  is set to -1,  $v_{\text{photon}}$  is set to 0,  $v_{\text{TAG}}$  is maximized similar to Eq. 6, and the yield is calculated as  $v_{\text{TAG}}/-v_{\text{starch}}$ .

This results in theoretical maximum yields of 1.62 g reproducing biomass/mol photon (when grown on nitrate), 3.24 g starch/mol photon, 3.24 g CHO/mol photon, 1.33 g TAG/mol photon, and 0.39 g TAG/g starch (Appendix B).

### **A.3.3 Discussion of assumptions in metabolic network**

The large difference in magnitude of the aforementioned yields illustrates the importance of using a yield specific for each biomass constituent rather than using an average photosynthetic yield for carbon fixation. Nevertheless, uncertainty remains about the exact values of these yields. This is mainly due to assumptions for compartmentalization and transport of carbon intermediates between compartments. For example, in the model it is assumed that GAP, 3PG, and glucose can be freely transported over the chloroplast membrane in both directions. This allows for balancing of reducing power (NAD(P)H) between the chloroplast and cytosol/mitochondria, that cannot be transported directly. Namely, using these transporters, 3PG can be exported from the chloroplast to the cytosol/mitochondria where it can be reduced to GAP using excess NADH from the cytosol/mitochondria. GAP can then be transferred back to the chloroplast where it is oxidized to 3PG to provide NADPH in the chloroplast. This shuttle could enhance the maximum yields in the case that NADH production in the cytosol/mitochondria exceeds the requirements for NADH in the cytosol/mitochondria. The contribution of this shuttle to the biomass and starch/carbohydrate yield is negligible (Appendix B). However, the predicted yields of TAG on photons and TAG on starch would be reduced from 1.33 to 1.15 g/mol and from 0.39 to 0.21 g/g, respectively, if these transporters would not operate in both directions (Appendix B). Because such a metabolic loss seems unrealistic and because a similar shuttle is described for *C. reinhardtii* when grown on acetate (Johnson & Alric, 2013), these transporters are assumed to be bidirectional.

### **A.4 Carbon partitioning**

In section A.2, the net biomass specific photosynthetic rate is derived. This rate provides the amount of photons that are available for the production of new biomass. This new biomass can consist out of different biomass constituents that can be produced simultaneously and in variable ratios (Fig. 7.1D). This section describes the partitioning of photons towards these different biomass constituents. Together with the yields calculated in section A.3, this carbon partitioning allows calculation of the biomass specific production rate of each biomass constituent.

It is assumed that in all cases the available photosynthetic capacity is first used to fulfil maintenance requirements ( $m_s$ ; mol photon (g DW h)<sup>-1</sup>; node 1 in Fig. 7.1D). This biomass specific maintenance coefficient is assumed to be independent of the cultivation conditions and physiological state of the biomass, but assumed to be proportional to the fraction of reproducing biomass in the total biomass (*i.e.* proportional to  $Q/Q_{max}$ ). It is thus assumed that storage products such as TAG and starch do not have maintenance requirements.

It is assumed that when the extracellular nitrogen concentration (N) is above 0, all remaining photosynthetic capacity that is not used for cell maintenance, is used for the synthesis of reproducing biomass (X). When no extracellular nitrogen is available, the synthesis of reproducing biomass is completely impaired (Eq. 7) and the remaining photosynthetic capacity is used for the production of TAG, starch, and other carbohydrates (CHO) (node 2 Fig. 7.1D).

$$q_x = \begin{cases} Y_{x,hv} \left( \overline{q_{hv}} - m_s \frac{q}{Q_{max}} \right) & \text{if } N > 0 \\ 0 & \text{if } N = 0 \end{cases} \quad \text{Eq. 7}$$

The ratio in which these products are made during nitrogen starvation is variable and is dependent on the extent of nitrogen starvation. This carbon partitioning during nitrogen starvation is highly complex and many regulatory mechanisms can be active simultaneously. These can enhance or counteract each other. Analyses of the transcriptome in various microalgae species shows that the activity of fatty acid synthesis, glycolysis, oxidative PPP, TCA cycle, and the gluconeogenesis are regulated at the transcription level (Blaby et al., 2013; Li et al., 2014; Rismani-Yazdi et al., 2012; Valenzuela et al., 2012; Yang et al., 2013). In addition, the activity of some of these pathways is also regulated by allosteric interactions (Hunter & Ohlrogge, 1998). Furthermore, production rates of TAG and storage carbohydrates can be influenced by competition for substrate, *i.e.* intermediates of glycolysis (Fan et al., 2012; Msanne et al., 2012). This is supported by observations that TAG synthesis is enhanced in starchless mutants (Breuer et al., 2014; de Jaeger et al., 2014; Li et al., 2010a). Finally, inter-conversion of biomass constituents can occur during nitrogen starvation (Breuer et al., 2014; Roessler, 1988). What makes modelling carbon partitioning during nitrogen starvation even more complex is that the partitioning of carbon changes when nitrogen starvation progresses (Breuer et al., 2014; Fan et al., 2012; Gardner et al., 2013; Msanne et al., 2012).

Mechanistic modelling of all these regulatory mechanisms is currently not realistic and certainly will result in an over complicated model. Nevertheless, accurate description of the carbon partitioning is required to model the biomass productivity because the various biomass constituents have very different photosynthetic yields (section A.3). Therefore an empirical approach is chosen to describe the carbon partitioning during nitrogen starvation.

Besides starch and TAG, also other biomass constituents are produced during nitrogen starvation. It is assumed that these other biomass constituents are carbohydrates other than starch (CHO) and could represent cell wall or structural carbohydrates. As observed by (Breuer et al., 2014), the contribution of these other biomass constituents to biomass dry weight is relatively constant and contributes approximately 30% to the biomass dry weight during nitrogen starvation in *S. obliquus* (Fig. A.3).

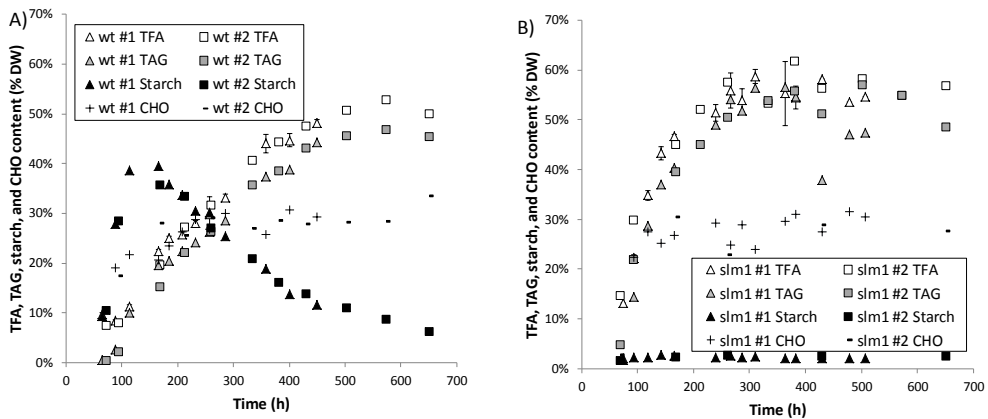


**Fig. A.3** Biomass composition of wt **(A)** and the slm1 starchless mutant **(B)** of *S. obliquus* during nitrogen starvation (nitrogen was depleted after 70-80h of cultivation). In the wt, the starch content (% of DW) increased rapidly during initial nitrogen starvation followed by degradation of starch. The TAG and total fatty acid (TFA) content (% of DW) increased more slowly and the CHO content (% of DW) remained more or less constant. In the starchless mutant, no starch was produced. As a consequence TAG was more rapidly accumulated. Also in the starchless mutant, the CHO content remained more or less constant throughout the entire cultivation. The CHO content was calculated as the difference between the dry weight concentration and the sum of the reproducing biomass (it is assumed that the amount of reproducing biomass does not change after the depletion of nitrogen from the culture medium), starch, and TAG concentration. Experimental data derived from (Breuer et al., 2014).

This biomass specific CHO production rate ( $q_{CHO}$ ) is included such that the CHO content in the biomass dry weight (% of DW) remains constant (node 3 in Fig. 7.1D).

Mathematically, this is achieved using an equation that partitions all photons towards CHO synthesis when the CHO content in the biomass newly produced during nitrogen starvation is below a critical value ( $\chi_{CHO}$ ) and partitions no photons towards CHO synthesis when this CHO content exceeds  $\chi_{CHO}$ . (Eq. 8). When the integration step-size is chosen small enough, this results in a constant CHO content.

$$q_{CHO} = \begin{cases} 0 & \text{if } \frac{CHO}{CHO + TAG + Starch} > \chi_{CHO} \\ \frac{\text{Available photons}}{(\overline{q_{hv}} - m_s \frac{Q}{Q_{max}})} \cdot \underbrace{\text{De novo CHO production}}_{Y_{CHO,hv}} & \text{if } \frac{CHO}{CHO + TAG + Starch} \leq \chi_{CHO} \end{cases} \quad \text{Eq. 8}$$

The photosynthetic capacity that is not used for CHO synthesis during nitrogen starvation is used for the synthesis of TAG and starch (node 4 Fig. 7.1D). During initial nitrogen starvation, most photons are used for the synthesis of starch, but when nitrogen starvation progresses most and eventually all of these remaining photons are used for the synthesis of TAG (Fig. A.4A).

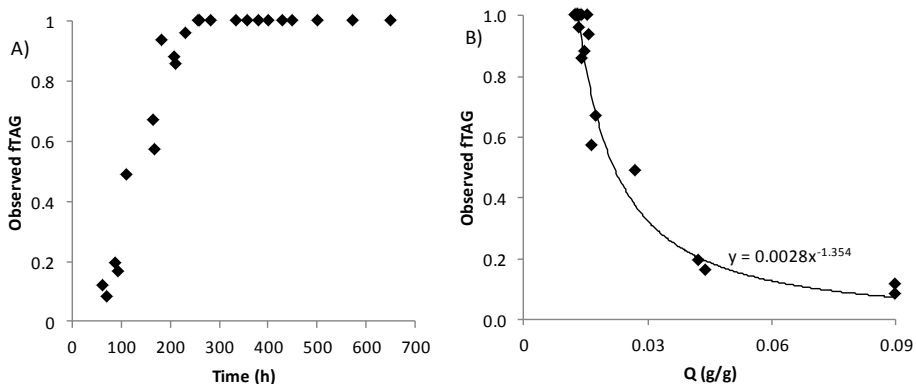


**Fig. A.4** Carbon partitioning between starch and TAG, expressed as the fraction of photons partitioned towards TAG ( $f_{TAG}$ ) in nitrogen depleted wt *S. obliquus*. **A:**  $f_{TAG}$  increases progressively to 1 when nitrogen starvation progresses. After this point,  $f_{TAG}$  remains equal to 1 and starch degradation and inter-conversion to TAG is initiated. **B:**  $f_{TAG}$  correlates non-linear to the biomass nitrogen content ( $Q$ ). This correlation is used to describe the partitioning between TAG and starch by the model (Eq. 9). Nitrogen was depleted after 70-80 h of cultivation. Experimental data derived from (Breuer et al., 2014).

The fraction of photons partitioned towards TAG (at node 4 in Fig. 7.1D), from now on called  $f_{TAG}$ , correlates non-linear to the cellular nitrogen content (state variable  $Q$ ) (Fig. A.4B; Eq. 9). Due to the empirical nature of this equation, this equation does not



guarantee that the value for  $f_{TAG}$  is always smaller or equal to 1. Therefore,  $f_{TAG}$  is set to 1 in the model when the predicted  $f_{TAG}$  exceeds 1.

$$f_{TAG} = \min \left\{ p_A \cdot Q^{-p_B} \right\} \quad \text{Eq. 9}$$

In the *slm1* starchless mutant, no starch is produced and the photosynthetic capacity that is used to produce starch in the wt, is used for the production of TAG in the *slm1* starchless mutant (Breuer et al., 2014). Therefore, the partition coefficient  $f_{TAG}$  is assumed to always be equal to 1 in the *slm1* starchless mutant.

When nitrogen starvation progresses, the accumulated starch is degraded again. These degradation products can subsequently contribute to TAG synthesis (Breuer et al., 2014). It is assumed that during initial nitrogen starvation no starch is degraded, but when the nitrogen content decreases below a critical nitrogen content ( $Q_{deg}$ ), degradation of starch follows 0<sup>th</sup> order kinetics with rate  $r_{starch,TAG}^{max}$  (node 5 in Fig. 7.1D). It is assumed that all degraded starch is used for the synthesis of TAG and that degradation of the starch that is produced during nitrogen starvation can continue until this starch is completely degraded (node 5 in Fig. 7.1D; Eq. 10).

$$r_{starch,TAG} = \begin{cases} 0 & \text{if } Q > Q_{deg} \text{ or Starch} = 0 \\ r_{starch,TAG}^{max} & \text{if } Q \leq Q_{deg} \text{ and Starch} > 0 \end{cases} \quad \text{Eq. 10}$$

This results in the biomass specific production rates of TAG and starch as presented in Eq. 11 and 12.

$$q_{TAG} = \left( \frac{\text{Available photons}}{\overline{q_{hv}} - m_s \frac{Q}{Q_{max}}} - \frac{\text{Photons remaining after CHO production}}{\frac{q_{CHO}}{Y_{CHO,hv}}} \right) \cdot \left( \underbrace{f_{TAG} Y_{TAG,hv}}_{\text{De novo TAG production}} + \underbrace{r_{starch,TAG} Y_{TAG,starch}}_{\text{Conversion of starch to TAG}} \right) \quad \text{Eq. 11}$$

$$q_{Starch} = \left( \frac{\text{Available photons}}{\overline{q_{hv}} - m_s \frac{Q}{Q_{max}}} - \frac{\text{Photons remaining after CHO production}}{\frac{q_{CHO}}{Y_{CHO,hv}}} \right) \cdot \left( \underbrace{(1 - f_{TAG}) Y_{Starch,hv}}_{\text{De novo starch production}} - \underbrace{r_{starch,TAG}}_{\text{Starch degradation}} \right) \quad \text{Eq. 12}$$

**A.5 Material balances**

A set of ordinary differential equations (ODEs) was used to describe the change in reproducing biomass (X), TAG, starch, CHO, and dissolved nitrogen (N) concentration using the biomass specific production rates as derived in section A.4, resulting in Eq. 13-17 for a batch cultivation.

$$\frac{dX}{dt} = q_X c_x \quad \text{Eq. 13}$$

$$\frac{dTAG}{dt} = q_{TAG} c_x \quad \text{Eq. 14}$$

$$\frac{dStarch}{dt} = q_{Starch} c_x \quad \text{Eq. 15}$$

$$\frac{dCHO}{dt} = q_{CHO} c_x \quad \text{Eq. 16}$$

$$\frac{dN}{dt} = q_N c_x \quad \text{Eq. 17}$$

Since nitrogen is only a constituent of reproducing biomass, the biomass specific nitrogen uptake rate ( $q_N$  in Eq. 17) is dependent on the production rate of reproducing biomass and the nitrogen content of reproducing biomass (Eq. 18). It is assumed that the nitrogen content of reproducing biomass is constant and equal to the maximum nitrogen content ( $Q_{max}$ ).

$$q_N = -q_X Q_{max} \quad \text{Eq. 18}$$

Notice that Eq. 17 and Eq. 18 do not prevent nitrogen from being taken up when the nitrogen concentration becomes zero. However,  $q_N$  will be 0 at a nitrogen concentration of 0 because  $q_X$  is forced to zero in that case (Eq. 7).

The total biomass concentration ( $c_x$ ) is calculated as the sum of X, TAG, Starch, and CHO (Eq. 19).

$$c_x = X + TAG + Starch + CHO \quad \text{Eq. 19}$$

The cellular nitrogen content (Q) of the total biomass is calculated using Eq. 20.

$$Q = \frac{Q_{max}X}{c_x} \quad \text{Eq. 20}$$

Eq. 13-17 were integrated using the 4<sup>th</sup>/5<sup>th</sup> order Runge-Kutta algorithm using the MATLAB *ode45* function to yield the concentrations as a function of time.

TAG, Starch, and CHO refer to the amounts of TAG, Starch, and CHO made after nitrogen depletion and do not include the amount of TAG, Starch, and CHO present in the biomass that is made during nitrogen replete conditions because this is already part of the reproducing biomass,  $X$  (section A.3). The experimentally measured biomass, however, does include the starch and CHO present in the reproducing biomass (TAG in reproducing biomass is negligible). For model validation, the simulated starch and CHO content are therefore corrected for the amount present in the reproducing biomass. This is done using Eq. 21 and 22.

$$\text{Starch content} = \frac{\chi_{\text{Starch},X}X + \text{Starch}}{c_x} \quad \text{Eq. 21}$$

$$\text{CHO content} = \frac{\chi_{\text{CHO},X}X + \text{CHO}}{c_x} \quad \text{Eq. 22}$$

In which,  $\chi_{\text{starch},X}$  and  $\chi_{\text{CHO},X}$  represents the fraction of starch and CHO in reproducing biomass and are assumed to be, respectively, 0.1 and 0.288 g/g for the wt and 0 and 0.288 g/g for the *slm1* starchless mutant, based on experimental observations (section A.2). It is assumed that this  $\chi_{\text{starch},X}$  is not used for inter-conversion into TAG when nitrogen starvation progresses.

## A.6 Parameter estimation and model validation

### A.6.1 Treatment of experimental data

The model was validated using nitrogen run-out cultivations of both the wt and the *slm1* starchless mutant of *S. obliquus* using the data presented by (Breuer et al., 2014). In these cultivations, the algae were inoculated at a low biomass density (less than 0.05 g/l) and cultivated at an incident light intensity of 100  $\mu\text{mol m}^{-2} \text{s}^{-1}$  until the biomass density reached 0.3-1 g/l after which the light intensity was increased to 500  $\mu\text{mol m}^{-2} \text{s}^{-1}$ . In these cultivations an initial amount of 10 mM  $\text{KNO}_3$  was supplied, which was completely consumed at a biomass concentration of 1.5 g/l. The results of the duplicate cultivations were combined and treated as a single dataset. Their time-axes were shifted

such that the experimental data of both duplicates overlaid. The first experimental point, immediately after setting the light intensity to  $500 \mu\text{mol m}^{-2} \text{s}^{-1}$ , was used as the initial (boundary) condition for integration and was considered  $t=0$  (Table A.1). All results after the increase in light intensity, until the point where the biomass concentration started to decrease substantially (cell decay), were used for parameter estimation.

The incident light intensity, light path of the reactor, absorption cross section and nitrogen content of nitrogen replete cells were directly derived from the experimental conditions or observations, and were used as constants in the model (Table A.1). Parameters related to partitioning of photons between TAG and starch and degradation of starch were only relevant for the wt, because it is assumed that  $f_{\text{TAG}}$  (Eq. 9) is always equal to 1 in the *slm1* starchless mutant. This results in 8 parameters to be estimated for the wt and 4 parameters to be estimated for the *slm1* starchless mutant

#### **A.6.2 Initial parameter estimation from experimental data**

Initial values for all parameters were determined from the experimental data and used as the starting point for parameter estimation as follows.  $q_{\text{hv}}^{\text{max}}$  was estimated at  $0.077 \text{ mol photon (g DW h)}^{-1}$  from an assumed maximum specific growth rate of  $3 \text{ g g}^{-1} \text{ day}^{-1}$  and a biomass yield of  $1.62 \text{ g/mol}$ .  $Q_{\text{min}}$  was estimated at  $0.012$  and  $0.014 \text{ g N (g DW)}^{-1}$  for the wt and *slm1* starchless mutant, respectively, from the nitrogen content in nitrogen replete biomass (9%) and the observed maximum increase in dry weight concentration after the depletion of nitrogen.  $m_s$  was assumed to be 0 as the initial value due to the uncertainty related to this value.  $p_A$  and  $p_B$  were estimated to be  $0.003$  and  $1.328$  using Fig. A.4B.  $\chi_{\text{CHO}}$  was estimated to be  $0.3 \text{ g CHO (g DW)}^{-1}$  from Fig. A.3.  $Q_{\text{deg}}$  was estimated at  $0.014 \text{ g N (g DW)}^{-1}$  from the biomass concentration at which the volumetric starch concentration was highest.  $r_{\text{starch,TAG}}^{\text{max}}$  was estimated at  $0.693 \text{ mg starch (g DW h)}^{-1}$  from the observed average starch degradation rate.

#### **A.6.3 Final parameter estimation by minimizing sum of squared differences**

Subsequently, parameters were estimated by minimizing the normalized sum of squared differences (ssq) between model predictions and experimentally observed dry weight concentration and starch and TAG contents throughout the cultivation (Eq. 23).

$$ssq = \sum_t \left( \frac{c_x^{model}(t) - c_x^{exp}(t)}{c_x^{exp}(t)} \right)^2 + \left( \frac{TAG\ content^{model}(t) - TAG\ content^{exp}(t)}{TAG\ content^{exp}(t)} \right)^2 + \left( \frac{Starch\ content^{model}(t) - Starch\ content^{exp}(t)}{Starch\ content^{exp}(t)} \right)^2 \quad \text{Eq. 23}$$

Because local minima might exist, first, a Monte-Carlo algorithm was used in which the ssq was calculated for combinations of parameters that were randomly distributed around the aforementioned values from S6.2 (using ranges of  $\pm 20$ , 50, 20, 20, 20, 100, and 100% for  $q_{hv}^{max, replete}$ ,  $Q_{min}$ ,  $p_A$ ,  $p_B$ ,  $\chi_{CHO}$ ,  $r_{starch, TAG}^{max}$ , and  $Q_{deg}$ , respectively).

The combinations of model-parameter values that resulted in the lowest ssq-values were manually evaluated and it was confirmed that the trends of the model were consistent with the trends as observed in the experimental data.

Second, the combination of parameters that was considered best to fit the experimental data was subsequently further optimized using unconstrained non-linear optimization (Matlab: fminsearch) to yield the values as presented in Table A.1.

**Table A.1** Estimated parameters, constants, and boundary conditions used for solving the material balances for the wt and slm1 starchless mutant of *S. obliquus*.

Estimated parameters	units	wt	slm1
$q_{hv}^{max, replete}$	mol photon (g DW h) <sup>-1</sup>	0.0642	0.0423
$Q_{min}$	g N (g DW) <sup>-1</sup>	0.0108	0.0151
$m_s$	mmol photon (g DW h) <sup>-1</sup>	0.100	0.100
$p_A$	-	$2.491 \cdot 10^{-3}$	
$p_B$	-	1.509	
$\chi_{CHO}$	g CHO (g DW) <sup>-1</sup>	0.367	0.405
$r_{starch, TAG}^{max}$	g Starch (g DW h) <sup>-1</sup>	$0.516 \cdot 10^{-3}$	
$Q_{deg}$	g N (g DW) <sup>-1</sup>	0.0144	
Constants	units	wt	slm1
$Q_{max}$	g N (g DW) <sup>-1</sup>	0.090	0.090
$\alpha_{replete}$	m <sup>2</sup> g <sup>-1</sup>	0.200	0.200
$z$	m	0.020	0.020
$I_0$	μmol m <sup>-2</sup> s <sup>-1</sup>	500	500
Initial values (boundary conditions)	units	wt	slm1
$c_x$	g m <sup>-3</sup>	120	550
TAG, Starch, and CHO	g m <sup>-3</sup>	0	0
N	g NO <sub>3</sub> -N m <sup>-3</sup>	129	91

When the model was simulated using these parameters it can be seen that the model closely follows the experimental data and is able to reproduce all trends in the evolution of the biomass concentration and composition in the experimental data (Fig. A.5).

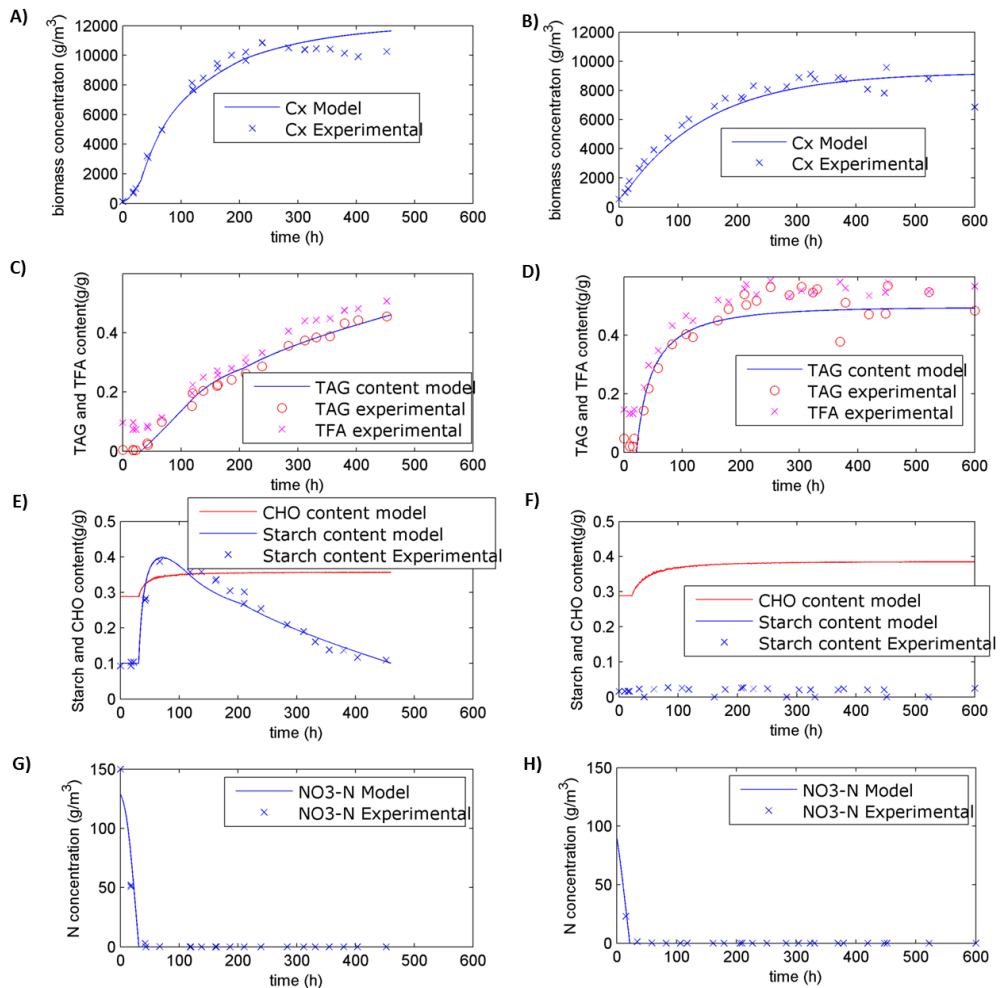


**Fig. A.5** Model simulations using the parameters as presented in Table A.1 compared to the experimental data. **(A,C,E,G)** wt *S. obliquus*. **(B,D,F,H)** *slm1* starchless mutant *S. obliquus*. **(A,B)** biomass dry weight concentration ( $\text{g/m}^3$ ), **(C,D)** TAG and TFA content (% DW), **(E,F)** starch and CHO content (% DW), **(G,H)** dissolved NO<sub>3</sub>-N concentration ( $\text{g NO}_3\text{-N/m}^3$ ). Experimental data is derived from (Breuer et al., 2014). As explained by (Breuer et al., 2014), after NO<sub>3</sub> was consumed, biomass formation continued. In the wild-type, starch accumulation started immediately after the depletion of nitrogen and accumulated to 40% of dry weight. Hereafter starch was degraded again. TAG accumulation also commenced shortly after NO<sub>3</sub> depletion and continued until the end of the cultivation. In the *slm1* starchless mutant, no starch is produced and the photosynthetic capacity that would otherwise have been used for starch synthesis is directed towards TAG synthesis. This resulted therefore in higher TAG synthesis rates in the *slm1* starchless mutant than in the wt and this is reflected by the higher TAG contents during initial nitrogen starvation in the *slm1* starchless mutant. **Continues next page.**

**Fig. A.5 (continued).** The maximum time-averaged TAG yield and volumetric TAG productivity were increased in the *slm1* starchless mutant from 0.144 to 0.217 g/mol and from 0.265 to 0.359 g (l day)<sup>-1</sup> as a consequence of this higher initial TAG synthesis rate (Breuer et al., 2014). The amounts of starch and CHO predicted by the model refer to the amounts of starch and CHO produced after nitrogen depletion. The simulated CHO and starch contents are therefore corrected for the amounts of CHO and starch, that were already present in the reproducing biomass at the start of nitrogen starvation, using the contents of starch and CHO in the reproducing biomass as explained in section A.5. When model simulations are performed using these parameters, it can be seen that the model closely represents the experimental data and that this model can successfully describe the trends observed in biomass formation and carbon partitioning during a batch process that includes both nitrogen replete growth and nitrogen starvation.

#### **A.6.4 Parameter sensitivity**

Especially the parameters related to starch degradation in the wt were difficult to estimate because starch synthesis and starch degradation could occur simultaneously (starch turnover). This was reflected by identification of several local minima with closely related ssq values but substantially different estimated parameters.

Although the model is well able to reproduce the experimental data, there are some complications when using the nitrogen content as a proxy for the physiological state in specific cases. For example, when nitrogen starvation progresses, up to 75% of the starch that is initially produced during nitrogen starvation is degraded and converted into TAG. This results in a large loss in biomass because the yield at which starch can be converted into TAG is only 0.39 g/g (section A.3). During this period photosynthesis continues, producing additional TAG. The net result of these two processes is a large change in biomass composition, but not a large change in cellular nitrogen content. This can make the model very sensitive to changes in parameters related to the cellular nitrogen content, such as for example the nitrogen content at which starch degradation is initiated ( $Q_{deg}$ ). A better understanding of the physiology and regulation behind carbon partitioning and photosynthesis during nitrogen starvation is required to model these processes more mechanistically.

### **A.7 Impact of model parameters on photosynthetic TAG yield**

#### **A.7.1 Model simulations and ranges of parameter values**

Using the validated model, the impact of various model parameters, that represent, or can be influenced by, the reactor design, process design, carbon-partitioning mechanism, or photosynthetic machinery were investigated. To do so, model simulations were performed using Monte-Carlo-sampled combinations of the incident light intensity

( $I_0$ ), biomass concentration at the onset of nitrogen starvation ( $C_{X,n=0}$ ), and reactor thickness ( $z$ ), and for combinations of the incident light intensity, the pigmentation at the onset of nitrogen starvation ( $\alpha_{replete}$ ), and the maximum photosynthetic rate ( $q_{hv}^{max}$ ). This was done for the carbon-partitioning mechanism of both the wt and *slm1* starchless mutant (blue symbols in Fig. 7.2). As a reference, these simulations were also performed in which the values for  $C_{X,n=0}$ ,  $z$ ,  $\alpha_{replete}$ , and  $q_{hv}^{max}$  were kept at the values estimated from the experimental data (section A.6; red symbols in Fig. 7.2; Table A.2). These parameters were sampled within the range as presented in Table A.2. All other parameters were used according to Table A.1. For each of these simulations, only the nitrogen starvation period was simulated. The desired biomass concentration at the onset of nitrogen depletion ( $C_{X,n=0}$ ) was therefore used as the initial biomass concentration (completely constituting from biomass constituent X) and an initial nitrogen concentration of  $0 \text{ g m}^{-3}$  was used. Because in the validation experiments nitrogen was depleted at a biomass concentration of approximately  $1.5 \text{ g/l}$ ,  $C_{X,n=0}$  was set to  $1500 \text{ kg/m}^3$  for the reference simulations.

Using these parameter values, eq. 13-17 were integrated for a time interval between 0-1300 h. Subsequently, the maximum time-averaged TAG yield on light was calculated using the obtained results (section A.7.2). It was confirmed that this time-interval was sufficiently large to ensure that the maximum time-averaged yields was always within the integration interval. For each combination of parameters, this procedure was repeated 1000 times to generate 1000 combinations of parameter values and their corresponding maximum time-averaged TAG yield. In Fig. 7.2, these maximum time-averaged yields were plotted versus the incident light intensity of that simulation to obtain a plot that describes the variability in the maximum time-averaged yield as a consequence of variation in either  $z$  and  $C_{X,n=0}$  or  $\alpha_{replete}$  and  $q_{hv}^{max}$  as a function of the incident light intensity.

Two examples of these simulated cultivations are shown in Fig. A.6.



**Table A.2** Ranges in which parameters were varied for the different sets of simulations.  $I_0$ : incident light intensity,  $z$ : reactor thickness (optical light path),  $c_{x,n=0}$ : biomass concentration at the onset of nitrogen depletion,  $\alpha_{replete}$ : pigmentation of nitrogen replete biomass (at onset of nitrogen starvation),  $q_{hv}^{max}$ : maximum photosynthetic rate of nitrogen replete biomass (at onset of nitrogen starvation). All parameters that are not listed were chosen according to Table A.1. The corresponding results are shown in Fig. 7.2A-D, as indicated between brackets in the column header of this table.

Parameter	wild-type reference (red crosses Fig. 7.2 A,C)	wild-type variable $z$ and $c_{x,n=0}$ (blue crosses Fig. 7.2A)	wild-type variable $\alpha_{replete}$ and $q_{hv}^{max}$ (blue crosses Fig. 7.2C)	starchless mutant reference (red crosses Fig. 7.2 B,D)	starchless mutant variable $z$ and $c_{x,n=0}$ (blue crosses Fig. 7.2 B)	starchless mutant variable $\alpha_{replete}$ and $q_{hv}^{max}$ (blue crosses Fig. 7.2D)
$I_0$ ( $\mu\text{mol m}^{-2} \text{s}^{-1}$ )	200-1500	200-1500	200-1500	200-1500	200-1500	200-1500
$z$ (m)	0.02	0.01-0.06	0.02	0.02	0.01-0.06	0.02
$c_{x,n=0}$ ( $\text{g m}^{-3}$ )	1500	750-3000	1500	1500	750-3000	1500
$\alpha_{replete}$ ( $\text{m}^2 \text{g}^{-1}$ )	0.2	0.2	0.1-0.3 (+/- 50%) <sup>1</sup>	0.2	0.2	0.1-0.3 (+/- 50%) <sup>1</sup>
$q_{hv}^{max}$ ( $\text{mol g}^{-1} \text{h}^{-1}$ )	0.064	0.064	0.032-0.096 (+/- 50%) <sup>1</sup>	0.042	0.042	0.021-0.063 (+/- 50%) <sup>1</sup>

<sup>1</sup>The values for  $\alpha_{replete}$  and  $q_{hv}^{max}$  were varied +/- 50% from the reference value as presented in Table A.1.

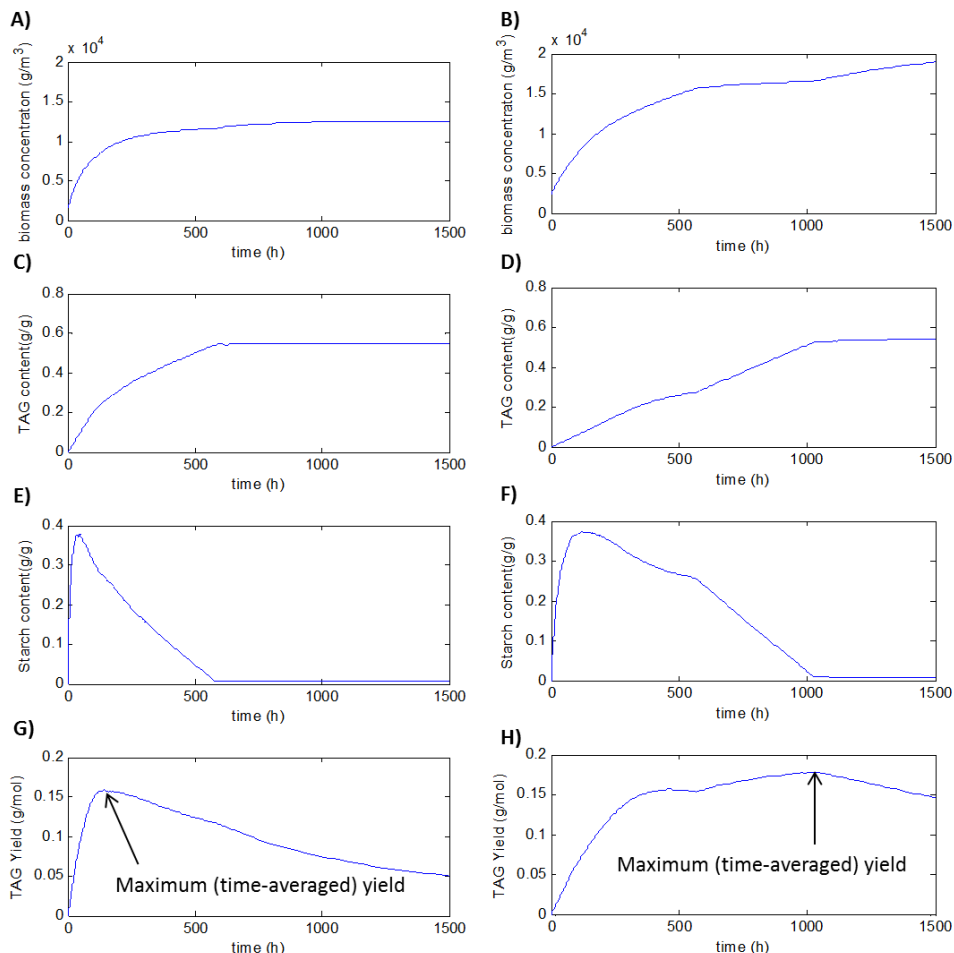


**Fig. A.6** Simulations for the wt using  $z=0.02$  m and  $C_{x,n=0} = 1500$  g m<sup>-3</sup> (**A,C,E,G**) and simulations using  $z = 0.04$  m and  $C_{x,n=0} = 2500$  g m<sup>-3</sup> (**B,D,F,H**). (**A,B**) biomass dry weight concentration (g/m<sup>3</sup>), (**C,D**) TAG and TFA content (% DW), (**E,F**) starch and CHO content (% DW), (**G,H**) Time-averaged yield throughout the simulated cultivation (g TAG/mol photon). This time-averaged TAG yield is calculated for each time point as the yield between  $t=0$  and that time-point (time-averaged yield) and corrected for the light energy needed to produce the initial biomass concentration using an assumed yield of 1 g/mol for this biomass. The maximum (time-averaged) yield is then derived as the maximum value for that simulation, as indicated by the arrow in figures G and H. This maximum yield thus represents the yield that would be achieved when the culture would be harvested at the optimal time-point for harvesting (*i.e.* an optimized process duration). In both simulations an incident light intensity of  $500 \mu\text{mol m}^{-2} \text{s}^{-1}$  and an initial nitrogen concentration of 0 were used ( $t=0$  thus refers to the onset of nitrogen starvation). All other parameters used were as listed in Table A.1. As shown in Fig. B, the biomass productivity increases after 1000 h. This is a result of the completion of starch degradation at this point (Fig. F). Before this point, starch turnover to TAG occurs simultaneously with *de novo* TAG synthesis. **Continues next page.**

**Fig. A.6 (continued).** Starch to TAG turnover occurs with a yield of 0.39 g/g (section A.3) and thus counteracts the increase in dry weight as a result of *de novo* synthesis (section A.6.4). After starch degradation is completed, only *de novo* TAG synthesis remains and this results in an increased biomass productivity.

### A.7.2 Calculation of the maximum time-averaged TAG yield on light

The time-averaged TAG yield on light is calculated for each time-point as the amount of TAG produced in the period between that time-point and the start of nitrogen depletion, divided by the amount of light supplied in that period (Fig. A.6G,H). The light energy needed to produce the initial biomass (*i.e.*, to produce  $c_{x,n=0}$ ) was included using the assumption that this biomass can be made at a net photosynthetic yield of 1 g/mol.

This time-averaged TAG yield varies throughout the cultivation (Fig. A.6G,H) and the maximum time-averaged TAG yield on light was retrieved as the maximum among these yields (Eq. 24; as indicated with the arrows in Fig. A.6G,H). It thus represents the yield at the time-point when harvesting would result in the highest yield. It is thus assumed that process duration is optimized. Note that this is not necessarily at the time-point when TAG accumulation is complete or when TAG contents are highest (section A.8.2).

$$\text{Maximum time averaged yield} = \max_t \left[ \frac{\text{TAG}(t)}{\frac{I_0 \cdot t}{z} + \frac{c_{x,n=0}}{1}} \right] \quad \text{Eq. 24}$$

In Eq. 24, TAG(t), represents the TAG concentration (g/m<sup>3</sup>) at time t,  $I_0$  represents the incident light intensity, z represents the reactor thickness, and  $c_{x,n=0}$  represents the biomass concentration at the onset of nitrogen depletion. The division of  $c_{x,n=0}$  by 1 represents the photosynthetic yield of 1 g/mol at which this initial biomass is made.

## A.8 Optimizing the TAG yield

### A.8.1 Light intensity and reactor design

The incident light intensity has the most prominent impact on the photosynthetic TAG yield among all parameters investigated. The predicted TAG yield increases up to threefold when the incident light intensity is reduced from 1500 to 200  $\mu\text{mol m}^{-2} \text{s}^{-1}$  (Fig. 7.2A,B; comparing scenarios 3, 4, and 6 to 1, 2, and 5). This is consistent with previously published experimental data (Breuer et al., 2013b), and is a result of increased photosaturation at high light intensities (Fig. 7.1A-C). Although solar irradiation provides a high incident light intensity to a certain ground area, photobioreactor design can be used to control the incident light intensity into the culture

without reducing the total amount of light provided to the photobioreactor, a principle called light dilution (Cuaresma et al., 2011; Posten, 2009; Wijffels & Barbosa, 2010; Zemke et al., 2013). This can be accomplished by building reactors that have a sharp angle between the incident light and the reactor surface (vertically oriented reactors). In this case, refraction at the reactor surface causes light from a certain ground area to be distributed over a larger reactor area inside the photobioreactor and reflections redistributes the direct sunlight on parts of the photobioreactor to self-shaded parts of the photobioreactor to provide a more homogeneous illumination (Fig. A.7). In Fig. A.7C it is calculated that an angle between the solar irradiation and reactor surface of  $83^\circ$  (angle  $\theta_1$  in Fig. A.7A) will result in a 10-fold reduction of the light intensity entering the photobioreactor (light intensity at  $I_2$  compared to light intensity at  $I_G$  and  $I_0$ ). Whether such an angle is feasible in vertically oriented reactors depends on the altitude and azimuth of the sun (Slegers et al., 2011) (Fig. A.7B), which is in turn dependent on geographic location, time of day, and season. Such an angle could be achieved at all times if the reactor is tilted from its vertical plane towards the sun. This is however likely to result in major engineering challenges with respect to mixing and aeration.

Furthermore, high mixing rates can be used to provide very short light/dark cycles to which the microalgae are exposed. When flashes of a high light intensity are compared to a continuous illumination with the lower average light intensity, it can be seen that the photosynthetic efficiency during these high light intensity flashes approaches that of the photosynthetic efficiency during the continuous lower light intensity when these cycles are short enough (in the order of more than 10 Hz) (Posten, 2009; Vejrazka et al., 2013). High biomass densities can help to reduce the required mixing rate because of the steep light gradients associated with high biomass densities. In these steep light gradients, zones in the photobioreactor that perceive a high light intensity are smaller and lower mixing rates are needed to ensure a short exposure to these high light intensity zones.

Although reactor design can help to reduce photoinhibition and increase the TAG yield up to threefold, it comes at the cost of increased photobioreactor construction costs due to the larger reactor surface area or increased costs and energy consumption associated with high mixing rates.

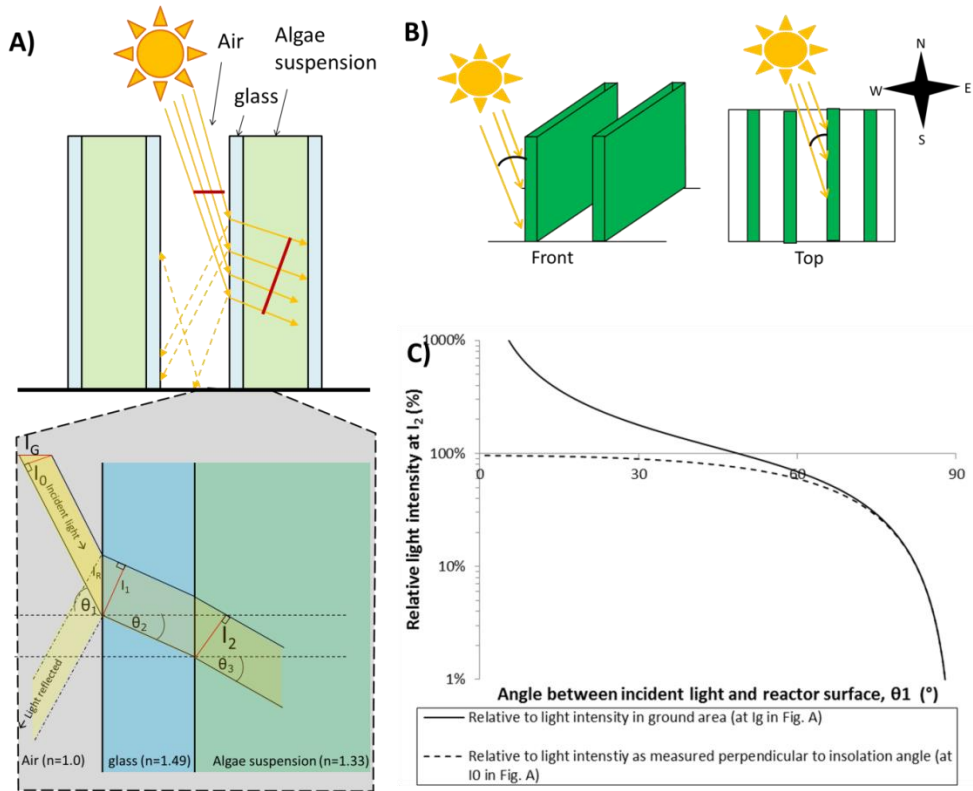


**Fig. A.7** Vertically oriented reactors can help to redistribute incident sunlight of a high light intensity to a larger reactor area and reduce the incident light intensity in the photobioreactor using refraction and reflection at the reactor surface. **(A)**: Refraction at the reactor surface causes light from a certain ground area to be distributed over a larger photobioreactor area (as illustrated by the yellow arrows and red lines). Reflections redistribute the direct sunlight on the illuminated parts of the photobioreactor to shaded parts of the photobioreactor to provide a more homogeneous illumination (as illustrated by the yellow dotted lines). Both the contribution of reflection and refraction increase with increasing angle between the reactor surface and the incident light flux (angle  $\theta_1$ ). Reflection nearly exclusively occurs at the air/glass interface (reflections between the glass/algae-suspension interface are negligible). Figure is not to scale and angles are exaggerated to illustrate the mechanisms. **(B)**: The angle between the incident light flux and the reactor surface ( $\theta_1$  in Fig. A) is determined by the altitude (left) and azimuth (right) of the sun relative to the reactor surface (as measured in the spherical coordinate system). **(C)**: Incident light intensity entering the microalgal culture measured perpendicular to the light flux ( $I_2$  in Fig. A) relative to the incident light intensity in a certain ground area ( $I_G$  in Fig. A; solid line) and relative to the light intensity measured perpendicular to the solar light flux ( $I_0$  in Fig. A; dotted line). A relative light intensity of 100% indicates no change in light intensity and all light intensities below 100% indicate a reduction in incident light intensity. It can be seen that vertically oriented reactors only decrease the light intensity relative to the light intensity in a certain ground area above solar angles of approximately  $50^\circ$  ( $\theta_1$  in Fig. A). **Continues next page.**

**Fig. A.7 (continued).** Below this solar angle, vertically oriented reactors actually concentrate the light and horizontally oriented photobioreactors would be more beneficial. At an angle of  $83^\circ$  of the solar light flux perpendicular to the reactor surface ( $\theta_1$  in Fig. A), a 10-fold light dilution would be accomplished. Light reflection is calculated using the Fresnel equations and light refraction is calculated using Snell's law, as explained by for example (Slegers et al., 2011). Refraction indices ( $n$ ) were obtained from (Lee et al., 2014). In these calculations, the geometry of a flat panel photobioreactor is assumed and it is assumed that all incident light is parallel to the insolation angle (no diffuse light).

### A.8.2 Process design

The impact of the initial biomass concentration and reactor thickness (light path) is commonly investigated (Zemke et al., 2013). At too low biomass concentrations or too short light paths, light is only partly absorbed and this results in decreased yields, reflected by the outliers present in Fig. 7.2A,B. When the light path or biomass concentration are increased beyond the point where all light is absorbed, dark zones form in the photobioreactor. This can reduce the yield due to increased cell maintenance requirements. As a consequence, an optimum in biomass concentration is often observed (Michels et al., 2014; Zemke et al., 2013). In our simulations, the reactor light path and biomass concentration show a similar effect on the TAG yield on light. As described by (Lee et al., 2014), it is in fact the product of the biomass concentration and light path that determines the yield. In our case, a very wide optimum is observed due to the low maintenance coefficient. In conclusion, it appears that there is little variation in the yield as long as the biomass concentration and reactor thickness (light path) are chosen such that all light is absorbed by the culture, consistent with observations by for example (Zemke et al., 2013).

When the outliers as a result of incomplete light absorption are ignored, the reactor light path and the biomass concentration at the onset of nitrogen starvation caused a 14% variation in the time-averaged TAG yield for the wt (Fig. 7.2A; scenarios 2 and 4 compared to 1 and 3). Higher biomass densities and longer light paths resulted in higher yields. This variation is not observed for the *slm1* starchless mutant. This variation in the wt is a consequence of the carbon partitioning mechanism. Although the time-scales differ, no difference in photosynthetic TAG yields are predicted in the wt as a function of biomass concentration or light path up to the point where starch degradation is initiated. But after starch degradation is initiated, *de novo* TAG synthesis is dependent on the photosynthetic rate. TAG production as a result of starch degradation, on the other hand, follows 0<sup>th</sup> order kinetics. As a consequence, at low biomass specific irradiances, starch turnover has a relatively higher contribution to TAG synthesis than *de novo* TAG

synthesis. This boosts the net TAG yield (Fig. A.6). This does not occur in the *slm1* starchless mutant because all available photosynthetic capacity is immediately directed towards TAG synthesis.

As illustrated in Fig. A.6, the harvesting moment of the culture also affects the achieved TAG yield. When harvested too early, only little TAG is produced and when harvested too late, the photosynthetic efficiency decreases too much resulting in a lower yield. In all simulations an optimum moment for harvesting is observed. In our simulations, it is assumed that the process duration is always optimized and this optimum in yield is used as the output for each simulation (*i.e.*, the maximum time-averaged yield; eq. 24). Among all simulations, the predicted TAG content at the point where this maximum time-averaged yield was achieved was  $36\pm12\%$  and  $37\pm2\%$  of DW for the wt and *slm1* starchless mutant, respectively. The larger variability in the predicted TAG content in the wt is a result of the interaction between *de novo* TAG synthesis and turnover of starch, whose relative contributions are dependent on the biomass specific illumination as mentioned above. Also the optimal process duration is much shorter for the *slm1* starchless mutant than for the wt ( $114\pm79$  and  $488\pm396$  h after nitrogen depletion, respectively).

Suboptimal cultivation conditions, such as suboptimal pH or temperature values, can result in a several fold decrease in TAG yield (Breuer et al., 2013b). In this work it is assumed that these values are continuously kept at their optimal values.

### **A.8.3 Strain improvement**

Strain improvement can be used to improve carbon partitioning towards TAG synthesis or can be used to improve the photosynthetic efficiency.

#### **A.8.3.1 Carbon partitioning**

Starchless mutants have shown to be able to direct the photosynthetic capacity, that is directed to starch synthesis in the wild-type, towards TAG synthesis (Breuer et al., 2014). Previously it has been shown that this can result in a more than 50% increase in TAG yield (Breuer et al., 2014). Our model simulations predict that this improvement varies as a function of the incident light intensity between 40 and 48% when the reference conditions for the wt and *slm1* starchless mutant are compared (Fig. 7.2A,B; scenarios 5 and 6 compared to 1 and 3). Even when the best cases of the wt and *slm1* starchless mutant are compared, the *slm1* starchless mutant outperforms the wt by 22-

29% (Fig. 7.2A,B; scenarios 5 and 6 compared to 2 and 4). The reason why the relative improvement of the best-case is lower than the relative improvement of the reference cases, is because the potential for improvement with respect to optimization of  $c_{x,n=0}$  and  $z$  is larger for the wt than for the *slm1* starchless mutant (section A.8.2).

Even in these starchless mutants, not all photosynthetic capacity is directed towards TAG synthesis. Further improvements might thus be possible if the activity of these other competing pathways are reduced.

Although a large part of the photosynthetic capacity is directed towards TAG synthesis during nitrogen starvation, the photosynthetic capacity itself is reduced due to a reduction in the photosynthetic efficiency during nitrogen starvation (Fig. 7.1A-C).

Unfortunately, during nitrogen replete conditions no TAG is produced (Breuer et al., 2012). Large improvements could thus be achieved if microalgae can be engineered to produce TAG under nitrogen replete conditions or if the reduction in photosynthetic efficiency during nitrogen starvation can be minimized. The trigger that causes TAG to be produced during nitrogen starvation remains unknown and as a consequence it has not been accomplished so far to engineer microalgae to produce substantial amounts of TAG under nitrogen replete conditions.

#### **A.8.3.2 Photosynthetic machinery**

A general trend towards higher yields at lower pigmentations (Fig. A.8C,D) and higher yields at higher maximum photosynthetic rates (Fig. A.8E,F) is observed. A decrease in pigmentation and an increase in maximum photosynthetic rate could reduce photosaturation and help to improve the photosynthetic TAG yield (Fig. 7.2C,D).

Although, the room for improvement was higher at a light intensity of  $1500 \mu\text{mol m}^{-2} \text{s}^{-1}$  (76 and 55% improvement for the wt and *slm1* starchless mutant, respectively; comparing scenarios 7 and 9 to 1 and 5, respectively) than at a light intensity of  $200 \mu\text{mol m}^{-2} \text{s}^{-1}$  (13 and 24% improvement for the wt and *slm1* starchless mutant, respectively; comparing scenarios 8 and 10 to 3 and 6, respectively), the photosynthetic efficiency at low light intensities can also be enhanced substantially by improvements to the photosystem. This is because during nitrogen starvation, the photosaturating light intensity decreases compared to nitrogen replete conditions (Fig. 7.1A-C). Engineering the photosynthetic machinery is often presented as an alternative to light dilution, but this model illustrates that these techniques can be complementary to the use of light dilution.

A reduction in pigmentation can be achieved in so called antennae mutants (Melis, 2009; Melis et al., 1999) and the maximum photosynthetic rate could be improved by de-



bottlenecking the photosynthetic chain (Peterhansel et al., 2008). This could for example be addressed by increasing the number of electron carriers in the photosystem (Chida et al., 2007) or by increasing the activity of rubisco or other rate limiting enzymes for CO<sub>2</sub> fixation (Sukenik et al., 1987). For example, it was calculated by (Zhu et al., 2007), using an evolutionary algorithm, that a redistribution of the enzymes in the carbon metabolism could improve the maximum photosynthetic rate almost twofold. Evolution optimized the composition of this machinery towards a composition that contributes to long term viability and robustness and not towards maximum photosynthetic rates. Furthermore this machinery is adapted towards environmental conditions such as atmospheric CO<sub>2</sub> concentrations (Zhu et al., 2007). Conditions in photobioreactors might be very different as it is common practice to use air enriched in CO<sub>2</sub> to aerate a photobioreactor (for example using flue gasses). Optimization of the photosynthetic machinery towards these conditions using laboratory evolution might thus substantially improve the photosynthetic performance. In addition to engineering of the photosystem, photo-acclimation also affects the pigmentation and maximum photosynthetic rate (Melis et al., 1999). Photo-acclimation prior to the onset of nitrogen starvation could therefore potentially also affect the photosynthetic performance during nitrogen starvation. The range in which  $q_{hv}^{max}$  and  $\alpha_{replete}$  are chosen in these simulations is chosen arbitrarily (+/- 50% of the reference-case values), and it remains to be proven that these biological parameters can be altered without negatively affecting other physiological traits. The absolute improvement in the TAG yield should therefore be interpreted with caution. Nevertheless, the ranges in which these parameters were varied seem realistic based on natural variation in these parameters (Horton, 2000; Melis, 2009; Melis et al., 1999; Sukenik et al., 1990; Zhu et al., 2007). Thus, although the potential for improvement is dependent on what realistically can be expected from changes to the photosystem, this work illustrates that an improvement in maximum photosynthetic rate and reduction in absorption cross section could be a tool to improve photosynthetic TAG production.

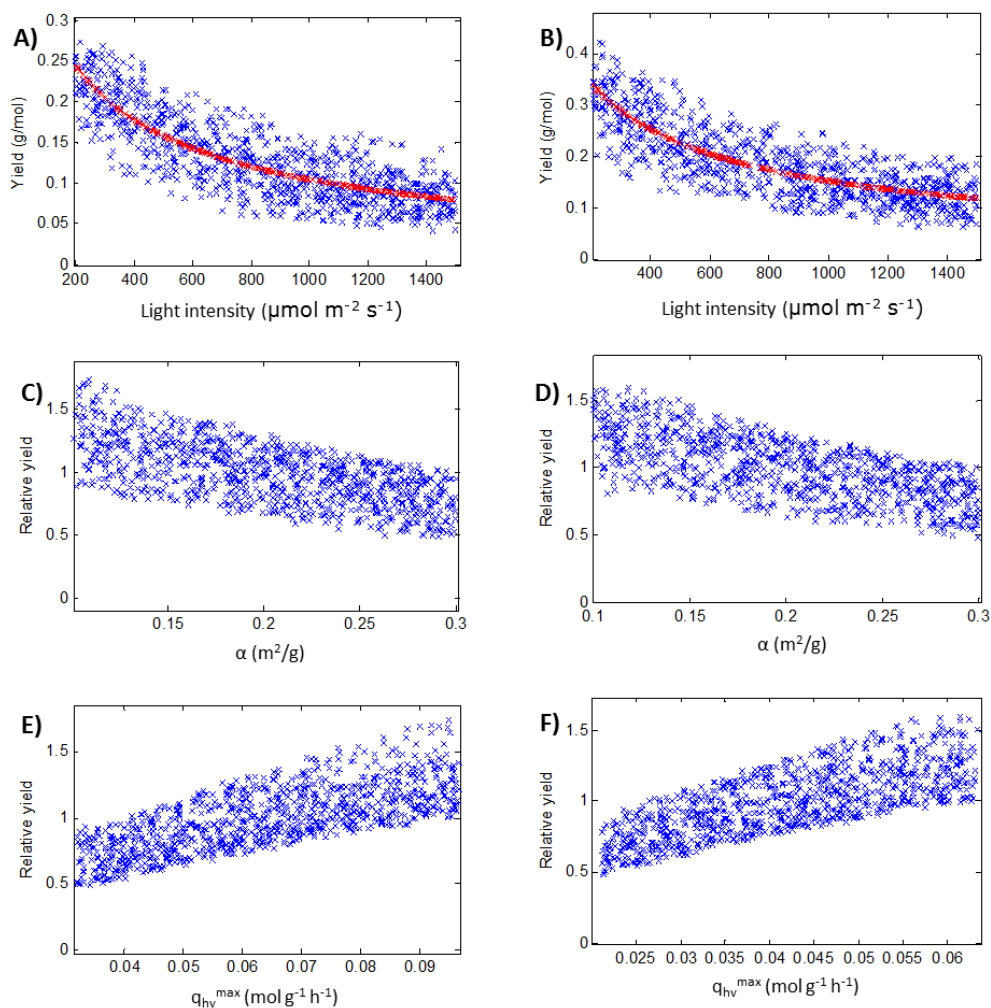


**Fig. A.8** Impact of a variation in  $\alpha_{\text{replete}}$  and  $q_{\text{hv}}^{\text{max}}$  on the maximum time-averaged TAG yield (**A,B**). To illustrate the contribution of  $\alpha_{\text{replete}}$  and  $q_{\text{hv}}^{\text{max}}$ , the yield for each combination of  $\alpha_{\text{replete}}$  and  $q_{\text{hv}}^{\text{max}}$  is normalized to the yield predicted at the same incident light intensity and the values for  $\alpha_{\text{replete}}$  and  $q_{\text{hv}}^{\text{max}}$  from Table A.1 (red symbols in A,B)(from now on called the relative yield). This normalisation is necessary to be able to isolate the effect of  $\alpha_{\text{replete}}$  and  $q_{\text{hv}}^{\text{max}}$  from the large impact of the incident light intensity. A relative yield of 1 represents no change, relative yields above 1 represent an improvement and relative yields below 1 represent a decrease in TAG yield compared to the reference case. The photosynthetic TAG yield decreases with increasing pigmentation (**C, D**) and increases with increasing  $q_{\text{hv}}^{\text{max}}$  (**E, F**). (**A, C, E**): wt. (**B, D, F**): *slm1* starchless mutant. Figure **A,B** corresponds to **Fig. 7.2C,D**.

## A.9 Extrapolation of yields to areal productivities

### A.9.1 Calculation of areal productivity

The areal productivity can be calculated by multiplying the insolation in the photosynthetic active radiation (PAR) spectrum with the projected maximum time-averaged yield of TAG on photons as obtained from the model simulations (Fig. 7.2), when it is assumed that all incident sunlight to a certain area can be converted to TAG at this photosynthetic TAG yield. An insolation of  $6480 \text{ MJ m}^{-2} \text{ year}^{-1}$  is assumed, corresponding to the insolation of Southern Europe. This productivity is then corrected for losses during nocturnal respiration (it is assumed that during the night 10% of the biomass, including TAG, is respired but no additional physiological responses occur as a result of day/night cycles). Furthermore, this productivity is corrected for an assumed annual two month downtime of the photobioreactor, which includes cleaning, turnover, and cultures losses (Eq. 25).

$$\text{Areal productivity (g TAG m}^{-2} \text{ day}^{-1}) = Y_{\text{TAG}} \cdot \frac{I \cdot \text{PAR}}{E \cdot 365} \cdot (1 - r) \cdot (1 - \text{downtime}) \quad \text{Eq. 25}$$

In which  $Y_{\text{TAG}}$  is the maximum time-averaged TAG yield (as obtained using the simulations from section A.7 and as presented in Fig. 7.2A-D),  $I$  the annual insolation ( $6480 \text{ MJ m}^{-2} \text{ year}^{-1}$ ),  $\text{PAR}$  the fraction of photons in the PAR spectrum (0.42 J/J (Breuer et al., 2013b)),  $E$  the average molar energy of photons in the PAR spectrum (0.217 MJ/mol (Breuer et al., 2013b)),  $r$  the fraction lost to nocturnal respiration (0.1), and downtime the fraction of time that the photobioreactor is not operational (2/12).

### A.9.2 Scenarios for optimization

Ten different scenarios for the areal TAG productivity were chosen for which the areal productivity is calculated from the corresponding projected maximum time-averaged TAG yields, as summarized in Table A.3. These projected areal TAG productivities are presented in Fig. 7.2E.

**Table A.3** Scenarios for extrapolation of yields to areal productivities. The scenarios correspond to the scenarios presented in Fig. 7.2E using the yields presented by the numbered circles in Fig. 7.2A-D.

	<b>Description of scenario</b>	<b>wt or starchless mutant</b>	<b>Light intensity (<math>\mu\text{mol m}^{-2} \text{s}^{-1}</math>)</b>	<b>Yield (g TAG/mol photon)</b>
1	Base case. The base case is calculated for the wild-type using the TAG yield that would be obtained without light dilution (highest light intensity; $1500 \mu\text{mol m}^{-2} \text{s}^{-1}$ ). This yield was estimated using the model parameters estimated from the experimental data (red symbols in Fig. 7.2A).	wt	1500	0.080
2	Optimized $z$ and $C_{x,n=0}$ . Similar to 1, but with an optimized reactor thickness and biomass concentration at the onset of nitrogen starvation (upper blue crosses at $1500 \mu\text{mol m}^{-2} \text{s}^{-1}$ in Fig. 7.2A).	wt	1500	0.091
3	Optimal use of light dilution. Similar to 1, but with the assumption that light dilution is maximally exploited such that the TAG yield that can be achieved is similar to the TAG yield achieved at the lowest simulated light intensity ( $200 \mu\text{mol m}^{-2} \text{s}^{-1}$ ).	wt	200	0.244
4	Optimized $z$ and $C_{x,n=0}$ and light dilution. Combination of 2 and 3.	wt	200	0.278
5	Starchless mutant. The starchless mutant scenario is calculated for the <i>slm1</i> starchless mutant that has an improved carbon partitioning towards TAG during nitrogen starvation. It is calculated using the TAG yield that would be obtained without light dilution (highest light intensity; $1500 \mu\text{mol m}^{-2} \text{s}^{-1}$ ). This yield was estimated from the red symbols in Fig. 7.2B.	starchless mutant	1500	0.118
6	Optimal use of light dilution and starchless mutant. Similar to 3, but now for the <i>slm1</i> starchless mutant.	starchless mutant	200	0.340
7	Enhanced photosynthetic machinery. Similar to 1, but with the optimal values for $a_{\text{replete}}$ and $q_{\text{hv}}^{\text{max}}$ (upper blue crosses at $1500 \mu\text{mol m}^{-2} \text{s}^{-1}$ in Fig. 7.2C).	wt	1500	0.142
8	Optimal use of light dilution and enhanced photosynthetic machinery. Combination of scenario 3 and 7.	wt	200	0.273
9	Enhanced photosynthetic machinery and starchless mutant. Similar to 7, but for the <i>slm1</i> starchless mutant.	starchless mutant	1500	0.186
10	Optimal use of light dilution, enhanced photosynthetic machinery, and starchless mutant. Combination of scenario 5 and 9.	starchless mutant	200	0.421
	Theoretical maximum	-	-	1.33

### A.10 List of symbols

Symbol	Unit	Description
$\alpha$	$\text{m}^2 \text{g}^{-1}$	Absorption cross section
$\alpha_{\text{replete}}$	$\text{m}^2 \text{g}^{-1}$	Absorption cross section of nitrogen replete cells
$P_A$	-	Coefficient A for carbon partitioning
$P_B$	-	Coefficient B for carbon partitioning
$C_x$	$\text{g m}^{-3}$	Biomass concentration
$C_{x,n=0}$	$\text{g m}^{-3}$	Biomass concentration at the onset of nitrogen depletion
CHO	$\text{g m}^{-3}$	Concentration of residual biomass produced after nitrogen depletion
$f_{\text{TAG}}$	$\text{mol mol}^{-1}$	Fraction of photons portioned towards starch and TAG that is utilized for TAG production
$\Psi_N$	$\text{mol mol}^{-1}$	Photosynthetic quantum yield during nitrogen starvation
$I_0$	$\text{mol m}^{-2} \text{s}^{-1}$	Incident light intensity
$m_s$	$\text{mol (g DW s)}^{-1}$	Maintenance coefficient
$N$	$\text{g NO}_3\text{-N m}^{-3}$	Extracellular nitrate-N concentration
$Q$	$\text{g g}^{-1}$	Cellular nitrogen content
$Q_{\text{deg}}$	$\text{g g}^{-1}$	Cellular nitrogen content at which starch inter-conversion to TAG is initiated
$Q_{\text{max}}$	$\text{g g}^{-1}$	Maximum cellular nitrogen content
$Q_{\text{min}}$	$\text{g g}^{-1}$	Minimum cellular nitrogen content
$\overline{q_{hv}}$	$\text{mol g}^{-1} \text{s}^{-1}$	Biomass specific photon utilization rate, averaged throughout the reactor
$q_{hv}^{\text{max}}$	$\text{mol g}^{-1} \text{s}^{-1}$	Maximum photosynthetic rate
$q_{hv}^{\text{max, replete}}$	$\text{mol g}^{-1} \text{s}^{-1}$	Maximum photosynthetic rate of nitrogen replete cells
$q_i$	$\text{g g}^{-1} \text{s}^{-1}$	Biomass specific production/consumption rate of component i
$r_{\text{starch, TAG}}$	$\text{g (g DW s)}^{-1}$	Inter-conversion rate of starch to TAG
$r_{\text{starch, TAG}}^{\text{max}}$	$\text{g (g DW s)}^{-1}$	Maximum inter-conversion rate of starch to TAG
Starch	$\text{g m}^{-3}$	Concentration of starch produced after nitrogen depletion
$t$	h	Time
TAG	$\text{g m}^{-3}$	Concentration of TAG produced after nitrogen depletion
$X$	$\text{g m}^{-3}$	Concentration of reproducing biomass
$X_{\text{CHO}}$	$\text{g CHO (g DW)}^{-1}$	CHO content in the newly biomass produced after nitrogen depletion, excluding the reproducing biomass
$X_{\text{CHO, X}}$	$\text{g CHO (g DW)}^{-1}$	CHO content in reproducing biomass
$X_{\text{starch, X}}$	$\text{g g}^{-1}$	Starch content in reproducing biomass
$Y_{i,j}$	$\text{g mol}^{-1}$ or $\text{g g}^{-1}$	Yield of component i on component j (subscript hv refers to photons)
$z$	m	Light path of reactor

## Appendix B: Metabolic network.

### B.1 Lumping protein synthesis

stoichiometry of amino acid synthesis normalized to the synthesis of 1 amino acid Stoichiometry from Kliphuis et al. 2011																			
Amino acid	MW	N	abundance	substrates										cofactors					
				3PG	GLU	GLN	AKG	PYR	AcCoA	PEP	E4P	R5P	GAP	OXA	FUM	FORM	SUCC	GLYOX	NH4
SER	105	1	5.50%		-1	-1		1											
CYS	121	1	1.20%		-1	-1													
ALA	89	1	11.10%			-1		1	-1										
VAL	117	1	5.90%			-1		1	-2										-1
LEU	131	1	9.30%			-1		1	-2	-1							1	-1	
PHE	131	1	4.50%			-1		1			-2	-1						-1	-1
TYR	181	1	3.10%			-1		1			-2	-1					1	-1	-1
TRYP	204	2	0.10%		-1		-1	1	1		-2	-1	-1	1			1	-1	-3
ASP	133	1	4.70%			-1		1							-1				
ASN	132	2	4.70%				-1	1							-1				-1
ARG	174	4	4.70%			-2	-1	2							-1	1			-4
PRO	115	1	5.90%			-1											-2		
HYDRPRO	115	1	1.30%			-1		-1									-2		
LYS	146	2	5.80%			-2		2	-1						-1			-1	-1
THR	119	1	5.70%			-1		1							-1			-2	-2
MET	149	1	2.20%		-1	-2		1	1						-1		-1	-4	-4
ILE	131	1	3.60%			-2		2	-1						-1			1	-3
GLY	75	1	9.40%			-1		1										-1	
GLU	147	1	5.00%			-1													
GLN	146	2	5.00%				-1												
HIS	155	3	1.70%			-1	-1	2					-1		-1	1	-1		2
polymerization			1																-4.306

net stoichiometric reaction (for production of 1 mol amino acid normalized protein)																			
Amino acid	MW	N	abundance	3PG	GLU	GLN	AKG	PYR	AcCoA	PEP	E4P	R5P	GAP	OXA	FUM	FORM	SUCC	GLYOX	NH4
SUM	124.40	1.34	1.004		-0.090	-1.069	-0.162	0.965	-0.486	-0.093	-0.154	-0.077	-0.018	0.001	-0.331	0.064	-0.039	0.013	-0.094
																			0.058
																			-0.035
																			-0.597
																			-5.083

Weight of protein after polymerization (amino acid monomer)	106.40 g/mol
nitrogen content	0.176 g/g

### B.2 Lumping DNA synthesis

DNA stoichiometry for the production of nucleotides according to Kliphuis et al. 2011																
Nucleotide	MW	N	abundance	substrates								cofactors				
				GLU	GLN	OXA	FORM	R5P	GLYOX	FUM	AKG	NH4	ATP	NADPH	NADH	
dATP	331	5	0.18	-1	-2	-2	-2	-1	-1	2	3		-11	-1		
dGTP	347	5	0.32		-2	-1	-2	-1	-1	1	2	-1	-12	-1	1	
dCTP	307	3	0.32	1	-2	-1		-1			1		-7	-1		
dTTP	322	2	0.18		-1	-1	-1	-1			1		-7	-3		
polymerization			1												-1.37	

Nucleotide	MW	N	abundance	GLU	GLN	OXA	FORM	R5P	GLYOX	FUM	AKG	NH4	ATP	NADPH	NADH	
SUM	326.82	3.82		1.00	0.14	-1.82	-1.18	-1.18	-1.00	-0.50	0.68	1.68	-0.32	-10.69	-1.36	0.32

weight of nucleotide before polymerization	326.82 g/mol
weight after polymerization	308.82 g/mol
nitrogen content	0.173 g/g

### B.3 Lumping RNA synthesis

RNA stoichiometry for the production of nucleotides according to Kliphuis et al. 2011															
Nucleotide	MW	N	abundance	substrates							cofactors				
				GLU	GLN	OXA	FORM	R5P	GLYOX	FUM	AKG	NH4	ATP	NADPH	NADH
nATP	347	5	0.16	-1	-2	-2	-2	-1	-1	2	3		-11		
nGTP	363	5	0.34		-2	-1	-2	-1	-1	1	2	-1	-12		1
nCTP	323	3	0.34	1	-2	-1		-1			1		-7		
nUTP	324	2	0.16		-1	-1		-1			1		-6		
polymerization			1										-0.4		

Nucleotide	MW	N	abundance	GLU	GLN	OXA	FORM	R5P	GLYOX	FUM	AKG	NH4	ATP	NADPH	NADH	
SUM	340.60	3.84		1.00	0.18	-1.84	-1.16	-1.00	-1.00	-0.50	0.66	1.66	-0.34	-9.58	0.00	0.34

weight of nucleotide before polymerization	340.60 g/mol
weight after polymerization	322.60 g/mol
nitrogen content	0.167 g/g

### B.4 Biomass composition

Biomass composition					
Component	MW monomer	MW polymer	Nitrogen content		
	(g/mol)	(g/mol)	(% DW)	% DW	mmol/g
Protein	124.40	106.40		17.6%	4.229522
Starch	180	162		0.0%	0.617284
Other carbohydrate	180	162		0.0%	1.777778
TAG (triolein)	885	885		0.0%	0
oleic acid	282	282		0.0%	0.35461
DNA	326.82	308.82		17.3%	0.006476
RNA	340.60	322.60		16.7%	0.185989
total				9%	100%

B.5 Stoichiometry of metabolic network

reaction number	1	2	3	4	5	6	7	8	9	10	11	12	13	14	15	16	17	18	19	20	21	22	23	24	25	26	27	28	29	30	31	32	33	34	35		
pathway	photosynt		gluconeogenesis										PPP										TCA cycle														
	linear photosynth	cycl photosynth	calvin cycle	cGAP --> c_3PG	c_3PG --> c_F16BP	c_F16BP --> c_F6P	c_F6P --> c_F16BP	c_F6P --> c_G6P	c_G6P --> c_starch	GAP transport	3PG transport	G6P transport	GAP --> 3PG	GAP --> glycerol	G6P --> R5P	R5P --> X5P	R5P + X5P --> E4P + F6P	X5P + E4P --> F6P + GAP	F6P --> G6P	3PG --> PEP	PEP --> PYR	PYR --> PEP	PYR --> AcCoA	PYR --> OXA	AcCoA + OXA --> CIT	CIT --> ISOCIT	ISOCIT --> aKG	aKG --> SUCC	SUCC --> FUM	FUM --> MAL	MAL --> OXA	ISOCIT --> GLYOX + SUCC	GLYOX + AcCoA --> MAL	c_aKG --> c_GLU	c_GLU --> c_GLN		
photon	-8	-2																																			
c_ATP	3	1	-9	1			-1		-1																												-1
c_NADPH	2	-6	1																																		-1
c_NADH																																					
c_GAP			1	-1	-2					-1																											
c_3PG				1							-1																										
c_F16BP					1	-1	1																														
c_F6P					1	-1	-1																														
c_G6P								1	-1			-1																									
c_starch									1																												
ATP													1	-1							1	-2		-1			1										
NADH													1											1			1	1	1			1					
NADPH														-1	2																						
GAP										1			-1	-1			1																				
3PG											1		1							-1																	
G6P												1			-1				1																		
glycerol6P													1																								
R5P															1	-1	-1																				
X5P																1	-1	-1																			
E4P																	1	-1																			
F6P																	1	1	-1																		
PEP																			1	-1	1																
PYR																				1	-1	1															
AcCoA																					1	-1														-1	
OXA																						1	-1									1					
CIT																							1	-1													
ISOCIT																								1	-1										-1		
aKG																									1	-1											
c_aKG																										1	-1									-1	
SUCC																											1	-1					1				
FUM																												1	-1								
MAL																													1	-1					1		
GLYOX																																	1	-1			
GLU																																				1	-1
c_GLU																																					1
c_GLN																																					1
c_NH4																																				-1	-1
c_NO2																																					
NO2																																					
NO3																																					
c_AcCoA																																					
c_FA																																					
FA																																					
TAG																																					
Protein																																					
DNA																																					
RNA																																					
boundaries																																					
lb	0	0	0	-10	-10	0	0	-10	-10	-10	-10	-10	-10	-10	0	0	0	0	-10	-10	0	0	-10	-10	0	0	-10	-10	0	-10	-10	-10	0	0	0	0	
ub	10	10	10	10	10	10	10	10	10	10	10	10	10	10	10	10	10	10	10	10	10	10	10	10	10	10	10	10	10	10	10	10	10	10	10	10	







## **Chapter 8** General discussion

**Abstract**

Global demands for food commodities and biofuels are rapidly increasing. Availability of arable land to produce these products using conventional agriculture is limited. Novel sources for these commodities are therefore highly desired. Microalgae-derived products are a promising source for these commodities because microalgae have a much higher areal productivity and can be cultivated on non-arable land. Before these microalgal products can be commercialized, it is important that their production processes have a positive energy balance and have a competitive cost-price. This is commonly evaluated in techno-economic (TE) and life cycle assessment (LCA) studies. Most of these studies use biodiesel production as their case-study and conclude that the cost-price is currently several folds higher than that of vegetable-oil-derived biodiesel. Estimated net energy ratios (energy contained in products divided by energy consumed in production process) are mostly unfavourable or near unity.

Most studies use input values for microalgae production that are poorly supported by practical data or scientific knowledge. To use more realistic input values in these studies, trustworthy physiological data should be included. Important data that should be included are photosynthetic efficiency and carbon partitioning. Secondary metabolites such as TAG are only produced during prolonged nitrogen starvation, during which the photosynthetic efficiency is lower than during nitrogen replete conditions. The data reported in this thesis provide more realistic inputs for techno-economic and LCA studies. It is concluded that in most TE and LCA studies the microalgal TAG productivity is over-estimated by 3 to 6-fold. If these lower productivities would have been used in these TE and LCA studies, it would have resulted in a 2 to 3.5-fold higher cost-price and specific energy consumption (MJ/kg product). Engineered improvements in productivity and microalgal performance can decrease energy consumption and cost-price, but in addition to that, photobioreactors and downstream processing unit operations with a reduced cost and energy consumption need to be developed to commercialize commodity products from microalgae.

### 8.1 Microalgal products as a substitute for plant products

Global demands for fuel, energy and food are rapidly increasing (Godfray et al., 2010). At the same time, fossil resources are being depleted and concerns for greenhouse gas emissions and climate change are increasing. Terrestrial plants can be used as a resource for fuel and energy production, but availability of arable land is limited and the productivity of agricultural crops is reaching a ceiling (Godfray et al., 2010). Sustainable and renewable alternative sources are therefore needed. Microalgae have the potential to supplement or substitute crop-derived products for food, feed, fuel, and chemicals. Microalgae can be seen as 'microplants' with capabilities to produce large quantities of oil (triacylglycerol or TAG). The fatty acid composition of these oils is similar to that of oil-crops and is considered a vegetable oil and can be used as food ingredients (Draaisma et al., 2013). These oils can also be used for the production of biodiesel (Chisti, 2007). Starch and other carbohydrates can also be produced by microalgae can also be used in food or feed. These carbohydrates could be fermented to produce bio-ethanol or organic acids that can be used for, for example, the production of biopolymers. Proteins derived from microalgae can be used in food as well (Becker, 2007; Draaisma et al., 2013; Schwenzfeier et al., 2011). In addition to these commodities, some microalgae species produce higher-value products that are used as for example food-supplements, such as carotenoids (e.g.  $\beta$ -carotene, astaxanthin, lutein) or long-chain poly-unsaturated fatty acids (LC-PUFA) such as eicosapentaenoic acid (EPA; C20:5 $\omega$ 3) or docosahexaenoic acid (DHA; C22:6 $\omega$ 3) (Benemann et al., 1987). LC-PUFAs are products for which currently no vegetable source exists. Other products, such as for example  $\beta$ -carotene, can be produced in higher concentrations by some microalgae species than in crops (Table 8.1).

Microalgae have several advantages over terrestrial plants. Microalgae can achieve much higher photosynthetic efficiencies and as a result much higher areal productivities can be accomplished. Using photobioreactors, microalgae can be cultivated on land that is not suitable for agriculture. Some microalgae species can grow efficiently on salt water and potentially these can even be cultivated off-shore. Furthermore, in closed photobioreactors water losses due to evaporation can be minimized. As a result, in theory, very little fresh water is needed for their cultivation. In photobioreactors fertilizer losses to the environment can be prevented and nutrients can be recycled by anaerobic digestion of the residual biomass after product recovery (Chisti, 2013). Because of these advantages, biofuels derived from microalgae are often considered 3<sup>rd</sup> generation biofuels.

At the same time, microalgae also have some disadvantages that need to be overcome. For their high productivities, microalgae rely on cultivation in photobioreactors. The construction and operation of photobioreactors adds to costs and energy consumption. Furthermore, in contrast to crops, all microalgal products are located within a single cell. This provides challenges for harvesting, extraction and refinery because the co-products have to be valorised to prevent large losses. Finally, the biomass dry weight concentration in photobioreactors is typically much lower than biomass concentrations in heterotrophic processes and the dry matter content of crop-derived products. This introduces challenges for harvesting and refinery of the biomass.

**Table 8.1 (continues next page).** Range in which the macro-biomass constituents vary in photoautotrophically-grown microalgae and applications for various biomass constituents of microalgae. The biochemical composition is highly variable and is dependent on the microalgae species as well as environmental conditions. Nitrogen starvation is commonly used to produce secondary metabolites.

<b>Biomass constituent</b>	<b>Application</b>	<b>Abundance (%DW)</b>	<b>Cultivation strategy to produce component</b>	<b>Examples of recommended species</b>	<b>Reference</b>
TAG	biodiesel, edible oil	0-50	Prolonged nitrogen starvation	<i>Scenedesmus obliquus</i> , <i>Chlorella zofingiensis</i> , <i>Nannochloropsis sp.</i>	<b>(chapter 3)</b> (Chisti, 2007; Draaisma et al., 2013; Mulders et al., 2014a)
Starch	food, feed, fermentation to bio-ethanol or organic acids (biopolymers)	5-50	Harvest during early nitrogen starvation	<i>Chlorella sorokiniana</i> , <i>S. obliquus</i> , <i>Dunaliella tertiolecta</i> , <i>Chlamydomonas reinhardtii</i>	(Draaisma et al., 2013)
Protein	food, feed	5-50	Optimal growth conditions (nitrogen replete)	Various green microalgae	<b>(chapter 3)</b> (Becker, 2007; Draaisma et al., 2013; Schwenzfeier et al., 2011)

**Table 8.1 (continued).**

residual biomass (e.g. cellulosic biomass)	bio-ethanol, organic acids (biopolymers), methane production	10-30	Strategy for cultivation should not aim to produce residual biomass. The produced residual biomass can be valorised biomass		<b>(chapter 5 &amp; 6)</b>
LC-PUFA ( $\omega$ -3 fatty acids)	food-supplement, aquaculture feed	0-5	Optimal growth conditions (dark acclimated)	<i>Phaeodactylum tricornutum</i> , <i>Isochrysis galbana</i> , <i>Nannochloropsis sp.</i>	<b>(chapter 3)</b> (Draaisma et al., 2013)
carotenoids (e.g. $\beta$ -carotene, astaxanthin)	food-supplement, aquaculture feed	0-10	Prolonged nitrogen starvation, high light intensity	<i>Dunaliella salina</i> , <i>Haematococcus pluvialis</i> , <i>Chlorella zofingiensis</i>	(Lamers et al., 2012; Lamers et al., 2010; Mulders et al., 2014b)

## 8.2 Economic and energetic feasibility

Potentially, microalgae can be more sustainable and have a much higher productivity than terrestrial plants, but advances are needed to make their commodity products cost-effective and energy neutral/positive. Most techno-economic (TE) and life-cycle assessment (LCA) studies focus on biodiesel or whole biomass production as their case-study (Table 8.2). Although never employed on a commercial scale (for phototrophic processes), typically the flow sheet as presented in Fig. 8.1 is used. Here, microalgae with a high TAG content are cultivated in an open pond or closed photobioreactor, the biomass is then harvested, oil is subsequently extracted, and the extracted oil is transesterified to alcohol-esters (usually fatty acid methyl esters). In some cases, the residual biomass is anaerobically digested for biogas production and recovery of nutrients.

Calculated cost-prices for biodiesel or whole-biomass that are produced using current microalgal technology range from 2.0 to 25.2 €/kg (Table 8.2). These values largely exceed the market-price of vegetable oils of 0.5-1 €/kg (Klok et al., 2014).

Predicted net energy ratio (NER) values (energy in products divided by energy consumed in production, not considering the absorbed sunlight) for biodiesel or microalgal biomass production range from 0.03-1.6 (Table 8.2). NER values above 1 mean a net production of energy and NER values below 1 mean that more energy is consumed than energy that is produced. This means that according to most LCA studies,

current microalgae cultivation would consume more energy than what is produced in the form of biodiesel and biogas. According to others, marginally more energy is produced than is consumed. Processes with a NER value below 1 can never be feasible for energy applications. Even processes with NER values marginally above 1 are not economically feasible, because the majority of the produced energy then needs to be used for the process itself. For example, in the case of a process with a NER value of 2, 50% of the output needs to be re-used in the process to generate the energy required in the process. This reduces the overall productivity twofold. Ideally, NER values above 7 are desired (Chisti, 2013). Biodiesel from rape and soya is estimated to have NER values of 2 (Scott et al., 2010) and diesel derived from fossil oil has a NER value of 5.25 (Batan et al., 2010).

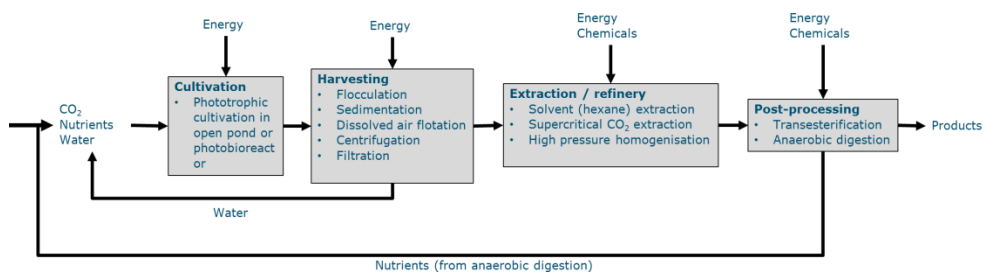


**Fig. 8.1.** Flow sheet for typical microalgal biodiesel process. Commonly used or proposed unit operations are shown as examples. For a more detailed description of this flow sheet or unit operations, see for example (Slegers et al., 2014).

From these studies it can be concluded that substantial improvements in costs and energy use are required to commercialize phototrophic microalgal products. At the same time, these estimates suffer from large uncertainties in their predictions. This arises from large uncertainties in input parameters. Experience with commercial large-scale phototrophic algae cultivation is limited to production of dried microalgal biomass, containing high value components such as LC-PUFA or carotenoids, that is used for food supplements or as aquaculture feed. TE and LCA studies therefore heavily rely on assumptions, extrapolations from lab-scale data, and data from other technologies such as wastewater treatment (e.g. for flocculation or open pond construction) or processing of vegetable biomass (e.g. for extraction/refinery).

The input values for the cultivation step introduces one of the largest uncertainties in these TE and LCA studies. At the same time, a large part of both the operational and investment costs and the energy consumption is used in the cultivation step (Fig. 8.2). This makes it very important to use reliable input values for the cultivation step.



**Table 8.2.** Reported NER and cost-price values for biodiesel or biomass production.

Reported NER values (MJ energy produced/MJ energy consumed)	Reported cost-prices
Microalgae	
<ul style="list-style-type: none"><li>• 0.3-1.6, biodiesel (Slegers et al., 2014)<sup>2</sup></li><li>• 0.51-1.34, biodiesel (Lardon et al., 2009)<sup>2</sup></li><li>• 0.03-0.73, biodiesel (Passell et al., 2013)<sup>2</sup></li><li>• 0.95, biomass (Clarens et al., 2010)<sup>2</sup></li><li>• 0.33-1.5, biodiesel (Quinn et al., 2013)<sup>2</sup></li><li>• 0.13-0.64, biodiesel (Brentner et al., 2011)</li><li>• 1.07, biodiesel (Batan et al., 2010)</li><li>• 0.16, biomass (Acien et al., 2012)<sup>2</sup></li></ul>	<ul style="list-style-type: none"><li>• 17.8-25.2 €/kg oil (Richardson et al., 2014)<sup>1</sup></li><li>• 4.16-5.96 €/kg biomass (Norsker et al., 2011)</li><li>• 2.2-3.7 €/kg oil (Delrue et al., 2012)<sup>1</sup></li><li>• 2.0-4.2 €/kg oil (Davis et al., 2011)<sup>1</sup></li><li>• &gt;8.3 €/kg oil (Draaisma et al., 2013)</li><li>• pilot scale 69 €/kg biomass; large-scale 12.6 €/kg biomass (Acien et al., 2012)</li></ul>
Terrestrial plants	
<ul style="list-style-type: none"><li>• 2 (biodiesel from rape and soya) (Scott et al., 2010)</li><li>• 1.64 (biodiesel from soya) (Batan et al., 2010)</li></ul>	<ul style="list-style-type: none"><li>• 0.5-1 €/kg oil (various sources) (Klok et al., 2014)</li></ul>

<sup>1</sup>Calculated using 1 USD = €0.79; 1 litre oil = 0.9 kg

<sup>2</sup>Only for the operational energy consumption. Embedded energy (in construction and installation) is excluded from this NER ratio.

Most studies, however, mainly focus their calculations on the downstream part (after cultivation) and use the composition of the biomass stream (productivity, concentration, and composition) as a given boundary (Batan et al., 2010; Clarens et al., 2010; Quinn et al., 2013). Productivities that are used are commonly obtained by multiplication of the maximum photosynthetic efficiency of microalgae with maximum reported TAG contents. These high photosynthetic efficiencies are only achieved under low light intensities, but the light provided to the photobioreactor by sunlight is that of a high light intensity. These high light intensities will result in lower photosynthetic efficiencies. Furthermore, the photosynthetic efficiency is largely reduced under the conditions that result in high TAG contents (**chapters 3-7**). In some studies the impact of photobioreactor design is partly taken into account by using different productivities and TAG contents for different reactor designs (Brentner et al., 2011; Davis et al., 2011; Jorquera et al., 2010; Resurreccion et al., 2012). These reactor designs are often limited to the choice between an open pond or a closed photobioreactor and do not consider specific design or operational decisions. Penalties associated with suboptimal reactor designs for productivity or TAG content are chosen arbitrarily. Sometimes, the uncertainty in for example the productivity, TAG content, or biomass density is simulated using a random distribution for these parameters (Campbell et al., 2011; Delrue et al., 2012; Richardson

et al., 2014). But in these studies it is overlooked that these parameters are strongly interconnected. Only few studies include basic physiological behaviour such as nitrogen replete or nitrogen deplete algae cultivation (Lardon et al., 2009) or use operational data of pilot or commercial microalgae production facilities, of for example biomass containing LC-PUFAs (Acién et al., 2012; Passell et al., 2013).

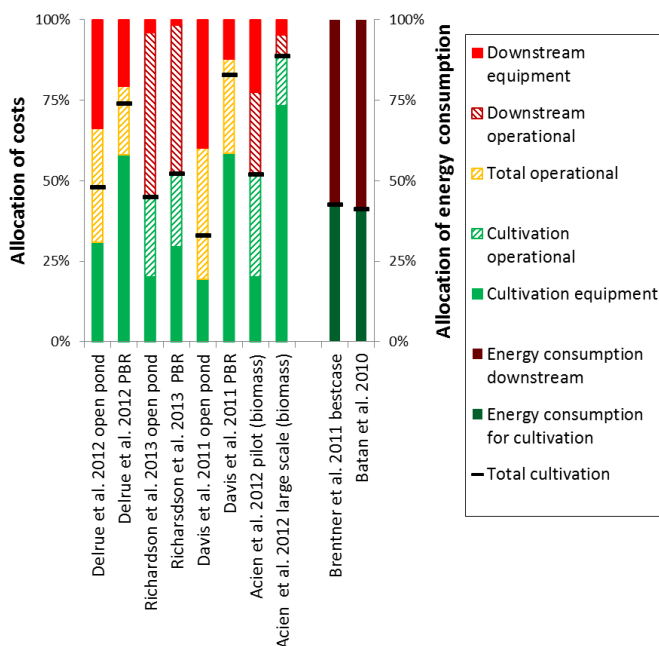


**Fig. 8.2.** Allocation of costs and energy consumption of operation and construction of the cultivation step and the downstream steps (including harvesting), from the studies presented in Table 8.2 that specify the allocation of costs or energy consumption. For the allocation of costs (studies shown on the left), a distinction is made between operational costs and construction/installation costs. Some studies only report the total operational costs (e.g. total labour). In these cases, the total operational cost is shown (orange). To calculate the contribution of the cultivation step for these cases, these total operational costs are allocated proportional to ratio of equipment costs for cultivation and equipment costs for downstream processing (as indicated with the black line). For allocation of energy consumption (studies shown on the right), only the studies that included embedded energy (construction and installation) are shown. These studies did not report the allocation of energy consumption between construction and operation, therefore the combined operational and construction energy consumption is presented.

Altogether, most studies assume biomass productivities between 15-30 g m<sup>-2</sup> day<sup>-1</sup>, oil contents between 25-50%, and biomass densities between 0.5-5 g/l. As will be illustrated in the subsequent paragraphs, these values overestimate the microalgal performance. As the outcomes of LCA and TE studies relies heavily on these assumed

input parameters, more-realistic combinations of input parameters for these studies are highly desired.

### **8.3 Microalgal response to nitrogen starvation – what can we expect from microalgae?**

To select reasonable input values for the microalgal productivity and biochemical composition that can be used in TE and LCA studies, it is important to understand the basics of the microalgal physiology. Both the photosynthetic efficiency and biochemical composition are highly variable. These do not only differ between microalgae species, but are also highly dependent on cultivation conditions. Under balanced growth conditions, very high photosynthetic efficiencies can be accomplished, but under these conditions almost no secondary metabolites such as TAG are produced. The most common technique to induce accumulation of these secondary metabolites is the use of nitrogen starvation.

In such a batch cultivation, the cultivation is started with a certain amount of nitrogen. This nitrogen is used for growth and after several days, all nitrogen is depleted from the cultivation medium. After the depletion of nitrogen from the cultivation medium, photosynthesis and carbon assimilation continue and this assimilated carbon is used for the synthesis of secondary metabolites (Fig. 8.3). The physiological response to nitrogen starvation can be subdivided in the effects on *photosynthesis* and in the effects on *carbon partitioning*. Although the magnitude of these effects can vary between species, the same general trends are observed between microalgae species.

#### **8.3.1 Dynamics of nitrogen starvation**

##### **8.3.1.1 Photosynthesis**

The light intensity has a large impact on the photosynthetic efficiency. At low light intensities the highest photosynthetic efficiencies are accomplished. At this point, photosynthesis is limited by light absorption. When the light intensity increases beyond the photosaturating light intensity, the photosynthetic capacity becomes limiting. At this point, all light absorbed that exceeds the photosynthetic capacity is thermally dissipated. This reduces the photosynthetic efficiency (Box 1). High light intensities can easily result in a 2 to 5-fold reduction in the photosynthetic efficiency (**chapter 4, 6, and 7**). This reduction in photosynthetic efficiency at high light intensities occurs at both nitrogen replete cultivation and nitrogen depleted cultivation, but typically the reduction in photosynthetic efficiency is larger during nitrogen depleted conditions (**chapter 6 & 7**).

Also suboptimal temperatures and pH values can have a detrimental effect on the photosynthetic efficiency (**chapter 4**).

How the light intensity can influence the photosynthetic rate and photosynthetic efficiency is explained in more detail in Box 1.

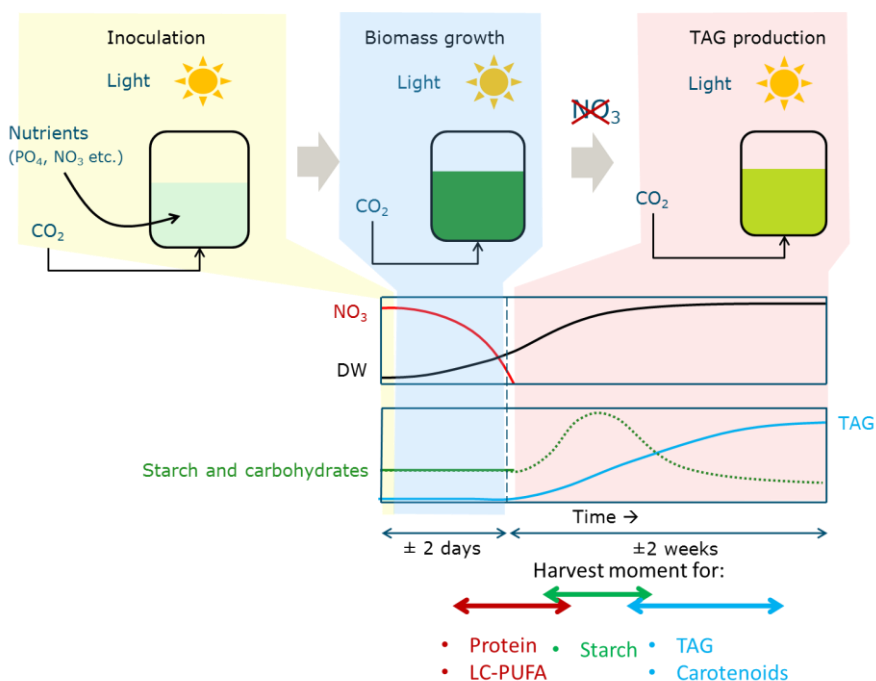


**Fig. 8.3.** Dynamics of nitrogen starvation in a batch cultivation. The cultivation is started with a certain amount of nitrogen. This nitrogen is used for growth and after several days, all nitrogen is depleted from the cultivation medium. Hereafter, photosynthesis and biomass formation continue and secondary metabolite accumulation is initiated. First, most of the photosynthetic capacity is partitioned towards carbohydrate synthesis. When nitrogen starvation progresses, gradually more is partitioned towards TAG. Finally, the accumulated carbohydrates are degraded again and their monomers are likely used as a substrate for TAG synthesis. The duration of this nitrogen starvation phase can be up to several weeks, even under high light conditions. The optimal moment for harvesting is dependent on the desired biomass composition. For proteins or LC-PUFA, harvesting can best be done before nitrogen depletion or early after nitrogen depletion. For carbohydrates, harvesting can best be performed during early nitrogen starvation. For a high TAG or carotenoids (in microalgae that can over-produce carotenoids) content, the best harvesting time is at late nitrogen starvation, but to maximize their yield on light, harvesting should occur before nitrogen starvation is completed.

During nitrogen starvation, the above mentioned responses to the light intensity still apply, but in addition various physiological changes occur that affect light harvesting,

the photosynthetic capacity, and photoinhibition. As explained in more detail in **chapter 7**, the pigmentation, pigment class composition, quantum yield, and photosynthetic capacity (maximum photosynthetic rate) change during nitrogen starvation. As a result, the photosynthetic efficiency progressively decreases during nitrogen starvation, but photosynthesis and carbon assimilation can continue, at progressively reducing rates, for up to several weeks in well-performing microalgae (Fig. 8.3).

Although similar general trends in the response to nitrogen starvation are observed for different microalgae species, quantitative differences in the photosynthetic response between microalgae species can be large (**chapter 3**). These can be generalized in the following two points (A and B in Fig. 8.5).

A) Duration of sustained high biomass productivity. Immediately after the depletion of nitrogen, biomass production continues with the same rate as before the depletion of nitrogen (**chapter 3**). When nitrogen starvation progresses further, the biomass productivity starts to decrease. How long microalgae can sustain their initial biomass productivity during nitrogen starvation (A in Fig. 8.5) is an important characteristic, because the biomass productivity during nitrogen starvation ultimately determines the productivity of secondary metabolites such as TAG.

How long microalgae can sustain their high biomass productivity can best be expressed as the fold-increase in biomass after the depletion of nitrogen, because this allows for comparison of different illumination conditions (e.g. light intensities, or biomass densities). For example, for what period (days) microalgae can retain their high photosynthetic efficiency is highly dependent on the light intensity, but until what fold-increase in biomass they can retain their high biomass productivity is mostly independent of the light intensity (**chapter 4 and 6**).

Some species, such as *I. galbana*, exhibit a decreased biomass productivity almost immediately after the depletion of nitrogen (Fig. 8.5). Other species, such as for example, *S. obliquus*, appear to be able to increase 4.5-fold in biomass concentration after the depletion of nitrogen before a noticeable decrease in biomass productivity is observed (**chapter 3**).

B) The maximum increase in biomass after nitrogen depletion. When the biomass productivity starts to decrease (after period A in Fig. 8.5), photosynthesis keeps to contribute to a further increase in biomass (B in Fig. 8.5). For example, *S. obliquus* was able to increase 7 to 8-fold in biomass concentration after the depletion of nitrogen

**(chapter 3 & 6).** *S. obliquus* appears to perform exceptionally well in this respect.

Some other microalgae species such as *I. galbana* or *Nannochloris* sp. were only able to increase 1.4 and 2.2-fold in biomass concentration after the depletion of nitrogen

**(chapter 3).**

For *S. obliquus* it was found that how much *S. obliquus* can maximally increase in biomass concentration during nitrogen starvation is not affected by the light intensity **(chapter 4 and 6)**, but is negatively affected by suboptimal pH and temperatures

**(chapter 4).**

**Box 1.** Photosynthesis and photosynthetic efficiency.

**Photosynthesis**

In photosynthesis, light is absorbed by light harvesting pigments. This light energy is used to liberate electrons from H<sub>2</sub>O to produce O<sub>2</sub>. These electrons are used to regenerate NADPH from NADP<sup>+</sup> and to produce ATP (photosynthesis). NADPH and ATP can subsequently be used for carbon fixation and downstream metabolism. Not all absorbed light energy is however used for photosynthesis and parts of the absorbed light are thermally dissipated. This reduces the photosynthetic efficiency.

Light influences the photosynthetic efficiency in several ways. These are discussed below and apply to both nitrogen replete and nitrogen-depleted conditions. In addition to that, nitrogen starvation also has additional effects on photosynthesis. There are discussed in **chapter 7**.

**(1) Photosaturation.** At low light intensities, photosynthesis is limited by the absorption of light. Under these conditions a high photosynthetic efficiency can be accomplished. At high light intensities, light absorption exceeds the photosynthetic capacity and excess light is thermally dissipated resulting in a decreased photosynthetic efficiency (Fig. 8.4). This is called photosaturation. Sometimes also called dynamic photoinhibition (but is very different from photoinhibition as mentioned under 2).

**(2) Photoinhibition.** Light induces damage to the photosystem (to the PSII D1 protein). This damage renders the photosystem un-functional and all photons absorbed by the antennae of this photosystem are then thermally dissipated. This damage is reversible, but at high light intensities, a larger proportion of the photosystems is damaged and un-functional. This reduces the photosynthetic efficiency (Fig. 8.4). Also when photoinhibited microalgae are suddenly exposed to a very low light intensity, this photoinhibition may temporarily persist **(chapter 6)** (Baroli & Melis, 1996; Neidhardt et al., 1998).

**(3) Photoacclimation.** The pigmentation and photosystem composition acclimates to the light intensity **(chapter 6)**. For example, the pigmentation can decrease up to twofold at high light intensities **(chapter 6)**. This decreases light absorption rates (when compared to a higher pigmentation at the same light intensity). Also the composition of the photosystem changes, which can affect both the photosynthetic capacity and quantum yield (Sukenik et al., 1987). Altogether these changes ultimately also affect the photosaturating light intensity and photosynthetic efficiency at high light intensities (MacIntyre et al., 2002).

Altogether, the photosynthetic efficiency can decrease 2 to 5-fold at high light intensities when compared to low light intensities (**chapter 4 & 6**).

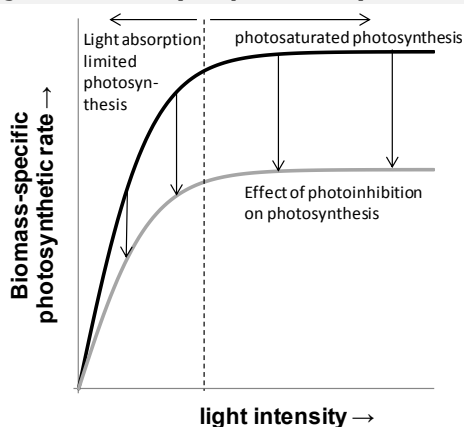


**Fig. 8.4.** Photosynthesis-irradiance response curve that shows the effects of photosaturation and photoinhibition. The curve presented in this figure represents the immediate photosynthetic response and does not include effects of acclimation (e.g. build-up or recovery from photoinhibition or change in pigmentation). The effects of photoacclimation on the photosynthesis-irradiance response curve are for example illustrated by (MacIntyre et al., 2002).

### Increasing the photosynthetic efficiency

By applying the above-mentioned knowledge, the photosynthetic efficiency at high light intensities could be increased by both reactor design or by strain improvement.

#### **Photobioreactor design**

(1) **Light dilution.** Photobioreactor design can reduce the incident light intensity without reducing the total amount of light provided to the photobioreactor, a principle called light dilution (**chapter 7**) (Posten, 2009). This can be done by exploiting reflections and refractions at the reactor surface. Light that falls onto a certain ground area is then redistributed over a larger reactor area. The resulting reduced incident light intensity can be used at a higher photosynthetic efficiency and because the total amount of light that enters the reactor remains unchanged, the areal productivity can be increased (as explained in more detail in **chapter 7**).

(2) **High mixing rates.** Furthermore, high mixing rates can improve the photosynthetic efficiency at high incident light intensities. In photobioreactors with a steep light gradients, microalgae are intermittently exposed to high and low light intensities (light:dark cycles). At low mixing rates, this will result in long light:dark cycles. In the high light intensity zones, the light intensity is saturating and excess light is thermally dissipated, decreasing the overall photosynthetic efficiency in the photobioreactor. Very high mixing rates in the photobioreactor can however result in very short light:dark cycles. When the duration of these light:dark cycles approach the time-scale of photosynthesis (light:dark cycles of more than 10 Hz), the photosynthetic efficiency no longer responds to the local light intensities, but approaches that of the (much lower) average light intensity (as explained in more detail in **chapter 7**). This can result in a

substantial increase in the net photosynthetic efficiency (Posten, 2009; Vejrazka et al., 2013; Vejrazka et al., 2011).

### **Strain improvement**

Strain improvement can help to increase the photosynthetic efficiency at high light intensities in various ways.

(1) Decreasing the pigmentation. Decreasing the pigmentation of microalgae reduces light absorption. This can increase the saturating light intensity, and reduce photosaturation at high light intensities (Huesemann et al., 2009; Melis, 2009; Melis et al., 1999).

(2) Increasing the maximum photosynthetic rate. Increasing the maximum photosynthetic rate could increase the light saturated light intensity and reduce photosaturation at high light intensities (Zhu et al., 2007).

(3) Increasing the pool size of photosynthetic intermediates. Similar to the beneficial effects of high mixing rates, increasing the pool size of photosynthetic intermediates (e.g. electron carriers) might provide a buffer that can temporarily store part of the electrons that are liberated by photosynthesis. These can subsequently be processed in the dark zones of the photobioreactor. This prevents dissipation of light absorbed in excess of the photosynthetic capacity. It therefore allows for a larger proportion of the light that is absorbed in the high-light intensity zones of the photobioreactor to be used for photosynthesis and can improve the net photosynthetic efficiency (Chida et al., 2007).

(4) Improving the photosynthetic efficiency during nitrogen starvation. The photosynthetic efficiency is largely reduced during nitrogen starvation. If microalgae are engineered such that they can retain their photosynthetic efficiency better during nitrogen starvation, this can improve the overall TAG productivity (Klok et al., 2014).

#### **8.3.1.2 Carbon partitioning**

During nitrogen replete conditions, the biochemical composition is rather constant and only minor variations are caused by acclimation to different light intensities (**chapter 6**). This biomass constitutes for the largest part out of proteins, structural carbohydrates (cell wall), starch, and structural lipids (cell, organelle, and thylakoid membranes) (**chapter 6 & 7**). Under these conditions almost no TAG is produced (**chapter 3**). During nitrogen starvation, protein can no longer be produced and the biochemical composition changes drastically. The photosynthetic capacity is then used for the production of secondary metabolites. In *S. obliquus*, approximately 70% of the biomass made during nitrogen starvation consists of the storage components starch and TAG. During initial nitrogen starvation in *S. obliquus*, most of the photosynthetic capacity is partitioned towards starch synthesis. When nitrogen starvation progresses, gradually more carbon is used for TAG synthesis. Finally, the accumulated carbohydrates are in turn degraded and their monomers are likely used as a substrate for TAG synthesis (Fig. 8.3; **chapter 5 & 6**). It is hypothesized that the observed carbon partitioning during



nitrogen starvation in *S. obliquus* is caused by competition between the fatty acid and starch synthesis pathway for a common carbon pre-cursor (**chapter 6**).

Similar responses are observed for other microalgae species. The simultaneous production of carbohydrates and TAG during initial nitrogen starvation (**chapter 3**) (Dillschneider & Posten, 2013; Fernandes et al., 2013; Klok et al., 2013b; Siaux et al., 2011) and the subsequent inter-conversion of carbohydrates to TAG (Li et al., 2011; Msanne et al., 2012; Roessler, 1988; Zhu et al., 2013) has also been observed for numerous other microalgae species. Quantitative differences between microalgae species can however be large. For instance, the carbon partitioning ratio between TAG and other biomass constituents can vary between microalgae species (C in Fig. 8.5). Maximum TAG contents, among the nine species investigated in **chapter 3**, varied from 5 to 40% (% of dry weight), and between 10 to 60% of the newly formed biomass was a result of TAG production. In the best performing species, however, little differences between maximum TAG contents were observed and these were all around 40% of dry weight (**chapter 3**).

In **chapter 5**, it was shown that the carbon partitioning towards TAG can be increased by eliminating the competing starch synthesis pathway in starchless mutants. All photosynthetic capacity that is used for starch synthesis in the wild-type was used for TAG production in the starchless mutant. This increased both the initial TAG production rate as well as the maximum TAG content.

The light intensity and other cultivation conditions such as temperature and pH can also affect carbon partitioning. For *S. obliquus*, the light intensity during nitrogen starvation had a minor effects on carbon partitioning. At high light intensities, slightly more starch is produced at the expense of TAG. The light intensity towards which *S. obliquus* is acclimated has no effect on carbon partitioning (**chapter 4 & 6**).

The pH and temperature had a large effect on both how much biomass can be made during nitrogen starvation, and on carbon partitioning. The maximum biomass concentration was reduced threefold at suboptimal pH and temperatures and 40 to 70% of the newly formed biomass was a result of fatty acid synthesis, among all combinations of pH and temperature tested. The maximum TAG content decreased up to 2-fold at suboptimal pH and temperatures, resulting in a 5-fold lower TAG yield on light (**chapter 4**). The conditions that resulted in the highest TAG contents coincided with the conditions that resulted in the highest photosynthetic efficiencies (**chapter 4**). The pH

and temperature also had a minor effect on the fatty acid composition of TAG (**chapter 4**).

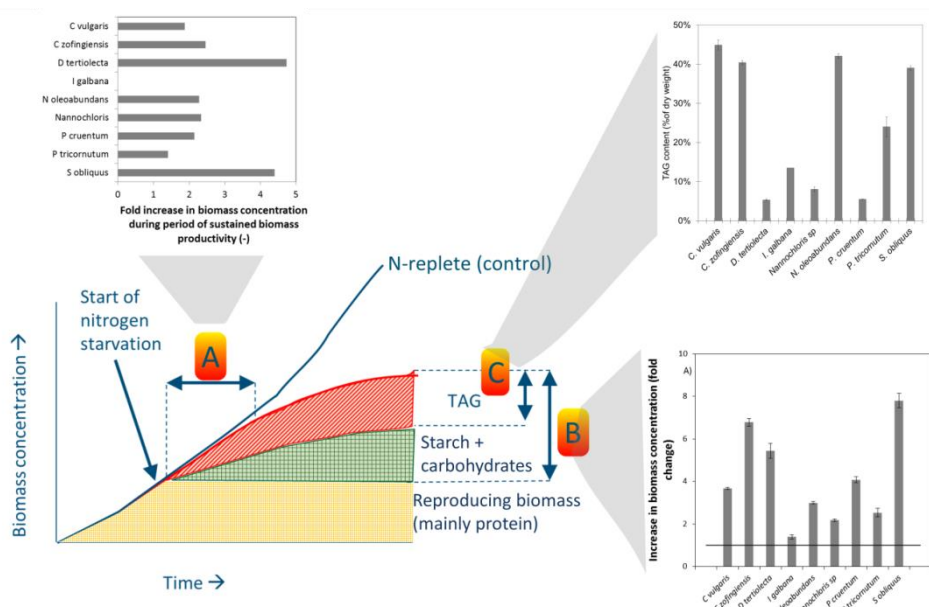


**Fig. 8.5.** Differences between microalgae species. Microalgae are characterized by (A) how long they can retain the same photosynthetic efficiency in the absence of a nitrogen source (fold-increase in dry weight); (B) the total amount of dry weight produced after the depletion in nitrogen (fold-increase in dry weight); and (C) the proportion of this biomass increase that is represented by TAG. Data is obtained from **chapter 3**.

### 8.3.2 Productivity and biochemical composition – Input parameters for TE and LCA studies

As discussed in the previous sections, the photosynthetic efficiency and biochemical composition are highly variable. Choosing the moment of harvesting in a batch cultivation is, together with the selection of the microalgae species, the best tool to control the biomass composition (Fig. 8.3 and Fig. 8.5). For proteins or LC-PUFA, harvesting can best be done before nitrogen depletion or during early nitrogen starvation. For starch or carbohydrate production, harvesting can best be performed during early nitrogen starvation. For high TAG or carotenoids contents in the biomass, best can be harvested at late nitrogen starvation, but to maximize their yields on light, harvesting should occur before nitrogen starvation is completed (Fig. 8.3; Table 8.1). These differences in the harvesting moment also have a large impact on the

photosynthetic efficiency and associated areal productivity, because the photosynthetic efficiency is reduced during nitrogen starvation.

These insights in the photosynthetic and carbon-partitioning response to nitrogen starvation, obtained in the experiments performed in **chapters 3-6** are used to provide realistic combinations for productivities, biochemical compositions, and nutrient consumption that could be used as input in LCA and TE studies (Table 8.3). This is done for six different scenarios in which the production of protein (scenarios 3 and 6), starch (scenario 4), and TAG are considered (scenarios 1, 2, and 5). For TAG production, harvesting at the moment that results in the highest productivity (scenarios 1 and 5) and harvesting at the moment that results in the highest TAG content is considered (scenario 2). Also the production of astaxanthin and EPA as a co-product are considered in scenario 5 and 6, respectively. The productivities and biochemical compositions of scenarios 1, 2, 4, and 5 were obtained using model simulations using the model as described in **chapter 7**, the values for scenario 3 were derived from the experimental data of **chapter 6**, and the values for scenario 6 were extrapolated from scenario 3 using the differences observed between *S. obliquus* and *P. tricornutum* in **chapter 3**, as explained in Supplementary Table 1.

#### Scenarios:

1. Production of TAG using the *slm1* starchless mutant of *S. obliquus* (**chapter 5**). The culture is harvested at the point where it would result in the highest TAG yield on light (and thus highest areal TAG productivity).
2. Production of TAG using the *slm1* starchless mutant of *S. obliquus* (**chapter 5**). The culture is harvested later to maximize the TAG content (% DW), at the expense of a lower TAG yield on light.
3. Protein production using wild-type *S. obliquus*. In this scenario, nitrogen replete cultivation is used to maximize protein production.
4. Starch production using wild-type *S. obliquus*. The culture is harvested at the point where it would result in the highest starch yield on light (and thus highest areal starch productivity).
5. Production of TAG with astaxanthin as a co-product in *C. zofingiensis*. The culture is harvested at the point where it would result in the highest TAG yield on light (and thus highest areal TAG productivity).
6. Production of proteins with EPA as a co-product in *P. tricornutum*. Nitrogen replete cultivation is used to maximize protein production.

For these scenarios, the biomass yield is provided for both a low ( $200 \mu\text{mol m}^{-2} \text{s}^{-1}$ ) and high ( $1500 \mu\text{mol m}^{-2} \text{s}^{-1}$ ) incident light intensity. In a photobioreactor, the incident light intensity is dependent on the time of day, season, and geographic location, but the majority of the light that is annually provided to a certain ground area, is that of a high incident light intensity. The yields calculated for the high light intensities are therefore most representative for the yields that could be achieved under outdoor conditions (*i.e.* the lowest yields in Table 8.3). These low yields that correspond to an incident light intensity of  $1500 \mu\text{mol m}^{-2} \text{s}^{-1}$  should therefore be considered the base-case.

Advanced reactor designs, however, can dilute this high incident light intensity over a larger reactor area to reduce the incident light intensity, without reducing the total amount of light entering the reactor (Box 1; **chapter 7**). Alternatively, microalgae could be engineered such that they can retain their photosynthetic efficiency at high light intensities (Box 1; **chapter 7**). Using these technologies, the biomass yield at high light intensities could approach that what is currently accomplished only at low light intensities. This should thus be considered future technology and corresponds to the yields at an incident light intensity of  $200 \mu\text{mol m}^{-2} \text{s}^{-1}$  (*i.e.* highest yields in Table 8.3).

To enable comparison of these biomass yields with input data commonly used for TE and LCA studies, these biomass yields are extrapolated to areal productivities using an insolation that corresponds to Southern Europe ( $6480 \text{ MJ m}^{-2} \text{ year}^{-1}$ ) and some basic assumptions for nocturnal respiration (10% of the biomass is respired in the night) and reactor downtime (in total 2 months annually), as described in **chapter 4**.

Nitrogen starvation has a major impact on the biomass yield/productivity. This is reflected by the large variation (3 to 4-fold) in biomass productivities between the different scenarios (Table 8.3). Also the incident light intensity has a large impact on the yield/productivity (Table 8.3). For high light intensities (no light dilution; base-case), the productivity is 2 to 4-fold lower than for the low light intensities (light dilution/improved strains; future-case). The reason that the difference in productivity between the low and high incident light intensities is not the same for each scenario is because the reduction in photosynthetic efficiency at high light intensities is dependent on the extent of nitrogen starvation (**chapter 6 & 7**; Table 8.3).

**Table 8.3.** Scenarios for production of commodities using microalgae. Values are derived from experimental data presented in **chapter 3-6** and (Mulders et al., 2014a) and model simulations using the model presented in **chapter 7**, as explained in Supplementary Table 1. For the biomass yield and productivity, ranges are presented. These depend on the incident light intensity. The highest values are derived from the lowest incident light intensities ( $200 \mu\text{mol m}^{-2} \text{s}^{-1}$ ; equivalent to low irradiance conditions or high irradiance conditions combined with future technology) and the lowest values are derived from high incident light intensities ( $1500 \mu\text{mol m}^{-2} \text{s}^{-1}$ ; base case, equivalent to direct sunlight around noon in high irradiance areas using current technology).

	scenario 1 Maximum TAG productivity	scenario 2 Maximum TAG content (% DW)	scenario 3 Protein production	scenario 4 Starch production (maximum productivity)	scenario 5 TAG (maximum productivity) + carotenoid production	scenario 6 Protein + EPA production
Species	<i>S. obliquus</i> <i>slm1</i>	<i>S. obliquus</i> <i>slm1</i>	<i>S. obliquus</i> wt	<i>S. obliquus</i> wt	<i>C. zofingiensis</i>	<i>P. tricornutum</i>
Cultivation mode	batch	batch	continuous or batch	batch	batch	continuous or batch
Harvest strategy	N-starvation	N-starvation	N-replete	Harvest during early N- starvation	N-starvation	N-replete
Biomass yield on light (g/mol)	0.22-0.80	0.15-0.51	0.60-1.20	0.35-1.37	0.21-0.68	0.32-0.60
Areal biomass productivity (g m <sup>-2</sup> day <sup>-1</sup> ) <sup>1</sup>	6-22	4-13	16-31	9-36	5-18	8-16
(co)-products (% DW)	0	0	0	0	0.3 (astaxanthin) <sup>3</sup>	3 (EPA)
Protein (% DW) <sup>4</sup>	15 ± 1	9 ± 0	45 ± 0	14 ± 1	7 ± 0	45 ± 0
Starch (% DW)	0 ± 0	0 ± 0	11 ± 4	37 ± 0	20 ± 2	0 ± 0 <sup>2</sup>
TAG (% DW)	40 ± 1	48 ± 1	0 ± 0	8 ± 1	34 ± 2	2 ± 0
Residual biomass <sup>5</sup> (% DW)	46 ± 1	44 ± 1	45 ± 4	42 ± 1	39 ± 0	53 ± 0
Nutrient usage (mg N/g DW)	29 ± 2	19 ± 1	90 ± 0	27 ± 2	13 ± 0	90 ± 0

<sup>1</sup>Using an insolation of  $6480 \text{ MJ m}^{-2} \text{ year}^{-1}$  (corresponding to Southern Europe) and the assumptions as presented in **chapter 4**.

<sup>2</sup>*P. tricornutum* and other diatoms do not produce starch, but produce chrysolaminarin instead.

<sup>3</sup>*C. zofingiensis* was chosen for this scenario because of its potential as a TAG producer. When aiming for maximum carotenoid production, other microalgae species that can accumulate much higher carotenoid contents, such as *D. salina* or *H. pluvialis* might be preferred.

<sup>4</sup>Estimated using a protein/N ratio of 5 (**chapter 7**).

<sup>5</sup>Residual biomass includes both residual biomass that is made under nitrogen replete conditions (non-protein biomass, including membranes, DNA, RNA, cell wall, etc) and residual biomass that is made during nitrogen starvation.

For the base-case scenarios (at high light intensities, representing no light dilution), the highest biomass productivity is for the protein production scenario using nitrogen replete conditions ( $16 \text{ g m}^{-2} \text{ day}^{-1}$ ; Table 8.3). For the TAG production scenarios this decreases to 4-6 g biomass m<sup>-2</sup> day<sup>-1</sup> at a TAG content of 34-48% of dry weight (Table 8.3). For future-case scenarios (at low light intensities), the highest biomass productivities are predicted for the protein and starch production scenarios ( $31\text{-}36 \text{ g m}^{-2} \text{ day}^{-1}$ ). With

regard to TAG production, future technology can increase the biomass productivity to 22 g m<sup>-2</sup> day<sup>-1</sup> at a TAG content of 40% of DW (scenario 1).

Scenarios 5 and 6 aim for commodity production (TAG and protein, respectively) with co-production of high-value components (astaxanthin and EPA, respectively). These scenarios therefore only aimed for maximal production of TAG and protein. For economical optimization (assuming the current market), optimization of maximal astaxanthin or EPA production might be favourable. It should, however, be taken into account that if microalgae are used for the production of commodities with co-production of high-value components in the ratio as presented in Table 8.3, the market for these high-value components will quickly be saturated, resulting in a decrease in their market value. Nevertheless, when aimed for maximal carotenoid production, much higher productivities could be achieved if chosen for a different species, such as *D. salina* or *H. pluvialis*. For EPA production, nitrogen replete cultivation, as is used for the current scenario, will also result in the highest EPA productivity. For example, in **chapter 3**, a twofold higher EPA productivity was found under nitrogen replete conditions than under nitrogen-depleted conditions.

These productivities are calculated using the assumption that the yields obtained under lab-scale conditions are similar to the yields that can be achieved under outdoor conditions, at the same light intensity, but with some penalties for nocturnal respiration (10% loss due to nocturnal respiration) and reactor downtime (2 months annually). The validity of this assumption is difficult to assess with current information due to large uncertainties (Box 2). Outdoor systems (for research purposes) that aim to achieve high productivities are scarce and mostly focus on the production of total biomass. As reviewed by (Slegers, 2014), biomass productivities in these systems range from 2.8 to 25.9 g m<sup>-2</sup> day<sup>-1</sup>, with an average productivity among these systems of 10.9 g m<sup>-2</sup> day<sup>-1</sup>. Experiences with nitrogen starvation in outdoor systems that aim for oil production are even more scarce, but range from 1.7-6.5 g total lipids m<sup>-2</sup> day<sup>-1</sup> (Bondioli et al., 2012) or from 1.7-3.2 g fatty-acyl lipids m<sup>-2</sup> day<sup>-1</sup> (Quinn et al., 2012). The productivities of these systems are consistent with the high light intensity scenarios of Table 8.3.

**Box 2.** From lab-scale to large-scale.

#### **Uncertainties introduced by outdoor cultivation**

Uncertainties in how lab-scale and outdoor cultivation correlate originate for a large part from limited understanding of the microalgal behaviour during day/night cycles. Day/night cycles not only cause oscillations in light intensity, but also in temperature, solar inclination, and light spectrum. Furthermore, these oscillations can vary largely

from day-to-day, or even from hour-to-hour, and are seasonally dependent. The time-scale of these different oscillations in environmental conditions varies and the effects of these environmental conditions are strongly interconnected. This complicates interpretation of their contribution. The net result of oscillations in these environmental conditions is complex and difficult to predict. This section aims to provide insights in the effects of and correlations between the most important environmental conditions that affect microalgal growth.

The photosynthetic efficiency is largely dependent on the light intensity and will therefore vary during the day. How the photosynthetic efficiency changes with light intensity is, however, also dependent on numerous other environmental conditions. For example, the temperature also affects the photosynthetic response to the light intensity (Bernard & Remond, 2012; Quinn et al., 2011a). The temperature can negatively affect the efficiency of the photosystems directly, but the temperature can also affect the catalytic capacity of Rubisco, which is often assumed to be the rate limiting step in carbon fixation. Because Rubisco activity is also dependent on the CO<sub>2</sub> concentration, the concentration of CO<sub>2</sub> in the cultivation medium can therefore affect how the temperature affects the photosynthetic response to the light intensity, especially near limiting CO<sub>2</sub> concentrations (Sage & Kubien, 2007). Oscillations in temperature can therefore cause non-trivial behaviour. Although oscillations in solar light intensity and environmental temperature are given, oscillations in light gradients and temperatures in the photobioreactor are highly dependent on photobioreactor design. For a given photobioreactor this can easily be taken into account, but this complicates projecting the outdoor performance of microalgae.

Microalgae synchronize their cell cycle to day/night cycles (de Winter et al., 2013). Oscillations in cell physiology as a result of their cell-cycle might add to this non-trivial behaviour. It has for example been observed by (de Winter et al., 2013; de Winter et al., 2014) that in a cell-cycle synchronized culture of *Neochloris oleoabundans*, at a constant light intensity, the biomass yield varies almost 2.5-fold during the cell-cycle, suggesting large oscillations in the photosynthetic efficiency. Only minor oscillations in biochemical composition occurred during these day/night cycles (de Winter et al., 2013; de Winter et al., 2014).

During the night, parts of the biomass are respired to fulfil energy requirements. This reduces the productivity and can result in larger oscillations in biochemical composition than observed during the cell-cycle under continuous illumination (Lacour et al., 2012). These energy requirements are highly dependent on metabolic activity and temperature. The contribution of this nocturnal respiration might therefore be very different from respiration estimated in lab-scale experiments. Furthermore, cellular respiration could be strongly affected by nitrogen starvation.

### **Bridging the gap**

To investigate how the performance of lab-scale and outdoor cultivation correlate, more experiences with outdoor cultivation are required. Here, it is important that not simply the productivity is quantified, but that changes in biochemical composition, photosynthetic efficiency, physiology, and process and illumination conditions are characterized in detail. This should be done for both day/night cycles and for day-to-day

variations. Especially for outdoor processes, it is essential that day-to-day variation in the process performance, as a result of variations in illumination and environmental conditions, is thoroughly investigated. Studies that quantify the biomass productivity during a short period of time might be able to estimate microalgal productivities that can be accomplished for long-term outdoor production. These studies are, however, not suitable to correlate the behaviour of microalgae under lab-scale to outdoor conditions. Models are an invaluable tool to compare outdoor performance with lab-scale performance. Models can account for these oscillations and day-to-day variations that are observed under outdoor cultivation. To do so, models can be validated using lab-scale data and subsequently used to simulate the measured oscillations in temperature and light intensity in the outdoor cultivation. These simulations can then be compared to the actual outdoor-performance to find discrepancies that could be a clue for different behaviour under outdoor conditions and lab-scale conditions. Attempts to gain insight on this topic are currently in progress (Acien et al., 2012; Bosma et al., 2014), and substantial advances can be expected on this topic in the coming years.

### Scaling up

Further uncertainties are introduced by up-scaling. Robustness of microalgae is an important characteristic that needs to be investigated. Microalgae with a wide and high temperature optimum close to the equilibrium temperature of the culture broth are desired to minimize losses in productivity or energy requirements for temperature control. The response to temporal deviations from these optima, for example at hot days or parts of the day, needs to be investigated. This robustness also includes the risk of contaminants or grazers. In a nitrogen-starved batch process, the risk of algae contaminants is minimal because the absence of nutrients inhibits multiplication of contaminants that enter the culture. Grazers on the other hand can be a large risk as they can destroy complete cultures in several days. Little is known of the likelihood that this will occur, however. But for example, (Richardson et al., 2014) assume a 8-20% biomass loss due to grazers (closed photobioreactor and open pond, respectively).

Maximal TAG yields on light achieved on a lab-scale are close to what realistically can be expected from microalgae. Lab-scale TAG yields as high as 0.3 g/mol can be achieved with wild-type microalgae (**chapter 6**) (Mulders et al., 2014a). The most optimistic theoretical maximum yield is 1.33 g/mol, as calculated using flux balance analysis (**chapter 7**), but achieving these theoretical maximum yields is unrealistic because of inherent losses due to photosaturation, co-product formation, and reductions in photosynthetic efficiency during nitrogen starvation (Box 3). It was calculated in **chapter 7** that by a combination of technological advances, a maximum practical TAG yield on light of 0.45 g/mol can be achieved (Box 3). These high yields are achieved at low light intensities, several fold reductions in this yield occur at high light intensities as a result of photo-saturation (**chapter 4, 6, 7**). This reduces the maximum practical TAG yield to approximately 0.15 g/mol at high light intensities (**chapter 7**). The future-case



scenarios in Table 8.3 are close to this maximum practical TAG yield on light of 0.45 g TAG/mol and improvements that largely exceed these future-case values seem unlikely (Box 3; **chapter 7**).

**Box 3. Maximum practical TAG yield.**

Under lab-scale conditions, the microalgae behaviour can be well predicted and the performance on lab-scale is close to what can be expected from microalgae. Lab scale yields can be as high as 0.3 g/mol (**chapter 6**)(Mulders et al., 2014a). In **chapter 7**, it was calculated that the absolute theoretical maximum TAG yield on light is 1.33 g/mol. This suggests that a 4-fold increase is possible. However, achieving such theoretical maximum yields is unrealistic. This theoretical maximum is based on an optimal metabolism that directs all absorbed light towards TAG at the theoretical maximum photosynthetic efficiency (8 photons/2 electrons). Here it is also assumed that transport and co-factor utilization between different cellular compartments is optimally balanced. In practice, photosynthesis never achieves 100% efficiency. Even at moderately low light intensities this can at best be approximately 80% (**chapter 6 & 7**). If these more conservative assumptions are used, but still assuming that all light is directed towards TAG synthesis, this will reduce the maximum TAG yield to 0.8-1 g/mol (**chapter 7**)(Klok, 2013). Furthermore, nitrogen starvation severely reduces the photosynthetic efficiency. Because retaining the photosynthetic efficiency relies for a part on protein synthesis to repair photo-induced damage (photo-inhibition), it is difficult to avoid a reduction in photosynthetic efficiency under conditions where protein synthesis is impaired (**chapter 7**). Finally, TAG only contributes to a maximum of 50-60% to the biomass DW. Co-product formation is thus inevitable, especially when it is considered that TAG is only made during nitrogen starvation and a preceding biomass formation phase is required (**chapter 7**).

By considering these changes, it was calculated in **chapter 7** that by a combination of low light intensities, starchless mutants, an improved photosynthetic machinery, and when the moment of harvesting is optimized, the maximum practical achievable yield is approximately 0.45 g/mol. This yield thus provides an upper limit on what yield realistically can be expected from microalgal TAG production.

Further improvements might be possible if microalgae can be engineered such that they produce large amounts of TAG under nitrogen replete conditions. In this case, the reduction in photosynthetic efficiency during nitrogen starvation can be circumvented.

### 8.3.3 Consequences for the outcomes of TE and LCA studies

Microalgal productivities commonly assumed in TE and LCA studies typically range from 15-30 g m<sup>-2</sup> day<sup>-1</sup> (Campbell et al., 2011; Davis et al., 2011; Delrue et al., 2012; Lardon et al., 2009; Quinn et al., 2013). Most commonly 30 g m<sup>-2</sup> day<sup>-1</sup> is used for photobioreactors and 15 g m<sup>-2</sup> day<sup>-1</sup> is used for open ponds. TAG or oil contents assumed in these TE and LCA studies typically range from 25-50%, but most commonly 50% is used. The corresponding TAG productivity is thus 3 to 6-fold higher in most TE and LCA studies, than what is found for the base-case TAG production scenarios in Table

8.3, where biomass productivities of 4-6 g biomass m<sup>-2</sup> day<sup>-1</sup> at a TAG content of 34-48% of dry weight are projected. Even when advanced photobioreactor designs are used that can efficiently and homogeneously dilute the incident light, or when engineered microalgae are used that can achieve high photosynthetic efficiencies at high light intensities (Box 1), the TAG productivity is still only 60% of what is commonly assumed as the base-case for most LCA and TE studies (low light intensity scenario 1 in Table 8.3).

This lower areal productivity has a major impact on the outcomes of these TE and LCA studies. Photobioreactor construction and operation is a major contributor to costs and energy consumption in the total production process (Table 8.2). When it is assumed that roughly 50% of all costs and energy are consumed in the cultivation step, that photobioreactor construction and operation costs as well as energy use scale linearly to occupied land area (€/m<sup>2</sup>, and MJ/m<sup>2</sup>), and that the costs of harvesting and downstream processing are proportional to the total amount of biomass processed (€/kg DW and MJ/kg DW), a 3 to 6 fold overestimation of the areal productivity will result in a 2 to 3.5-fold underestimation of the cost-price and specific energy consumption (MJ/kg product).

The motivation for considering microalgae as a substitute for crops to produce commodities is the much lower (arable) land use of microalgae. The conservative base-case TAG productivities from scenarios 1, 2, and 5 range from 1.7 to 2.4 g TAG m<sup>-2</sup> day<sup>-1</sup> and optimistic future-case TAG productivities range up to 8.8 g TAG m<sup>-2</sup> day<sup>-1</sup>. This is much higher than TAG productivities of commonly used terrestrial oil crops that range from 0.1-1.4 g m<sup>-2</sup> day<sup>-1</sup> (**chapter 7**). When the values from Table 8.3 are used, land use for microalgal products will increase compared to current estimates (Campbell et al., 2011; Davis et al., 2011; Delrue et al., 2012; Lardon et al., 2009; Quinn et al., 2013), but is still several folds lower than that for agricultural crops.

#### **8.4 Concluding remarks**

Most techno-economic (TE) and life cycle analysis (LCA) studies that evaluate microalgae production use biodiesel production as their case-study and conclude that the cost-price is currently several folds higher than that of vegetable oil derived biodiesel. Net energy ratios are mostly unfavourable or near unity. Substantial improvements in cost-price and specific energy consumption are thus needed to commercialize commodity products from microalgae. The cultivation step introduces the largest uncertainty in these studies and often arbitrary values are used for microalgal

performance. Therefore values are presented that can be used as more reasonable input values for these TE and LCA studies. Base-case productivities that were found are 3 to 6-fold lower than the productivities commonly used in LCA and TE studies.

Approximately half of the costs and energy consumption in the process are consumed in the cultivation process. When the outcomes of existing TE and LCA studies are re-considered using these new base-case productivities, the cost-price of TAG and specific energy consumption increases 2 to 3.5-fold. When the highest yields that can be accomplished under optimized lab-scale conditions are reproduced in outdoor cultivation, productivities near what is currently assumed in TE and LCA studies seem feasible.

Improvements that can be made in microalgal productivity can thus help to decrease the cost-price, but are still insufficient to realize the reduction in cost-price that is required to commercialize commodity products. Additional advances in photobioreactor design are needed to reduce costs and energy use. Also, downstream processing unit operations specifically designed to treat algal biomass (e.g. flocculation/sedimentation of microalgae, wet-extraction of oil, fractionation of biomass constituents) can reduce costs and energy consumption in the downstream process. Further improvements are possible when co-products are valorised (most TE and LCA studies only consider the production of biodiesel), photobioreactors are operated at higher biomass densities to reduce energy consumption and costs for harvesting (most TE and LCA studies assume biomass densities between 0.5-5 g/l, but on a lab-scale, much higher biomass densities of 10-15 g/l could easily be achieved; **chapter 3, 5, 6**), or when nitrogen starvation is used to reduce nutrient requirements (commonly, nutrient consumption corresponding to nutrient replete cultivation is considered, but a 5 to 10-fold reduction in nutrient consumption can be accomplished when nitrogen starvation is used).

Future research should therefore not only focus at improving lab-scale microalgae performance, but also on reproducing lab-scale performance under outdoor conditions, reducing photobioreactor costs and energy footprint, and obtaining microalgae that can have a high photosynthetic efficiency at high light intensities, during nitrogen starvation, and at high temperatures.

Scenario	Explanation of scenarios and assumptions
1	Results derived from the model presented in <b>chapter 7</b> , simulated using incident light intensities of 200 and 1500 $\mu\text{mol m}^{-2} \text{s}^{-1}$ and an amount of nitrogen consistent with the validation experiments of that chapter (10 mM, resulting in depletion of nitrogen at a biomass concentration of 1.5 g/l). Yields, and biomass compositions are consistent with values found under experimental conditions ( <b>chapter 3, 4, 5, and 6</b> ). The values for the biomass yield and biochemical composition at the time-point where the time-averaged TAG yield on light was maximal were used.
2	Similar to scenario 1, with the exception that the values for the biomass yield and biochemical composition at the time-point where the TAG content reached approximately 90-95% of the maximal value were used.
3	Biomass compositions and yields from <b>chapter 6</b> were used, from the experiments that were performed at 200 and 1500 $\mu\text{mol m}^{-2} \text{s}^{-1}$ . These data were obtained in a light limited, nitrogen replete, chemostat cultivation at a biomass density of 1.5 g/l.
4	Similar to scenario 1, with the exception that the values for the biomass yield and biochemical composition at the time-point where the time-averaged starch yield on light was maximal were used.
5	It is assumed that <i>Chlorella zofingiensis</i> can achieve similar performance as the wild-type <i>S. obliquus</i> , as observed in <b>chapter 3</b> and (Mulders et al., 2014a). Results were derived from the model presented in <b>chapter 7</b> , simulated using incident light intensities of 200 and 1500 $\mu\text{mol m}^{-2} \text{s}^{-1}$ and an amount of nitrogen consistent with the validation experiments. Yields, and biomass compositions are consistent with values found under experimental conditions ( <b>chapter 3</b> ) (Mulders et al., 2014a). The values for the biomass yield and biochemical composition at the time-point where the time-averaged TAG yield on light was maximal were used. An astaxanthin content of 3 mg/g was used, that is consist with the astaxanthin content when also the TAG content is high (Mulders et al., 2014a).
6	Extrapolation of scenario 3, using differences observed between <i>S. obliquus</i> and <i>P. tricornutum</i> in experimental data from <b>chapter 3</b> . In this case, <i>P. tricornutum</i> produced half of the biomass compared to <i>S. obliquus</i> under identical conditions (50% lower photosynthetic efficiency). EPA content is assumed to be similar as found in <b>chapter 3</b> .

**Supplementary table 1.** Assumptions made in the scenarios for production of microalgae-derived commodities.





# References

- Acíén, F.G., Fernández, J.M., Magán, J.J., Molina, E. 2012. Production cost of a real microalgae production plant and strategies to reduce it. *Biotechnology Advances*, **30**(6), 1344-1353.
- Aguirre, A.-M., Bassi, A. 2013. Investigation of biomass concentration, lipid production, and cellulose content in *Chlorella vulgaris* cultures using response surface methodology. *Biotechnology and Bioengineering*, **110**(8), 2114-2122.
- Apt, K.E., Behrens, P.W. 1999. Commercial developments in microalgal biotechnology. *Journal of Phycology*, **35**(2), 215-226.
- Asada, K. 2006. Production and Scavenging of Reactive Oxygen Species in Chloroplasts and Their Functions. *Plant Physiology*, **141**(2), 391-396.
- Bar, E., Rise, M., Vishkautsan, M., Arad, S. 1995. Pigment and Structural Changes in *Chlorella zofingiensis* upon Light and Nitrogen Stress. *Journal of Plant Physiology*, **146**(4), 527-534.
- Baroli, I., Melis, A. 1996. Photoinhibition and repair in *Dunaliella salina* acclimated to different growth irradiances. *Planta*, **198**(4), 640-646.
- Batan, L., Quinn, J., Willson, B., Bradley, T. 2010. Net Energy and Greenhouse Gas Emission Evaluation of Biodiesel Derived from Microalgae. *Environmental science & technology*, **44**(20), 7975-7980.
- Becker, E.W. 2007. Micro-algae as a source of protein. *Biotechnology Advances*, **25**(2), 207-210.
- Ben-Amotz, A., Tornabene, T.G., Thomas, W.H. 1985. Chemical profile of selected species of microalgae with emphasis on lipids. *Journal of Phycology*, **21**(1), 72-81.
- Benemann, J.R., Tillett, D.M., Weissman, J.C. 1987. Microalgae biotechnology. *Trends in Biotechnology*, **5**(2), 47-53.
- Berges, J.A., Charlebois, D.O., Mauzerall, D.C., Falkowski, P.G. 1996. Differential Effects of Nitrogen Limitation on Photosynthetic Efficiency of Photosystems I and II in Microalgae. *Plant Physiology*, **110**(2), 689-696.
- Bernard, O. 2011. Hurdles and challenges for modelling and control of microalgae for CO<sub>2</sub> mitigation and biofuel production. *Journal of Process Control*, **21**(10), 1378-1389.
- Bernard, O., Remond, B. 2012. Validation of a simple model accounting for light and temperature effect on microalgal growth. *Bioresour Technol*, **123**, 520-7.



- Blaby, I.K., Glaesener, A.G., Mettler, T., Fitz-Gibbon, S.T., Gallaher, S.D., Liu, B., Boyle, N.R., Kropat, J., Stitt, M., Johnson, S., Benning, C., Pellegrini, M., Casero, D., Merchant, S.S. 2013. Systems-Level Analysis of Nitrogen Starvation-Induced Modifications of Carbon Metabolism in a *Chlamydomonas reinhardtii* Starchless Mutant. *The Plant Cell Online*.
- Bligh, E.G., Dyer, W.J. 1959. A rapid method of total lipid extraction and purification. *Canadian Journal of Biochemistry and Physiology*, **37**(8), 911-917.
- Bondioli, P., Della Bella, L., Rivolta, G., Chini Zittelli, G., Bassi, N., Rodolfi, L., Casini, D., Prussi, M., Chiaramonti, D., Tredici, M.R. 2012. Oil production by the marine microalgae *Nannochloropsis* sp. F&M-M24 and *Tetraselmis suecica* F&M-M33. *Bioresource Technology*, **114**, 567-572.
- Bosma, R., de Vree, J.H., Slegers, P.M., Janssen, M., Wijffels, R.H., Barbosa, M.J. 2014. Design and construction of the microalgal pilot facility AlgaePARC. *Algal Research*(0).
- Boyle, N.R., Morgan, J.A. 2009. Flux balance analysis of primary metabolism in *Chlamydomonas reinhardtii*. *Bmc Systems Biology*, **3**.
- Boyle, N.R., Page, M.D., Liu, B., Blaby, I.K., Casero, D., Kropat, J., Cokus, S.J., Hong-Hermesdorf, A., Shaw, J., Karpowicz, S.J., Gallaher, S.D., Johnson, S., Benning, C., Pellegrini, M., Grossman, A., Merchant, S.S. 2012. Three Acyltransferases and Nitrogen-responsive Regulator Are Implicated in Nitrogen Starvation-induced Triacylglycerol Accumulation in *Chlamydomonas*. *Journal of Biological Chemistry*, **287**(19), 15811-15825.
- Brentner, L.B., Eckelman, M.J., Zimmerman, J.B. 2011. Combinatorial life cycle assessment to inform process design of industrial production of algal biodiesel. *Environmental science & technology*, **45**(16), 7060-7.
- Breuer, G., de Jaeger, L., Artus, V., Martens, D.E., Springer, J., Draaisma, R.B., Eggink, G., Wijffels, R.H., Lamers, P.P. 2014. Superior triacylglycerol (TAG) accumulation in starchless mutants of *Scenedesmus obliquus*: (II) evaluation of TAG yield and productivity in controlled photobioreactors. *Biotechnology for Biofuels* **7**(70), 70.
- Breuer, G., Evers, W.A.C., de Vree, J.H., Kleinegris, D.M.M., Martens, D.E., Wijffels, R.H., Lamers, P.P. 2013a. Analysis of Fatty Acid Content and Composition in Microalgae. *J Vis Exp*, **80**, e50628.
- Breuer, G., Lamers, P.P., Martens, D.E., Draaisma, R.B., Wijffels, R.H. 2013b. Effect of light intensity, pH, and temperature on triacylglycerol (TAG) accumulation

- induced by nitrogen starvation in *Scenedesmus obliquus*. *Bioresource Technology*, **143**(0), 1-9.
- Breuer, G., Lamers, P.P., Martens, D.E., Draaisma, R.B., Wijffels, R.H. 2012. The impact of nitrogen starvation on the dynamics of triacylglycerol accumulation in nine microalgae strains. *Bioresource Technology*, **124**(0), 217-226.
- Burczyk, J., Grzybek, H., Banaś, J., Banaś, E. 1970. Presence of cellulase in the algae *Scenedesmus*. *Experimental Cell Research*, **63**(2-3), 451-453.
- Camacho Rubio, F., Sánchez Mirón, A., Cerón García, M.C., García Camacho, F., Molina Grima, E., Chisti, Y. 2004. Mixing in bubble columns: a new approach for characterizing dispersion coefficients. *Chemical Engineering Science*, **59**(20), 4369-4376.
- Campbell, P.K., Beer, T., Batten, D. 2011. Life cycle assessment of biodiesel production from microalgae in ponds. *Bioresource Technology*, **102**(1), 50-56.
- Caspar, T., Huber, S.C., Somerville, C. 1985. Alterations in Growth, Photosynthesis, and Respiration in a Starchless Mutant of *Arabidopsis thaliana* (L.) Deficient in Chloroplast Phosphoglucomutase Activity. *Plant Physiology*, **79**(1), 11-17.
- Chen, W., Zhang, C., Song, L., Sommerfeld, M., Hu, Q. 2009. A high throughput Nile red method for quantitative measurement of neutral lipids in microalgae. *Journal of Microbiological Methods*, **77**(1), 41-47.
- Chida, H., Nakazawa, A., Akazaki, H., Hirano, T., Suruga, K., Ogawa, M., Satoh, T., Kadokura, K., Yamada, S., Hakamata, W., Isobe, K., Ito, T.-i., Ishii, R., Nishio, T., Sonoike, K., Oku, T. 2007. Expression of the Algal Cytochrome c6 Gene in *Arabidopsis* Enhances Photosynthesis and Growth. *Plant and Cell Physiology*, **48**(7), 948-957.
- Chisti, Y. 2007. Biodiesel from microalgae. *Biotechnology Advances*, **25**(3), 294-306.
- Chisti, Y. 2013. Constraints to commercialization of algal fuels. *Journal of Biotechnology*, **167**(3), 201-214.
- Clarens, A.F., Resurreccion, E.P., White, M.A., Colosi, L.M. 2010. Environmental Life Cycle Comparison of Algae to Other Bioenergy Feedstocks. *Environmental science & technology*, **44**(5), 1813-1819.
- Cooper, M.S., Hardin, W.R., Petersen, T.W., Cattolico, R.A. 2010. Visualizing "green oil" in live algal cells. *Journal of Bioscience and Bioengineering*, **109**(2), 198-201.
- Cuaresma, M., Janssen, M., Vílchez, C., Wijffels, R.H. 2011. Horizontal or vertical photobioreactors? How to improve microalgae photosynthetic efficiency. *Bioresource Technology*, **102**(8), 5129-5137.

- da Silva, A.F., Lourenço, S.O., Chaloub, R.M. 2009. Effects of nitrogen starvation on the photosynthetic physiology of a tropical marine microalga *Rhodomonas* sp. (Cryptophyceae). *Aquatic Botany*, **91**(4), 291-297.
- Davis, R., Aden, A., Pienkos, P.T. 2011. Techno-economic analysis of autotrophic microalgae for fuel production. *Applied Energy*, **88**(10), 3524-3531.
- de Jaeger, L., Verbeek, R., Springer, J., Eggink, G., Wijffels, R.H. 2014. Superior triacylglycerol (TAG) accumulation in starchless mutants of *Scenedesmus obliquus*: (I) mutant generation and characterisation. *Biotechnology for Biofuels*, **7**(69), 69.
- de Mooij, T., Janssen, M., Cerezo-Chinarro, O., Mussgnug, J., Kruse, O., Ballottari, M., Bassi, R., Bujaldon, S., Wollman, F.-A., Wijffels, R. 2014. Antenna size reduction as a strategy to increase biomass productivity: a great potential not yet realized. *Journal of Applied Phycology*, 1-15.
- de Winter, L., Klok, A.J., Cuaresma Franco, M., Barbosa, M.J., Wijffels, R.H. 2013. The synchronized cell cycle of *Neochloris oleoabundans* and its influence on biomass composition under constant light conditions. *Algal Research*, **2**(4), 313-320.
- de Winter, L., Schepers, L.W., Cuaresma, M., Barbosa, M.J., Martens, D.E., Wijffels, R.H. 2014. Circadian rhythms in the cell cycle and biomass composition of *Neochloris oleoabundans* under nitrogen limitation. *Journal of Biotechnology*, **187**(0), 25-33.
- Delrue, F., Setier, P.A., Sahut, C., Cournac, L., Roubaud, A., Peltier, G., Froment, A.K. 2012. An economic, sustainability, and energetic model of biodiesel production from microalgae. *Bioresource Technology*, **111**(0), 191-200.
- Dillschneider, R., Posten, C. 2013. A Linear Programming Approach for Modeling and Simulation of Growth and Lipid Accumulation of *Phaeodactylum tricornutum*. *Energies*, **6**(10), 5333-5356.
- Dong, H.-P., Williams, E., Wang, D.-z., Xie, Z.-X., Hsia, R.-c., Jenck, A., Halden, R., Li, J., Chen, F., Place, A.R. 2013. Responses of *Nannochloropsis oceanica* IMET1 to Long-Term Nitrogen Starvation and Recovery. *Plant Physiology*, **162**(2), 1110-1126.
- Draaisma, R.B., Wijffels, R.H., Slegers, P.M., Brentner, L.B., Roy, A., Barbosa, M.J. 2013. Food commodities from microalgae. *Current opinion in biotechnology*, **24**(2), 169-177.
- Droop, M.R. 1968. Vitamin B12 and Marine Ecology. IV. The Kinetics of Uptake, Growth and Inhibition in *Monochrysis Lutheri*. *Journal of the Marine Biological Association of the United Kingdom*, **48**(03), 689-733.

- Dunahay, T., Jarvis, E., Dais, S., Roessler, P. 1996. Manipulation of microalgal lipid production using genetic engineering. *Applied Biochemistry and Biotechnology*, **57-58**(1), 223-231.
- Falkowski, P.G., Raven, J.A. 2007. *Aquatic photosynthesis*. Princeton University Press.
- Fan, J., Yan, C., Andre, C., Shanklin, J., Schwender, J., Xu, C. 2012. Oil accumulation is controlled by carbon precursor supply for fatty acid synthesis in *Chlamydomonas reinhardtii*. *Plant and Cell Physiology*, **53**(8), 1380-1390.
- Fernandes, B., Teixeira, J., Dragone, G., Vicente, A.A., Kawano, S., Bišová, K., Přibyl, P., Zachleder, V., Vítová, M. 2013. Relationship between starch and lipid accumulation induced by nutrient depletion and replenishment in the microalga *Parachlorella kessleri*. *Bioresource Technology*, **144**(0), 268-274.
- Folch, J., Lees, M., Sloane Stanley, G.H.S. 1956. A simple method for the isolation and purification of total lipides from animal tissues. *J Biol Chem*, **226**, 497-509.
- Gardner, R., Peters, P., Peyton, B., Cooksey, K.E. 2010. Medium pH and nitrate concentration effects on accumulation of triacylglycerol in two members of the chlorophyta. *Journal of Applied Phycology*, **23**(6), 1005-1016.
- Gardner, R.D., Lohman, E., Gerlach, R., Cooksey, K.E., Peyton, B.M. 2013. Comparison of CO<sub>2</sub> and bicarbonate as inorganic carbon sources for triacylglycerol and starch accumulation in *Chlamydomonas reinhardtii*. *Biotechnology and Bioengineering*, **110**(1), 87-96.
- Geider, R., Macintyre, Graziano, L., McKay, R.M. 1998a. Responses of the photosynthetic apparatus of *Dunaliella tertiolecta* (Chlorophyceae) to nitrogen and phosphorus limitation. *European Journal of Phycology*, **33**(4), 315-332.
- Geider, R.J., La Roche, J., Greene, R.M., Olaizola, M. 1993. Response of the photosynthetic apparatus of *phaeodactylum tricornutum* (Bacillariophyceae) to nitrate, phosphate, or iron starvation. *Journal of Phycology*, **29**(6), 755-766.
- Geider, R.J., MacIntyre, H.L., Kana, T.M. 1998b. A Dynamic Regulatory Model of Phytoplanktonic Acclimation to Light, Nutrients, and Temperature. *Limnology and Oceanography*, **43**(4), 679-694.
- Godfray, H.C.J., Beddington, J.R., Crute, I.R., Haddad, L., Lawrence, D., Muir, J.F., Pretty, J., Robinson, S., Thomas, S.M., Toulmin, C. 2010. Food Security: The Challenge of Feeding 9 Billion People. *Science*, **327**(5967), 812-818.
- Gouveia, L., Oliveira, A.C. 2008. Microalgae as a raw material for biofuels production. *Journal of Industrial Microbiology & Biotechnology*, **36**(2), 269-274.

- Griffiths, M.J., Harrison, S.T.L. 2009. Lipid productivity as a key characteristic for choosing algal species for biodiesel production. *Journal of Applied Phycology*, **21**(5), 493-507.
- Griffiths, M.J., Hille, R.P., Harrison, S.T.L. 2014. The effect of nitrogen limitation on lipid productivity and cell composition in *Chlorella vulgaris*. *Appl Microbiol Biotechnol*, **98**(5), 2345-2356.
- Griffiths, M.J., Hille, R.P., Harrison, S.T.L. 2011. Lipid productivity, settling potential and fatty acid profile of 11 microalgal species grown under nitrogen replete and limited conditions. *Journal of Applied Phycology*, **24**, 989-1001.
- Griffiths, M.J., Hille, R.P., Harrison, S.T.L. 2010. Selection of Direct Transesterification as the Preferred Method for Assay of Fatty Acid Content of Microalgae. *Lipids*, **45**(11), 1053-1060.
- Grima, E.M., Medina, A.R., Giménez, A.G., Perez, J.A., Camacho, F.G., Sánchez, J.L.G. 1994. Comparison Between Extraction of Lipids and Fatty Acids from microalgal biomass. *JAOCs*, **71**(9), 955-959.
- Guarnieri, M.T., Nag, A., Smolinski, S.L., Darzins, A., Seibert, M., Pienkos, P.T. 2011. Examination of Triacylglycerol Biosynthetic Pathways via De Novo Transcriptomic and Proteomic Analyses in an Unsequenced Microalga. *PLoS one*, **6**(10), e25851.
- Guckert, J.B., Cooksey, K.E. 1990. Triglyceride accumulation and fatty acid profile changes in *Chlorella* (Chlorophyta) during high pH-induced cell cycle inhibition. *Journal of Phycology*, **26**(1), 72-79.
- Guckert, J.B., Cooksey, K.E., Jackson, L.L. 1988. Lipid solvent systems are not equivalent for analysis of lipid classes in the micro eukaryotic green alga. *Journal of Microbiological Methods*, **8**, 139-149.
- Guedes, A.C., Meireles, L.A., Amaro, H.M., Malcata, F.X. 2010. Changes in Lipid Class and Fatty Acid Composition of Cultures of *Pavlova lutheri*, in Response to Light Intensity. *Journal of the American Oil Chemists' Society*, **87**(7), 791-801.
- Guschina, I.A., Harwood, J.L. 2006. Lipids and lipid metabolism in eukaryotic algae. *Progress in Lipid Research*, **45**(2), 160-86.
- Hodaifa, G., Martínez, M.E., Sánchez, S. 2010a. Influence of pH on the culture of *Scenedesmus obliquus* in olive-mill wastewater. *Biotechnology and Bioengineering*, **14**(6), 854-860.
- Hodaifa, G., Martínez, M.E., Sánchez, S. 2010b. Influence of temperature on growth of *Scenedesmus obliquus* in diluted olive mill wastewater as culture medium. *Engineering in Life Sciences*, **10**(3), 257-264.

- Horton, P. 2000. Prospects for crop improvement through the genetic manipulation of photosynthesis: morphological and biochemical aspects of light capture. *Journal of experimental botany*, **51**(suppl 1), 475-485.
- Hu, Q., Sommerfeld, M., Jarvis, E., Ghirardi, M., Posewitz, M., Seibert, M., Darzins, A. 2008. Microalgal triacylglycerols as feedstocks for biofuel production: perspectives and advances. *The Plant Journal*, **54**(4), 621-639.
- Huerlimann, R., de Nys, R., Heimann, K. 2010. Growth, lipid content, productivity, and fatty acid composition of tropical microalgae for scale-up production. *Biotechnology and Bioengineering*, **107**(2), 245-257.
- Huesemann, M.H., Hausmann, T.S., Bartha, R., Aksoy, M., Weissman, J.C., Benemann, J.R. 2009. Biomass Productivities in Wild Type and Pigment Mutant of *Cyclotella* sp. (Diatom). *Applied Biochemistry and Biotechnology*, **157**(3), 507-526.
- Hunter, S.C., Ohlrogge, J.B. 1998. Regulation of Spinach Chloroplast Acetyl-CoA Carboxylase. *Archives of Biochemistry and Biophysics*, **359**(2), 170-178.
- Iverson, S.J., Lang, S.L.C., Cooper, M.H. 2001. Comparison of the bligh and dyer and folch methods for total lipid determination in a broad range of marine tissue. *Lipids*, **36**(11), 1283-1287.
- Jakob, T., Wagner, H., Stehfest, K., Wilhelm, C. 2007. A complete energy balance from photons to new biomass reveals a light- and nutrient-dependent variability in the metabolic costs of carbon assimilation. *Journal of experimental botany*, **58**(8), 2101-12.
- Janssen, M., Janssen, M., de Winter, M., Tramper, J., Mur, L.R., Snel, J., Wijffels, R.H. 2000. Efficiency of light utilization of *Chlamydomonas reinhardtii* under medium-duration light/dark cycles. *Journal of Biotechnology*, **78**(2), 123-137.
- Jassby, A.D., Platt, T. 1976. Mathematical Formulation of the Relationship Between Photosynthesis and Light for Phytoplankton. *Limnology and Oceanography*, **21**(4), 540-547.
- Johnson, X., Alric, J. 2013. Central carbon metabolism and electron transport in *Chlamydomonas reinhardtii*, metabolic constraints for carbon partitioning between oil and starch. *Eukaryotic Cell*, **12**, 776-793.
- Jorquera, O., Kiperstok, A., Sales, E.A., Embiruçu, M., Ghirardi, M.L. 2010. Comparative energy life-cycle analyses of microalgal biomass production in open ponds and photobioreactors. *Bioresource Technology*, **101**(4), 1406-1413.
- Kandilian, R., Pruvost, J., Legrand, J., Pilon, L. 2014. Influence of light absorption rate by *Nannochloropsis oculata* on triglyceride production during nitrogen starvation. *Bioresource Technology*, **163**(0), 308-319.

- Kliphuis, A.M., Klok, A.J., Martens, D.E., Lamers, P.P., Janssen, M., Wijffels, R.H. 2012. Metabolic modeling of *Chlamydomonas reinhardtii*: energy requirements for photoautotrophic growth and maintenance. *Journal of Applied Phycology*, **24**(2), 253-266.
- Klok, A.J. 2013. *Lipid production in microalgae (PhD thesis)*. Wageningen University.
- Klok, A.J., Lamers, P.P., Martens, D.E., Draaisma, R.B., Wijffels, R.H. 2014. Edible oils from microalgae: insights in TAG accumulation. *Trends in Biotechnology*, **32**(10), 521-528.
- Klok, A.J., Martens, D.E., Wijffels, R.H., Lamers, P.P. 2013a. Simultaneous growth and neutral lipid accumulation in microalgae. *Bioresource Technology*, **134**(0), 233-243.
- Klok, A.J., Verbaanderd, J.A., Lamers, P.P., Martens, D.E., Rinzema, A., Wijffels, R.H. 2013b. A model for customising biomass composition in continuous microalgae production. *Bioresource Technology*, **146**, 89-100.
- Kolber, Z., Zehr, J., Falkowski, P. 1988. Effects of Growth Irradiance and Nitrogen Limitation on Photosynthetic Energy Conversion in Photosystem II. *Plant Physiology*, **88**(3), 923-929.
- Krienitz, L., Bock, C. 2012. Present state of the systematics of planktonic coccoid green algae of inland waters. *Hydrobiologia*, **698**(1), 295-326.
- La Russa, M., Bogen, C., Uhmeyer, A., Doebbe, A., Filippone, E., Kruse, O., Mussgnug, J.H. 2012. Functional analysis of three type-2 DGAT homologue genes for triacylglycerol production in the green microalga *Chlamydomonas reinhardtii*. *Journal of Biotechnology*, **162**(1), 13-20.
- Lacour, T., Sciandra, A., Talec, A., Mayzaud, P., Bernard, O. 2012. Diel variations of carbohydrates and neutral lipids in nitrogen-sufficient and nitrogen-starved cyclostat cultures of *Isochrysis* sp. . *Journal of Phycology*, **48**(4), 966-975.
- Lamers, P.P., Janssen, M., De Vos, R.C.H., Bino, R.J., Wijffels, R.H. 2012. Carotenoid and fatty acid metabolism in nitrogen-starved *Dunaliella salina*, a unicellular green microalga. *Journal of Biotechnology*, **162**(1), 21-27.
- Lamers, P.P., Janssen, M., De Vos, R.C.H., Bino, R.J., Wijffels, R.H. 2008. Exploring and exploiting carotenoid accumulation in *Dunaliella salina* for cell-factory applications. *Trends in Biotechnology*, **26**(11), 631-638.
- Lamers, P.P., van de Laak, C.C.W., Kaasenbrood, P.S., Lorier, J., Janssen, M., De Vos, R.C.H., Bino, R.J., Wijffels, R.H. 2010. Carotenoid and fatty acid metabolism in light-stressed *Dunaliella salina*. *Biotechnology and Bioengineering*, **106**(4), 638-648.

- Lardon, L., Hélias, A., Sialve, B., Steyer, J.-P., Bernard, O. 2009. Life-Cycle Assessment of Biodiesel Production from Microalgae. *Environmental science & technology*, **43**(17), 6475-6481.
- Laurens, L.M.L., Dempster, T.A., Jones, H.D.T., Wolfrum, E.J., Van Wychen, S., McAllister, J.S.P., Rencenberger, M., Parchert, K.J., Gloe, L.M. 2012. Algal Biomass Constituent Analysis: Method Uncertainties and Investigation of the Underlying Measuring Chemistries. *Analytical Chemistry*, **84**(4), 1879-1887.
- Lee, E., Pruvost, J., He, X., Munipalli, R., Pilon, L. 2014. Design tool and guidelines for outdoor photobioreactors. *Chemical Engineering Science*, **106**(0), 18-29.
- Lee, J.Y., Yoo, C., Jun, S.Y., Ahn, C.Y., Oh, H.M. 2010. Comparison of several methods for effective lipid extraction from microalgae. *Bioresour Technol*, **101**(1 Supplement), S75-7.
- Lepage, G., Roy, C.C. 1984. Improved recovery of fatty acid through direct transesterification without prior extraction or purification. *Journal of Lipid research*, **25**, 1391-1396.
- Li, J., Han, D., Wang, D., Ning, K., Jia, J., Wei, L., Jing, X., Huang, S., Chen, J., Li, Y., Hu, Q., Xu, J. 2014. Choreography of Transcriptomes and Lipidomes of Nannochloropsis Reveals the Mechanisms of Oil Synthesis in Microalgae. *The Plant Cell Online*.
- Li, Y., Han, D., Hu, G., Dauvillee, D., Sommerfeld, M., Ball, S., Hu, Q. 2010a. Chlamydomonas starchless mutant defective in ADP-glucose pyrophosphorylase hyper-accumulates triacylglycerol. *Metabolic Engineering*, **12**(4), 387-391.
- Li, Y., Han, D., Hu, G., Sommerfeld, M., Hu, Q. 2010b. Inhibition of starch synthesis results in overproduction of lipids in Chlamydomonas reinhardtii. *Biotechnology and Bioengineering*, **107**(2), 258-268.
- Li, Y., Han, D., Sommerfeld, M., Hu, Q. 2011. Photosynthetic carbon partitioning and lipid production in the oleaginous microalga Pseudochlorococcum sp. (Chlorophyceae) under nitrogen-limited conditions. *Bioresource Technology*, **102**(1), 123-129.
- Li, Y., Horsman, M., Wang, B., Wu, N., Lan, C.Q. 2008. Effects of nitrogen sources on cell growth and lipid accumulation of green alga Neochloris oleoabundans. *Applied Microbiology and Biotechnology*, **81**(4), 629-636.
- Liu, J., Yuan, C., Hu, G., Li, F. 2012. Effects of Light Intensity on the Growth and Lipid Accumulation of Microalga Scenedesmus sp. 11-1 Under Nitrogen Limitation. *Applied Biochemistry and Biotechnology*, **166**(8), 2127-2137.



- Lv, J.-M., Cheng, L.-H., Xu, X.-H., Zhang, L., Chen, H.-L. 2010. Enhanced lipid production of *Chlorella vulgaris* by adjustment of cultivation conditions. *Bioresource Technology*, **101**(17), 6797-6804.
- MacIntyre, H.L., Kana, T.M., Anning, T., Geider, R.J. 2002. Photoacclimation of photosynthesis irradiance response curves and photosynthetic pigments in microalgae and cyanobacteria. *Journal of Phycology*, **38**(1), 17-38.
- Mairet, F., Bernard, O., Masci, P., Lacour, T., Sciandra, A. 2011. Modelling neutral lipid production by the microalga *Isochrysis aff. galbana* under nitrogen limitation. *Bioresource Technology*, **102**(1), 142-149.
- Mata, T.M., Martins, A.A., Caetano, N.S. 2010. Microalgae for biodiesel production and other applications: A review. *Renewable and Sustainable Energy Reviews*, **14**(1), 217-232.
- Maxwell, K., Johnson, G.N. 2000. Chlorophyll fluorescence—a practical guide. *Journal of experimental botany*, **51**(345), 659-668.
- Melis, A. 2009. Solar energy conversion efficiencies in photosynthesis: Minimizing the chlorophyll antennae to maximize efficiency. *Plant Science*, **177**(4), 272-280.
- Melis, A., Neidhardt, J., Baroli, I., Benemann, J. 1999. Maximizing Photosynthetic Productivity and Light Utilization in Microalgae by Minimizing the Light-Harvesting Chlorophyll Antenna Size of the Photosystems. in: *BioHydrogen*, Springer US, pp. 41-52.
- Michels, M.H.A., Slegers, P.M., Vermuë, M.H., Wijffels, R.H. 2014. Effect of biomass concentration on the productivity of *Tetraselmis suecica* in a pilot-scale tubular photobioreactor using natural sunlight. *Algal Research*, **4**(0), 12-18.
- Moody, J.W., McGinty, C.M., Quinn, J.C. 2014. Global evaluation of biofuel potential from microalgae. *Proceedings of the National Academy of Sciences*, **111**(23), 8691-8696.
- Msanne, J., Xu, D., Konda, A.R., Casas-Mollano, J.A., Awada, T., Cahoon, E.B., Cerutti, H. 2012. Metabolic and gene expression changes triggered by nitrogen deprivation in the photoautotrophically grown microalgae *Chlamydomonas reinhardtii* and *Coccomyxa* sp. C-169. *Phytochemistry*, **75**(0), 50-59.
- Mulders, K.J.M., Janssen, J.H., Martens, D.E., Wijffels, R.H., Lamers, P.P. 2014a. Effect of biomass concentration on secondary carotenoids and triacylglycerol (TAG) accumulation in nitrogen-depleted *Chlorella zofingiensis*. *Algal Research*, **6**, Part A(0), 8-16.

- Mulders, K.J.M., Lamers, P.P., Martens, D.E., Wijffels, R.H. 2014b. Phototrophic pigment production with microalgae: biological constraints and opportunities. *Journal of Phycology*, **50**(2), 229-242.
- Mulders, K.J.M., Weesepeel, Y., Lamers, P.P., Vincken, J.P., Martens, D.E., Wijffels, R.H. 2013. Growth and pigment accumulation in nutrient-depleted *Isochrysis* aff. *galbana* T-ISO. *J Appl Phycol*, **25**(5), 1421-1430.
- Neidhardt, J., Benemann, J., Zhang, L., Melis, A. 1998. Photosystem-II repair and chloroplast recovery from irradiance stress: relationship between chronic photoinhibition, light-harvesting chlorophyll antenna size and photosynthetic productivity in *Dunaliella salina* (green algae). *Photosynthesis Research*, **56**(2), 175-184.
- Norsker, N.-H., Barbosa, M.J., Vermuë, M.H., Wijffels, R.H. 2011. Microalgal production — A close look at the economics. *Biotechnology Advances*, **29**(1), 24-27.
- Ort, D.R. 2001. When There Is Too Much Light. *Plant Physiology*, **125**(1), 29-32.
- Packer, A., Li, Y., Andersen, T., Hu, Q., Kuang, Y., Sommerfeld, M. 2011. Growth and neutral lipid synthesis in green microalgae: a mathematical model. *Bioresource Technology*, **102**(1), 111-7.
- Pal, D., Khozin-Goldberg, I., Cohen, Z., Boussiba, S. 2011. The effect of light, salinity, and nitrogen availability on lipid production by *Nannochloropsis* sp. *Applied Microbiology and Biotechnology*, **90**(4), 1429-41.
- Passell, H., Dhaliwal, H., Reno, M., Wu, B., Ben Amotz, A., Ivry, E., Gay, M., Czartoski, T., Laurin, L., Ayer, N. 2013. Algae biodiesel life cycle assessment using current commercial data. *Journal of Environmental Management*, **129**(0), 103-111.
- Peterhansel, C., Niessen, M., Kebeish, R.M. 2008. Metabolic Engineering Towards the Enhancement of Photosynthesis†. *Photochemistry and Photobiology*, **84**(6), 1317-1323.
- Popovich, C.A., Damiani, C., Constenla, D., Martinez, A.M., Freije, H., Giovanardi, M., Pancaldi, S., Leonardi, P.I. 2012. *Neochloris oleoabundans* grown in enriched natural seawater for biodiesel feedstock: evaluation of its growth and biochemical composition. *Bioresource Technology*, **114**, 287-93.
- Posten, C. 2009. Design principles of photo-bioreactors for cultivation of microalgae. *Engineering in Life Sciences*, **9**(3), 165-177.
- Prézelin, B.B., Matlick, H.A. 1983. Nutrient-dependent low-light adaptation in the dinoflagellate *Gonyaulax polyedra*. *Marine Biology*, **74**(2), 141-150.

- Pruvost, J., Van Vooren, G., Cogne, G., Legrand, J. 2009. Investigation of biomass and lipids production with *Neochloris oleoabundans* in photobioreactor. *Bioresource Technology*, **100**(23), 5988-5995.
- Pruvost, J., Van Vooren, G., Le Gouic, B., Couzinet-Mossion, A., Legrand, J. 2011. Systematic investigation of biomass and lipid productivity by microalgae in photobioreactors for biodiesel application. *Bioresource Technology*, **102**(1), 150-158.
- Quinn, J., de Winter, L., Bradley, T. 2011a. Microalgae bulk growth model with application to industrial scale systems. *Bioresource Technology*, **102**(8), 5083-92.
- Quinn, J.C., Catton, K., Wagner, N., Bradley, T.H. 2011b. Current Large-Scale US Biofuel Potential from Microalgae Cultivated in Photobioreactors. *BioEnergy Research*, **5**(1), 49-60.
- Quinn, J.C., Smith, T.G., Downes, C.M., Quinn, C. 2013. Microalgae to biofuels lifecycle assessment — Multiple pathway evaluation. *Algal Research*, **4**(0), 116-122.
- Quinn, J.C., Yates, T., Douglas, N., Weyer, K., Butler, J., Bradley, T.H., Lammers, P.J. 2012. Nannochloropsis production metrics in a scalable outdoor photobioreactor for commercial applications. *Bioresour Technol*, **117**, 164-71.
- Radakovits, R., Jinkerson, R.E., Darzins, A., Posewitz, M.C. 2010. Genetic Engineering of Algae for Enhanced Biofuel Production. *Eukaryotic Cell*, **9**(4), 486-501.
- Ral, J.-P., Colleoni, C., Wattebled, F., Dauvillée, D., Nempont, C., Deschamps, P., Li, Z., Morell, M.K., Chibbar, R., Purton, S., d'Hulst, C., Ball, S.G. 2006. Circadian Clock Regulation of Starch Metabolism Establishes GBSSI as a Major Contributor to Amylopectin Synthesis in *Chlamydomonas reinhardtii*. *Plant Physiology*, **142**(1), 305-317.
- Ramazanov, A., Ramazanov, Z. 2006. Isolation and characterization of a starchless mutant of *Chlorella pyrenoidosa* STL-PI with a high growth rate, and high protein and polyunsaturated fatty acid content. *Phycological Research*, **54**(4), 255-259.
- Ratledge, C., Cohen, Z. 2008. Microbial and algal oils: Do they have a future for biodiesel or as commodity oils? *Lipid Technology*, **20**(7), 155-160.
- Renaud, S.M., Thinh, L.-V., Parry, D.L. 1999. The gross chemical composition and fatty acid composition of 18 species of tropical Australian microalgae for possible use in mariculture. *Aquaculture*, **170**(2), 147-159.

- Renaud, S.M., Thinh, L.V., Lambrinidis, G., Parry, D.L. 2002. Effect of temperature on growth, chemical composition and fatty acid composition of tropical Australian microalgae grown in batch cultures. *Aquaculture*, **211**(1-4), 195-214.
- Renaud, S.M., Zhou, H.C., Parry, D.L., Thinh, L.-V., Woo, K.C. 1995. Effect of temperature on the growth, total lipid content and fatty acid composition of recently isolated tropical microalgae *Isochrysis* sp., *Nitzschia closterium*, *Nitzschia paleacea*, and commercial species *Isochrysis* sp. (clone T.ISO). *Journal of Applied Phycology*, **7**(6), 595-602.
- Resurreccion, E.P., Colosi, L.M., White, M.A., Clarens, A.F. 2012. Comparison of algae cultivation methods for bioenergy production using a combined life cycle assessment and life cycle costing approach. *Bioresource Technology*, **126**(0), 298-306.
- Richardson, J.W., Johnson, M.D., Zhang, X., Zemke, P., Chen, W., Hu, Q. 2014. A financial assessment of two alternative cultivation systems and their contributions to algae biofuel economic viability. *Algal Research*, **4**(0), 96-104.
- Rismani-Yazdi, H., Haznedaroglu, B., Hsin, C., Peccia, J. 2012. Transcriptomic analysis of the oleaginous microalga *Neochloris oleoabundans* reveals metabolic insights into triacylglyceride accumulation. *Biotechnology for Biofuels*, **5**(1), 74.
- Rodolfi, L., Chini Zittelli, G., Bassi, N., Padovani, G., Biondi, N., Bonini, G., Tredici, M.R. 2009. Microalgae for oil: Strain selection, induction of lipid synthesis and outdoor mass cultivation in a low-cost photobioreactor. *Biotechnology and Bioengineering*, **102**(1), 100-112.
- Roessler, P.G. 1988. Effects of silicon deficiency on lipid-composition and metabolism in the diatom *cyclotella-cryptica*. *Journal of Phycology*, **24**(3), 394-400.
- Rubio, F.C., Camacho, F.G., Sevilla, J.M.F., Chisti, Y., Grima, E.M. 2003. A mechanistic model of photosynthesis in microalgae. *Biotechnology and Bioengineering*, **81**(4), 459-473.
- Ryckebosch, E., Muylaert, K., Foubert, I. 2011. Optimization of an Analytical Procedure for Extraction of Lipids from Microalgae. *Journal of the American Oil Chemists' Society*, **89**(2), 189-198.
- Sage, R.F., Kubien, D.S. 2007. The temperature response of C3 and C4 photosynthesis. *Plant, Cell & Environment*, **30**(9), 1086-1106.
- Santos, A.M., Janssen, M., Lamers, P.P., Evers, W.A.C., Wijffels, R.H. 2012. Growth of oil accumulating microalga *Neochloris oleoabundans* under alkaline-saline conditions. *Bioresource Technology*, **104**, 593-599.

- Schenk, P.M., Thomas-Hall, S.R., Stephens, E., Marx, U.C., Mussgnug, J.H., Posten, C., Kruse, O., Hankamer, B. 2008. Second Generation Biofuels: High-Efficiency Microalgae for Biodiesel Production. *BioEnergy Research*, **1**(1), 20-43.
- Schwenzfeier, A., Wierenga, P.A., Gruppen, H. 2011. Isolation and characterization of soluble protein from the green microalgae *Tetraselmis* sp. *Bioresource Technology*, **102**(19), 9121-9127.
- Scott, S.A., Davey, M.P., Dennis, J.S., Horst, I., Howe, C.J., Lea-Smith, D.J., Smith, A.G. 2010. Biodiesel from algae: challenges and prospects. *Current opinion in biotechnology*, **21**(3), 277-86.
- Sheehan, J., Dunahay, T., Benemann, J., Roessler, P. 1998. A look back at the us department of energy aquatic species program: biodiesel from algae. National renewable energy lab. NREL/TP-580-24190.
- Siaut, M., Cuiné, S., Cagnon, C., Fessler, B., Nguyen, M., Carrier, P., Beyly, A., Beisson, F., Triantaphylidès, C., Li-Beisson, Y., Peltier, G. 2011. Oil accumulation in the model green alga *Chlamydomonas reinhardtii*: characterization, variability between common laboratory strains and relationship with starch reserves. *BMC Biotechnology*, **11**(1), 7.
- Simionato, D., Block, M.A., La Rocca, N., Jouhet, J., Maréchal, E., Finazzi, G., Morosinotto, T. 2013. The Response of *Nannochloropsis gaditana* to Nitrogen Starvation Includes De Novo Biosynthesis of Triacylglycerols, a Decrease of Chloroplast Galactolipids, and Reorganization of the Photosynthetic Apparatus. *Eukaryotic Cell*, **12**(5), 665-676.
- Simionato, D., Sforza, E., Corteggiani Carpinelli, E., Bertucco, A., Giacometti, G.M., Morosinotto, T. 2011. Acclimation of *Nannochloropsis gaditana* to different illumination regimes: effects on lipids accumulation. *Bioresource Technology*, **102**(10), 6026-32.
- Slegers, P. 2014. *Scenario studies for algae production (PhD thesis)*. Wageningen Universiteit (Wageningen University).
- Slegers, P.M., Koetzier, B.J., Fasaei, F., Wijffels, R.H., van Straten, G., van Boxtel, A.J.B. 2014. A model-based combinatorial optimisation approach for energy-efficient processing of microalgae. *Algal Research*, **5**(0), 140-157.
- Slegers, P.M., Wijffels, R.H., van Straten, G., van Boxtel, A.J.B. 2011. Design scenarios for flat panel photobioreactors. *Applied Energy*, **88**(10), 3342-3353.
- Solovchenko, A.E., Khozin-Goldberg, I., Didi-Cohen, S., Cohen, Z., Merzlyak, M.N. 2007. Effects of light intensity and nitrogen starvation on growth, total fatty acids and

- arachidonic acid in the green microalga *Parietochloris incisa*. *Journal of Applied Phycology*, **20**(3), 245-251.
- Sukenik, A., Bennett, J., Falkowski, P. 1987. Light-saturated photosynthesis — Limitation by electron transport or carbon fixation? *Biochimica et Biophysica Acta (BBA) - Bioenergetics*, **891**(3), 205-215.
- Sukenik, A., Bennett, J., Mortain-Bertrand, A., Falkowski, P.G. 1990. Adaptation of the Photosynthetic Apparatus to Irradiance in *Dunaliella tertiolecta*: A Kinetic Study. *Plant Physiology*, **92**(4), 891-898.
- Takagi, M., Karseno, Yoshida, T. 2006. Effect of salt concentration on intracellular accumulation of lipids and triacylglyceride in marine microalgae *Dunaliella* cells. *Journal of Bioscience and Bioengineering*, **101**(3), 223-226.
- Takagi, M., Watanabe, K., Yamaberi, K., Yoshida, T. 2000. Limited feeding of potassium nitrate for intracellular lipid and triglyceride accumulation of *Nannochloris* sp. UTEX LB1999. *Applied Microbiology and Biotechnology*, **54**(1), 112-117.
- Valenzuela, J., Mazurie, A., Carlson, R., Gerlach, R., Cooksey, K., Peyton, B., Fields, M. 2012. Potential role of multiple carbon fixation pathways during lipid accumulation in *Phaeodactylum tricornutum*. *Biotechnology for Biofuels*, **5**(40), 1-17.
- Van Vooren, G., Le Grand, F., Legrand, J., Cuiné, S., Peltier, G., Pruvost, J. 2012. Investigation of fatty acids accumulation in *Nannochloropsis oculata* for biodiesel application. *Bioresource Technology*, **124**(0), 421-432.
- Vejrazka, C., Janssen, M., Benvenuti, G., Streefland, M., Wijffels, R. 2013. Photosynthetic efficiency and oxygen evolution of *Chlamydomonas reinhardtii* under continuous and flashing light. *Applied Microbiology and Biotechnology*, **97**(4), 1523-1532.
- Vejrazka, C., Janssen, M., Streefland, M., Wijffels, R.H. 2011. Photosynthetic efficiency of *Chlamydomonas reinhardtii* in flashing light. *Biotechnology and Bioengineering*, **108**(12), 2905-2913.
- Waltz, E. 2009. Biotech's green gold? *Nature Biotechnology*, **27**(1), 15-18.
- Wang, Z., Benning, C. 2011. *Arabidopsis thaliana* Polar Glycerolipid Profiling by Thin Layer Chromatography (TLC) Coupled with Gas-Liquid Chromatography (GLC). *J Vis Exp*(49), e2518.
- Wang, Z.T., Ullrich, N., Joo, S., Waffenschmidt, S., Goodenough, U. 2009. Algal Lipid Bodies: Stress Induction, Purification, and Biochemical Characterization in Wild-

Type and Starchless *Chlamydomonas reinhardtii*. *Eukaryotic Cell*, **8**(12), 1856-1868.

Welch, R.W. 1977. A micro-method for the estimation of oil content and composition in seed crops. *Journal of the Science of Food and Agriculture*, **28**(7), 635-638.

Wijffels, R.H., Barbosa, M.J. 2010. An outlook on microalgal biofuels. *Science*, **329**(5993), 796-9.

Wijffels, R.H., Barbosa, M.J., Eppink, M.H.M. 2010. Microalgae for the production of bulk chemicals and biofuels. *Biofuels, Bioproducts and Biorefining*, **4**(3), 287-295.

Xin, L., Hong-ying, H., Yu-ping, Z. 2011. Growth and lipid accumulation properties of a freshwater microalga *Scenedesmus* sp. under different cultivation temperature. *Bioresource Technology*, **102**(3), 3098-3102.

Yamaberi, K., Takagi, M., Yoshida, T. 1998. Nitrogen depletion for intracellular triglyceride accumulation to enhance liquefaction yield of marine microalgal cells into a fuel oil. *Journal of Marine Biotechnology*, **6**(1), 44-48.

Yang, C., Hua, Q., Shimizu, K. 2000. Energetics and carbon metabolism during growth of microalgal cells under photoautotrophic, mixotrophic and cyclic light-autotrophic/dark-heterotrophic conditions. *Biochemical Engineering Journal*, **6**(2), 87-102.

Yang, Z.-K., Niu, Y.-F., Ma, Y.-H., Xue, J., Zhang, M.-H., Yang, W.-D., Liu, J.-S., Lu, S.-H., Guan, Y., Li, H.-Y. 2013. Molecular and cellular mechanisms of neutral lipid accumulation in diatom following nitrogen deprivation. *Biotechnology for Biofuels*, **6**(1), 67.

Zemke, P., Sommerfeld, M., Hu, Q. 2013. Assessment of key biological and engineering design parameters for production of *Chlorella zofingiensis* (Chlorophyceae) in outdoor photobioreactors. *Applied Microbiology and Biotechnology*, **97**(12), 5645-5655.

Zhu, S., Huang, W., Xu, J., Wang, Z., Xu, J., Yuan, Z. 2013. Metabolic changes of starch and lipid triggered by nitrogen starvation in the microalga *Chlorella zofingiensis*. *Bioresource Technology*, **152**(0), 292-298.

Zhu, X.-G., de Sturler, E., Long, S.P. 2007. Optimizing the Distribution of Resources between Enzymes of Carbon Metabolism Can Dramatically Increase Photosynthetic Rate: A Numerical Simulation Using an Evolutionary Algorithm. *Plant Physiology*, **145**(2), 513-526.





# Summary

Global demands for food and biofuels are rapidly increasing as a result of an increasing world population, wealth of developing countries, depleting fossil resources, and concerns for climate change. Their production currently relies mainly on the cultivation of agricultural crops. The availability of arable land, fresh water, and nutrients are major challenges that need to be overcome to supply in these demands. Novel sustainable and renewable sources for both food-commodities and biofuels are therefore highly desired. Microalgal-derived products are often considered as a promising substitute for these commodities.

Cultivation of microalgae has several advantages over the use of traditional agricultural crops. Microalgae can achieve much higher areal productivities, do not require arable land and can potentially even be cultivated off-shore. Current estimates, however, claim that a several fold reduction in cost-price needs to be realized before the production of bulk products using microalgae can become feasible.

Although microalgae could be a source for a large variety of commodities, the work presented in this thesis focusses on the production of triacylglycerol (TAG). These TAGs are similar to vegetable oils and can be used as an edible oil and can be used for the production of biodiesel.

To commercialize TAG production by microalgae, a high TAG productivity is desired to reduce the cost-price. To achieve these high TAG productivities, a quantitative understanding of the physiological processes affecting microalgal TAG production is essential. TAG is a secondary metabolite and during balanced growth conditions, only negligible amounts of TAG are produced. The most commonly used technique to induce TAG accumulation in microalgae is to expose them to nitrogen starvation. Some microalgae species can accumulate up to 50% of their dry weight as TAG under these conditions. Nitrogen starvation does not only induce TAG production, many other cellular processes, including photosynthesis, are affected at the same time.

When generalized, the microalgal TAG productivity is determined by the amount of light absorbed, the efficiency at which this light is used to fixate carbon (photosynthetic efficiency), and the proportion of this carbon that is partitioned towards TAG. The photosynthetic efficiency and carbon partitioning are highly variable in microalgae and a detailed understanding of the physiology behind photosynthesis and carbon partitioning during nitrogen starvation could thus lead to strategies to improve the TAG productivity. The aim of this thesis is therefore to obtain a quantitative understanding of the physiology of TAG production that is induced by nitrogen starvation.

Microalgae produce a large variety of lipid-classes. Only part of these lipids are triacylglycerols or other fatty acyl-lipids (fatty acid containing lipids). **Chapter 2** describes an analytical method to analyse the fatty acid content and composition in microalgae. This analytical procedure is based on a sequence of mechanical cell disruption, solvent based lipid extraction in chloroform:methanol, transesterification of fatty acids to fatty acid methyl esters (FAMES), and identification and quantification of FAMES using gas chromatography (GC-FID). One of the main advantages of this method is the small sample size required for analysis and the possibility to extend the method with a solid phase extraction step to separate TAGs from polar fatty-acyl lipids.

Large differences exist between microalgae species in their response to nitrogen starvation. It is therefore important for large scale TAG production to select an appropriate species. In **chapter 3**, differences and similarities between microalgae species with respect to their response to nitrogen starvation were investigated with the aim to select a promising microalga for TAG production. From a literature survey among 96 microalgae species, nine promising species were selected (*Chlorella vulgaris*, *Chlorella zofingiensis*, *Dunaliella tertiolecta*, *Isochrysis galbana*, *Nannochloris* sp., *Neochloris oleoabundans*, *Porphyridium cruentum*, *Phaeodactylum tricornutum* and *Scenedesmus obliquus*). The biomass productivity and TAG production of these species were investigated in detail during both nitrogen replete and nitrogen depleted conditions. It was found that all of these species continued with photosynthesis and carbon assimilation during nitrogen starvation. Most species were able to maintain an unchanged biomass productivity during initial nitrogen starvation compared to nitrogen replete conditions, and were able to increase several folds in biomass concentration after the depletion of nitrogen. The duration during which these species could retain their high biomass productivity and the total amount of biomass produced after nitrogen was depleted, varied greatly between species (between a 1.4 and 7.8-fold increase in biomass after the depletion of nitrogen). Also, large differences were observed between species in the maximum TAG content, ranging from 5 to 45% of dry weight. It was found that in all species, other components were accumulated simultaneously with TAG. TAG could only account for up to half of the biomass produced during nitrogen starvation.

*S. obliquus* achieved the highest TAG productivity, was able to accumulate large quantities of TAG (more than 35% of dry weight), and retained an unchanged biomass productivity for the longest period of time during nitrogen starvation (after the depletion of nitrogen, a 4.5-fold increase in biomass concentration was achieved before a

reduction in biomass productivity became apparent). *S. obliquus* was therefore chosen as the most suitable species for TAG production and used in all further studies.

**Chapter 4** continues with *S. obliquus*, and describes how the light intensity, pH, and temperature affect the response of *S. obliquus* to nitrogen starvation, and associated TAG production. It was found that TAG could be produced in the ranges pH 5-9, temperature of 20-35°C, and incident light intensity of 200-1500  $\mu\text{mol m}^{-2} \text{s}^{-1}$ . The light intensity did not affect the maximum TAG content. The light intensity did, however, have a major effect on the photosynthetic efficiency. As a result, the TAG yield on light (g TAG/mol photon) was 5-fold lower at high light intensities compared to low light intensities. Suboptimal pH values and temperatures resulted in an up to 5-fold lower TAG yield on light and 2-fold lower maximum TAG content. The optimum conditions found for TAG accumulation coincided with the optimum found for growth. This was at the lowest light intensity, pH 7, and a temperature of 27.5°C. A yield of 0.263 g fatty acids/mol photon was achieved under these conditions. The fatty acid composition of TAG was not affected by the light intensity, but the degree of fatty acid unsaturation increased with decreasing temperature and pH.

In the previous chapters it was found that during nitrogen starvation, only approximately half of the biomass produced during nitrogen starvation is TAG, and that other biomass constituents are thus produced simultaneously. Elimination of competing pathways can potentially improve the TAG productivity. In **chapter 5**, carbon-partitioning was therefore investigated in both the wild-type and the *slm1* starchless mutant of *S. obliquus*. It was found that during initial nitrogen starvation, starch is accumulated to up to 40% of dry weight in wild-type *S. obliquus*. During initial nitrogen starvation, TAG was produced simultaneously with starch, but at a much lower rate. When nitrogen starvation progressed, starch accumulation stopped while TAG accumulation continued. Hereafter, the initially accumulated starch was degraded again and the degradation products were most-likely used as a substrate for TAG synthesis. It was found that the starchless mutant diverted all photosynthetic capacity, that was used for starch synthesis in the wild-type, towards TAG synthesis. This resulted in much higher TAG accumulation rates during initial nitrogen starvation. Furthermore, it was found that the efficiency of photosynthesis was not negatively affected in this starchless mutant. Altogether, the TAG yield on light increased by 51%, from 0.144 to 0.217 g/mol in this *slm1* starchless mutant of *S. obliquus* compared to the wild-type. The maximum TAG content was also enhanced in the starchless mutant from 45 to 57% of dry weight.

These results illustrated that the capacity of the TAG synthesis machinery is not limiting the TAG production rate. This chapter thus showed that elimination of competing pathways is a feasible strategy to increase the TAG productivity, even in the most oleaginous microalgae.

The mechanism behind the simultaneous starch and TAG production was investigated in more detail in **chapter 6**. It was investigated how this carbon partitioning, and the photosynthetic efficiency during nitrogen starvation, are influenced by the light intensity during nitrogen starvation and by the photoacclimated state at the onset of nitrogen starvation. To be able to independently investigate the impact of light intensity during nitrogen starvation and the impact of the photoacclimated state at the onset of nitrogen starvation, a novel experimental setup was developed. In this experimental setup, cultivations were started as nitrogen replete, light limited, chemostat cultivations. This was done at both a low and a high incident light intensity to obtain two differently photoacclimated cultures. As a result of photoacclimation, these differently photoacclimated cultures had large differences in their pigmentation, pigment class composition and composition of their photosystem. Once steady-state conditions were achieved, the chemostat operation was terminated and cultivation was continued as a nitrogen-depleted batch cultivation, at both a low and a high incident light intensity. It was found that the carbon partitioning ratio between starch and fatty acids strongly correlated to the extent of nitrogen starvation, quantified by the biomass nitrogen content. At all times, approximately 70% of the newly produced biomass was accounted for by production of starch and fatty acids. Immediately after nitrogen depletion, the ratio between fatty acid and starch production was 1:4. The ratio progressively increased to 100% fatty acid production when nitrogen starvation progressed. Hereafter, the initially accumulated starch was degraded while fatty acid synthesis continued. The differences in pigmentation and pigment class composition, caused by photoacclimation to different incident light intensities in the nitrogen replete chemostats, persisted during nitrogen starvation. This did however not affect the photosynthetic efficiency or carbon partitioning during nitrogen starvation. The light intensity had a major impact on the photosynthetic efficiency in both the nitrogen replete and deplete cultures. When compared to low light intensities, the photosynthetic efficiency at a high light intensity was reduced almost 2-fold during nitrogen replete conditions and the fatty acid yield on light during nitrogen starvation was reduced threefold. The light intensity during nitrogen starvation had a minor impact on how the fatty acid:starch synthesis ratio progressed during nitrogen starvation. At high light intensities, slightly more

carbon was partitioned towards starch synthesis. Based on these observations, it was proposed that the observed carbon partitioning is caused by competition for a common carbon pre-cursor between the starch and fatty acid synthesis pathway, and not by an overflow-metabolism-like response.

Using the insights from the previous chapters and existing literature, a mechanistic model was developed, in **chapter 7**, that describes TAG production during nitrogen starvation. This model constitutes of a photosynthesis module and a carbon partitioning module. The photosynthesis module describes light absorption, the amount of photons used for photosynthesis and the amount that is thermally dissipated as a function of the light intensity and extent of nitrogen starvation. The carbon partitioning module describes the partitioning of photons, as a function of the extent of nitrogen starvation, over reproducing biomass (made during nitrogen replete conditions), cellular maintenance, starch, TAG, and residual biomass. In addition, it describes the inter-conversion of starch to TAG. To include the differences in energetic requirements for production of these different biomass constituents, this module uses a different yield (g/mol or g/g) for each individual biomass constituent. These yields were calculated from the stoichiometry of the metabolic network using flux balance analysis. Between different biomass constituents, these yields varied up to threefold, illustrating the importance of using a yield specific for each biomass constituent rather than an average yield for photosynthesis. The model was validated using the experimental data from both the wild-type and starchless mutant of *S. obliquus* from chapter 5, and described the experimental data very well.

Subsequently, this model was used to investigate how TAG production could be improved by advances in reactor design and strain improvement. It was concluded that the incident light intensity is the most important factor determining the TAG yield on light. It was illustrated how advances in reactor design, using light dilution techniques, can improve the productivity 3-fold (from 2.1 to 6.3 g m<sup>-2</sup> day<sup>-1</sup>). Engineering of the photosystem could improve productivity by 50-75% at high light intensities (from 2.1 to 3.7 g m<sup>-2</sup> day<sup>-1</sup>). Starchless mutants can improve the productivity by 50% and further advances seem possible if other competing pathways are reduced. In areas with an insolation corresponding to Southern Europe, combinations of the aforementioned technologies could improve the productivity to up to 10.9 g TAG m<sup>-2</sup> day<sup>-1</sup> and productivities up to 8.8 g TAG m<sup>-2</sup> day<sup>-1</sup> seem feasible with current state-of-the-art technology.

The research performed in this thesis clearly underlines the potential of microalgae as a source of commodity products, because the productivities that can be expected from microalgae largely exceed productivities accomplished by terrestrial plants ( $2.1\text{--}8.8\text{ g m}^{-2}\text{ day}^{-1}$  in microalgae compared to  $0.1\text{--}1.4\text{ g m}^{-2}\text{ day}^{-1}$  in commonly used agricultural oil-crops). This does however not guarantee economic success or a positive energy balance.

**Chapter 8** evaluates the outcomes of techno-economic and life cycle analysis (LCA) studies that investigated the cost-price and net energy ratio of microalgal products. Most of these studies use biodiesel production from microalgal TAGs as their case-study. These studies conclude that with current technology, the cost-price for biodiesel is too high and that more energy is consumed in the production process than what is produced in the form of biodiesel. It was also found that the biomass productivity and biochemical composition associated with the cultivation of microalgae are large uncertainties in the input for these studies. This chapter therefore presents several scenarios for microalgal cultivation (various products). For each scenario, productivities, biochemical compositions, and nutrient requirements are provided that can be used as more realistic input values for techno-economic and LCA studies. These values are derived from the outcomes of the previous chapters. It was concluded that the TAG productivity is commonly overestimated by 3 to 6-fold in techno-economic and LCA studies. According to these studies, approximately half of the costs and energy are used in the cultivation step. It was therefore concluded that these techno-economic and LCA studies underestimate the cost-price and energy consumption by 2 to 3.5-fold. The future improvements in productivity that might be accomplished according to chapter 7, could potentially improve the productivity such that it approaches the productivity that is commonly assumed as the base-case in current techno-economic and LCA studies. These advances in productivity can thus help to reduce the cost-price and specific energy consumption, but in addition, a reduction in costs and energy consumption of photobioreactors is needed before microalgal TAG production can be commercialized.

Altogether, this thesis provides a quantitative understanding of the factors that influence photosynthesis and carbon partitioning during nitrogen starvation. Using these insights, it is illustrated how the TAG productivity could be increased. Estimates for productivities and biochemical composition that can be achieved in a production process were made. These can help to estimate and reduce the cost-price and specific energy consumption for microalgal TAG production. This can ultimately help to enable the replacement of current sources of fossil and vegetable oil.





# Samenvatting

De wereldwijde vraag naar grondstoffen voor levensmiddelen en biobrandstoffen stijgt snel als een gevolg van een groei in wereldpopulatie, economische groei van ontwikkelingslanden, and zorgen voor klimaatverandering. De productie van deze grondstoffen gebeurt grotendeels door middel van landbouwgewassen. Het garanderen van voldoende beschikbaarheid van landbouwgrond, zoet water, en voedingstoffen is een grote uitdaging om in de vraag naar deze grondstoffen te voorzien. Er is daarom een grote vraag naar nieuwe duurzame en hernieuwbare grondstoffen voor zowel levensmiddelen en biobrandstoffen. Producten die uit microalgen verkregen kunnen worden, worden vaak gezien als een veelbelovende vervanging voor deze grondstoffen. Het kweken van microalgen heeft een aantal voordelen ten opzichte van het gebruik van traditionele landbouw gewassen. Microalgen hebben een veel hogere productiviteit dan traditionele landbouwgewassen, hebben geen landbouwgrond nodig en kunnen in potentie zelfs op zee gekweekt worden. Desalniettemin laten huidige schattingen zien dat een reductie van meerdere malen in kostprijs gerealiseerd moet worden voordat de productie van bulk producten met microalgen economisch haalbaar is. Hoewel een verscheidenheid aan producten gemaakt kan worden uit microalgen, richt dit werk zich op de productie van triacylglycerol (TAG). Deze TAGs zijn vergelijkbaar met plantaardige olie en kunnen gebruikt worden als een eetbare olie en als een grondstof voor de productie van biodiesel.

Een hoge TAG productiviteit is nodig om op commerciële schaal TAG te produceren met behulp van microalgen zodat de kostprijs verlaagd kan worden. Om deze hoge productiviteiten te kunnen behalen is er een kwantitatief begrip nodig van de fysiologische processen die een rol spelen in TAG productie door microalgen. TAG is een secundair metaboliet dat onder optimale groei condities in verwaarloosbare hoeveelheden gemaakt wordt. De meest gebruikte techniek om te zorgen dat microalgen veel TAG maken is door de microalgen bloot te stellen aan stikstofuithongering. Onder deze condities kunnen sommige microalgensoorten tot wel 50% van hun eigen gewicht ophopen als TAGs. Deze stikstofuithongering zorgt echter niet alleen voor dat TAGs opgehoopt worden, het heeft ook een effect op een hoop andere cellulaire processen, waaronder bijvoorbeeld fotosynthese.

In algemene zin kan de TAG productiviteit uitgedrukt worden als de hoeveelheid licht die geabsorbeerd wordt, vermenigvuldigd met de efficiëntie waarmee CO<sub>2</sub> gefixeerd wordt (fotosynthetische efficiëntie) en het aandeel van het gefixeerde CO<sub>2</sub> dat gebruikt wordt om TAG te maken (koolstof partitionering).

Zowel de fotosynthetische efficiëntie en de koolstof partitionering zijn erg variabel in microalgen. Een gedetailleerd begrip van de fysiologie achter fotosynthese en de

koolstof partitieverhouding tijdens stikstofuithongering kan helpen om strategieën te bedenken om de TAG productiviteit te verhogen. Het doel van dit proefschrift is daarom een kwantitatief begrip te verkrijgen van de fysiologie achter TAG productie tijdens stikstofuithongering.

Microalgen produceren een grote verscheidenheid aan vetklassen. Slechts een deel van deze vetten zijn TAGs of andere vetzuurhoudende vetten. **Hoofdstuk 2** beschrijft een analytische methode om de vetzuurhoeveelheid en vetzuursamenstelling in microalgen te meten. Deze analytische procedure is gebaseerd op een opvolging van mechanische cel disruptie, oplosmiddel gebaseerde vetextractie in chloroform en methanol, transesterificatie van vetzuren naar vetzuur methyl esters (FAMES) en identificatie en kwantificatie van FAMES met behulp van gaschromatografie (GC-FID). Een van de belangrijkste voordelen van deze methode is de kleine hoeveelheid materiaal die nodig is om de analyse uit te voeren en de mogelijkheid om de methode uit te breiden met een vaste fase extractie stap om TAGs van polaire vetten te scheiden.

Er bestaan grote verschillen in hoe microalgen soorten reageren op stikstofuithongering. Het is daarom belangrijk om de juiste microalgen soort te kiezen waarmee op grote schaal TAG geproduceerd kan worden. **Hoofdstuk 3** onderzoekt daarom de verschillen en overeenkomsten tussen microalgen soorten met betrekking tot hoe ze reageren op stikstofuithongering met het uiteindelijke doel om een geschikte microalg voor TAG productie te vinden. Uit een literatuuronderzoek onder 96 microalgensoorten zijn negen veelbelovende soorten geselecteerd (*Chlorella vulgaris*, *Chlorella zofingiensis*, *Dunaliella tertiolecta*, *Isochrysis galbana*, *Nannochloris* sp., *Neochloris oleoabundans*, *Porphyridium cruentum*, *Phaeodactylum tricornutum* and *Scenedesmus obliquus*). De biomassa productiviteit en TAG productie van deze soorten zijn in detail onderzocht voor zowel stikstofrijke en stikstofloze condities. Er is gevonden dat alle microalgensoorten doorgaan met fotosynthese en koolstofassimilatie tijdens stikstofuithongering. De meeste microalgensoorten waren in staat om dezelfde biomassa productiviteit te handhaven tijdens initiële stikstofuithongering als tijdens stikstofrijke condities. Deze soorten waren ook in staat om meerdere malen toe te nemen in biomassa concentratie nadat de stikstof uitgeput was. Hoe lang deze microalgensoorten deze hoge biomassa productiviteit konden volhouden en hoeveel biomassa gemaakt kon worden nadat de stikstof uitgeput was varieerde erg tussen de soorten (tussen een 1,4 en 7,8 keer toename in biomassa concentratie nadat stikstof uitgeput was). Er waren ook grote verschillen tussen de soorten in de maximale TAG fractie die opgehoopt kon worden.

Deze maximale TAG fractie varieerde tussen de 5 en 45% van het drooggewicht. Er was gevonden dat alle microalgensoorten ook andere biomassabestandsdelen tegelijkertijd met TAG ophoopten. TAG productie kon maximaal de helft van de biomassa toename tijdens de stikstofuithongering verklaren.

De microalg *S. obliquus* behaalde de hoogste TAG productiviteit, was in staat om grote hoeveelheden TAG op te hopen (meer dan 35% van het totale drooggewicht), en kon het langste een onveranderde biomassa productiviteit handhaven nadat stikstof uitgeput was (een toename in biomassa concentratie van 4,5 keer was behaald voordat een afname van de biomassa productiviteit was waargenomen). *S. obliquus* was daarom gekozen als de meest geschikte microalgensoort om TAG mee te produceren en deze microalg is gebruikt in al het vervolgonderzoek beschreven in dit proefschrift.

**Hoofdstuk 4** beschrijft hoe de lichtintensiteit, pH, en de temperatuur de reactie van *S. obliquus* op stikstofuithongering beïnvloed. Er is gevonden dat TAG geproduceerd kan worden tussen pH 5 en 9, een temperatuur van 20 en 35°C, en een ingaande lichtintensiteit van 200 tot 1500  $\mu\text{mol m}^{-2} \text{s}^{-1}$ . De licht intensiteit had geen effect op de maximale TAG fractie. De lichtintensiteit had echter wel een groot effect op de fotosynthetische efficiëntie. Als een consequentie daarvan was de TAG opbrengst op licht (g TAG/mol fotonen) ongeveer 5-voud lager onder hoge lichtintensiteiten dan onder lage lichtintensiteiten. Suboptimale pH waarden en temperaturen kunnen de TAG opbrengst op licht ook tot wel 5-voud verlagen en kunnen ook de maximale TAG fractie met 2-voud verlagen. De optimale condities voor TAG productie vielen samen met het optimum voor groei. Dit was bij de laagste licht intensiteit, pH 7, en een temperatuur van 27.5°C. Een opbrengst van 0.263 g vetzuren per mol fotonen was behaald onder deze condities. De vetzuur samenstelling van TAG was niet beïnvloed door de lichtintensiteit, maar de onverzadigingsgraad nam toe met afnemende temperatuur en pH.

In de vorige hoofdstukken was er gevonden dat tijdens stikstofuithongering slechts de helft van de biomassa die geproduceerd wordt een gevolg is van TAG productie en dat andere biomassa bestandsdelen tegelijkertijd geproduceerd worden. Eliminatie van concurrerende metabole routes kan mogelijk de TAG productiviteit verhogen. In **hoofdstuk 5** is daarom het koolstofverdelingsmechanisme van zowel het wild-type en van de *slm1* zetmeeldeficiënte mutant van *S. obliquus* onderzocht. Er is bevonden dat tijdens initiële stikstofuithongering, zetmeel opgehoopt wordt tot wel 40% van het drooggewicht in het wild-type van *S. obliquus*. In deze periode wordt TAG tegelijkertijd met zetmeel geproduceerd maar wel in een langzamer tempo. Wanneer de

stikstofuithongering verder vordert, dan stopt zetmeel ophoping maar TAG ophoping gaat door. Hierna wordt het initieel opgehoopte zetmeel weer afgebroken en worden de afbraakproducten waarschijnlijk gebruikt als een substraat voor TAG productie. Er is gevonden dat de zetmeeldeficiënte mutant de volledige fotosynthetische capaciteit die gebruikt wordt om zetmeel te maken in het wild-type, herdistributeert naar TAG productie. Dit zorgde voor veel hogere TAG ophopingssnelheden tijdens initiële stikstofuithongering. Verder was er gevonden dat de fotosynthetische efficiëntie niet negatief beïnvloed werd door de zetmeeldeficiëntie. Samen zorgde dit voor een toename van 51% in de TAG opbrengst op licht, van 0.144 naar 0.217 g/mol. De maximale TAG fractie was ook verbeterd in de zetmeeldeficiënte mutant, van 45 naar 57% van het drooggewicht. Deze resultaten laten zien dat de capaciteit van het TAG synthese mechanisme niet limiterend is voor TAG productie. Dit hoofdstuk laat ook zien dat eliminatie van concurrerende metabole routes een goede strategie is om de TAG productiviteit te verhogen, ook in microalgen die uit zichzelf al veel TAG produceren.

Het mechanisme achter de gelijktijdige zetmeel en TAG ophoping is in meer detail onderzocht in **hoofdstuk 6**. Er is onderzocht hoe de koolstof partitie-verhouding en de fotosynthetische efficiëntie tijdens stikstofuithongering afhankelijk zijn van de lichtintensiteit tijdens de stikstofuithongering en van de licht-geacclimeerde staat op het moment van stikstof uitputting. Om in staat te zijn om het effect van de lichtintensiteit tijdens de stikstofuithongering en het effect van de licht-geacclimeerde staat op het moment van stikstof-uitputting gelijktijdig en onafhankelijk te onderzoeken is een nieuwe experimentele opstelling ontwikkeld. In deze opstelling zijn de kweken begonnen als licht gelimiteerde chemostaat kweken met voldoende stikstof in het groeimedium. Deze kweken zijn uitgevoerd bij zowel een lage als een hoge ingaande lichtintensiteit om op deze manier twee verschillend licht-geacclimeerde kweken te verkrijgen. Door licht-acclimatie hebben deze verschillende licht-geacclimeerde culturen een groot verschil in hun pigmentatie, pigment samenstelling en samenstelling van het fotosysteem. Op het moment dat in deze kweken een 'steady-state' situatie verkregen was, was de chemostaat controle gestopt en zijn de kweken voortgezet als een stikstof-uitgeputte batch kweek, bij zowel een lage als een hoge lichtintensiteit. Er is bevonden dat de koolstof-partitie verhouding tussen zetmeel en vetzuren sterk afhankelijk is van de mate van stikstofuithongering, welke gekwantificeerd is als de fractie stikstof in de biomassa. Ten aller tijden kan ongeveer 70% van de biomassa productie tijdens de stikstofuithongering verklaard worden door zetmeel en vetzuur productie. Meteen na stikstof uitputting was de verhouding tussen vetzuur en zetmeel

productie 1 op 4. Deze verhouding nam geleidelijk toe tot 100% vetzuur productie wanneer de stikstofuithongering verder vorderde. Hierna werd zetmeel weer afgebroken en waarschijnlijk gebruikt als een substraat voor vetzuur synthese.

De verschillen in pigmentatie en pigment samenstelling, die een gevolg waren van licht-acclimatie tijdens de chemostaat kweken met voldoende stikstof die bij verschillende lichtintensiteiten uitgevoerd waren, bleven zichtbaar tijdens de stikstofuithongeringsfase. Dit had echter geen effect op de fotosynthetische efficiëntie of op de koolstof-partitie verhouding tijdens de stikstof uithongering. De lichtintensiteit had echter wel een grote invloed op de fotosynthetische efficiëntie, zowel tijdens de stikstofuithongeringsfase als tijdens groei met afdoende stikstof. Vergeleken met lage lichtintensiteiten nam de fotosynthetische efficiëntie bijna 2-voud af onder afdoende-stikstof condities en de vetzuur opbrengst op licht nam bijna 3-voud af. De lichtintensiteit tijdens stikstof uithongering had een kleine invloed op hoe de vetzuur:zetmeel synthese verhouding zich ontwikkelde tijdens stikstofuithongering. Bij hoge lichtintensiteiten werd een iets lagere vetzuur:zetmeel productie verhouding waargenomen. Gebaseerd op de observaties in dit hoofdstuk werd er voorgesteld dat het waargenomen koolstof-partitie mechanisme veroorzaakt wordt door competitie tussen de twee metabole routes voor een gedeeld koolstof-substraat, en niet door een 'overflow' metabolisme als vaak wordt aangenomen.

Op basis van de inzichten uit de vorige hoofdstuk en bestaande literatuur is een mechanistisch model ontwikkeld, beschreven in **hoofdstuk 7**, dat TAG productie tijdens stikstofuithongering beschrijft. Dit model bestaat uit een fotosynthese module en een koolstofpartitionerings module. De fotosynthese module beschrijft absorptie van licht, het aandeel van de fotonen dat gebruikt wordt voor fotosynthese en het aandeel dat thermisch gedissipeerd wordt als een functie van de lichtintensiteit en de mate van stikstofuithongering. De koolstofpartitionerings module beschrijft de verdeling van fotonen, als een functie van de mate van stikstofuithongering, tussen celonderhoud, reproducerende biomassa (de biomassa die gemaakt wordt tijdens groei in de aanwezigheid van stikstof), zetmeel, TAG, en residuele biomassa productie. Verder beschrijft deze module de omzetting van zetmeel naar TAG. Er zijn verschillen in de energetische benodigdheden om deze verschillende bestandsdelen te maken. Om de verschillen mee te nemen gebruikt deze module een opbrengstverhouding (g product/mol foton of g product/g substraat) specifiek voor elk biomassa bestandsdeel. Deze opbrengstverhoudingen zijn uitgerekend aan de hand van de stoichiometrie van het metabole netwerk door middel van 'flux balance analysis'. Deze

opbrengstverhoudingen kunnen tot wel drievoud variëren tussen de verschillende biomassa bestandsdelen. Dit benadrukt het belang om opbrengstverhoudingen specifiek voor elk biomassabestandsdeel te gebruiken en om niet een gemiddelde opbrengstverhouding voor fotosynthese te gebruiken. Het model is gevalideerd aan de hand van experimentele data van zowel het wild-type en de zetmeeldeficiënte mutant van *S. obliquus* uit hoofdstuk 5, en het model is in staat om de experimentele data nauwkeurig te beschrijven.

Vervolgens is het model gebruikt om te onderzoeken hoe de TAG productiviteit verbeterd kan worden door middel van reactor ontwerp en stamverbetering. Er is geconcludeerd dat de ingaande lichtintensiteit de belangrijkste factor is die de TAG opbrengst op licht bepaald. Dit hoofdstuk laat zien hoe verbeteringen in reactor ontwerp, door middel van lichtverduunningstechnieken, de productiviteit met een factor drie kunnen verbeteren (van 2,1 naar 6,3 g m<sup>-2</sup> dag<sup>-1</sup>). Verbeteren van het fotosysteem kan de productiviteit met 50 tot 75% verbeteren bij hoge licht intensiteiten (van 2,1 naar 3,7 g m<sup>-2</sup> dag<sup>-1</sup>). Zetmeeldeficiënte mutanten kunnen de productiviteit met 50% verbeteren en verdere verbeteringen lijken mogelijk als de activiteit van andere concurrerende metabole routes verminderd wordt. In gebieden met een hoeveelheid zonlicht vergelijkbaar met zuid Europa kunnen combinaties van voorgenoemde technologieën de productiviteit tot wel 10,9 g TAG m<sup>-2</sup> dag<sup>-1</sup> verhogen en productiviteiten tot 8,8 g TAG m<sup>-2</sup> dag<sup>-1</sup> lijken haalbaar met huidige 'state-of-the-art' technologie.

Het onderzoek dat is uitgevoerd voor dit proefschrift laat duidelijk het potentieel van microalgen zien als een bron van bulkproducten. De potentiële productiviteiten die behaald kunnen worden met microalgen zijn namelijk veel hoger dan de productiviteiten die behaald kunnen worden met traditionele landbouwgewassen (2,1-8,8 g m<sup>-2</sup> dag<sup>-1</sup> in microalgen vergeleken met 0,1-1,4 g m<sup>-2</sup> dag<sup>-1</sup> in veelgebruikte olie gewassen). Deze hoge productiviteit garandeert echter geen economisch succes of positieve energie balans. **Hoofdstuk 8** evalueert daarom de uitkomsten van techno-economische en 'life cycle' analyse (LCA) studies die de kostprijs en netto energie verhouding (energie geproduceerd/energie geconsumeerd) van producten die uit microalgen verkregen zijn evalueren. De meeste van deze studies nemen biodiesel productie uit TAGs van microalgen als voorbeeld. Deze studies concluderen dat met huidige technologie de kostprijs van biodiesel te hoog is en dat er meer energie gebruikt wordt in het productie proces dan wat er gemaakt wordt in de vorm van biodiesel. Er is bevonden dat de biomassa productiviteit en de biomassa samenstelling van microalgen een grote

onzekerheid is in deze studies. Om hier meer inzicht in te geven presenteert dit hoofdstuk daarom een aantal scenario's voor het kweken van microalgen (gericht op verschillende producten). Voor elk scenario worden getallen gegeven voor de biomassa productiviteit, biomassa samenstelling en nutriënten gebruik die als input gebruikt kunnen worden voor techno-economische en LCA studies. Deze waarden zijn verkregen aan de hand van de vindingen uit de vorige hoofdstukken. Op basis hiervan is geconcludeerd dat de TAG productiviteit vaak drie- tot zesvoudig wordt overschat in veel techno-economische en LCA studies. Volgens deze studies wordt ongeveer de helft van de kosten en energie gebruikt in de microalgenkweek stap in het biodiesel productieproces. Dit betekent dat deze techno-economische en LCA studies de kostprijs en energie consumptie 2 tot 3,5 keer onderschatten. Toekomstige verbeteringen in productiviteit die behaald kunnen worden volgens hoofdstuk 7 kunnen potentieel bijdragen tot een productiviteit die vergelijkbaar is met de productiviteit die vaak als uitgangssituatie wordt aangenomen in huidige techno-economische en LCA studies. Deze verbeteringen in productiviteit kunnen dus helpen om de kostprijs en energieconsumptie te verlagen, maar in aanvulling daarop is een verlaging van kosten en energiegebruik van fotobioreactoren nodig voordat TAG productie met behulp van microalgen economisch en energetisch haalbaar is.

Alles bij elkaar geeft dit proefschrift een kwantitatief begrip van de factoren die fotosynthese en koolstofverdeling tijdens stikstofuithongering beïnvloeden. Aan de hand van deze inzichten is laten zien hoe de TAG productiviteit verbeterd kan worden. Verder zijn schattingen voor de productiviteit en biomassa samenstelling die gehaald kunnen worden in een productieproces gegeven. Deze kunnen helpen om de kostprijs en energiegebruik in te schatten en te verlagen. Dit kan uiteindelijk bijdragen in het vervangen van huidige fossiele en plantaardige bronnen van olie door olie verkregen uit microalgen.







# Dankwoord

Met het schrijven van dit dankwoord komen vier jaar onderzoek bij Bioprocess Engineering tot een eind. Een uitdagende en leuke tijd waarin ik veel heb geleerd. Een tijd waarin ik veel mooie herinneringen heb opgedaan die ik nooit zal vergeten. Zowel dit proefschrift als deze herinneringen zouden er niet geweest zijn zonder velen van jullie. Ik wil deze laatste bladzijdes van mijn proefschrift daarom graag gebruiken om jullie hiervoor te bedanken.

Ten eerste wil ik graag mijn begeleiders bedanken. **René, Dirk en Packo**, bedankt dat jullie me de kans gegeven hebben om mijn promotieonderzoek bij jullie te doen. Jullie hebben me veel vrijheid gegeven en me altijd gestimuleerd om het uiterste uit mezelf te halen. Ik vond het heel fijn dat ik altijd kon binnenlopen en jullie tijd maakten als ik iets wilde bespreken. Alles was bespreekbaar en jullie dachten graag mee met mijn ideeën. Jullie waren kritisch maar tegelijkertijd motiverend. Wat ik zelf wilde stond voor jullie altijd centraal. Bedankt daarvoor. Ik had me geen fijnere begeleiders kunnen voorstellen! **René**, je had altijd een helder beeld van waar we stonden en wat er moest gebeuren. Je maakte het mogelijk om effectief beslissingen te nemen. Je was altijd helder en eerlijk over hoe je over dingen dacht maar gaf me de ruimte om mijn eigen visie te ontwikkelen. Bedankt! **Packo**, bedankt voor de vele, en vooral lange, discussies en brainstorm sessies. Die hebben me erg geholpen om op nieuwe ideeën te komen en om alles op een rijtje te krijgen. **Dirk**, bedankt dat je me hielp met het zien van het grotere plaatje en je kritische houding die me hielp om alles goed en helder te beargumenteren.

**René D.**, heel erg bedankt voor je grote betrokkenheid en interesse in mijn onderzoek. Je belangstelling was voor mij erg motiverend en je visie en wensen vanuit de toepassing geredeneerd waren heel erg leerzaam. Je hebt je altijd erg ingezet in het geven van feedback op mijn onderzoek en artikelen. Bedankt daarvoor. Ik vond het een hele fijne samenwerking. **Marcia, Ingrid, Hui, Hans-Gerd, Peter**, en andere collega's van Unilever, bedankt voor de fijne samenwerking. Jullie dachten graag mee met vragen die ik had, hielpen met (het ontwikkelen van) analyses die we zelf niet konden, en ik vond het altijd erg interessant om te zien wat jullie allemaal deden.

**Lenny**, zonder jou had dit proefschrift er zeker niet uitgezien zoals het er nu uit ziet. De starchless mutant die je gemaakt hebt en waarnaar we samen vervolgonderzoek gedaan hebben is zonder twijfel een van de meest spannende onderwerpen in dit proefschrift. Ik

vond het altijd fijn om je als collega-aio in ons project te hebben en onze vindingen en plannen te bespreken. Veel succes met de laatste lootjes!

**Jannik** and **Valentin**, thank you for your contributions to this thesis. **Jannik**, you were the first student that I supervised together with **Anne**. You were working on a very challenging and exciting project on a proof of concept for a two-reactor system. You managed this really well, learned really quickly, and was able to work very independently, which made your project a success! **Valentin**, you were really passionate about algae and were convinced that 'your' starchless mutant was the best! You were hard working, self-motivating and eager to learn. The result of that is that your work is the foundation of chapter 5 of this thesis! Thank you both for your enthusiasm. It was a pleasure to work together.

**Fred, Sebas**, en **Wendy**, bedankt voor al jullie ondersteuning in het lab. Ik verbaasde me steeds over jullie gedetailleerde kennis over hoe alle methodes, apparaten en onderdelen werken. Ik heb daar veel van geleerd. Als er een probleem was waren jullie er meteen om mee te kijken en het op te lossen. Dat nam vaak veel zorgen weg. Bedankt daarvoor!

**Lenneke, Pascale, Jacqueline**, en **Jeroen**. Toen ik net op de vakgroep aankwam hebben jullie me meteen opgenomen in de labuitje commissie. Dat bleek een fantastische manier om kennis te maken met de vakgroep en daar heb ik vanaf het begin erg veel plezier in gehad. Ik voelde me daarom meteen thuis. Tijdens de vergaderingen kwam van vergaderen weinig terecht, maar ik denk dat daardoor het labuitje alleen maar een groter succes geworden is.

**Anne, Kim, Lenneke, Lenny, Marjon**, en **Tim**, samen hebben we het eerste young algaeeneers symposium neergezet. Ik vond dit een hele leuke en leerzame ervaring. Het resultaat is iets waar ik erg trots op ben en een succes waar ik van te voren alleen maar over durfde te dromen.

**Kim, Pascale, Jacqueline**, jullie waren mijn kamergenoten in de eerste jaren op de vakgroep. Jullie waren er om mee te lachen, maar ook om stoom af te blazen als de stress toenam of om mee te denken als ik met een probleem zat. Bedankt voor alle steun en lol die we gehad hebben. Ik denk er regelmatig met weemoed aan terug.

**Lenneke, Lenny, Rupali**, and **Catalina**, after the movement you became my office mates. Going to the office was a lot more fun thanks to you!

**Marcel**, je was altijd beschikbaar om gedetailleerde uitleg te geven over fotosynthesemechanismen en allerlei andere onderwerpen, of om feedback te geven op mijn werk. Bedankt daarvoor en bedankt voor je bijdrage aan hoofdstuk 7! **Agi**, thank you for all the weird conversations we could have. They really made me laugh! **Kim**, je bent zonder twijfel een van de meest vrolijke en enthousiaste personen die ik ken en weet daarmee iedereen in een goed humeur te brengen. Bedankt! **Lenneke**, bedankt voor het organiseren van de vele borrels, kerstdiners en andere activiteiten. **Marjon**, bedankt voor al je vrolijkheid in het lab, en dat het je lukte om '632' een beetje in het gareel te houden! **Giulia**, thank you for all your enthusiasm to continue with the model! **Mathieu**, bedankt voor alle grappige discussies die we konden hebben in de koffiecorner. **Miranda & Marina**, bedankt voor jullie hulp met het regelen van van-alles-en-nog-wat. **Douwe**, bedankt voor al je enthousiaste uitleg over transcriptomics, genexpressie, statistiek, en overige adviezen. **Gerard**, bedankt voor al je adviezen en practical jokes. **Youri, Agi, Lenneke, Catalina, Ward, Joao (or should I say "mr. van der Zee"?), Tim, Mark, Josue, Carl, Luci, Kiira, Pauline, Jeroen, Rafael, Ilse**, and many others, thank you for all the fun at the BBQs and Friday afternoon drinks! **All members of BPE**, you made working at BPE very enjoyable. You helped to turn all brainstorm days, PhD trip, and conferences we attended together into cheerful events! Thank you for all the fun at the many department drinks and coffee breaks. I will definitely miss those!

**Pascalie, Erik, Marlinda, Lies, Annemieke**, en **Jasper**, het was fijn om jullie als huisgenoten te hebben. Bedankt voor de gezelligheid, soms hoognodige afleiding, en adviezen.

**Ralph** en **Tim**, bedankt dat jullie mijn paranimfen willen zijn.

**Marco** en **Marluus**, jullie hebben me altijd gesteund en gestimuleerd om te gaan doen wat ik graag wil doen. Bedankt voor alle belangstelling en waardevolle adviezen. **Cecile, Sijmen**, en **Rinske**, bedankt voor al jullie interesse de afgelopen jaren. **Rinske** bedankt voor de taxi-service naar Schiphol waar ik veelvuldig gebruik van heb mogen maken.

- Guido -







## About the author

Guido Breuer was born in Amsterdam, The Netherlands, on January 25, 1987. He went to the Bonaventura college in Leiden where he obtained his VWO diploma in 2004.

In 2004 he started his studies 'Life Science and Technology' at the University of Leiden and Technical University of Delft. He graduated from his BSc in 2008 on the topic of the solubility and crystallization of fumaric acid. Hereafter he continued with his MSc. During his MSc he focussed on bioprocess engineering in the 'cell factory' theme of his studies. During this MSc program he performed research on the degradation of cellulose-fibres in wastewater treatment plants during an internship at Waternet. In addition, he also gained experience on industrial fermentation technology during an internship at DSM where he performed research on enzyme production.

After he obtained his MSc degree in 2010, he started his PhD research at the Bioprocess Engineering department of the Wageningen University, where he worked in the 'emerald oils' project on triacylglycerol production in microalgae and which resulted in the writing of this thesis.





# List of publications

- Breuer G**, Lamers P.P., Janssen M., Wijffels R.H., Martens D.E.: Opportunities to improve the areal TAG productivity of microalgae. *manuscript submitted*.
- Breuer G**, Martens D.E., Draaisma R.B., Wijffels R.H., Lamers P.P.: Photosynthetic efficiency and carbon partitioning in nitrogen-starved *Scenedesmus obliquus*. *manuscript submitted*.
- Breuer, G.**, de Jaeger, L., Artus, V., Martens, D.E., Springer, J., Draaisma, R.B., Eggink, G., Wijffels, R.H., Lamers, P.P. 2014. Superior triacylglycerol (TAG) accumulation in starchless mutants of *Scenedesmus obliquus*: (II) evaluation of TAG yield and productivity in controlled photobioreactors. *Biotechnology for Biofuels* 7, 70.
- Breuer, G.**, Evers, W.A.C., de Vree, J.H., Kleinegris, D.M.M., Martens, D.E., Wijffels, R.H., Lamers, P.P. 2013. Analysis of Fatty Acid Content and Composition in Microalgae. *J Vis Exp*, e50628.
- Ruiken, C.J., **Breuer, G.**, Klaversma, E., Santiago, T., van Loosdrecht, M.C.M. 2013. Sieving wastewater – Cellulose recovery, economic and energy evaluation. *Water Res*, 47(1), 43-48.
- Breuer, G.**, Lamers, P.P., Martens, D.E., Draaisma, R.B., Wijffels, R.H. 2013. Effect of light intensity, pH, and temperature on triacylglycerol (TAG) accumulation induced by nitrogen starvation in *Scenedesmus obliquus*. *Bioresource Technology*, 143, 1-9.
- Breuer, G.**, Lamers, P.P., Martens, D.E., Draaisma, R.B., Wijffels, R.H. 2012. The impact of nitrogen starvation on the dynamics of triacylglycerol accumulation in nine microalgae strains. *Bioresource Technology*, 124, 217-226.

# Overview of completed training activities

## Discipline specific activities

### Courses

Bio-energy production from crop plants and algae (Wageningen, The Netherlands, 2012)

Process economics and cost engineering (Enschede, The Netherlands, 2014)

### Conferences

Netherlands biotechnologie symposium (Ede, The Netherlands, 2012)<sup>2</sup>

9<sup>th</sup> European workshop on algal biotechnology (Potsdam, Germany, 2012)<sup>1</sup>

1<sup>st</sup> Young algaeneers symposium (Wageningen, The Netherlands, 2012)<sup>1,3</sup>

9<sup>th</sup> European congress of chemical engineering (ECCE), (The Hague, The Netherlands, 2013)<sup>2</sup>

Algal biomass, biofuels & bioproducts (Toronto, Canada, 2013)<sup>1</sup>

2<sup>nd</sup> Young algaeneers symposium (Montpellier & Narbonne, France, 2014)<sup>1</sup>

BIO Pacific rim summit on industrial biotechnology and bioenergy (San Diego, USA, 2014)<sup>2</sup>

## General courses

VLAG PhD week (Baarlo, The Netherlands, 2011)

PhD competence assessment

Scientific writing (Wageningen, The Netherlands, 2012)

Presentation skills (Wageningen, The Netherlands, 2012)

Communication in Interdisciplinary Research (Wageningen, The Netherlands, 2012)

Project and time management (Wageningen, The Netherlands, 2012)

Effective behaviour in your professional surroundings (Wageningen, The Netherlands, 2012)

### **Optionals**

Trip to Bioprocess Engineering group Karlsruhe Institute of Technology (KIT), and Algen biotechnologie group University of Bielefeld (Germany, 2011)

BPE PhD symposia and brainstorm days (Wageningen, 2011, 2012, 2013, 2014)<sup>2</sup>

Visit to University of Nantes (Saint-Nazaire, France, 2013)<sup>2</sup>

PhD trip (Spain, 2012)<sup>1,2</sup>

<sup>1</sup>Poster

<sup>2</sup>Presentation

<sup>3</sup>Organisation

---

This study was carried out at the Bioprocess Engineering Group of Wageningen University, Wageningen, The Netherlands and was supported by Unilever and the Food and Nutrition Delta program of Agentschap NL (FND 10007).

Printing: Ridderprint BV

Edition: 350 copies

Guido Breuer, 2015



